

Geostatistical Categorical Variable Modeling using
Optimization Techniques with Truncated Plurigaussian
Simulation

by

Samaneh Sadeghi

A thesis submitted in partial fulfillment of the requirements for the degree of

Doctor of Philosophy

in

Mining Engineering

Department of Civil and Environmental Engineering
University of Alberta

© Samaneh Sadeghi, 2017

Abstract

Stochastic simulation of rock types is a major area of continuing research. Rock types account for the majority of heterogeneity in mineral/ petroleum deposits, and a good understanding of the geometry and spatial distribution of natural phenomena is required for reliable resource and reserve estimation. Integrating geological concepts in geostatistical modeling is important in order to provide realistic geological models. The resulting models are practical and reasonable if they provide a reliable reproduction of the true underlying structure of the subsurface.

A methodology has been developed to construct geostatistical models that reproduce features inferred from data and are consistent with geologic understanding of the deposit. The main idea is to transfer essential geological features to the geostatistical models, particularly when there is a clear ordering between categories. In deposits with complicated ordering structures, truncated plurigaussian simulation (TPG) is a flexible method for simulating facies categories. This is a modeling technique which relies on simulating multiple underlying Gaussian variables to represent a categorical variable. TPG simulation utilizes truncation masks for mapping categorical variables to a continuous space. Therefore, an optimized truncation mask is required to best represent the contacts and transitions between facies categories with respect to the geological interpretations.

In addition, continuity of the categories is controlled by the variogram of each Gaussian variable. Finding the variogram model of the underlying Gaussian variable is essential to reproduce the target indicator variograms of facies categories and is an important challenge of TPG simulation.

TPG simulation is improved through adopting optimization techniques for modeling the underlying Gaussian variables and the categorical variable. A novel technique is developed which allows for the reproduction of the spatial continuity of facies categories by automatically inferring the optimum variogram models for the underlying Gaussian deviates. Implementation of this methodology demonstrates improvement in the modeling of complicated geologic features and in accounting for changes in the categories proportions. Reasonable reproductions of the transitions observed in the data as well as the categorical data observations from the production data are achieved.

*To my parents, **Noorbanoo** and **Hoosein**, for their support and unconditional love
and
my twin sister, **Dr. Samira**, for her friendship and words of motivation*

Acknowledgements

I would like to express my deepest appreciation to my supervisor, Dr. Jeffery B. Boisvert. It has been a rewarding opportunity for me to work under his supervision. I thank him for his excellent ideas, for his patience and for all the time he spent with me. Without his guidance, constant encouragement and support, this thesis could never have been possible.

I wish to express my sincere appreciation and gratitude to Dr. Clayton V. Deutsch, director of the Center of Computational Geostatistics (CCG) for his precious assistance, guidance, and support which built a strong base for my knowledge.

I would like to take this opportunity to extend my gratitude to Dr. Clayton V. Deutsch, Dr. Juliana Leung and Dr. Yashar Pourrahimian for being part of my supervisory committee and to Dr. Ming Ye for being my external examining committee. I thank them all for dedicating their time to reviewing this thesis and providing constructive and insightful comments.

I acknowledge the financial support of the member companies of the CCG. I also would like to acknowledge the support of administrative staff of Civil and Environmental Engineering at University of Alberta, especially, Alice Da Silva and Arlene Figley for their daily contribution which is essential to the success of the student's school.

A special note of gratitude goes to my fianc, **Navid** who is my best friend, for his love, enthusiasm, strength, companionship, and encouragement to finish my doctoral studies.

Many thanks to my friends and my great colleagues, Dr. Vahid Dehdari, Dr. Maryam Hadavand, Dr. Mehdi Rezvandehy, Dr. Daniel A. Silva, Mostafa Hadavand, Dr. John Manchuk, Felipe Pinto and Jianan Qu for encouragement and for making my days in the CCG lab pleasant. And especially thanks to Diogo Silva for his collaboration, kindness support, and excited discussions during this program.

Special gratitude is extended to my best friends, Mohammad Sharifi, Meisam Norouzi, and Shaghayegh Hosseinpour for their motivation and support. They were an important source of distraction when I required it.

Last, but not the least, I would like to thank my family for their unending love and unconditional support throughout my life. They have always been there for me when I needed them and have been instrumental in every success of my life.

Table of Contents

- 1 Introduction** **1**
 - 1.1 Motivation and Problem Statement 2
 - 1.2 Thesis Statement 4
 - 1.3 Approach 5
 - 1.4 Outline 7

- 2 Background and Literature Review** **9**
 - 2.1 Random Function 10
 - 2.2 Stationarity 11
 - 2.3 Indicator Variables 12
 - 2.4 Transition Probabilities 14
 - 2.5 Gradient Optimization Technique 16
 - 2.6 Categorical Variable Modeling 19
 - 2.7 Sequential Indicator Simulation 19
 - 2.8 Multiple Point Statistics (MPS) 20
 - 2.9 Truncated Gaussian/Plurigaussian Simulation 22
 - 2.9.1 One-Gaussian Function 24
 - 2.9.2 Threshold Definition 26
 - 2.9.3 Link between Thresholds and Proportions 27
 - 2.9.4 M-Gaussian Functions 29
 - 2.10 Object Based Modeling 30
 - 2.11 Event Based Modeling 32
 - 2.12 Discussion 33

3	TPG Framework and Mask Optimization	34
3.1	Mask Optimization	34
3.1.1	Discretized Mask	34
3.1.2	Object Based Mask	46
3.2	Summary	51
4	TPG Simulation with Locally Varying Proportions (LVP)	52
4.1	Conditional Simulation in TPG Simulation	53
4.2	Locally Varying Mask with Thresholds	55
4.3	MDS Mask	58
4.4	Locally Varying Mask with MDS Mask	61
4.5	Case Study	62
4.6	Summary	70
5	Correlation between Underlying Gaussian RFs in TPG Simulation	72
5.1	Correlation Matrix	73
5.2	Effect of Correlated Gaussian RFs on TPG Realizations	78
5.3	Effect of Correlated Gaussian RFs on Mask	83
5.4	Summary	90
6	Variogram Optimization in TPG Simulation	91
6.1	Variogram Optimization	91
6.2	Variogram Optimization using Local Refinement	93
6.3	Variogram Optimization using a Neural Network	102
6.3.1	Artificial Neural Network (ANN)	102
6.3.2	Application	105
6.4	Variogram Optimization by Iteratively Adding Complexity	110
6.4.1	Application	111
6.5	Summary	120
7	Case Study	122
7.1	Available Data	122
7.1.1	Data Analysis	124
7.1.2	Global Mask	127

7.2	Variogram Optimization of Underlying Gaussian Realizations	128
7.3	Locally Varying Proportions	140
7.4	Summary	147
8	Summary and Future work	149
8.1	Mask Optimization	150
8.2	Correlated Gaussian functions	152
8.3	Variogram Optimization	153
8.4	Remarks	154
8.5	Future Work	154
	Bibliography	156
A	Appendix	168
A.1	Locally Varying Mask with Linear Thresholds	168
	A.1.1 Truncating Conditional Gaussian for Threshold Mask	170
A.2	Locally Varying Mask with MDS	173
	A.2.1 Truncating Conditional Gaussian for MDS Mask	176
A.3	Correlation Coefficient in Truncated Plurigaussian Simulation	178
A.4	Covariance Map Optimization	181

List of Tables

3.1	Summary of input iterations for perturbation.	44
3.2	Objective values for different masks.	44
3.3	Categories proportion of data, initial truncated realization and final truncated realization.	50
4.1	Mineral deposit declustered proportions in DH data.	63
4.2	Summary of the integrated proportions in truncated realization using TPG method.	66
6.1	Summary of results for created ANN for different activation functions. .	108
6.2	Summary of the percent error in each parameter for each activation function.	109
7.1	Red Dog model coordinate limits.	123
7.2	Red Dog model declustered proportions in DH data and BH data. . . .	127
7.3	Summary of optimized variogram parameters using proposed optimization for both Gaussian deviates and one nested structure.	130
7.4	Red Dog model reproduced proportions among 100 unconditional simulations.	130
7.5	Red Dog model reproduced the declusterd proportions among 100 simulations with two structures.	132
7.6	Summary of optimized variogram parameters for two Gaussian deviates and two nested structures.	132
7.7	Summary of performance in transition probabilities reproduction.	145
7.8	Summary of performance in reproduction of BH data using different methods.	146

List of Figures

1.1	The Pennsylvanian strata.	3
1.2	Simple demonstration of modeling deposits with TPG simulation with two underlying Gaussian deviates for three rock types.	6
2.1	A string of data showing transition between $K = 3$ categories and relative transition probability matrix.	16
2.2	Top: outcrop of a typical carbonate reservoir along the San Juan River in Utah. Bottom: a geological model of the Pennsylvanian algal mounds in outcrops (Galli, Le Loch, Geffroy, & Eschard, 2006).	24
2.3	Masks for Paradox basin (Armstrong et al., 2011). Right: mask for the upper part and left: mask for lower part.	25
2.4	Sketch of a synthetic 2D geological region with $K = 3$ categories.	26
2.5	Truncation of a Gaussian distribution with two thresholds (t_1 & t_2).	27
2.6	Complex deepwater geological features (Pyrzcz, McHargue, Clark, Sullivan, & Strebelle, 2012).	31
3.1	Sample of discretized mask by $2^3 \times 2^3 = 64$ blocks and optimized mask.	35
3.2	Discretization of mask based on different scales.	35
3.3	Lag orientations.	38
3.4	Illustration of how selected locations in the mask are changed	39
3.5	Required CPU time (seconds) for updating transition probabilities in the objective function.	40
3.6	Annealing schedule.	42
3.7	Top: two generated realizations of standard Gaussian RV. Bottom left: bivariate object based mask and bottom right: truncated realization.	43

3.8	Random masks with discretization of $8 \times 8 = 64$ blocks.	43
3.9	Final mask and final truncated realization for random mask number one.	45
3.10	Annealing temperatures procedure and objective function reduction related to mask number one.	45
3.11	Rotating and Shifting an ellipse.	47
3.12	Top: two generated realizations of standard Gaussian RV. Bottom left: bivariate object based mask and bottom right: truncated realization.	48
3.13	Top left: initial mask and top right: related initial truncated realization. Bottom left: final mask bottom right: final truncated realization.	50
4.1	Masks for $K = 4$ categories and $M = 2$ Gaussian functions (modified from Armstrong et al. (2011)).	56
4.2	Sample truncation rule for truncating bivariate Gaussian functions for 9 categories ($F_k, k = 1, 2, \dots, 9$) with eight thresholds (t_1, \dots, t_8).	57
4.3	Locally varying masks of threshold based mask for one cross section of a synthetic example.	58
4.4	Evolution of MDS method for four categories (J. L. Deutsch & Deutsch, 2014).	61
4.5	Locally varying masks in TPG simulation with a MDS mask for one cross section of a synthetic example.	62
4.6	Location map of available drill hole data and projection onto a North-East and East-Elevation plans.	63
4.7	Left: Global threshold based mask and right: MDS mask for a mineral deposit with four rock types.	64
4.8	Global VPC for the mineral deposit.	65
4.9	Plan view of generated trend model for rock types based on the data sets at elevation 600(m).	65
4.10	Top: plan view of optimized threshold mask and bottom: plan view of optimized MDS mask at elevation 900(m) for 140 locations in the simulated domain.	66
4.11	Plan view of generated trend model for rock types based on the data sets at elevation 900(m)	67

4.12	Left: plan view of trend model and right: plan view of up scaled trend model for rock types.	68
4.13	Plan view of optimized up scaled MDS mask for composited elevations 870-900(m) for 128 blocks in the simulated domain.	69
4.14	3D view of simulated realizations	70
4.15	Simulated realizations at elevation 700 (m) using TPG simulation and SIS simulation methods.	70
5.1	Gaussian realization Y_1 and Y_2 and corresponding variograms	76
5.2	Mask for $K = 4$ categories using two Gaussian deviates.	76
5.3	Evaluation of proportion of category one using four thresholds.	78
5.4	Truncated realization for different correlation between Gaussian deviates ($\rho \in (-0.98, 0.98)$) when consider global thresholds (mask).	79
5.5	Scatter plot of variation of correlation between Gaussian deviates $(-0.98, 0.98)$	80
5.6	Scatter plot of Gaussian deviates with $\rho = 0.98$ and global mask.	81
5.7	Categories proportions for each correlation coefficient with same mask.	81
5.8	Variogram map of Gaussian RFs	82
5.9	Truncated realization for different correlation between Gaussian deviates (from -0.98 to 0.98).	84
5.10	Variation of thresholds	85
5.11	Variogram map of category number one with different correlation coefficients.	86
5.12	Variogram map of category number two with different correlation coefficients.	87
5.13	Variogram map of category number three with different correlation coefficients.	88
5.14	Variogram map of category number four with different correlation coefficients.	89
6.1	Schematic of refinement of two parameters. Large Xs represent the value of parameters for coarse optimization and the highlighted X indicates the best pare of nugget effect and range parameters. The refinement around the highlighted X provides optimal values.	94

6.2	Location map of available data.	95
6.3	Experimental and fitted variograms in horizontal (red) and vertical (blue) directions for available rock types.	96
6.4	Global threshold based mask with four rock types.	97
6.5	Variogram reproductions of horizontal direction(gray lines). Red and black lines represent variogram model of rock types and and the average reproduction of 50 realizations.	99
6.6	Balanced reproduction of model variograms of all four rock types with TPG method (gray lines), and the average of 50 realizations (black line).	100
6.7	Input proportion reproduction for all four categories with TPG simulation for 50 realizations. The input proportions are shown with the black line.	101
6.8	Transition probability matrix of data and averaged transition probability matrix of rock types for 50 simulated realizations colored by transition probability values from zero to one.	101
6.9	Schematic representation of ANN	103
6.10	McCulloch-Pitts model of a neuron (McCulloch & Pitts, 1943).	104
6.11	Different types of activation functions. Top from left to right: Gaussian, Piecewise linear. Bottom from left to right: Sigmoid, Softplus and Rectified linear.	105
6.12	Underlying Gaussian realizations (500×500 cells).	106
6.13	MDS mask with 3 categories and a corresponding truncated bigaussian simulation.	106
6.14	Designed neural network with full connections and one hidden layer.	108
6.15	Polar plot of the lag vectors to calculate the objective function (C. V. Deutsch & Cockerham, 1994).	112
6.16	Work flow for covariance map optimization of categorical variable in TPG simulation method.	113
6.17	Underlying Gaussian realizations.	115
6.18	Left: truncation rule using MDS mask and right: categorical data.	115
6.19	Slice of representation of covariance of off sets for each available category colored by covariance values.	116

6.20	Experimental and fitted variograms model in major (red) and minor (blue) horizontal directions.	116
6.21	Input proportion reproduction for all three categories with TPG simulation for 100 realizations. The input proportions are showed with the black line.	117
6.22	Reproduction of model variograms with TPG in major (red) and minor (blue) directions using two Gaussian deviates and one nested structures (left) and two nested structures (right) for all three categories.	118
6.23	Underlying Gaussian realizations and categorical data.	119
6.24	Slice through the representation of covariance of off sets. Top: using the initial variogram parameters and bottom: using the optimum variogram parameters for three available categories.	120
7.1	Experimental indicator and fitted variograms in horizontal direction (red) and vertical direction (blue).	124
7.2	Top: location map of available DH data, middle: projected onto a North-East cross section, and bottom: North-Elevation cross sectional view. . .	125
7.3	Top: location map of available BH and DH data and bottom: DH data verses BH data an East-North cross sectional view.	126
7.4	Red Dog Global truncation rule	127
7.5	slices of 3D representation of covariance of off sets for data for four available rock types colored by covariance values.	129
7.6	Red Dog data variogram parameters for two Gaussian deviates and one nested structure	131
7.7	Slices of a 3D representation of covariance of off sets using optimized variogram parameters for four available rock types with two nested structures.133	
7.8	Reproduction of model variograms with TPG using two Gaussian deviates and two nested structures	134
7.9	Truncation rule based on the MDS with three Gaussian deviates.	135
7.10	Reproduction of model variograms with TPG using three Gaussian deviates	136

7.11 Slices of a 3D representation of covariance of off sets using optimized variogram parameters for four available rock types with three Gaussian deviates colored by covariance values.	137
7.12 Percent error in variogram reproduction of rock types	138
7.13 Reproduction of model variograms with MCS based method	139
7.14 3D view of generated trend model for each plate based on the data sets.	141
7.15 Global VPC for the Red Dog deposit.	142
7.16 Cross section through generated Gaussian realizations with the optimized variograms.	142
7.17 3D view of simulated realizations (Red Dog data)	143
7.18 Global proportion reproduction for all four rocks with TPG simulation with threshold based mask for 50 unconditional realizations. The declustered global proportions are indicated with the black solid line.	144
7.19 Global proportion reproduction for all four rocks with TPG simulation with MDS mask for 50 unconditional realizations. The declustered global proportions are indicated with the black solid line.	144
7.20 Error in transition probability reproduction using TPG methods and BSIS method colored by absolute error between transition probabilities.	145
7.21 The error in matching categorical observations from BH data in TPG methods and BSIS method	147

List of Symbols

Symbol	Definition	First Use
D	Domain of interest	10
R^n	N-dimensional space	10
Ω	Set of all possible outcomes	10
a	A set of outcomes	10
P	The assignment of probabilities to the outcomes	10
u	Location/Point in the N-dimensional space	10
$Z(\mathbf{u})$	Random variable(RV) at location u	10
$z(\mathbf{u})$	A realization/outcome of the RV $Z(\mathbf{u})$ at location u	10
$F_z(\mathbf{u}; \mathbf{z})$	CDF of the RV $Z(u)$	10
$E\{.\}$	Expected value of a RV	10
$Var\{.\}$	Variance of a RV	11
$Cov\{Z_1, Z_2\}$	Covariance function between RVs $Z(\mathbf{u}_1), Z(\mathbf{u}_2)$	11
K	Number of categories	12
$I_k(\mathbf{u})$	Indicator variable corresponding to category k	12
p_k	The probability of occurrence of an outcome/ category	12
$E\{I_k\}$	Expected value of an indicator I_k	12
$Var\{I_k\}$	Variance of an indicator I_k	13
H	Entropy	13
γ_k	Indicator variogram of $I_k(\mathbf{u})$	13
$\gamma_{kk'}$	Cross indicator variogram between $I_k(\mathbf{u})$ and $I_{k'}(\mathbf{u} + \mathbf{h})$	14
C_k	Indicator covariance of $I_k(\mathbf{u})$	14
$C_{kk'}$	Cross covariance between $I_k(\mathbf{u})$ and $I_{k'}(\mathbf{u} + \mathbf{h})$	14

$\mathbf{tp}_{kk'}$	Transition probability from category k to category k'	14
O	Optimization objective function	16
\mathbf{g}	Gradient of an objective function	16
α_i	Step size at the point \mathbf{x}_i	18
μ	Mean of the Gaussian distribution	25
σ^2	Variance of the Gaussian distribution	25
G	Standard Gaussian CDF	26
t_i	i^{th} threshold	27
cp_k	Cumulative proportion of category k	28
T	Annealing temperature parameter	36
pr	Probability of change	36
k_b	A natural constant which relates temperature to energy	36
O	Objective function	37
nD	Number of directions for scanning the domain	37
$\mathbf{tp}_{kk'}(\mathbf{h})^{data}$	Transition probability of categories in the data	37
$\mathbf{tp}_{kk'}(\mathbf{h})^{real}$	Transition probability of categories in the realization	37
δ	A constant scalar in the annealing schedule	41
M	Number of underlying Gaussian RFs	55
ρ	Correlation coefficient	73
$Y(\mathbf{u})$	Gaussian random function	74
f	Probability density function	77

List of Abbreviations

Abbrv.	Definition	First Use
TPG	Truncated plurigaussian	4
TGS	Truncated Gaussian simulation	4
LVP	Locally varying proportions	5
MDS	Multidimensional scaling	7
RF	Random function	9
RV	Random variable	10
CDF	Cumulative distribution function	10
PDF	Probability density function	10
SRF	Stationary random function	11
SIS	Sequential indicator simulation	19
MPS	Multiple point statistics	19
TPG	Truncated Gaussian simulation	19
SNESIM	Single normal equation simulation	21
SA	Simulated Annealing	34
MDS	Multidimensional Scaling	51
VPC	Vertical Proportion Curve	64
NN	Neural Network	91
ANN	Artificial Neural Network	102
LU	Lower Triangular Matrix - Upper Triangular Matrix	111
Zn	Zinc grade	122
DH	Drill hole data	123
BH	Blasthole data	123

BSIS	Block sequential indicator simulation	140
------	---	-----

Chapter 1

Introduction

There are limited natural resources in the world. Generally for the purpose of cost-efficiency in the petroleum or mining industries, properties of interest such as minerals and hydrocarbons are measured for a limited number of locations, and later, are estimated or predicted for the remaining larger areas of deposit or reservoir. Therefore, a good understanding of the behavior of these sources is essential to best predict the rock properties at unsampled locations. Geostatistics is a statistical methodology that has been applied to geological phenomena and quantitative numerical models for uses of planning ([A. Journel and Huijbregts \(1978\)](#); [Matheron \(1971\)](#)). Geostatistics considers all the available information to allow researchers to predict the properties of interest at unsampled locations for the whole area of interest and to assess the uncertainty in the predictions. Dealing with different types of data with complex variation is possible through geostatistics.

Simulation of categories is a common challenge in geostatistics. Defining the categorical variables that encode rock types, mineralization, facies, or vein occurrences is often the first step in any modeling in mining, petroleum engineering and environmental sciences studies. Categorical variables represent a specific environment or units, which are geologically homogeneous. In other words, categorical variables separate stationary domains. Categorical variables such as classes of grade or porosity (rich, medium and poor), or rock lithotype (silt, limestone, sandstone, shale) define the area in a deposit that can be separated into a stationary set of categories. The variability of contentious

properties, such as grade, is higher between the rock types than within a rock type. Therefore, attention should be paid to the categorical modeling first for accurate and effective models of the continuous variables.

1.1 Motivation and Problem Statement

Categorical variable modeling has a significant impact on resource estimation as the heterogeneity between categories is often significantly larger than the heterogeneity within a category; accurate categorical variable modeling is important. Characterization of complex geological features and patterns is challenging. This work focuses on three challenges related to categorical variable modeling. First, the categorical variable model should reproduce known geological features of a domain to obtain a realistic and reliable model. The development of geostatistical methods to simulate models that result in realistic geological distributions of heterogeneities which match the spatial continuity of available data is an important contribution.

Second, stationarity is a crucial assumption required by most geostatistical techniques. The wrong decision of stationarity can lead to unrealistic models when data belong to separate populations with different statistics. Due to different mineralization systems, the geological phenomena may alter changes through the areal extent. Also, it is possible to have multiple mineralization settings connected vertically in a deposit which result in various transitions between rock types. These changes have to be taken into account in modeling.

In categorical variable modeling, proportions of categories are essential input parameters and frequently follow a trend calculated from available data. One way to account for changes in the depositional setting is the use of non-stationarity statistics. Non-stationarity statistics allows for consistency with the conceptual model and variables. Proper modeling should be adapted to account for these transitions and impose trends in the simulation.

Lastly, capturing the correct ordering of categories that are genetically ordered because of the depositional process in the domains is another important key in categorical

variable modeling. When the ordering relationships or transition probabilities between rock types are known, for instance when sandstone is followed by shale and then volcanic rock, geostatistical techniques should honor and reproduce these transitions in the final geostatistical model; these types of ordering relationships are usually difficult to control.

To demonstrate the concept of the above issues, consider Figure 1.1 which displays the Pennsylvanian strata with very complex transitions between rock types. Due to diverse geological conditions, there are lateral and vertical variations in thickness and composition. The sandstones and shales frequently transition laterally into each other and the shales may connect laterally and vertically into limestones and coals. Reproduction of these complex ordering structures while accounting for the variation of proportion of rock types is essential when using any geostatistical techniques to generate reliable models.

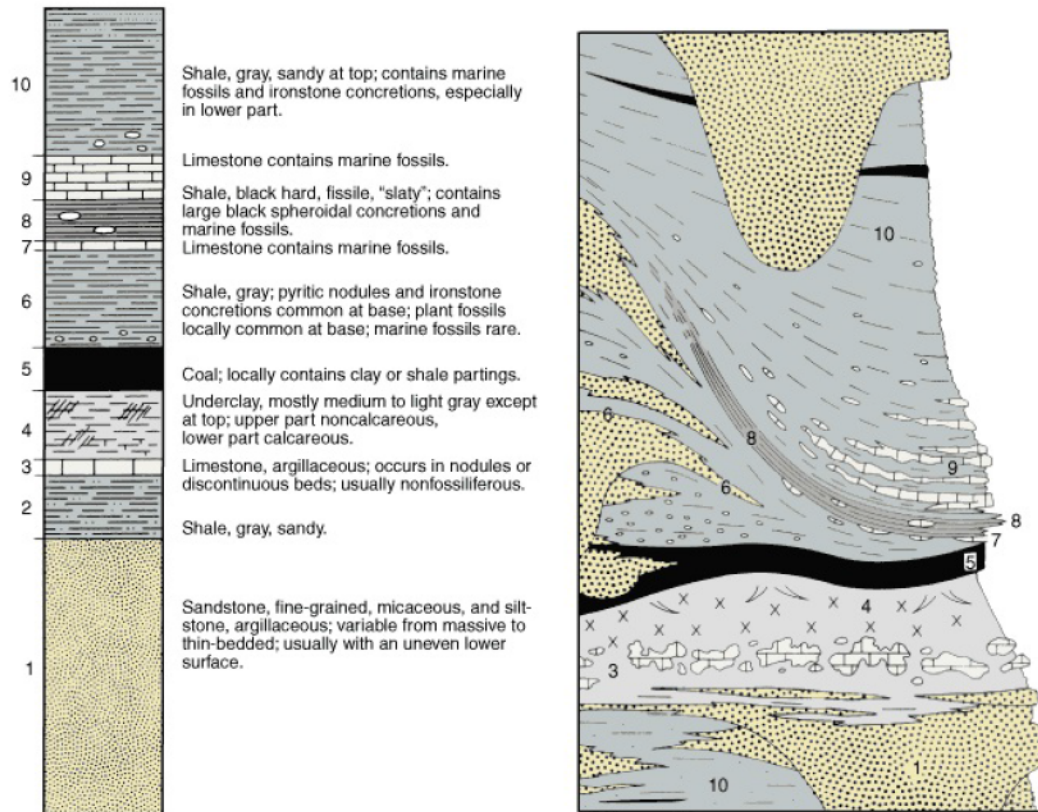


Figure 1.1: The Pennsylvanian strata. Left: the geological description. Right: typical layering with laterally discontinuous feature (Pennsylvanian, n.d.).

Truncated plurigaussian (TPG) simulation is one of the categorical variable modeling algorithms which is capable of addressing mentioned challenges in categorical variable modeling. Development of this technique is the fundamental objective of this thesis.

Truncated Plurigaussian Simulation

TPG simulation is a variogram based technique and is a powerful method for modeling geology with known ordering of categories. The main benefit is its flexibility in representing complex lateral and vertical categories transitions. TPG simulation simulates a number of continuous standard normal variables that are then discretized into categorical variables based on truncation rules or masks which define the geological relationship between categories. Truncated Gaussian simulation (TGS) was developed in the late 1980s for simulating lithotypes in oil reservoirs ([Matheron et al., 1987](#)) using only one Gaussian variable and then generalized to TPG simulation ([Galli, Beucher, Le Loch, Doligez, et al., 1994](#)) for more than one Gaussian variable.

1.2 Thesis Statement

The main goal of this thesis is to improve categorical variable modeling with TPG simulation through addressing the following major issues:

1. Honoring the correct ordering of categories with optimization of flexible truncation rules;
2. Honoring locally varying proportions with different truncation rules;
3. Capturing the spatial continuity of individual categories by variogram optimization of underlying Gaussian functions;

Addressing the above issues will allow for TPG simulation to construct more reliable categorical variable models. Improvement is measured by cross validation analyses as well as comparison of the model to the existing methodologies.

1.3 Approach

TPG simulation is capable of dealing with complexly ordered spatial structures by simulating a number of Gaussian realizations and then using the mask to convert the continuous values into categories. Honoring the correct ordering of categories in TPG simulation is achieved by optimization of these truncation rules. Geological interpretation can be transferred to modeling through the truncation mask. The masks also control categorical proportions; therefore having a methodology that is able to account for locally varying proportions (LVP) of categories in the domain is necessary.

TPG simulation requires the generation of a number of Gaussian realizations to be truncated to categorical models. To do so, the variogram model of the underlying variogram/covariance function for each of the underlying Gaussian functions is required. These variograms should be selected in such a way that the categorical variables in the simulated realizations have the correct spatial continuity after truncation. A novel optimization is proposed in this thesis that attempts to select the optimum input variograms to best reproduce the spatial structure of each categorical variable.

A TPG framework that automatically generates the required mask to reproduce known input statistics is developed. This mask matches the known relationships from existing data and also accounts for LVP of categories in the domain.

A simple demonstration of TPG simulation to simulate three rock types is provided in Figure 1.2. First indicator variograms of rock types are calculated from the available data set. In this example, two underlying Gaussian deviates are employed to define the contacts between rock types. The correct ordering of rock types is achieved by optimization of the truncation rules. The next step after defining a mask is to find the optimum variogram model to simulate two underlying Gaussian deviates. In the optimized mask, distribution of the rock type one versus the other two is controlled by Gaussian realization one (horizontal axis), and the distribution of rock type two and three are controlled by Gaussian realization two (vertical axis) of Figure 1.2(c).

Variogram optimization of the underlying Gaussian realization is necessary to find the optimum variogram models that best reproduce the spatial distribution of rock

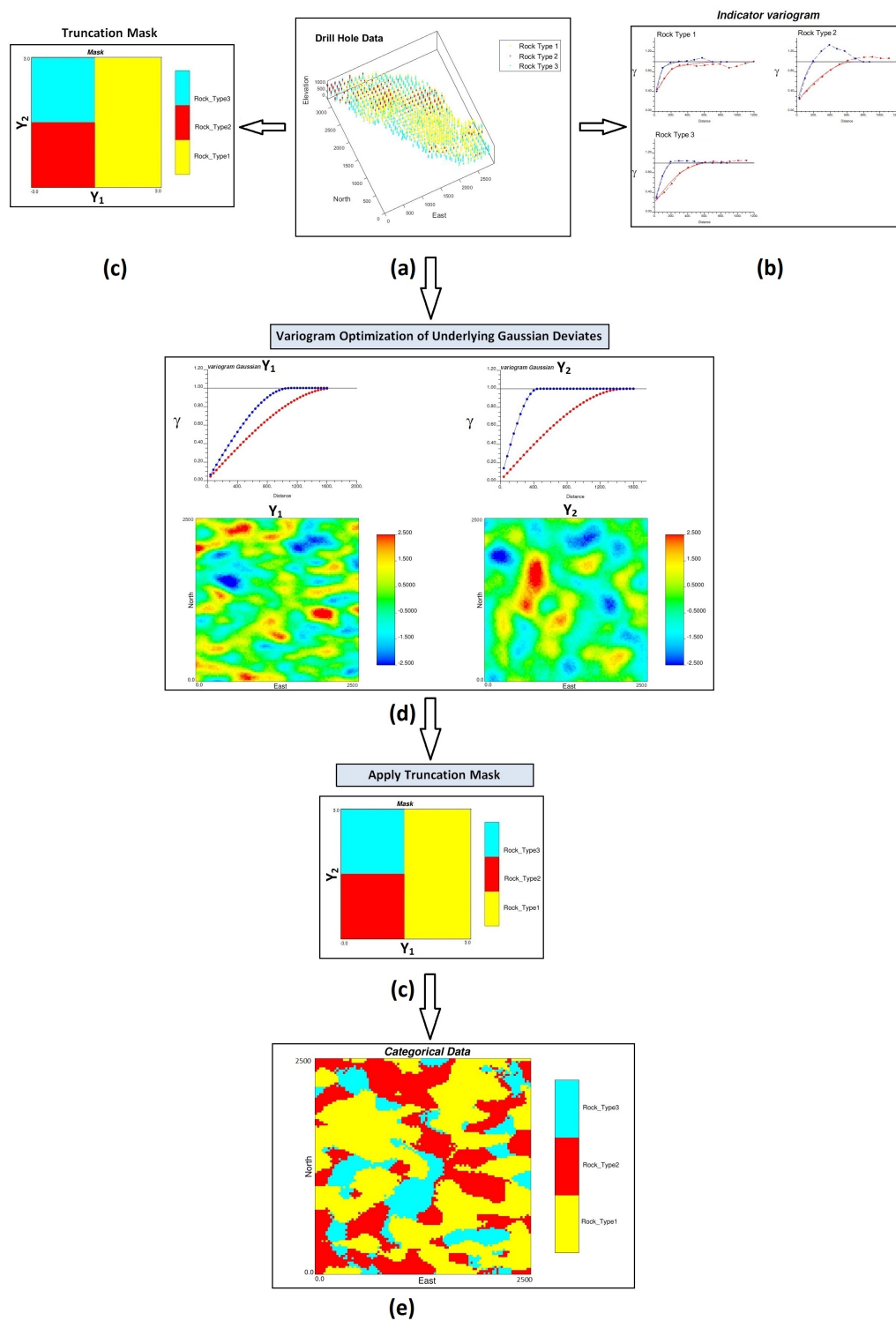


Figure 1.2: Simple demonstration of modeling deposits with TPG simulation with two underlying Gaussian deviates for three rock types.

types after truncation. In the final step, simulated Gaussian realizations are truncated to categorical variables using the optimized mask.

TPG simulation is performed in Gaussian units. The truncation mask can be established based on the global proportion or LVP of categories. In TPG simulation process, several conditions and statistics have to be satisfied. The final truncated realization should reproduce the transition probability between categories, global/ local proportions as well as indicator variogram of categories. In Chapter 2, TPG simulation is explained in detail.

1.4 Outline

Chapter 2 presents the necessary background on geostatistical categorical variable modeling and describes TPG simulation framework. This chapter presents reviews of different methodologies for categorical variable modeling.

Chapter 3 demonstrates the generation and optimization of two different flexible types of truncation rules: a discretized mask and an object based mask in the content of TPG simulation. The implementations of the proposed masks are tested using a synthetic 2D example.

Chapter 4 introduces two additional masks: a threshold mask and multidimensional scaling (MDS) mask. A methodology to handle spatial changes in the categories' proportions is proposed. LVP of categories in the domain is considered for both masks and is demonstrated on a porphyry deposit.

Chapter 5 describes the effect of the correlation between underlying Gaussian functions in TPG simulation. The impacts on simulation, the mask, as well as the variograms are demonstrated.

Chapter 6 presents three methodologies for variogram optimization. A novel optimization method is developed to find the optimum variogram parameters in TPG simulation that results in models that match the spatial continuity of categories.

Chapter 7 demonstrates the developed methodologies on an illustrative case study based on a porphyry deposit. Production data in the form of blast holes are used

to verify and confirm TPG models generated. Comparison to traditional work flow demonstrates the improvement obtained using the proposed TPG implementation.

Finally, **Chapter 8** summarizes the main contributions of this dissertation. Future work is also discussed. The description of developed software is provided in **Appendix A**.

Chapter 2

Background and Literature Review

The following chapter explains the backgrounds for TPG simulation and presents common geostatistical techniques for categorical variable modeling.

Geostatistical techniques model the uncertainty at unsampled locations and simulate realizations of the joint uncertainty at many unsampled locations using statistical models that are based on the random function (RF) theory.

Geostatistics is a set of the theoretical concepts of spatial RF modeling that [Matheron \(1962\)](#) established and first applied to mineral deposits. The origins of geostatistics are also due to the pioneering work of D. G. Krige in the Witwatersrand gold fields in South Africa in the late 1950s when he was challenged with the problem of estimating grades ([Sichel \(1952\)](#); [Krige \(1951\)](#)). [Matheron \(1962, 1965\)](#) provided theoretical support for the estimation of unbiased mineral resources.

Kriging is a best linear unbiased prediction (BLUP) in spatial statistics that leads to proper predictions from observed data. The word kriging in spatial statistics is synonymous with optimally predicting or optimal prediction at unsampled locations using nearby correlated data. [Matheron \(1963\)](#) and [Gandin and Hardin \(1965\)](#) were the first to publish a definitive development of spatial kriging. Also, the concept of a *regionalized variable* was developed by [Matheron \(1965\)](#) and constitutes the foundational elements of geostatistics.

An important development in geostatistics is the use of simulation methods ([Math-](#)

eron (1973); A. G. Journel (1974); David (1977)). Simulation provides equally probable realizations of the distributions of regionalized variable and creates a group of stochastic models or realizations which describe the natural phenomena with a practical fluctuations and variability. Simulations are utilized as a measure of uncertainty that comes from a limited amount of data and demonstrate higher local variability.

2.1 Random Function

The theoretical formalism of geostatistics was established by Matheron (1962). Often, a random variable (RV) refers to one variable. Basically, characterization of any unsampled value z is introduced as a RV of Z . The uncertainty of an unknown value is defined by the probability distribution of Z models (Pyrcz & Deutsch, 2014). When RV is location dependent, then the result is often called an RF. The spatially distributed variable is called a regionalized variable.

For a certain domain $D \subset R^n$ and a probability space (Ω, a, P) , an RF is a function of two variables $Z(\mathbf{u}, \omega)$ so that for each $u \in D$ the variable $Z(\mathbf{u}, \cdot)$ is a RV on (Ω, a, P) . Each of the functions $Z(\cdot, \omega)$ specified on D as the variable of the RF at $\omega \in \Omega$ is a realization of the RF($z(u)$).

The probability that the value of an RV is less than a specified threshold is a cumulative distribution function (CDF) (Eq. 2.1).

$$F_z(\mathbf{u}; \mathbf{z}) = Prob\{Z(\mathbf{u}) \leq \mathbf{z}\} \quad (2.1)$$

The CDF could be summarized by parameters such as the expected value. The weighted average of an RV which can be thought of as the center of mass in a probability density function (PDF) is called the expected value. The expected value is also named as the first moment (Eq. 2.2).

$$E\{Z(\mathbf{u})\} = m(\mathbf{u}), \mathbf{u} \in D \quad (2.2)$$

The second moment or variance is the other key parameters in probability theory which measures how far a set of numbers are spread in Eq. 2.3.

$$Var\{Z(\mathbf{u})\} = \sigma^2(\mathbf{u}) = E\{(Z(\mathbf{u}) - m(\mathbf{u}))^2\}, \mathbf{u} \in D \quad (2.3)$$

Covariance also shows how much two RVs or two locations (\mathbf{u}_1 & \mathbf{u}_2) change together and measures the relation between them. In other words, the expected value of the difference in one RV from its mean multiplied by the difference in the other RV from its mean is defined as the covariance between two RVs (Eq. 2.4).

$$Cov\{Z(\mathbf{u}_1), Z(\mathbf{u}_2)\} = E\{(Z(\mathbf{u}_1) - m(\mathbf{u}_1))(Z(\mathbf{u}_2) - m(\mathbf{u}_2))\}, \mathbf{u}_1, \mathbf{u}_2 \in D \quad (2.4)$$

Usually, probability distribution is summarized with the mean, variance and covariance functions.

2.2 Stationarity

When multiple categories are involved in modeling, it is important to be able to show whether or not the statistical properties, such as the mean, histogram, correlation, and variogram, are constant within a given category. All statistical analysis requires a decision of how to pool data. Pooling data in a histogram assumes they come from the same population and the global histogram is the same for all locations in modeling domain (first order stationarity). The decision of stationarity gives significance to the CDF of the variable ($F_z(\mathbf{u}; \mathbf{z})$) which shows that at any certain location, there can be only one realization. There is a need to identify separate domains with separate stationary random function (SRF) models that are deemed more consistent with the mathematical assumptions of a SRF (i.e. stationarity). When a RF is stationary, its moments are invariant under translation and the phenomenon is homogeneous in space. Therefore, stationarity entails that the statistical properties of a variable of interest is

constant within the domain.

Usually there is non-stationarity in proportions of categories due to geological trends and changes in depositional setting. This non-stationarity is considered in the simulation by adopting locally varying statistics in this work.

2.3 Indicator Variables

Different geological classifications such as structure, mineralogy, alteration and lithology are considered in different geological domains, and the data are subset within them. Categorical variable models are created to separate stationary domains of the subsurface and encode rock types, mineralization, or facies.

Consider having K mutually exclusive and exhaustive categories, $k = 1, 2, \dots, K$. The list of categories is exhaustive which means location \mathbf{u} belongs to one and only one of these K categories. $I_k(\mathbf{u})$ is the indicator variable related to category k . The indicator is set to 1 if \mathbf{u} in k and zero otherwise (Eq. 2.5):

$$I_k(\mathbf{u}) = \begin{cases} 1 & \text{if category } k \text{ is present at location } \mathbf{u} \\ 0 & \text{otherwise} \end{cases} \quad (2.5)$$

Generating the spatial models for discrete classes is the main purpose of simulating categorical variables.

Indicator Statistics

The expected value of an indicator variable is equal to the proportion of that variable ($E\{I_k\} = p_k$). The second moment or variance of an indicator is another important parameter which shows the variability of the variable and is also a function of the proportion (Eq. 2.6).

$$\begin{aligned}
Var\{I_k(\mathbf{u})\} &= E\{(I_k(\mathbf{u}) - p_k)^2\} \\
&= E\{I_k(\mathbf{u})^2\} - (p_k)^2 = p_k(1 - p_k), \quad \mathbf{u} \in D
\end{aligned}
\tag{2.6}$$

Entropy is another measurement which is useful to compute the variability of all values together.

Entropy

The idea of entropy is introduced in geology to quantify the uncertainty of probability density functions (Christakos, 1990). For a categorical variable with K probable events or outcomes, entropy (H) is calculated by Eq. 2.7:

$$H = - \sum_{k=1}^K p_k \ln(p_k)
\tag{2.7}$$

The probability of occurrence of each possible events is defined as p_k here and the sum of all the probabilities should be equal to one ($\sum_{k=1}^K p_k = 1$). When there is enough knowledge to determine which outcome (categorical variables) exactly will be at a certain location, the entropy is minimum (zero) for this instance ($p_k = 1$ for $I_k = 1$ and $p_k = 0$ for $I_k = 0$). When there is no information regarding what the true outcome could be, then $p_k = \frac{1}{K}$ for all $k = 1, 2, \dots, K$ result in the maximum possible entropy.

Indicator Variograms and Covariances

An indicator variogram (Eq. 2.8) is used to characterize the spatial relationships between the binary variables through indicator kriging, which predicts the probability of occurrence of a categorical variable at an unsampled location (Chiles and Delfiner (2009); Goovaerts (1997)).

$$2\gamma_k(\mathbf{h}) = E \{ [I_k(\mathbf{u}) - I_k(\mathbf{u} + \mathbf{h})]^2 \} \quad k = 1, 2, \dots, K
\tag{2.8}$$

Only the average transition from category k to any other category such as k' and from any other category (k') to category k from one location to another location is considered in the direct indicator variogram of category k . The cross indicator variogram between two categories (k and k') is defined as Eq. 2.9:

$$2\gamma_{kk'}(\mathbf{h}) = E \{ [I_k(\mathbf{u}) - I_k(\mathbf{u} + \mathbf{h})][I_{k'}(\mathbf{u}) - I_{k'}(\mathbf{u} + \mathbf{h})] \} \quad k' \neq k \quad (2.9)$$

The indicator covariance model is usually given by indicator variogram model. An indicator covariance and an indicator cross covariance between two categories (k and k') are defined as Eq. 2.10- 2.11, respectively.

$$C_k(\mathbf{h}) = C(0) - \gamma_k(\mathbf{h}) \quad k = 1, 2, \dots, K \quad (2.10)$$

where:

$C(0)$ - the covariance at lag zero or variance;

$$C_{kk'}(\mathbf{h}) = E \{ [I_k(\mathbf{u}) - I_k(\mathbf{u} + \mathbf{h})][I_{k'}(\mathbf{u}) - I_{k'}(\mathbf{u} + \mathbf{h})] \} \quad k' \neq k \quad (2.11)$$

2.4 Transition Probabilities

The global proportion of each category can be calculated from experimental data. The transition probability is a subset of the multiple point histogram for the specific case of two points, where the two points are normally adjacent. The transition probability matrix can be defined as a bivariate probability and is the probability of being category k' at location $\mathbf{u} + \mathbf{h}$ and location \mathbf{u} belongs to category k . The transition probability can be a measure of spatial variability (Carle & Fogg, 1996). Transition probability $\mathbf{tp}_{kk'}(\mathbf{h})$ is defined by a conditional probability Eq. 2.12 or Eq. 2.13:

$$\mathbf{tp}_{kk'} = Prob\{k' \text{ occurs at } \mathbf{u} + \mathbf{h} | k \text{ occurs at } \mathbf{u}\} \quad (2.12)$$

$$\begin{aligned} Prob(\mathbf{u} + \mathbf{h} \in I_{k'} | \mathbf{u} \in I_k) &= Prob(I_{k'}(\mathbf{u} + \mathbf{h}) = 1 | I_k(\mathbf{u}) = 1) \quad (2.13) \\ &= \frac{Prob(I_{k'}(\mathbf{u} + \mathbf{h}) = 1 \ \& \ I_k(\mathbf{u}) = 1)}{Prob(I_k(\mathbf{u}) = 1)} \\ &= \frac{E(I_{k'}(\mathbf{u} + \mathbf{h}) \cdot I_k(\mathbf{u}))}{E(I_k(\mathbf{u}))} \\ &= \frac{C_{kk'}(\mathbf{u}, \mathbf{u} + \mathbf{h})}{p_k(\mathbf{u})} \end{aligned}$$

where:

- $\mathbf{tp}_{kk'}$ - transition probability between location k and k' ;
- \mathbf{u} - a spatial location;
- \mathbf{h} - the lag (separation vector);
- k, k' - mutually exclusive categories such as geologic units or categories;

The transition probability matrix with K categories is defined as Eq.2.14. Simplified notation of \mathbf{tp} is used in the rest of thesis to represent transition probability matrix.

$$\mathbf{tp}(\mathbf{h}) = \begin{bmatrix} tp_{11} & tp_{12} & tp_{13} & \cdot & \cdot & \cdot & tp_{1K} \\ tp_{21} & tp_{22} & tp_{23} & \cdot & \cdot & \cdot & tp_{2K} \\ tp_{31} & tp_{32} & tp_{33} & \cdot & \cdot & \cdot & tp_{3K} \\ \cdot & & & \cdot & & & \cdot \\ \cdot & & & & \cdot & & \cdot \\ \cdot & & & & & \cdot & \cdot \\ tp_{K1} & tp_{K2} & tp_{K3} & \cdot & \cdot & \cdot & tp_{KK} \end{bmatrix} \quad (2.14)$$

Figure 2.1 displays a synthetic example of a string of data by downward transi-

tions for $K = 3$ categories and the transition probability matrix relative to one lag distance. The diagonal terms are the auto transition probabilities, or probability that the category does not transition. Cross terms are the probabilities of transitioning from category k to k' . These matrices are commonly collected both up and down a drill hole.

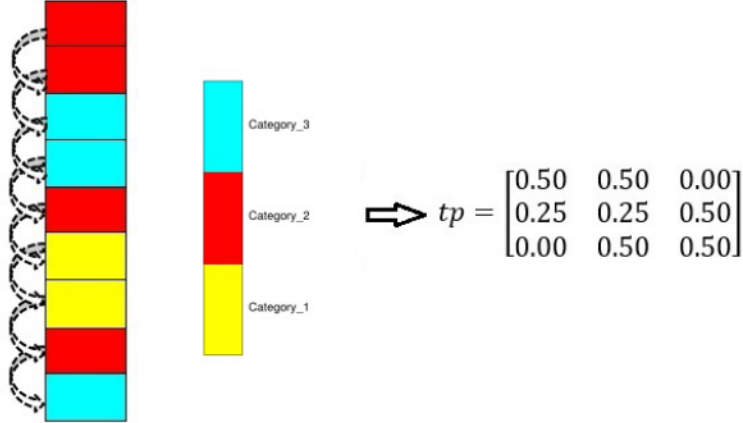


Figure 2.1: A string of data showing transition between $K = 3$ categories and relative transition probability matrix.

2.5 Gradient Optimization Technique

Different optimization techniques are used in this thesis. In this section, gradient optimization is introduced. In any optimization method, a set of n variables $X = \{x_1, \dots, x_n\}$ that influence the objective function (O) are adjusted in such a way to minimize $O(X)$. The gradient optimization uses gradient information related to the objective function, such as first and second derivatives of $O(X)$ with respect to the n variables (Eq. 2.15).

$$\mathbf{g}(X) = \left[\frac{\partial O}{\partial x_1} \quad \frac{\partial O}{\partial x_2} \quad \dots \quad \frac{\partial O}{\partial x_n} \right]^T \quad (2.15)$$

The gradient method is a class of optimization methods which depends on the function and gradient values at each iteration (Chong & Zak, 2013). Conjugate gradient is an iterative method which can be applied to sparse systems that are too large to be

handled by direct methods. The direction of search in each iteration depends on the local properties of the objective function. An effective method for the generation of conjugate directions is proposed by [Hestenes and Stiefel \(1952\)](#).

The Fletcher-Reeves method is a conjugate direction method. In this method, directions are generated sequentially in each iteration. Parameter α , which is an independent search parameter, is the key parameter in this method. A unique minimum for function $O(\mathbf{x})$ is obtained for some positive value of α . The parameters of α are determined by minimizing $O(\mathbf{x} + \alpha_i \mathbf{d}_i)$ with respect to α_i . Generally, a line search method is adopted to find these parameters. Here, \mathbf{d}_i is a conjugate direction with respect to $\mathbf{d}_{i-1}, \mathbf{d}_{i-2}, \dots, \mathbf{d}_0$ and can be found for convex and quadratic problems using Eq. 2.16:

$$\begin{aligned} \mathbf{d}_{i+1} &= -\mathbf{g}_{i+1} + \beta_i \mathbf{d}_i \\ \beta_i &= \frac{\mathbf{g}_{i+1}^T \mathbf{g}_{i+1}}{\mathbf{g}_i^T \mathbf{g}_i} \end{aligned} \tag{2.16}$$

where:

- \mathbf{d}_i - conjugate direction at the point \mathbf{x}_i ;
- \mathbf{g}_i - gradient at the point \mathbf{x}_i ;
- \mathbf{g}_i^T - transpose gradient at the point \mathbf{x}_i ;
- β_i - parameter to be added to the negative of the gradient at the new point to generate new direction;

So, for $i = 1, 2, \dots$ the conjugacy of the set of directions guarantees that (Eq. 2.17):

$$\begin{aligned} \frac{df(\mathbf{x}_i + \alpha_i \mathbf{d}_j)}{\mathbf{d}_j \alpha_i} &= \mathbf{g}_{i+1}^T \mathbf{d}_i = 0, \quad \text{for } 0 \leq j \leq i \\ \mathbf{g}_{i+1}^T \mathbf{d}_j &= 0, \quad \text{for } 0 \leq j \leq i \end{aligned} \tag{2.17}$$

where:

α_i - step size at the point \mathbf{x}_i ;

The Golden-section search method is a line search method that is used to determine α . This search method can be performed in each iteration until the desired accuracy in the minimum value of the objective function is achieved.

An implementation of the gradient algorithm is as follows:

1. Input \mathbf{x}_0 variables should be defined and the tolerance ε be initialized to stop the algorithm when the changes are not significant for all the variables.
2. Set $i = 0$ and compute gradient in the initial points \mathbf{g}_0 and set direction as $\mathbf{d}_0 = \mathbf{g}_0$. Here if $\frac{\partial O(\mathbf{a})}{\partial \mathbf{x}_j} = \frac{O(\mathbf{a} + \Delta \mathbf{x}_j) - O(\mathbf{a})}{\Delta \mathbf{x}_j}$ exist, then O has partial derivative with respect to \mathbf{x}_j at \mathbf{a} . A row vector whose elements are partial derivatives for \mathbf{x}_j is the gradient (Eq. 2.15).
3. Find α_i using golden-section search. The value of α minimizes $O(\mathbf{x} + \alpha_i \mathbf{d}_i)$. In this search, successive intervals are independent of n and iteration can be performed until the range of uncertainty or change in the value of the objective function is reduced below some tolerance ε . Then set $\mathbf{x}_{i+1} = \mathbf{x} + \alpha_i \mathbf{d}_i$ for the next iteration which defines the new points that satisfy the conditions.
4. This step is about stop criteria. The above process is continued, until there is not any significant improvement or the objective function has become lower than tolerance ε . If $\|\alpha_i \mathbf{d}_i\| < \varepsilon$, then output $\mathbf{x}^* = \mathbf{x}_{i+1}$ and $O(\mathbf{x}^*) = O(\mathbf{x}_{i+1})$, and stop.
5. If $i = n - 1$, set $\mathbf{x}_0 = \mathbf{x}_{i+1}$ and go to step 2.
6. Now the gradient of new points \mathbf{g}_{i+1} and β_i has to be calculated (Eq. 2.18):

$$\beta_i = \frac{\mathbf{g}_{i+1}^T \mathbf{g}_{i+1}}{\mathbf{g}_i^T \mathbf{g}_i} \quad (2.18)$$

The new direction is $\mathbf{d}_{i+1} = -\mathbf{g}_{i+1} + \beta_i \mathbf{d}_i$. Finally, Set $i = i + 1$ and repeat from step 3.

2.6 Categorical Variable Modeling

There are a number of techniques for the stochastic simulation of a categorical variable. The two main families methods are the cell based and object based methods ([Lantuéjoul \(2013\)](#); [Mattfeldt \(1996\)](#)). When the categorical variable can be identified from field observations, there are a large number of methods that can be used to generate a model (see review in [Koltermann and Gorelick \(1996\)](#); [De Marsily et al. \(2005\)](#)). In a cell based model, the categorical values are directly simulated cell-by-cell. The model is defined by a group of cells in two or three dimensions. Simulating cell-by-cell using a variogram/spatial covariance model supplied by the user is common ([Pyrzcz & Deutsch, 2014](#)). Sequential indicator simulation (SIS) ([A. G. Journel, 1983](#)), multiple point statistics (MPS) ([Alabert et al., 1989](#)), and truncated Gaussian simulation (TGS) or TPG simulation ([Galli et al., 1994](#)) are the three main cell based methods. Object based modeling and event based modeling are the two common techniques of object based methods for simulating categorical variables. Choosing the best approach for categorical variable modeling is highly dependent on the application ([C. V. Deutsch, 2002](#)).

2.7 Sequential Indicator Simulation

SIS was proposed by [Alabert \(1987\)](#) and [A. G. Journel \(1983\)](#) in the early 1980s. In SIS, simulated values are in the original space and inferred from the local indicator kriging-derived conditional distributions. Conventional categorical variable modeling approaches, such as SIS, are widely used and applied before grades, porosity, and permeability modelling to reproduce the spatial and geometric configuration of rock types ([A. Journel and Isaaks \(1984\)](#); [Dubrule \(1989\)](#); [Dubrule \(1993\)](#); [Langlais and Doyle \(1993\)](#); [Murray \(1994\)](#); [W. Xu \(1995\)](#)). SIS does not consider Gaussian assumptions and the conditional probability functions are inferred directly from the data. This non-parametric algorithm requires the binary transformation of continuous (eg. porosity or permeability) or categorical (eg. rock type) data into a series of indicator variables ([Goovaerts \(1997\)](#); [C. V. Deutsch, Journel, et al. \(1992\)](#)). To express the categorical

variable, SIS uses the indicator transform, and kriging is applied to the binary indicator transforms of the data to directly estimate conditional probabilities. SIS method has been used in many different studies as categorical soil variable simulation (C. Zhang & Li, 2007), simulation of categories for groundwater flow (Moysey & Knight, 2003), reservoir fluid flows (Seifert & Jensen, 1999) and uncertainty assessment of the spatial distribution of soil organic carbon (Delbari, Loiskandl, & Afrasiab, 2010), to name a few. The workflow is as follows:

1. Create a random path over the grid and for each cell:
2. Look for previously simulated values and nearby conditioning data
3. Use simple kriging or ordinary kriging to estimate the conditional probability for each category $k = 1, \dots, K$
4. Simulate a categorical value from the set of probabilities
5. Return to step 2 until simulating all nodes of the grid

Indicator based kriging and simulation methods have several weaknesses and limitations, as documented by several authors (Chiles and Delfiner (2009); Christakos (2012) Emery (2004)). This method generally is unable to capture the geometry of complex geological features (e.g. successive deposition and erosion). When the categorical variables follow obvious geometric forms, SIS is not recommended.

2.8 Multiple Point Statistics (MPS)

MPS is one approach for categorical variable modeling and does not rely on variogram models. This technique was first proposed by A. G. Journel and Alabert (1989) and then used in simulation by C. V. Deutsch (1992); Guardiano and Srivastava (1993); Strebelle and Journel (2000); Lyster (2009), to name a few. MPS accounts for the relations between more than two points at a time and is an alternative to the traditional kriging based methods. Unlike traditional geostatistics, MPS avoids the explicit definition of an RF. Categorical models that contain the complex nonlinear features in mineral deposits are generated by these techniques (Guardiano and Srivastava (1993);

A. G. Journel (2004)). The technique is based on the concept of single normal equations (SNE). Single normal equation simulation (SNESIM) is an efficient MPS algorithm that was first proposed by Guardiano and Srivastava (1993). Strebelle (2002) provides a review of the evolution of these MPS algorithms and a proposed efficient non-iterative algorithm (SNESIM).

In MPS, information regarding spatial heterogeneity of the reservoir is inferred from a training image that is a rasterized illustration of the categorical variables under study (Boucher, 2009) and can be viewed as the prior model of spatial structure (A. G. Journel & Zhang, 2006). A training image represents the geological heterogeneity and is a rock type model that is exhaustively populated by the rock types of interest (Boisvert, Pyrcz, and Deutsch (2007); C. V. Deutsch (1992)). The use of a data set as a training image guarantees that MPS is geologically realistic. However, an exhaustive data set that is representative of the deposit of interest is not often available.

Dimitrakopoulos, Mustapha, and Gloaguen (2010) introduced data-driven algorithms based on higher order moments known as cumulants for reproducing complex geologic patterns without appealing to training images. Other approaches implement secondary information for handling the reproduction of trends in simulations (Chugunova and Hu (2008); Straubhaar, Renard, Mariethoz, Froidevaux, and Besson (2011)). D. A. Silva and Deutsch (2014) used multiple training images simultaneously to reproduce geologic features from training images with the precise continuity and variability.

MPS facilitates conditioning. However, it is still computationally demanding (especially in terms of memory requirements). Moreover, a significant drawback of implementing MPS is the inference of a training image that accurately represents the characteristics and statistics of the domain of interest. To generate realistic realizations that accurately represent the phenomena under study, adopting a representative training image is important (Boisvert et al. (2007); A. G. Journel and Zhang (2006)). Also, the selection of template configurations and the availability of patterns in the training image are other complications of MPS (Arpat (2003); Lyster (2009)).

2.9 Truncated Gaussian/Plurigaussian Simulation

The TGS method simulates a continuous standard normal variable that is then discretized into categorical variables based on thresholds. This method is capable of dealing with ordered spatial structures. In the late 1980s, TGS was developed with the application in oil reservoirs (Matheron et al., 1987). TGS simulation models provide more straightforward and realistic transitions between categories than SIS (Galli et al., 1994). To simulate the geometry and internal architecture of a stratigraphic reservoir, TGS is an option. After truncation, appropriate values of porosity and permeability can be assigned to the known lithotype. When the categories appear in a sequential order in reservoirs, for instance, when sandstone is followed by shaly sandstone then shale, TGS is useful.

TPG simulation is an extension of TGS and is a powerful method for modeling geology and flexible in representing complex lateral and vertical categories transitions. The principle of this method was established by Galli et al. (1994). Normally, a maximum of two Gaussian functions are considered to represent relevant geological features in the models (Rondon (2009); Carrasco, Ibarra, Rojas, Le Loch, and Séguret (2007); Fontaine and Beucher (2006)). In the bigaussian method, truncation is characterized by the partition of a rectangle defined by the Gaussian realization, often referred to as the mask. Any number of combinations of categories can be considered in the model. As the relationships between categories become increasingly more complex, the truncation technique has to be flexible to account for these relationships. The main idea of the truncation is based mostly on permitting or not permitting some category contacts with either vertical or horizontal thresholds.

Some complex reservoir examples of primary diagenesis effects characteristic of carbonate sedimentary systems are explained by (Armstrong et al., 2011). TPG model is used for simulating geological domains in petroleum reservoirs and mineral deposits with the aim of assessing the uncertainty in the domain boundaries and improving the geological controls in the characterization of quantitative attributes (Remacre and Zapparoli (2003); Fontaine and Beucher (2006)).

The improvement of aquifer flow simulation responses using TPG model is shown by [Serrano, Guadagnini, Giudici, Guadagnini, and Riva \(2012\)](#); [Serrano, Guadagnini, Riva, Giudici, and Guadagnini \(2014\)](#). Also, a model for mineral proportion evaluation in an ore deposit is considered by [Emery \(2010\)](#). TPG simulation also has been used for fault facies modeling by [Fachri, Tveranger, Braathen, and Schueller \(2013\)](#). [Carrillat et al. \(2010\)](#) compared the application of different categorical variable modeling and TPG on a massive carbonate oil field. Distribution of facies for complicated reservoir models has been described by TPG simulation.

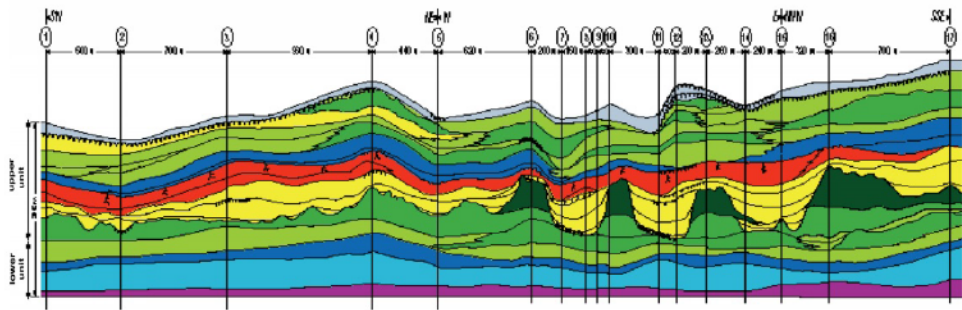
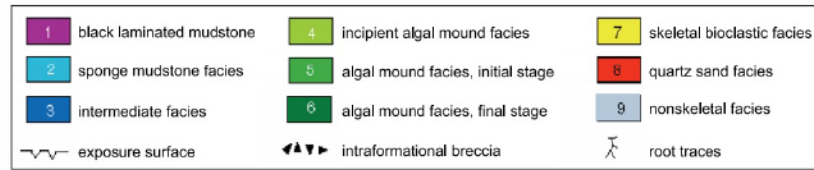
Figure 2.2 displays the sedimentary oil bearing formations in canyons along the San Juan River in Utah where phylloidal algal mounds of the Pennsylvanian age are exposed and can be modeled using TPG method ([Grammer, Eberli, Van Buchem, Stevenson, and Homewood \(1996\)](#); [Van Buchem et al. \(1998\)](#)). The threshold masks corresponding to this complex geological setting are illustrated in Figure 2.3. Two different masks are considered. The lower part is related to the platform progradation, and in the upper zone, algal mounds can be found. One Gaussian function is used for the simulation of the lower part, while in the upper part, because of the spatial organization of the mounds and intermound, categories have a more complex truncation rule.

Handling the locally varying proportions of categories in the threshold mask is straightforward. [C. Xu, Dowd, Mardia, and Fowell \(2006\)](#) increased the number of underlying Gaussian realizations of the threshold based mask to handle more complicated relationships between categorical variables. A general methodology using kernel regression is developed by [Allard, Dor, Biver, and Froidevaux \(2012\)](#) for the truncation mask to consider categorical variables and auxiliary latent variables. This method involves joint observation of the categorical and the Gaussian variables at the well locations and truncation is non-parametric to simultaneously consider more complex relations between categorical variables. Also, [J. L. Deutsch and Deutsch \(2014\)](#) considered a parametrized truncation mask with Voronoi tessellation.

The next sections explain the TGS and TPG methodology from a mathematical point of view.



(a) Carbonate reservoir



(b) Geological model

Figure 2.2: Top: outcrop of a typical carbonate reservoir along the San Juan River in Utah. Bottom: a geological model of the Pennsylvanian algal mounds in outcrops (Galli et al., 2006).

2.9.1 One-Gaussian Function

In TGS, the categorical assignment comes from one underlying continuous variable. A standard Gaussian RF ($N(0, 1)$ distribution) and then the classification of categorical domains are based on truncating the function according to a specified mask (thresholds) for representing different geometric patterns and contacts between geologic domains. An RV (Z) has a Gaussian distribution if it has PDF as Eq. 2.19:

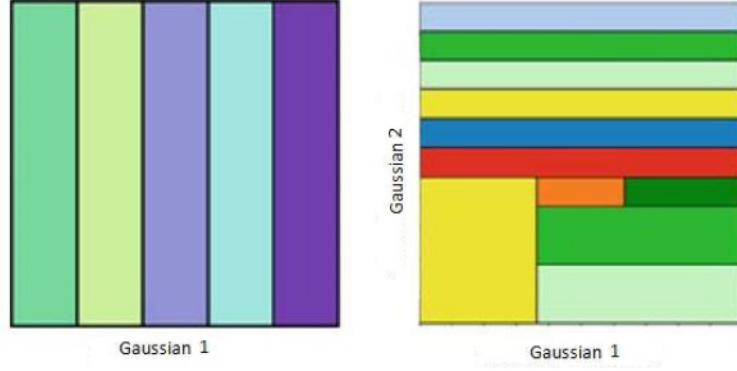


Figure 2.3: Masks for Paradox basin (Armstrong et al., 2011). Right: mask for the upper part and left: mask for lower part.

$$f(\mathbf{z}) = \frac{1}{\sigma\sqrt{2\pi}} e^{-\frac{1}{2}\left(\frac{\mathbf{z}-\mu}{\sigma}\right)^2} \quad (2.19)$$

where:

- μ - mean of the distribution;
- σ^2 - variance of the distribution;

μ and σ^2 can fully characterize the Gaussian distribution and therefore, by estimation of these two parameters, characterizing the conditional CDF at any point in D is simple. If $\{Z(\mathbf{u}), \mathbf{u} \in D\}$ is a Gaussian RF with covariance $C_Z(\mathbf{h})$, the multivariate Gaussian RF has following properties:

1. Any subset of the RF is also multivariate Gaussian
2. Any marginal distribution of $Z(\mathbf{u})$ has a Gaussian distribution
3. Distribution between any pairs of RVs ($Z(\mathbf{u})$, $Z(\mathbf{u} + \mathbf{h})$) is Gaussian and fully determined by the covariance function $C_Z(\mathbf{h})$
4. All conditional distributions of any subset of the RF Z with n known data are Gaussian (Eq. 2.20):

$$G_{Z(\mathbf{u}|(n))}(z(\mathbf{u}|(n))) = G\left(\frac{z - E\{Z(\mathbf{u})|(n)\}}{\sigma\{Z(\mathbf{u})|(n)\}}\right) \quad (2.20)$$

where:

G - the standard Gaussian (Normal) CDF;

To be able to apply TGS, a mask for representing geometric patterns and contacts between the geologic domains is required. The mask links the categorical variables (I_k , $k = 1, 2, \dots, K$) and the continuous variable $Z(\mathbf{u})$. Rectangular partitions (threshold based) for the mask are the most common type of masks. Figure 2.4 demonstrates a simple sketch for a domain with $K=3$ categories. In this domain, category one is in contact with category two, whereas category two is in contact with both category one and category three. This ordering of contacts between categories can be represented by partitioning a Gaussian RF that is divided by two lines (thresholds; t_1 and t_2), as in Figure 2.5. In this case, one Gaussian function is able to capture the spatial ordering relation between the geological categories.

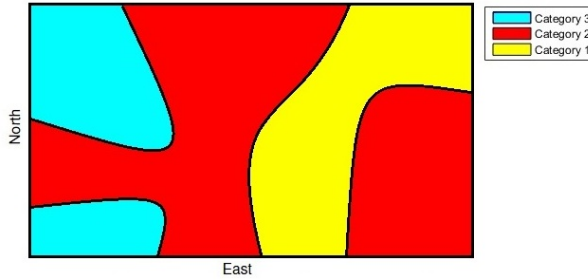


Figure 2.4: Sketch of a synthetic 2D geological region with $K = 3$ categories.

2.9.2 Threshold Definition

The thresholds define an area/volume of the multivariate Gaussian distribution assigned to categories. For two categories, consider $Z(\mathbf{u})$ as the simulated Gaussian function at location \mathbf{u} and $I_1(\mathbf{u})$ and $I_2(\mathbf{u})$ can be the indicators of the category one

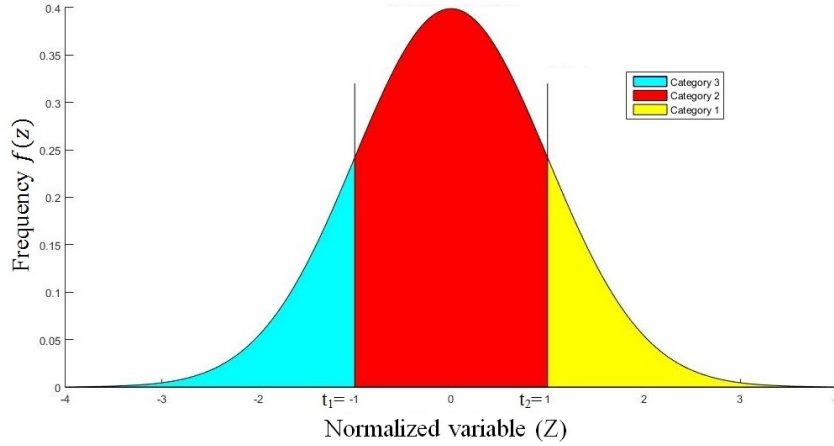


Figure 2.5: Truncation of a Gaussian distribution with two thresholds (t_1 & t_2).

and two, respectively. The mathematical equation of the truncation is Eq. 2.21:

$$I_1(\mathbf{u}) = 1 \quad \Leftrightarrow \quad -\infty \leq Z(\mathbf{u}) < t_1 \quad (2.21)$$

To simulate a variable with K possible categorical values, $K - 1$ thresholds have to be defined. The i^{th} category is defined by Eq. 2.22:

$$\mathbf{u} \in I_i \quad \Leftrightarrow \quad t_{i-1} \leq Z(\mathbf{u}) < t_i \quad (2.22)$$

There is an ordering relationship between the thresholds and K categories (Eq. 2.23).

$$t_1 \leq t_2 \leq \dots \leq t_i \leq t_{i+1} \leq \dots \leq t_{K-1} \quad (2.23)$$

2.9.3 Link between Thresholds and Proportions

The proportion of categories are usually obtained from the available drill hole or well data. There is a one-to-one relation between the proportion of categories and the threshold values for each of the masks. As for TGS, the probability of having category

k at \mathbf{u} defines the proportion of this category at that location (Eq. 2.24).

$$\begin{aligned}
 E\{I_k(\mathbf{u})\} &= p_k(\mathbf{u}) & (2.24) \\
 I_k(\mathbf{u}) = 1 &\Leftrightarrow t_{k-1} \leq Z(\mathbf{u}) < t_k
 \end{aligned}$$

where:

- $I_k(\mathbf{u})$ - indicator of the category k ;
- $Z(\mathbf{u})$ - the simulated Gaussian function at location \mathbf{u} ;
- t_{k-1} - the $(k-1)^{th}$ threshold on Gaussian function;
- t_k - the k^{th} threshold on Gaussian function;

Therefore:

$$\begin{aligned}
 p_k(\mathbf{u}) &= P(t_{k-1} \leq Z(\mathbf{u}) \leq t_k) & (2.25) \\
 &= P(-\infty < Z(\mathbf{u}) \leq t_i) - P(-\infty < Z(\mathbf{u}) \leq t_{k-1}) \\
 &= G(t_k) - G(t_{k-1})
 \end{aligned}$$

Using the normal distribution is conventional to generate the underlying Gaussian realization. The thresholds can be specified by the target global proportions for each category or with local proportions. Assuming the known proportions of each category experimentally $p_k(\mathbf{u})$ ($k = 1, \dots, K$), one can calculate the cumulative proportions (cp_k) (Eq. 2.26):

$$cp_k(\mathbf{u}) = \left[\sum_{i=1}^k p_i(\mathbf{u}) \right] \quad \mathbf{u} \in D \quad (2.26)$$

By construction, $cp_0 = 0$ and $cp_K = 1$. $K - 1$ thresholds are required for transforming the continuous Gaussian variables to K categories. The inversion of Eq. 2.25

results in the thresholds (Eq. 2.27):

$$\begin{aligned}
t_1 &= G^{-1}[p_1(\mathbf{u})] \\
t_2 &= G^{-1}[p_1(\mathbf{u}) + p_2(\mathbf{u})] \\
&\vdots \\
t_j &= G^{-1}[p_1(\mathbf{u}) + p_2(\mathbf{u}) + \cdots + p_j(\mathbf{u})] \\
&= G^{-1}[cp_j(\mathbf{u})], \quad j=1,2,\dots,K-1
\end{aligned} \tag{2.27}$$

Where t_j are the thresholds for the TGS and by construction $t_0 = -\infty$, $t_K = \infty$.

Therefore, for the example that is shown in Figure 2.4 the ordering relation between three categories can be defined by one Gaussian deviate. By using the specified mask in Figure 2.5 and considering the proportion of category one, two, and three as 0.159, 0.682, and 0.159, respectively, one can estimate the truncation of a Gaussian distribution with two thresholds (t_1 and t_2), as follows:

$$\left\{ \begin{array}{l} z(\mathbf{u}) \in I_3 \leftrightarrow Z(\mathbf{u}) < t_1 \\ z(\mathbf{u}) \in I_2 \leftrightarrow t_1 \leq Z(\mathbf{u}) < t_2 \\ z(\mathbf{u}) \in I_1 \leftrightarrow Z(\mathbf{u}) \geq t_2 \end{array} \right. \tag{2.28}$$

$$t_1 = G^{-1}[p_1(\mathbf{u}) = 0.159] = -1.0$$

$$t_2 = G^{-1}[p_1(\mathbf{u}) + p_2(\mathbf{u}) = 0.159 + 0.682] = 1.0$$

2.9.4 M-Gaussian Functions

To simulate the categories in a domain with more complicated ordered geological features, TPG simulation (≥ 2 Gaussian deviates) is a reasonable method. The area/volume of the multivariate Gaussian distribution between the variables is defined by thresholds. As we have $I_k(\mathbf{u}) = 1 \Leftrightarrow (Z_1(\mathbf{u}), Z_2(\mathbf{u}), \dots, Z_M(\mathbf{u})) \in D_k$, the probability of having category k at location \mathbf{u} when there are M Gaussian realizations can

be written as Eq. 2.29:

$$\begin{aligned}
 p_k(\mathbf{u}) &= P\{[Z_1(\mathbf{u}), Z_2(\mathbf{u}), \dots, Z_M(\mathbf{u})] \in D_k\} \\
 &= \int_{D_k} g_{\Sigma}(Z_1, \dots, Z_M) dz_M
 \end{aligned}
 \tag{2.29}$$

where:

- D_k - the subset of the Gaussian space which is assigned as category k ;
- g_{Σ} - the M-variate standard Gaussian function with mean of 0 and variance of 1;
- Σ - the correlation matrix;

2.10 Object Based Modeling

An important object based categorical variable modeling method is object based modeling. In the object based methods, parametrized geometries are placed sequentially into a domain model initialized with a background category. Some criteria such as target global proportion and data conditioning are applied to the model to stop the algorithm. To lay out a typical object based model, three key issues should be addressed (C. V. Deutsch, 2002): Geological shapes, method for object placement modification, and relevant data to constrain the resulting realization. Unconditional simulation with an object based algorithm is straight-forward and fast. Geometries are placed sequentially into a domain model until the global proportions of categories are reproduced. However, reproduction of dense data conditioning is difficult and needs time-consuming iterative procedures. For easier data conditioning, these methods have been combined with variogrambased techniques (e.g., Holden, Hauge, Skare, and Skorstad (1998); Shmaryan and Deutsch (1999); Viseur (1999); Oliver (2002); Vargas-Guzmán and Al-Qassab (2006)).

Object based facies models are visually attractive, and the categories represented

by geological shapes and realistic nonlinear continuity match the known geological features. Figure 2.6 shows a complex deepwater which was modeled by complicated channels using the object based method by [Pyrzcz et al. \(2012\)](#). Within the object, continuous property trends can be modeled that cannot usually be modeled with cell based methods. If geometries within the domain are well understood, object based models are appropriate. Object based modeling has been applied to a number of different geological settings and is popular in fluvial settings. [A. D. Miall \(1985\)](#) classified fluvial architectural elements based on their scales, bounding surfaces, texture, and internal geometries. Also, he explained fluvial sedimentary facies, basin analysis, and petroleum geology with more than 500 figures and 1000 references ([A. Miall, 2013](#)). With the work of Haldorsen and others ([H. Haldorsen and Chang \(1986\)](#); [H. H. Haldorsen, Lake, et al. \(1984\)](#); [Chiu, Stoyan, Kendall, and Mecke \(2013\)](#)), in the mid-1980s object based modeling became popular in petroleum reservoir modeling. [H. Haldorsen, MacDonald, et al. \(1987\)](#) modeled shale barriers as rectangular objects. There are many different examples of geological modeling of fluvial reservoirs using object based modeling. The mathematical model of a fluvial reservoir was studied by Holden et al. In their study the reservoir was divided into four discrete facies: channel, crevasses, barrier, and background. Realizations from the model are generated using the Metropolis-Hastings simulation algorithm with simulated annealing conditioning on the volume ratios and well observations ([Holden et al., 1998](#)).

Often object based models are constructed without considering local data and used as training images. Improved conditioning is necessary for object based modeling.

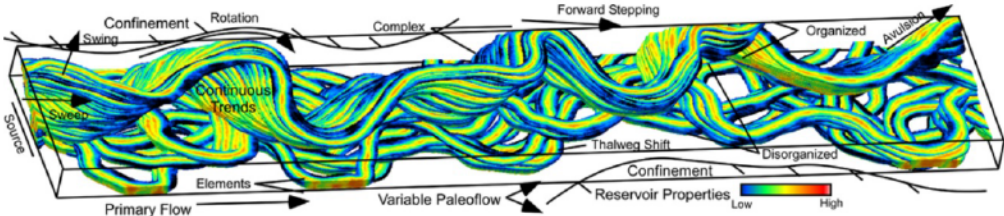


Figure 2.6: Complex deepwater geological features ([Pyrzcz et al., 2012](#)).

2.11 Event Based Modeling

Event based modelling, also known as process based, pseudo genetic, process mimicking or advanced object based models, is an extension of object based modelling in which the objects are placed in the model in a temporal sequence with rules to mimic the geologic processes associated with their deposition (Sun, Meakin, Jøssang, and Schwarz (1996); Xie, Cullick, Deutsch, et al. (2001); Pyrcz (2004); Pyrcz et al. (2012)). The geological complexity generated by event based modeling is appealing to many geologists. Conditioned event based models are difficult to construct and matching seismic data is rare. The result is the development of more complex models of heterogeneity and object inter-relationships, but conditioning is nearly impossible. Event based modelling has been used to generate realistic models of fluvial systems (Pyrcz, 2004). Process based forward simulation (Tetzlaff and Harbaugh (1989); Boisvert (2007)), event based modelling (Pyrcz, 2004), and unconditional object-based simulations (Pyrcz (2004); Maharaja (2008)) have been used to generate 3D training images.

A process based stochastic approach has also been used by Hu, Joseph, Dubrule, et al. (1994) to simulate the internal geometry of deltaic sandstone bodies. Process based models have been combined with object based and variogram based techniques (e.g., Xie et al. (2001); Pyrcz and Deutsch (2005); Teles, Delay, and De Marsily (2004); Pyrcz and Strebelle (2006); Reza, Pranter, and Weimer (2006)), though with limited success in data conditioning.

Process based and stochastic models provide satisfactory modelling for heterogeneous reservoirs by reproducing the depositional processes. When processes are known, process based stochastic models allow for the representation of realistic geometries and arrangements of different geological sets. Soft regional conditioning with seismic or hard conditioning at well data points is a challenging problem, limiting the practical use of event based models.

2.12 Discussion

Three main geostatistical algorithms for simulating categorical variables are SIS, MPS, TPG simulation and object/process based modeling. Classical geostatistical techniques condition data and assess uncertainty, but the models often lack geologic realism. In SIS, transitions between domains or rock types are not easily controlled and produce models of categorical variables that are fairly unstructured. Increasing levels of randomness, especially along the boundaries, is common when using SIS. In MPS, information regarding the spatial heterogeneity is inferred from a training image. MPS facilitates conditioning. However, the important issue of MPS is adopting a representative training image which can be very difficult. Also, object based models are considered when there are distinctive geological units in the domain that can be characterized with geometric parametrization. The major drawback of object based models is the honoring conditioning data.

In deposits with complicated ordering structures, when the ordering relationships or transition probabilities between rock types is known, TPG simulation is a flexible and powerful method for simulating facies categories. Its flexibility in representing complex lateral and vertical categories transitions is the important key of this simulation method. This thesis demonstrates the improvement of categorical variable modeling using TPG simulation through addressing common challenges in this methodology and improving the geological controls in the characterization of quantitative attributes by associating more information to the modeling.

Chapter 3

TPG Framework and Mask Optimization

Generation of the mask that reproduces the desired ordering structure is a preliminary step in TPG simulation. In this chapter, mask optimization of TPG modeling is explained and the optimization of two types of masks is introduced and discussed.

3.1 Mask Optimization

In TPG simulation, having a mask to convert the continuous Gaussian values simulated to categorical values is important. The layout of the mask must be chosen to reflect contacts between different categories. In this section, two types of masks (discretized and object based) are introduced in order to find the optimal mask to reproduce input statistics and global/local proportions.

3.1.1 Discretized Mask

The layout of the mask must be properly selected to suitably define the relationship between categories. To determine the ideal mask, an optimization algorithm is proposed based on simulated annealing (SA). In this approach an initial discretized mask is generated randomly and SA optimization is adopted to iteratively optimize the mask to match the spatial features in the final TPG realizations. An example of the initial discretized mask and optimized mask for three categories using two underlying Gaussian RFs is shown in Figure 3.1.

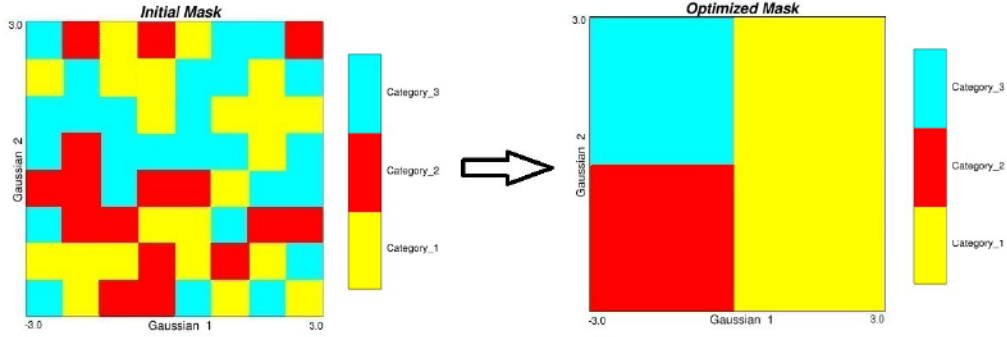


Figure 3.1: Sample of discretized mask by $2^3 \times 2^3 = 64$ blocks and optimized mask.

In the proposed methodology, seven discretization scales are proposed for discretizing a mask. A mask can be divided to $2^2 \times 2^2$ blocks and K categories are assigned randomly to these blocks. This discretization is coarser since there are only 16 blocks available. As illustrated in Figure 3.2, for instance, in the second image there are $2^3 \times 2^3 = 64$ blocks to be assigned to the categories. The finest discretization is $2^8 \times 2^8$ with 65536 blocks.

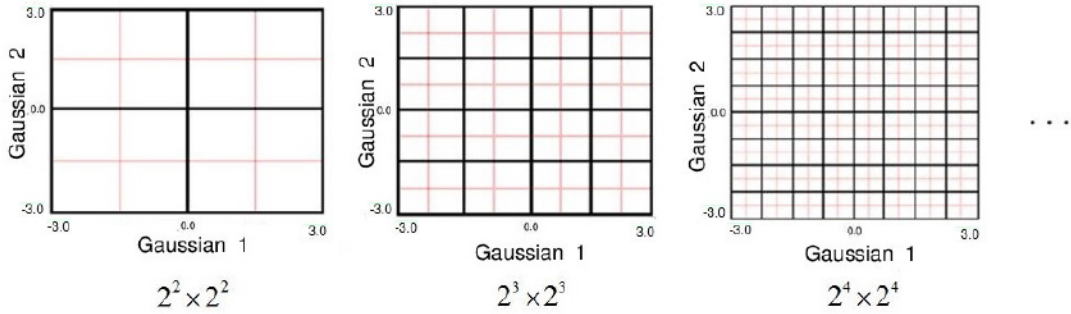


Figure 3.2: Discretization of mask based on different scales.

The optimization of the mask is applicable in any scale and SA changes the mask iteratively regarding the scale to minimize the difference between desired statistics and current statistics.

Mask Optimization with Simulated Annealing

SA can be considered as an extension of the Metropolis algorithm (Metropolis, Rosenbluth, Rosenbluth, Teller, & Teller, 1953) and as a global minimization technique. In optimization techniques, SA has found application in a wide range of application

areas including the integration of diverse data types (C. Deutsch & Tran, 2002), combinatorial problems (Rozenberg, Bck, & Kok, 2011), computer (VLSI) design (Mead & Ismail, 2012), image processing (Carnevali, Coletti, and Patarnello (1985); Jeng and Woods (1990); Antoniou and Lu (2007); Y. Zhang, Yan, Zou, Tao, and Zhang (2016)), genetic structures (Dupanloup, Schneider, & Excoffier, 2002), job shop scheduling (Xia & Wu, 2005) and many other difficult optimization problems. SA is one of the best approaches among local search algorithms (Michiels, Aarts, & Korst, 2007).

Temperature (T in Eq. 3.1) is an important parameter in SA. Typically, T starts high and temperature is reduced gradually. The structure of energy (or objective value) O_1 is changed to a structure of energy O_2 with probability (Eq. 3.1):

$$pr = e^{\frac{-(O_2 - O_1)}{k_b T}} \quad (3.1)$$

where:

- pr - the probability of change;
- T - the annealing temperature parameter;
- k_b - a natural constant which relates temperature to energy;

With the Metropolis algorithm (Metropolis et al., 1953), sometimes poor changes with a higher objective value than the current one ($O_2 > O_1$) are accepted. In SA, the rate of reduction of the optimization function (O) is controlled by the temperature distribution (the Boltzman distribution) using T . The probability of accepting poor exchanges increases as T increases. The accept probability distribution is specified by Eq. 3.2:

$$P(\text{accept}) = \begin{cases} 1 & \text{if } O_2 \leq O_1 \\ e^{\left(\frac{O_1 - O_2}{T}\right)} & \text{otherwise} \end{cases} \quad (3.2)$$

In the proposed optimization, special attention is paid to optimize the mask in order to match the desired input statistic, such as the transition probabilities between categories. The algorithm randomly accepts some changes that increase the objective function. Here, replacing a block with a specific category in the mask to another category is defined as a change. The application of the SA algorithm to mask optimization consists of six main steps:

1. The initial discretized mask is selected randomly.
2. The objective function which measures the closeness to the target feature is based on transition probabilities. Here, the objective function (Eq. 3.3) is defined by the sum of the square differences between transition probability of the data $\mathbf{tp}_{kk'}(\mathbf{h})^{data}$ and the simulated realization $\mathbf{tp}_{kk'}(\mathbf{h})^{realization}$ for a specific number of lag distances.

$$O(\mathbf{h}) = \sum_{d=1}^{nD} \sum_{k=1}^K \sum_{k'=1}^K (\mathbf{tp}_{kk'd}(\mathbf{h})^{data} - \mathbf{tp}_{kk'd}(\mathbf{h})^{realization})^2 \quad (3.3)$$

where:

nD - number of directions for scanning the domain to calculate transition probabilities;

K - number of categories;

$\mathbf{tp}_{kk'}(\mathbf{h})^{data}$ - transition probability of categories in the data set;

$\mathbf{tp}_{kk'}(\mathbf{h})^{real}$ - transition probability of categories in the simulated categorical realization;

Typically, probability matrices are inferred along the drill hole or wells upward and downward. Here, calculating the transition probability matrices along six different directions ($\theta_i, i = 1, \dots, 6$) as demonstrated in Figure 3.3 is proposed to add more flexibility for capturing the correct transition between categories.

3. The stopping criteria is needed in the optimization. In an iterative algorithm,

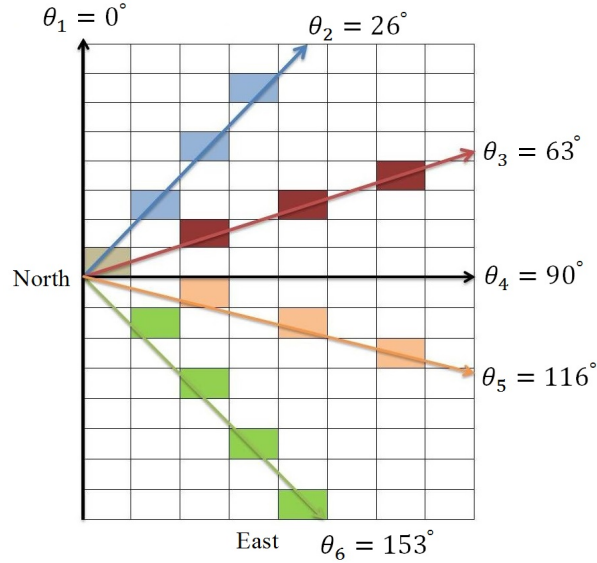


Figure 3.3: Lag orientations.

procedure should stop when the objective function is minimized. The algorithm here stops as follows:

- After reaching a specific temperature value
 - After a certain number of iterations
 - After no improvement in the objective function for number of iterations (no better solution)
4. Next step is related to the perturbation rules. The SA algorithm proceeds by visiting all the locations in the discretized mask along a random path. Procedure starts by truncation of Gaussian realizations into categories using the initial bivariate mask. The perturbation procedure is illustrated in Figure 3.4. First the process proceeds with random selection of one location in the mask at a time and then continues by checking the category of blocks in its neighborhood. As shown in Figure 3.4, if there is a difference between the category at a selected location (center block with yellow color in the figure which represents category one) and the surrounding categories, then in this step perturbation is accepted and the category at the selected location in the mask is changed to the one with a different category.

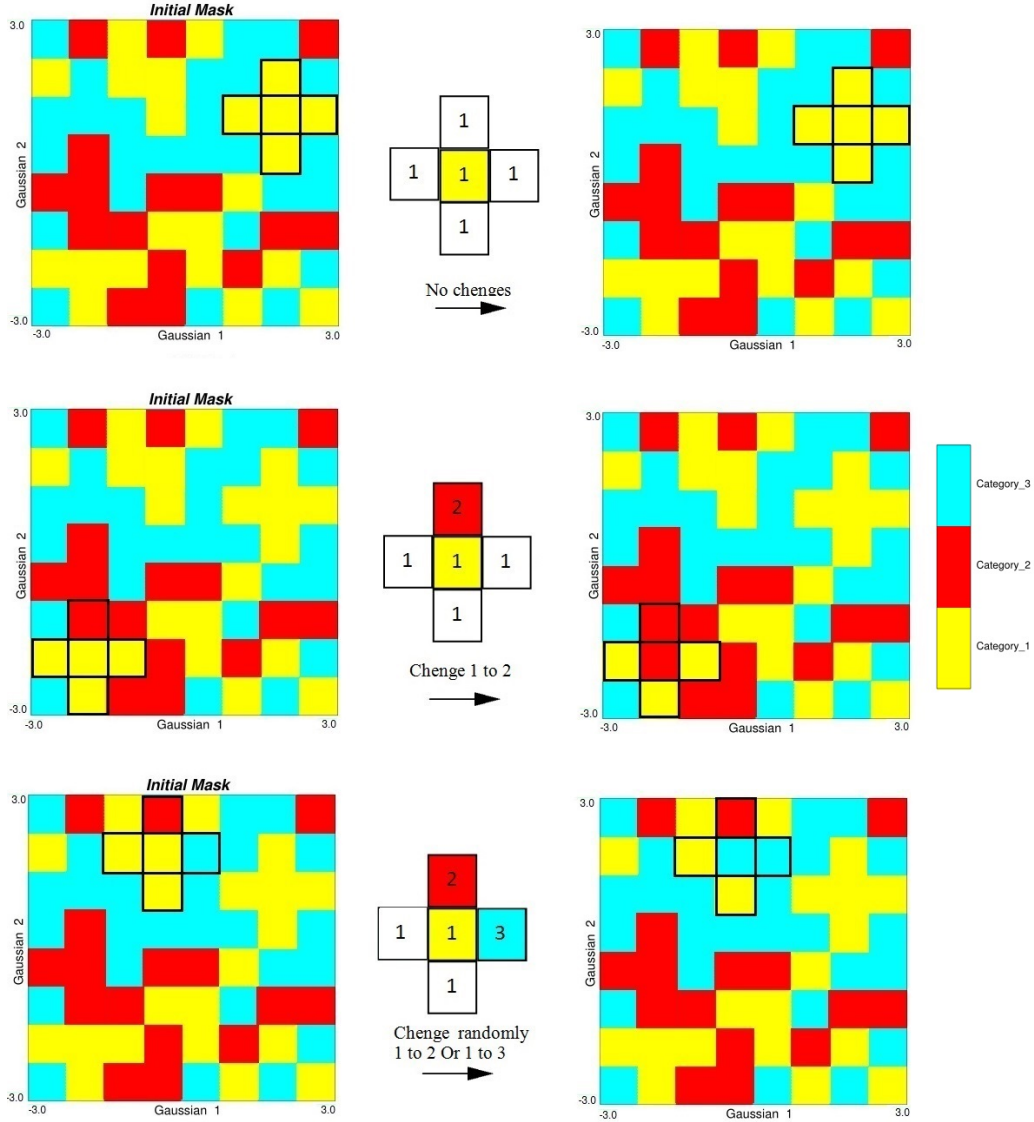


Figure 3.4: Illustration of how selected locations in the mask are changed. Yellow block in the center is the selected category in the mask and four other blocks in its four sides are considered as its neighbors.

5. The objective function is updated after each accepted perturbation. The objective function must be updated after each perturbation, but it is a CPU expensive operation. To improve the speed, the following implementation details are considered:

- Transition probability matrices are updated locally after each iteration. Rather than scanning the entire domain to build the transition probability matrices after each change, only the transitions between selected blocks

are updated for the number of considered lags. Figure 3.5 demonstrates the required CPU time for updating transition probabilities for different number of changes in the mask. If fewer than half of the blocks are changed, this improves CPU time.

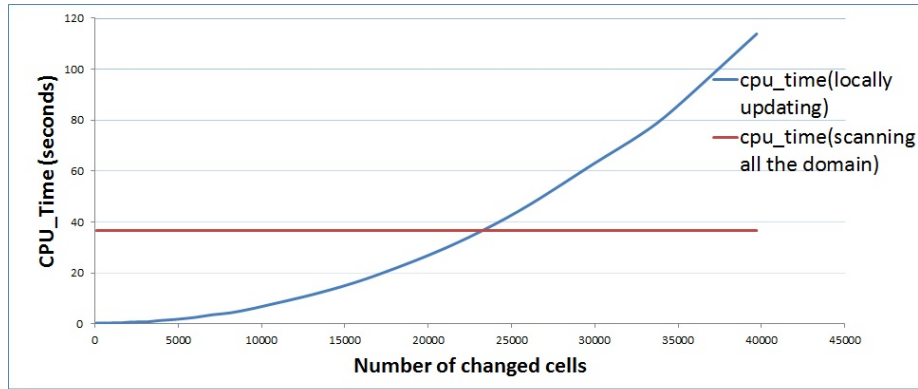


Figure 3.5: Required CPU time (seconds) for updating transition probabilities in the objective function.

- The objective function is updated after a specific percentage of changes in the mask for a certain number of iterations. The total number of iterations is divided in five steps and in each, a specific percentage of changes in the mask is applied. Percent of changes in each is considered as follows: 25%, 15%, 10%, 5%, and 1 block at a time of the total number of cells in the discretized mask. Therefore, in each iteration a specific number of changes is applied before updating the objective function. This updating procedure has two advantages. First the algorithm starts by changing 25% of blocks in the mask which may help to cover more space of uncertainty in the domain than changing only one block at a time. There is an increased chance to make large changes in the beginning and then the percentage of changes is reduced after obtaining an initially good solution. The second advantage is related to the CPU speed. Here also, the objective function is updated after each mentioned percentage of changes and it reduces the required CPU time.

6. The last step regards the annealing schedule. The annealing parameter (T) is

controlled by the cooling schedule. A number of annealing systems can be applied (Triki, Collette, and Siarry (2005); Van Laarhoven and Aarts (1987)). The change is always accepted if the objective function decreases. In this case, the simulation moves closer to the target statistics. However, there is also a probability that the simulation goes toward a local minimal. SA attempts to avoid becoming trapped in the local minimal by accepting some less optimal solutions. SA should start with a reasonably high initial temperature T_0 and should reduce the temperature as iterations progress. T_0 can be defined according to the formula Eq. 3.4 (Busetti, 2003):

$$T_0 = \frac{-\Delta O^+}{Ln(pr_0)} \quad (3.4)$$

where:

- pr_0 - acceptance probability of first increased objective function;
- ΔO^+ - difference between current and previous objective value;

After each iteration, the cooling temperature should be updated. The most common temperature decrement rule is Eq. 3.5 (Busetti, 2003):

$$T_{i+1} = \delta T_i \quad (3.5)$$

where:

- δ - a constant scalar in the range (0, 1), close to 1;

Also, an update for the temperature parameter in the starting point of each mentioned part is suggested here by increasing the temperature to a coefficient of the starting temperature of the previous part (Eq. 3.6) as shown in the annealing

schedule in Figure 3.6. To start the algorithm, $pr_0 = 0.95$ and $\delta = 0.95$ are adopted.

$$T_{st(i+1)} = \delta T_{st(i)} \quad st = 1, \dots, 4 \quad (3.6)$$

where:

- $T_{st(i)}$ - initial starting temperature of step i ;
- $T_{st(i+1)}$ - initial temperature of step $i+1$ which is a coefficient of initial starting temperature of previous stage i ;

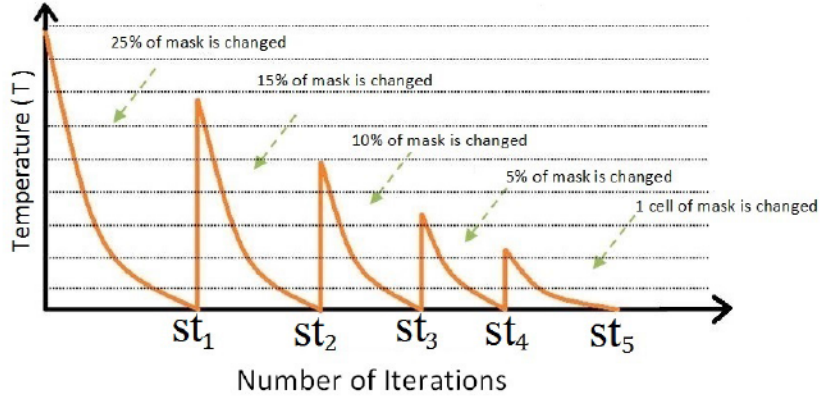


Figure 3.6: Annealing schedule.

Synthetic Case Study for Mask Optimization with SA

A synthetic categorical realization with the modeling grid of 256×256 blocks of $1 \times 1 \text{ m}^2$ has been used as the target feature (Figure 3.7, bottom right). Here $M = 2$ independent Gaussian realizations Z_1 and Z_2 are used. They are unconditionally simulated by sequential Gaussian simulation (SGSIM, (C. V. Deutsch et al., 1992)) with a spherical variogram model but different anisotropy (Figure 3.7, top). Based on the bivariate mask, the realizations are truncated.

Four random masks with discretization of $8 \times 8 = 64$ blocks are generated and proposed optimization with SA is applied at this scale (Figure 3.8). Input realizations are considered to be the same as the input realizations of target categorical realization.

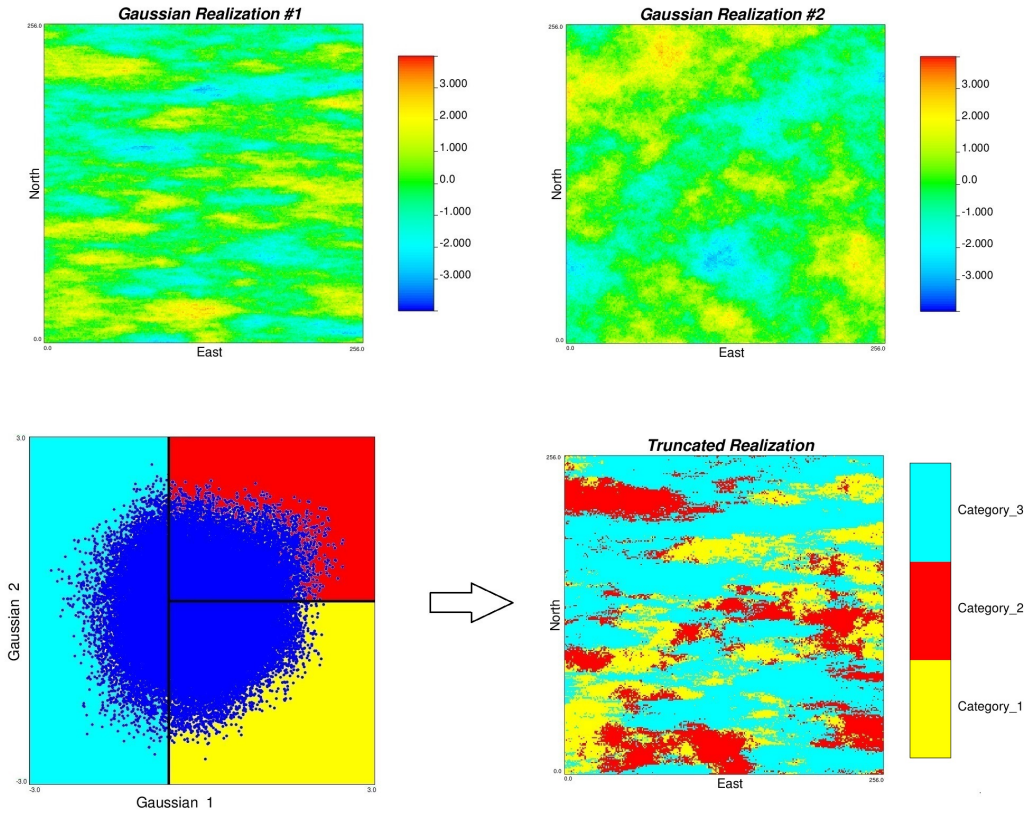


Figure 3.7: Top: two generated realizations of standard Gaussian RV. Bottom left: bivariate object based mask and bottom right: truncated realization.

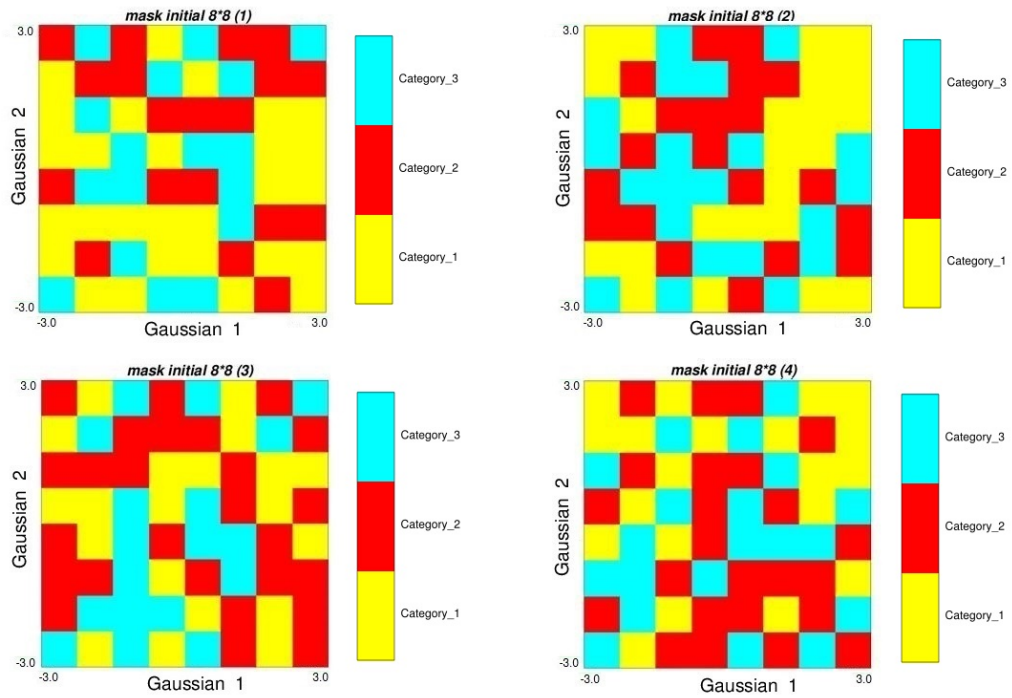


Figure 3.8: Random masks with discretization of $8 \times 8 = 64$ blocks.

The performance of the method and proposed procedure are evaluated using the mentioned random masks. In this case, the total number of 10000 iterations is specified to the optimization. The input number of iterations in each part is summarized in Table 3.1. Transition probabilities between categories for $nL = 10$ are considered for calculating the objective function (Eq. 3.3). Also Table 3.2 summarizes the initial objective values, final objective values, and iteration number that algorithm stopped for all four random masks.

Table 3.1: Summary of input parameters for perturbation.

Number of iterations to perturb the mask	
Total number of iterations	10000
Number of iterations with 25% changes at a time	1000
Number of iterations with 15% changes at a time	1500
Number of iterations with 10% changes at a time	2000
Number of iterations with 25% changes at a time	2000
Number of iterations with 1 block changes at a time	3500

Table 3.2: Objective values for different masks.

Mask #	Start obj.	End obj.	# of iterations
1	13.03	0.00	5154
2	8.74	0.00	5247
3	8.97	0.00	5850
4	21.64	0.00	5464

As shown in Table 3.2, the algorithm stopped with an objective equal to zero, indicating that the algorithm reproduced the optimum mask and the truncated realization shown in Figure 3.7. Figure 3.9 shows the final mask and final optimized truncated realization for mask number one as an example. The blue dots in the mask show the scatter plot of the underlying Gaussian realizations. Also, Figure 3.10 demonstrates the objective value reduction and annealing temperatures procedure related to mask number one.

The objective function started by value 13.03 and after around 2000 iterations reached close to zero (Figure 3.10(b)). In this example the optimum mask is reproduced. There are two locations in the mask which are different from the target mask (see

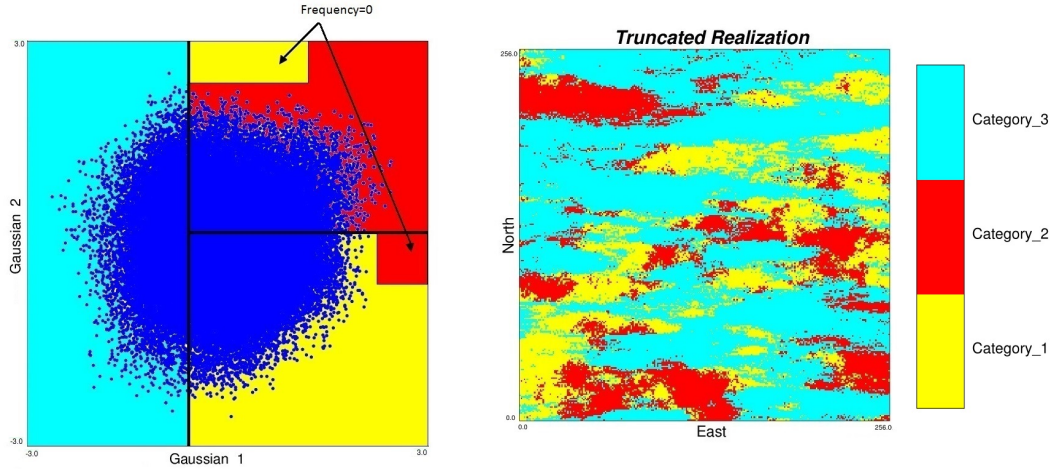
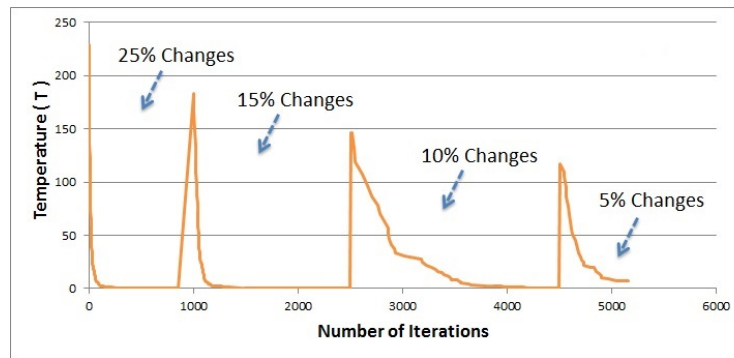
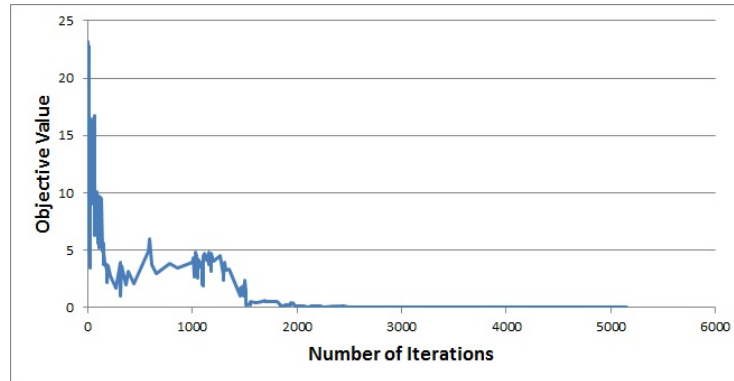


Figure 3.9: Final mask and final truncated realization for random mask number one.



(a) Annealing temperatures procedure



(b) Objective function reduction

Figure 3.10: Annealing temperatures procedure and objective function reduction related to mask number one.

Figure 3.9), but the frequency of the underlying Gaussian realizations in these areas is zero and those locations in the mask do not impact on the simulated realization.

The proposed methodology is an automatic mask optimization, which relies on the use of transition probabilities of categories to find the best mask's configuration. This mask starts with a random discretized mask and allows defining complex masks, but it is not efficient time-wise when the number of categories increases. Another limitation comes when the complexity of the relation between categories increases and more than two underlying Gaussian deviates are required to explain the transitions and contacts of categories. In the next section, an object based mask is introduced as an alternative to find the optimum truncation rule.

3.1.2 Object Based Mask

This section describes an object based mask to model spatial distributions between the categories in TPG realizations. Basically, any configuration can be considered for defining the relation between categories. Introducing objects into the mask can add flexibility for reproducing features observed in data and map the continuous variables to a categorical space. Here, objects control the contacts and transitions between categories. The proposed mask allows the use of any number of objects with different directions in the mask to capture the spatial distributions between the categories. The key to the approach is adapting objects with appropriate sizes and directions. The objects are characterized by some function or geometric shape and would be moved and scaled to get close to the configuration in the original model. In this work, objects are ellipses which are characterized by their center location in the X axis and Y axis, orientation and radius size. Each object can be shifted or rotated to produce different masks (Figure 3.11). An ellipse is defined as Eq. 3.7.

$$\frac{(x - x_0)^2}{R_a^2} + \frac{(y - y_0)^2}{R_b^2} = 1 \quad (3.7)$$

which is centered at some point (x_0, y_0) with radius (R_a, R_b) . The coordinates of the center point in an ellipse rotated by θ are found by Eq. 3.8:

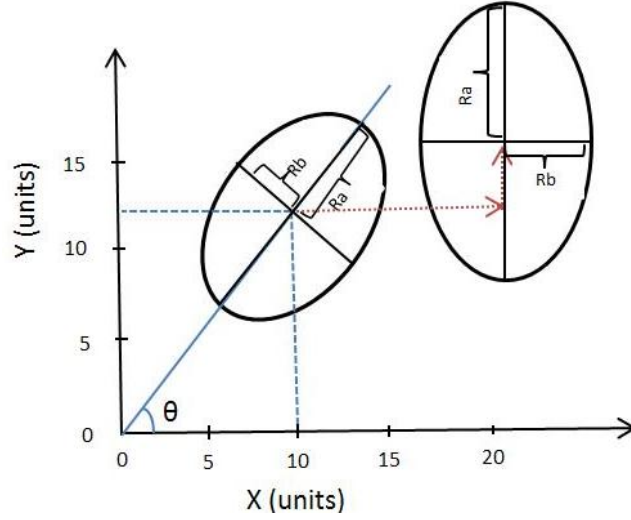


Figure 3.11: Rotating and Shifting an ellipse.

$$\begin{cases} x_{new} = x\cos\theta + y\sin\theta \\ y_{new} = y\cos\theta - x\sin\theta \end{cases} \quad (3.8)$$

Compared to the discretized mask explained in the Section 3.1.1, the object based mask reduces the randomness of initial masks. The optimization approach is based on gradient methods which are explained in Section 2.5 and the emphasis is placed on generating objects in the mask to find the optimum mask which honors the pattern statistics in the original model.

The number of shapes, initial coordinates, angel rotation, and radiuses are input parameters in the proposed procedure. Initially, shapes are randomly placed in the mask. The input realizations are discretized into categories by applying the mask. Also here, transition probabilities are used as the measure of spatial variability. Figure 3.12 shows the generated mask with three shapes and three categories and the related TPG realization.

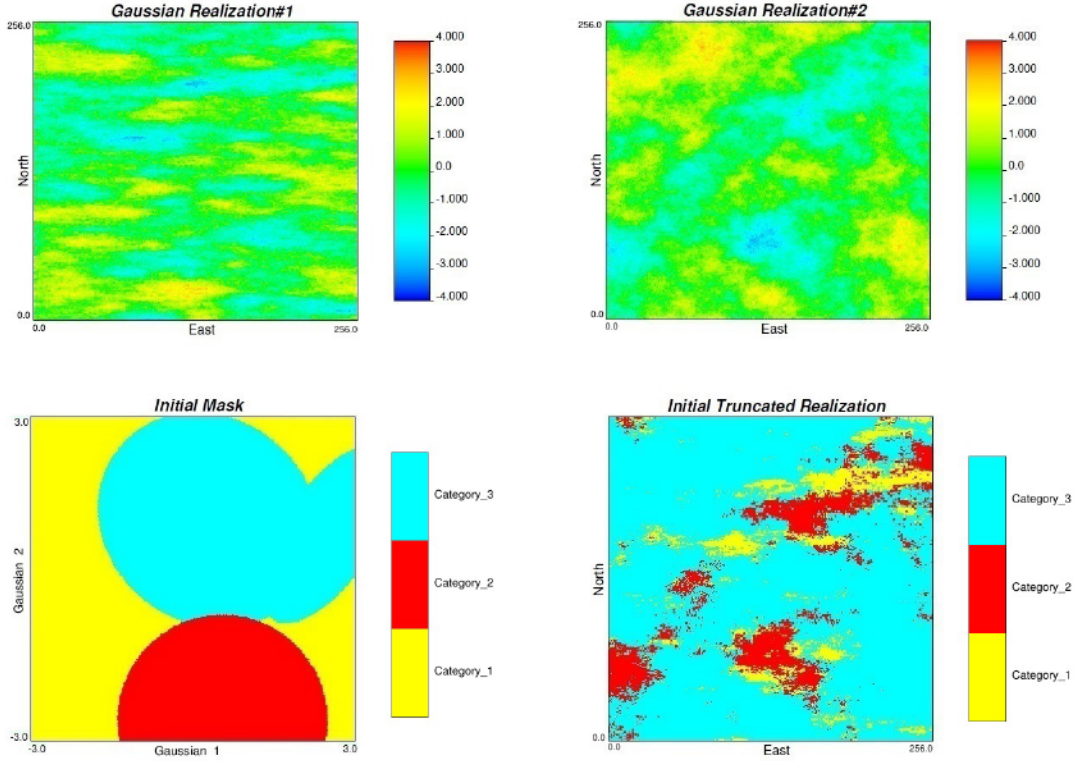


Figure 3.12: Top: two generated realizations of standard Gaussian RV. Bottom left: bivariate object based mask and bottom right: truncated realization.

Mask Optimization with Gradient Decent

Gradient algorithm is suitable for solving nonlinear optimization and unconstrained problems which the gradient can be calculated from objective function (O). The conjugate gradient method is an iterative method, so it can be applied to sparse systems that are too large to be handled by direct methods and is used here for mask optimization. This is a fast optimization and a solution can be found after a finite number of iterations. The objective function (O) is defined as in Eq. 3.3.

Here, the Fletcher-Reeves method (Fletcher & Reeves, 1964), which is a type of the conjugate gradient method, is used. The optimization is performed by using sequential search directions that allow a strict mathematical relationship between variables. The Fletcher-Reeves method attempts to approximately locate a local minimum of the objective function. Since only the first derivative term ($\frac{\partial O(\mathbf{a})}{\partial x_j} = \frac{O(\mathbf{a} + \Delta \mathbf{x}_j) - O(\mathbf{a})}{\Delta x_j}$) in the Taylor series is available from the defined objective function and the history of the

gradients to move is important to consider, the Fletcher-Reeves method is a suitable method.

In mask optimization, the very first step is to define the number of ellipses to be generated in the mask using initial random parameters. Gradient optimization is adopted to continuously and iteratively modify the initial parameters of ellipses in the mask until the objective function is minimized and target statistics of the truncated realization are close to the available data set. Each ellipse can be shifted or rotated in the mask (see Figure 3.11).

Synthetic Case Study for Mask Optimization with Gradient Optimization

Two Gaussian realizations with the modeling grid of 256×256 blocks of 1×1 m^2 are considered and truncated by the bivariate objects based mask into categories to generate a realization (Figure 3.12). The objective function is formulated to measure a mismatch between the transition probability of categories in the data set and simulated truncated realization. The initial parameters of the mask, center points, radiuses, and angels of objects are continuously modified until the objective function is minimized.

Three shapes with three categories are randomly placed into the mask. The objective value is calculated along 20 lags along six different directions ($\theta_i, i = 1, \dots, 6$ in Figure 3.3). The percent mismatch between the simulated realization with the object based mask optimization and the target categorical realization is calculated. There is a 5% mismatch between the simulated categories in the final truncated realization and target realization. Also, visually it is observed that the spatial feature of data is reproduced in simulated realization. The final TPG realization is shown in Figures 3.13.

Optimization began with the objective value of 245.69 and stopped with 1.45 in 20 iterations. A significant reduction is observed in the objective value, and the truncation of Gaussian realizations using the optimized mask reproduced the spatial distribution of target realization in the truncated simulated realization with small error. In general, there is no unique solution for the mask, but it could be seen that the method of object based mask optimization reproduced the simple categorical relationship in this

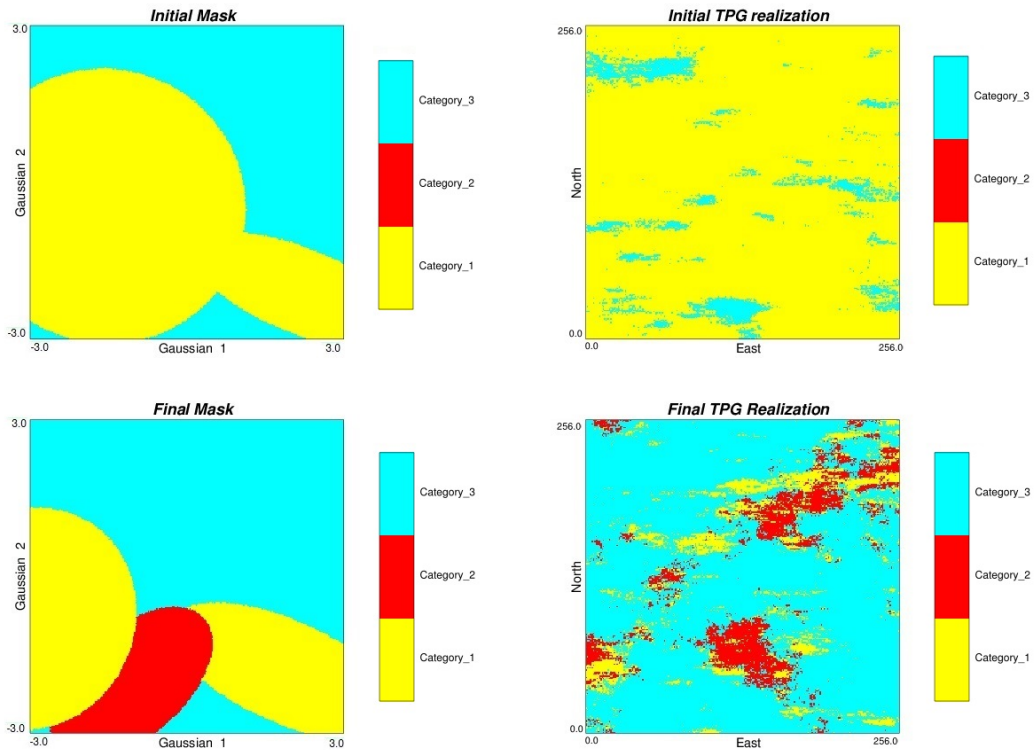


Figure 3.13: Top left: initial mask and top right: related initial truncated realization. Bottom left: final mask bottom right: final truncated realization.

example. The proposed algorithm also preserved the global proportion of categories in optimized truncated realization. Table 3.3 displays the proportions of categories in the target realization and the optimized truncated realization.

Table 3.3: Categories proportion of data, initial truncated realization and final truncated realization.

Category	Cat. 1	Cat. 2	Cat. 3
Proportion of data	0.093	0.118	0.789
Proportion of optimized realization	0.107	0.102	0.791

The object based mask is an automatic mask optimization method which uses gradient decent algorithm to find the optimum mask. This a fast optimization program for three to four categories. A different number of objects could be placed in the mask and the optimization procedure manages the size and number. Convex optimization problems can be solved quickly and reliably with a very large size of variables and constraints, but this efficiency is not true for non-convex optimization problems. Since

the defined objective function is not convex, the complexity of optimization increases as the number of objects and categories increases, and it becomes difficult to solve exactly in a reasonable time.

3.2 Summary

In this chapter, two methods for finding the truncation rule for TPG simulation are introduced. Depending on the complexity of ordering between categories in the data, the use of more complex masks to allow for flexible transition between categories is an option. The proposed masks work for truncation with two underlying Gaussian deviates. Limitation comes from the required CPU time for a more complex relationship between categories. When there is a complicated relation between categories, these masks may not be efficient.

Considering LVP is an important aspect of TPG simulation. In the next chapter, the threshold based mask and multidimensional scaling mask (MDS) are introduced. They are able to deal with the locally varying proportion of categories and allow for complex relationships between categories.

Chapter 4

TPG Simulation with Locally Varying Proportions (LVP)

The TPG model has been widely used to characterize heterogeneity in aquifers (Mariethoz, Renard, Cornaton, & Jaquet, 2009), oil reservoirs (Emery (2007); Galli et al. (2006)), and mineral deposits (Armstrong et al., 2011). Handling spatial changes in the categories proportion is an important requirement for categorical variable techniques. The determination of a truncation procedure for complicated geological environments is not obvious. The truncation rules control the proportions and ordering of categories in the simulation. In most cases, there is non-stationarity in proportions due to geological trends, and models with a global proportion of categories may not yield to the realistic results. The plurigaussian model can be generalized to account for lateral and vertical changes in the categories proportions. Relative proportions of categories need to be defined. Usually, this information comes from the analysis of wells/drill holes, outcrops, or remote sensing data. Beucher et al. (1993) and Ravenne, Galli, Doligez, Beucher, and Eschard (2002) used empirical proportions of observed data and interpolated to the whole space. Emery, Ortiz, and Cáceres (2008) proposed to model facies proportions with random fields rather than deterministic fields. Here, the use of locally varying masks is considered for the incorporation of trends. Two different mask frameworks are considered and programs (Appendix A.1, A.2) for TPG simulation with LVP are developed.

The first mask framework is defined by linear thresholds and is the typical type

of mask in standard TPG simulation algorithms. The second framework uses MDS method (Wickelmaier, 2003) to automatically calculate the optimal mask (J. L. Deutsch & Deutsch, 2014) and is generalized here to account for LVP.

A key requirement of the TPG method is to be able to condition the Gaussian RFs to actual categorical observations. The first available methods for conditional simulation in TPG are introduced. Then, the use of locally varying masks for both threshold based and MDS masks to deal with non-stationarity in domain are explained and the optimization of these two type of masks is discussed. Finally, a case study simulating rock types at a mineral deposit demonstrates the benefits of this method.

4.1 Conditional Simulation in TPG Simulation

The use of available data in the simulation is an important part of any geostatistical technique. In reality, categorical data, facies or rock types, are observed from well or drill holes. Transferring categorical data to continuous values for conditional simulation of underlying Gaussian deviates is an essential step in the TPG method. For conditioning, categorical data must be transferred into continuous Gaussian conditioning data.

There are two concerns here (C. V. Deutsch, 2002). The first issue is that the correct categories are maintained on back transformation. Therefore, the local proportions and corresponding thresholds must be considered. Second, since categorical variables are involved, spikes/ ties may occur and should be dealt with by constraining. To solve the problem of despiking, the simplest solution is to leave the spikes unaffected and consider the normal score transform of each category to the center of the class in the normal distribution (Eq. 4.1):

$$y(\mathbf{u}) = G^{-1}\left(\frac{cp_{k-1}(\mathbf{u}) + cp_k(\mathbf{u})}{2}\right) \quad (4.1)$$

where:

- K - number of categories;
- $y(\mathbf{u})$ - the normal score transform at location u ;
- $cp_k(\mathbf{u})$ - the cumulative proportions;

So, one method is the use of the centroid of each categorical class with respect to the truncation rule (C. V. Deutsch, 2002). But using fixed values may lead to incorrect uncertainty assessment. The use of centroid method is equivalent to assuming that underlying variables are known at sampled locations, but in reality, the values are unknown.

Another method for conditional simulation of the Gaussian variables in TPG is obtained using a stochastic approach, the Gibbs sampler, as proposed by Le Loch and Galli (1997). In the Gibbs sampler algorithm, multigaussian values at experimental points are generated iteratively from random Gaussian values. Kriging is applied at each point using the previous covariance model and a new value is allocated by adding the kriged value to a standard Gaussian variable with respect to the thresholds.

There are several advantages to using the stochastic approach, such as the theoretical consistency, speed and flexibility, especially when dealing with external geological information (Galli et al., 1994). On the other hand, there are some disadvantages such as considering a particular covariance model with the same anisotropy directions for all categories. The use of iterative fitting algorithm of generation of Gaussian values at conditioning points is suggested by Remacre and Zapparoli (2003). In this methodology, the spatial variation of the categories is considered in generation of Gaussian values with the Gibbs sampler algorithm.

The Gibbs sampler has an issue related to the inversion of the covariance matrix and moving search neighborhood when there are a large number of data available. Lantuéjoul, Desassis, and Fouedjio (2012) solved this issue by using a propagative version of the Gibbs sampler. Also, Emery, Arroyo, and Peláez (2014) modified the approach and used it in a TPG simulation with linear inequality constraints.

The problem of keeping facies observations at well locations using the data assimilation procedure is mentioned by Astrakova and Oliver (2015) as an important limita-

tion in the application of TPG. Merging the data assimilation algorithm (Levenberg-Marquardt approach (F. Zhang, Reynolds, Oliver, et al., 2003)) with an interior point formulation has been suggested to produce a good history matching algorithm.

As mentioned earlier, considering a specific covariance model with the same anisotropy directions for all categories is a drawback of using the stochastic approach. The use of the right spatial structure to simulate the unknown Gaussian values is suggested by (Astrakova, Oliver, and Lantuéjoul (2015); Emery et al. (2014); Arroyo, Emery, and Peláez (2012); Lantuéjoul et al. (2012); Galli et al. (1994)). However, the use of a single realization of underlying Gaussian variables may result in the underestimation of uncertainty. D. S. Silva and Deutsch (2016a) proposed the use of multiple realizations for transferring categorical values to Gaussian values at the sample data locations since there are multiple realizations for the underlying variables that give the correct categories on back transformation with the same spatial structure and the same truncation rule.

In this work, Eq. 4.1 is used to transform each category to the center of the class in the normal distribution but any data transformation can be used.

4.2 Locally Varying Mask with Thresholds

Threshold based or rectangular partitions for the mask are the most common geometry. Theoretically, one can use different geometry, but the layout of the mask must be properly selected. When the correlation matrix (Σ) and the domain of interest (D_k) are known, finding the thresholds and proportion of categories (p_k) is simple, but even with knowing all the p_k it is not possible to find the correlation matrix and D_k as there are many possible solutions. Here, a specific partitioning of Gaussian space into rectangles (with two Gaussian functions) is proposed. Figure 4.1 demonstrates an example of partitioning with two Gaussian deviates and four categories. The projection of rectangular boxes on the Gaussian axes defines the area of each box and the thresholds are assigned to each rectangular box. For M Gaussian functions, by knowing $2^M - 1$ of the thresholds. It is easy to find the last unknown threshold numerically using the

inversion of the Eq. 4.2.

$$\begin{aligned}
 p_k(\mathbf{u}) &= P\{[Z_1(\mathbf{u}), Z_2(\mathbf{u}), \dots, Z_M(\mathbf{u})] \in D_k\} \\
 &= \int_{D_k} g_{\Sigma}(Z_1, \dots, Z_M) dz_M
 \end{aligned}
 \tag{4.2}$$

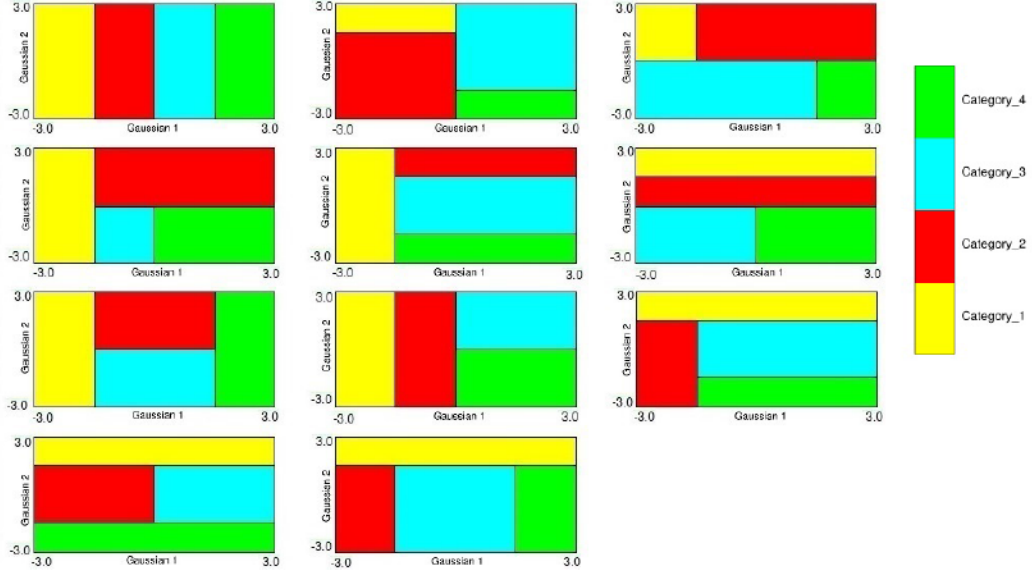


Figure 4.1: Masks for $K = 4$ categories and $M = 2$ Gaussian functions (modified from [Armstrong et al. \(2011\)](#)).

For M Gaussian functions and K categories, there are $K \times 2^M$ thresholds. There are many possible configurations even for a rectangular partition. As demonstrated in Figure 4.1, for $K = 4$ categories and $M = 2$ Gaussian functions there are 11 possible masks ([Armstrong et al., 2011](#)). Masks with linear thresholds can be defined based on geological knowledge of the frequency of intersections between categories. A program ("*tpgsim*") (Appendix, A.1) is developed to generate the threshold mask. This program is flexible and covers the most common combinations between categories. This mask is defined with three main zones (left, center, right). In this program users can easily define the mask between categories based on their geological knowledge. This relation is only defined with two parameters: the number of rectangles and the position of rectangles in each zone. The sample mask that is shown in Figure 4.2 is defined using

the relationship between nine categories. Notice that the number of rectangles should be equal to the number of categories. There are four categories in the left zone, two categories in the center zone, and three categories in the right zone. The order of categories to be placed in the mask in this program for the vertical position is from the left side to the right side and in the horizontal position is from bottom to the top. The thresholds can be specified by the target global proportions for each category or the local proportion. This local proportion could come from an aerial trend map or vertical trend.

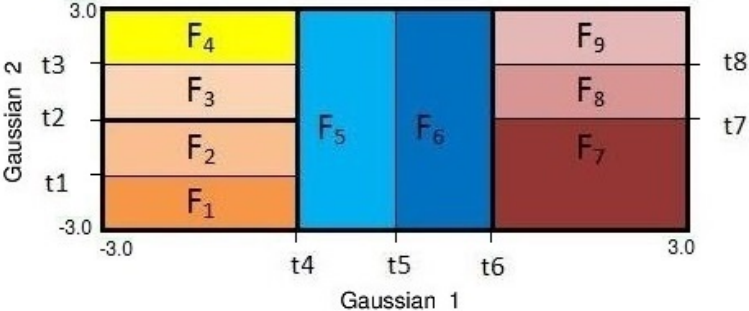


Figure 4.2: Sample truncation rule for truncating bivariate Gaussian functions for 9 categories ($F_k, k = 1, 2, \dots, 9$) with eight thresholds (t_1, \dots, t_8).

There is a one to one relation between the proportions and the thresholds. In the presence of a trend, thresholds of the mask are adjusted to match the local proportion of categories at each location. As explained in Section 4.1, the centroid of each categorical class with respect to the local truncation rules is used to transfer categorical data into continuous Gaussian conditioning data. Data and mask are paired based on the nearest neighbor. At each data location, the nearest local truncation rule based on the trend model is used for transformation. Figure 4.3 shows an example of how a mask can vary in a domain. For instance, category one has a higher proportion in lower elevations in the domain. As the proportion increases or decreases, thresholds are adjusted and created a new mask.

After one finds the locally varying masks and the conditioning data values, truncation using these outputs is straightforward. Output of the locally varying mask can be used as an input to another small utility program "truncation - tp" (Appendix,

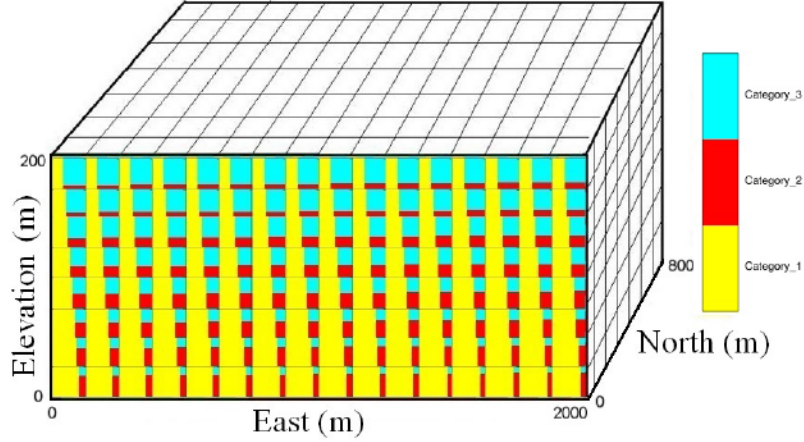


Figure 4.3: Locally varying masks of threshold based mask for one cross section of a synthetic example.

A.1.1) for truncating conditional Gaussian realizations to categorical realizations. In the standard linear threshold framework, the user is able to apply geological knowledge of the nature of the contacts between categories.

4.3 MDS Mask

In MDS mask, dissimilar categories are placed farther apart and similar categories close together based on the distance between categories. The multivariate space is then mapped using an eigen-decomposition. In this method, K categories are projected on M Gaussian variables using metric MDS (Wickelmaier, 2003) of the corrected non-transition probability matrix. These projected coordinates produce K M-dimensional control points. These K control points location are optimized iteratively to reduce the deviation between the desired proportions and integrated probabilities (J. L. Deutsch & Deutsch, 2014). The transition probabilities are used for the determination of a truncation structure using MDS. The probability of transitioning from category k to category k' can be calculated (Eq. 4.3):

$$\mathbf{tp}_{kk'} = Prob\{k' \text{ occurs at } u + h | k \text{ occurs at } u\} \quad (4.3)$$

The transition probability matrix with K categories is defined as Eq.4.4:

$$\mathbf{tp}(h) = \begin{bmatrix} tp_{11} & tp_{12} & tp_{13} & \cdot & \cdot & \cdot & tp_{1K} \\ tp_{21} & tp_{22} & tp_{23} & \cdot & \cdot & \cdot & tp_{2K} \\ tp_{31} & tp_{32} & tp_{33} & \cdot & \cdot & \cdot & tp_{3K} \\ \cdot & & & \cdot & & & \cdot \\ \cdot & & & & \cdot & & \cdot \\ \cdot & & & & & \cdot & \cdot \\ tp_{K1} & tp_{K2} & tp_{K3} & \cdot & \cdot & \cdot & tp_{KK} \end{bmatrix} \quad (4.4)$$

Transition probabilities are calculated from the transition between categories both upward and downward in a drill hole as illustrated in Figure 2.1. A symmetric MDS algorithm is considered in this method. To use the metric MDS method, a symmetric dissimilar matrix is required. The idea here is to convert the transition probability matrix from measuring similarity to a corrected not-transition probability matrix (\mathbf{tp}^{cs}) to measure dissimilarity between categories. The steps include the following:

1. After finding $K \times K$ transition probability matrix (\mathbf{tp}), convert it to not-transition probability matrix by calculating $\mathbf{tp}^c = 1 - \mathbf{tp}$;

$$\mathbf{tp}^c(h) = \begin{bmatrix} 1 - tp_{11} & 1 - tp_{12} & 1 - tp_{13} & \cdot & \cdot & \cdot & 1 - tp_{1K} \\ 1 - tp_{21} & 1 - tp_{22} & 1 - tp_{23} & \cdot & \cdot & \cdot & 1 - tp_{2K} \\ 1 - tp_{31} & tp_{32} & 1 - tp_{33} & \cdot & \cdot & \cdot & 1 - tp_{3K} \\ \cdot & & & \cdot & & & \cdot \\ \cdot & & & & \cdot & & \cdot \\ \cdot & & & & & \cdot & \cdot \\ 1 - tp_{K1} & 1 - tp_{K2} & 1 - tp_{K3} & \cdot & \cdot & \cdot & 1 - tp_{KK} \end{bmatrix} \quad (4.5)$$

2. Correct the not-transition probability matrix by averaging cross terms and setting the diagonal to zero (\mathbf{tp}^{cs});

$$\mathbf{tp}^{cs}(h) = \begin{bmatrix} 0 & 1 - \left(\frac{tp_{12}+tp_{21}}{2}\right) & \cdot & \cdot & \cdot & 1 - \left(\frac{tp_{1K}+tp_{K1}}{2}\right) \\ 1 - \left(\frac{tp_{12}+tp_{21}}{2}\right) & 0 & \cdot & \cdot & \cdot & 1 - \left(\frac{tp_{2K}+tp_{K2}}{2}\right) \\ 1 - \left(\frac{tp_{13}+tp_{31}}{2}\right) & 1 - \left(\frac{tp_{32}+tp_{23}}{2}\right) & \cdot & \cdot & \cdot & 1 - \left(\frac{tp_{3K}+tp_{K3}}{2}\right) \\ \cdot & \cdot & \cdot & \cdot & \cdot & \cdot \\ \cdot & \cdot & \cdot & \cdot & \cdot & \cdot \\ \cdot & \cdot & \cdot & \cdot & \cdot & \cdot \\ 1 - \left(\frac{tp_{1K}+tp_{K1}}{2}\right) & 1 - \left(\frac{tp_{2K}+tp_{K2}}{2}\right) & \cdot & \cdot & \cdot & 0 \end{bmatrix} \quad (4.6)$$

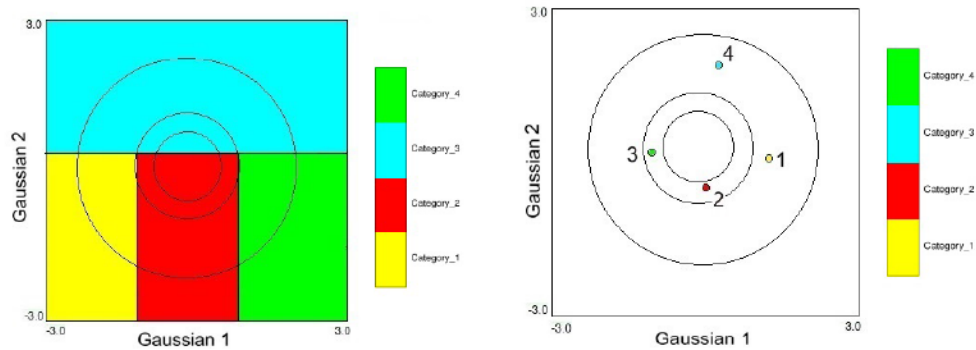
Now using a standard MDS algorithm, a centered not-transition probability matrix (\mathbf{tp}^{cs}) can be spectrally decomposed and projected on to M Gaussian deviates. Generally, the number of dimensions for projection is less than the number of categories K (at most $K - 1$). So, projected coordinates create K M-dimensional control points. These control points are rescaled to be mapped into a standard Gaussian unit.

In the last step, control point locations are optimized iteratively. A Voronoi decomposition of the control points is performed to define the polygon related to each category, and the multivariate Gaussian distribution is integrated over each Voronoi polygon. The control point locations are optimized to reduce the difference between the desired proportions and integrated probabilities.

For any location in the multivariate Gaussian domain, the category associated with this location is equal to the category associated with the nearest control point (Eq. 4.7):

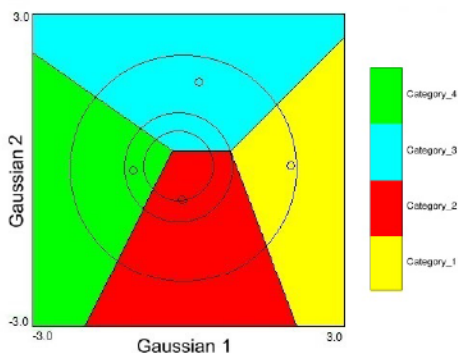
$$Z(\mathbf{u}) = \{Z(\mathbf{u}_{k'}) | (\mathbf{u} - \mathbf{u}_{k'}) \leq (\mathbf{u} - \mathbf{u}_k) \quad k = 1, \dots, K \quad k \neq k'\} \quad (4.7)$$

This framework has the benefit of requiring no user input regarding the nature of the mask. Figure 4.4 shows an example of the evolution of the MDS method for four categories and two Gaussian deviates.



(a) Initial mask integrated to the global proportions

(b) Rescaled MDS coordinates



(c) Optimized control points

Figure 4.4: Evolution of MDS method for four categories (J. L. Deutsch & Deutsch, 2014).

4.4 Locally Varying Mask with MDS Mask

In the presence of LVP, optimization begins with determination of the truncation mask for the first location in the grided domain. The K categories are projected on to M Gaussian variables using MDS. These projected coordinates compose control points which will be used for truncation of M underlying Gaussian realizations. Then optimization continues to determine the truncation mask for the next and other locations. In each step, the optimized control points of the previous location are considered as initial solution to the optimization. By the end of the optimization process, optimized MDS masks are constructed based on the LVP of categories at every location.

Figure 4.5 shows the locally varying mask in a domain with a bigaussian MDS mask. An optimization is performed at each location in the model to match the integrated

proportion of categories to the local proportions. A program "*mds_tpg_LVP*" is developed (Appendix, A.2) to deal with trends. Due to the nature of trend models which are smooth, finding the mask for every location may not be required. An up-scaling of the trend model while honoring the local heterogeneities in category properties is proposed as an option since proportions vary smoothly in the domain.

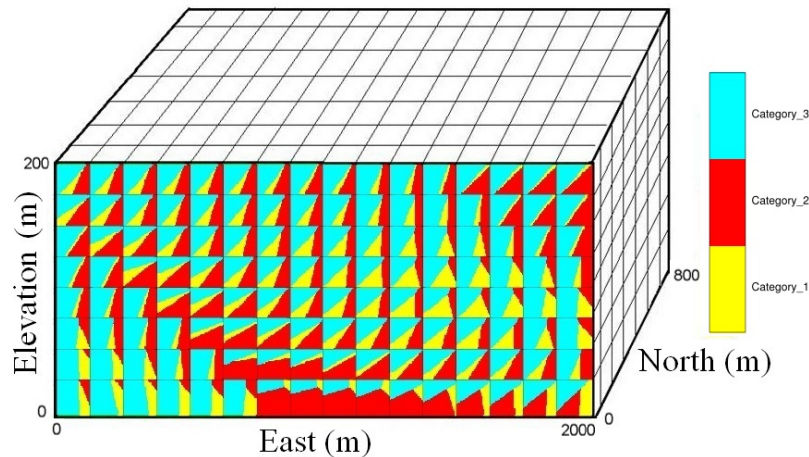


Figure 4.5: Locally varying masks in TPG simulation with a MDS mask for one cross section of a synthetic example.

After finding the locally varying mask and conditioning data values, truncating M underlying Gaussian functions using these outputs is straightforward. The output of a locally varying mask can be used as an input to "*trans_tpg_LVP*" (Appendix, A.2.1) for truncating conditional Gaussian realizations to categorical realization.

4.5 Case Study

A mineral deposit is simulated with data from 31 drill holes. The deposit has a number of well-defined layers. Drill holes contain measurements for the four different rock types. Figure 4.6 shows the available drill hole data and the projection onto East-North and North-Elevation slices. The geostatistical models are simulated at $10.0 \times 10.0 \times 10.0$ (m)³ resolution. The vertical drill holes are regularly spaced. The global proportion of rock types using cell declustering is summarized in Table 4.1.

Simulating the different rock types is the first step in geostatistical modeling before

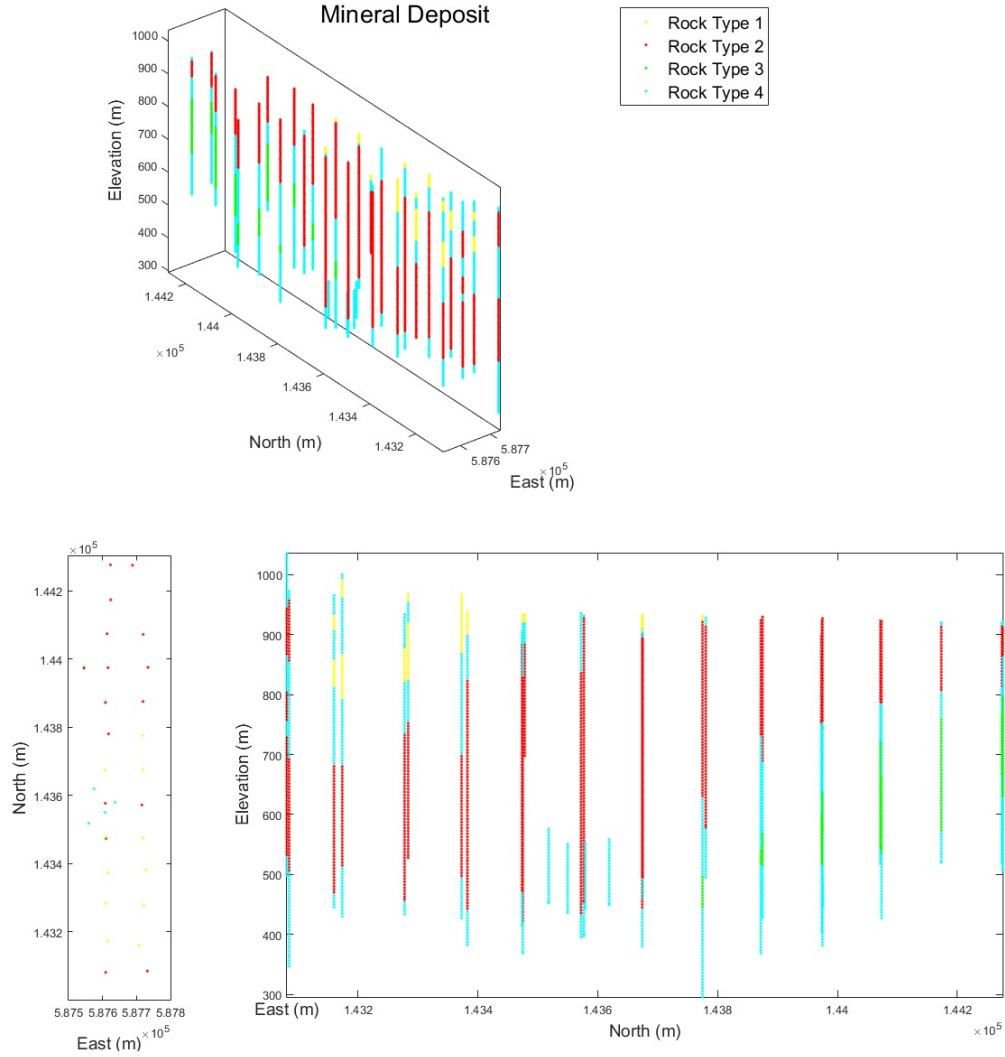


Figure 4.6: Location map of available drill hole data and projection onto a North-East and East-Elevation plans.

Table 4.1: Summary of rock types' declustered proportions in drill hole data.

	Rock Type 1	Rock Type 2	Rock Type 3	Rock Type 4
DH Prop.	0.048	0.497	0.081	0.382

assigning and simulating grades within the rock types. For this deposit, the transition probability matrix is calculated (Eq. 4.8). The transition probability matrix shows that rock type one is linked to rock type four, and we expect occasionally to see this rock type linked to rock type two. Also rock type three is related to rock type four more frequently. Figure 4.7 shows the global threshold mask and MDS mask.

$$\mathbf{tp}(h) = \begin{bmatrix} 0.9090 & 0.0050 & 0.0000 & 0.0860 \\ 0.0004 & 0.9816 & 0.0000 & 0.0180 \\ 0.0000 & 0.0000 & 0.9520 & 0.0490 \\ 0.0090 & 0.0240 & 0.0110 & 0.9570 \end{bmatrix} \quad (4.8)$$

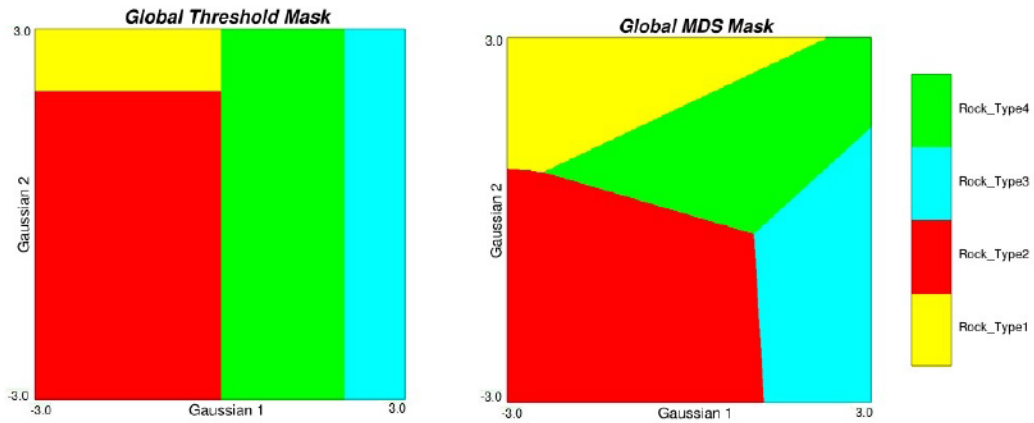


Figure 4.7: Left: Global threshold based mask and right: MDS mask for a mineral deposit with four rock types.

Due to no clear horizontal anisotropy, a horizontal omnidirectional is calculated for all four rock types. There is a non-stationary in the proportion of rock types in the deposit and some rock types are more probable to prevail in some areas than in others. For building a conceptual model of a deposit, understanding the spatial distribution of the categories and the geometry of the domain is essential. Vertical proportion curves (VPCs) provide information on the categories within the sequences. This method is useful to specify where the important vertical variation is likely to be, to decide about the non-stationarity. When the relative proportions of categories vary significantly within a domain, consequently non-stationarity exists. The spatial distribution of the proportions is shown in Figure 4.8.

Variation of the proportion of rock types in the vertical direction is observed clearly in Figure 4.8. Figure 4.9 shows the trend model that has been generated based on the data using the GSLIB "maketrend" program (Manchuk & Deutsch, 2011). The trend

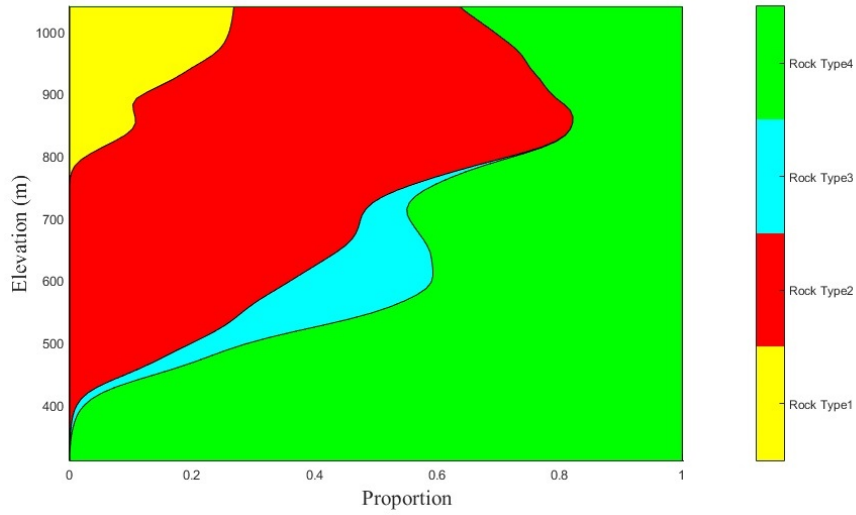


Figure 4.8: Global VPC for the mineral deposit.

model demonstrates the locally varying proportion of each plate in different locations of the area of interest.

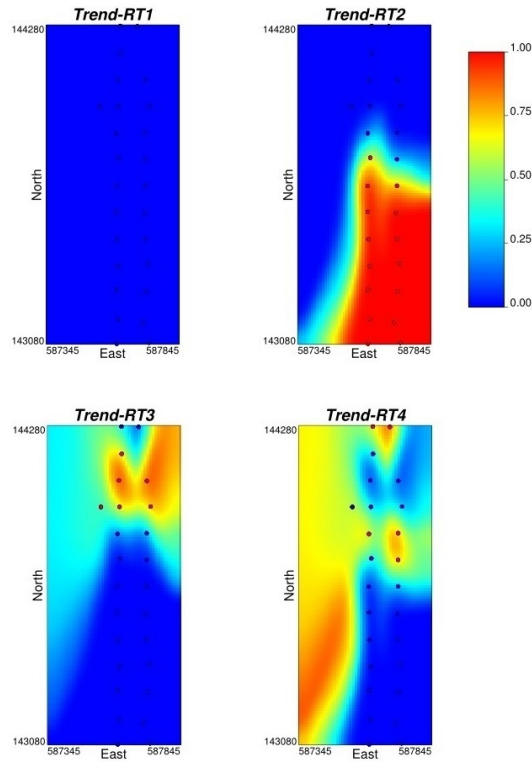


Figure 4.9: Plan view of generated trend model for rock types based on the data sets at elevation 600(m).

The locally varying mask is calculated for each mask in the model. To illustrate the reproduction of rock types' proportions in the simulated realization, Table 4.2 summarizes the proportion reproduction of the bench of elevation 600 (m) in the simulated realization using threshold based and MDS masks. Local proportions of rock types have been reproduced well.

Table 4.2: Summary of the integrated proportions in truncated realization using TPG method at elevation 600(m).

Proportion at elevation 600(m)	RT 1	RT 2	RT 3	RT 4
Trend model	0.000	0.372	0.221	0.407
Simulation with threshold mask	0.000	0.393	0.261	0.346
Simulation with MDS mask	0.000	0.335	0.246	0.419

Optimized locally varying masks at elevation 900(m) for 140 locations for both mask frameworks are shown in Figure 4.10. At this elevation, the probability of rock type three is very small and three other proportions vary smoothly (Figure 4.11). The proportion of rock type four increases gradually from East to West, while the proportion of rock type two decreases.

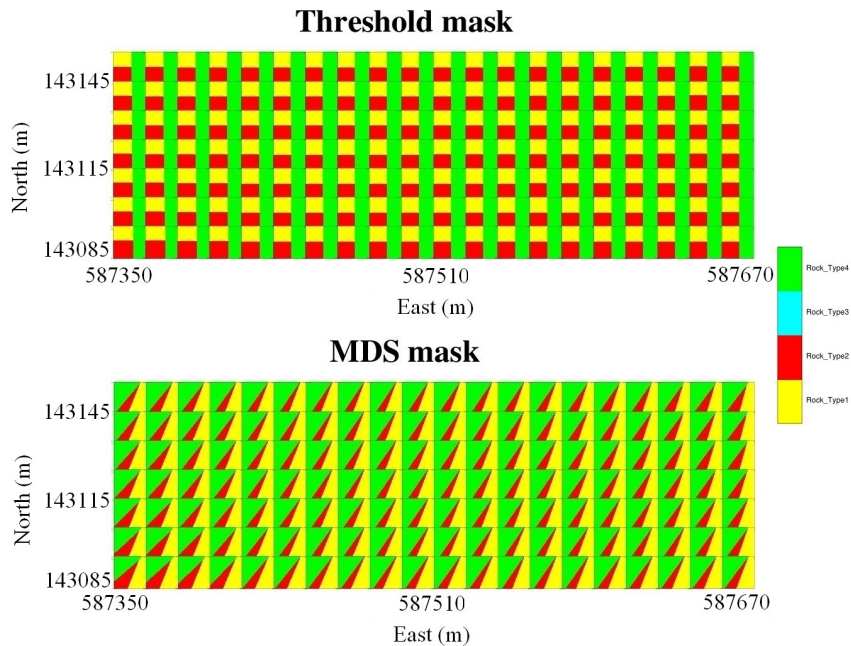


Figure 4.10: Top: plan view of optimized threshold mask and bottom: plan view of optimized MDS mask at elevation 900(m) for 140 locations in the simulated domain.

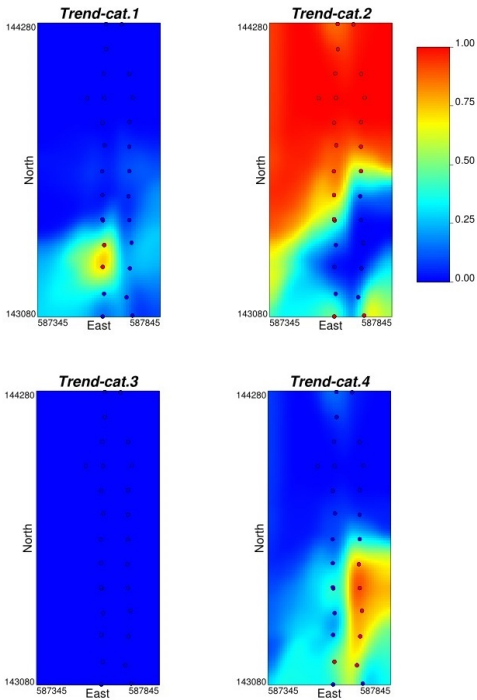


Figure 4.11: Plan view of generated trend model for rock types based on the data sets at elevation 900(m)

Since the trend is varying smoothly, the trend model is composited to $30 \times 50 \times 30 m^3$. Figure 4.12 right side demonstrates the up scaled trend model for composited elevations 870-900(m). The plan view of the MDS mask with the up scaled trend model for composited elevations is shown in Figure 4.12. Gradual variation of the mask based on the LVP is clearer in this Figure 4.13.

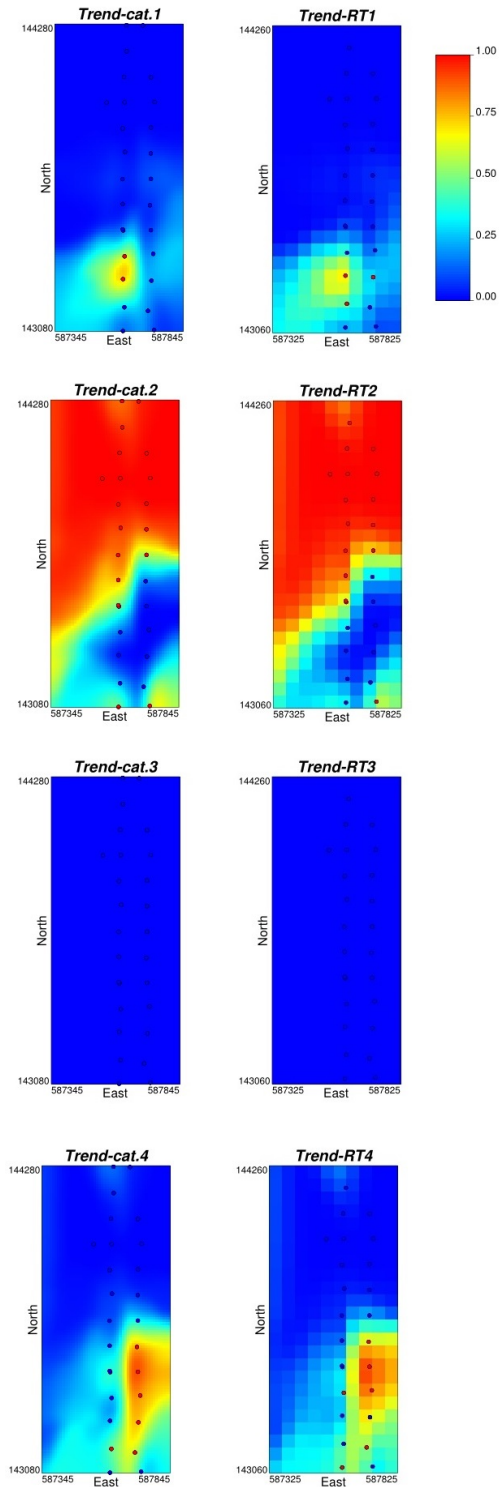


Figure 4.12: Left: plan view of trend model and right: plan view of up scaled trend model for rock types.

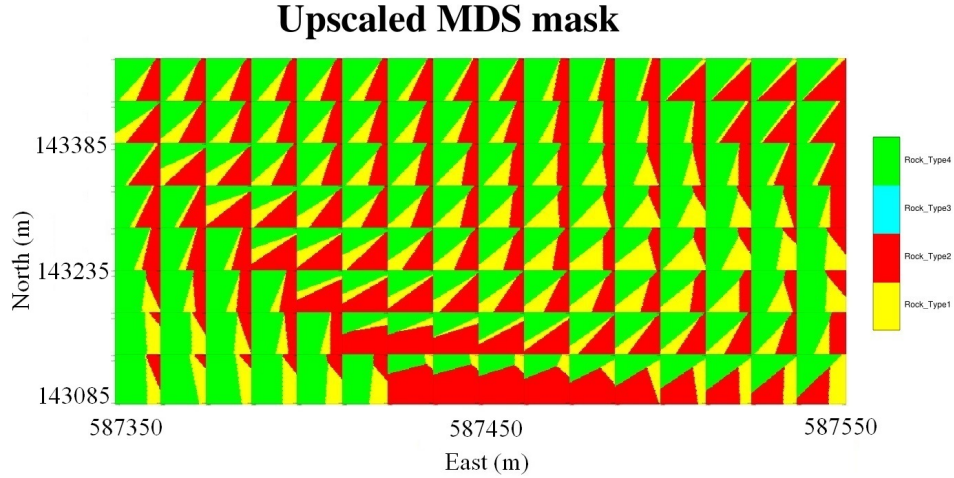


Figure 4.13: Plan view of optimized up scaled MDS mask for composited elevations 870-900(m) for 128 blocks in the simulated domain.

A comparison is performed between the results of TPG simulation using the proposed algorithm with SIS. A 3D view of TPG realization using these two type of masks and generated realization with SIS is demonstrated in Figure 4.14. To show the importance of considering a locally varying mask, simulated realizations without a trend model using only the global proportion of categories are shown in Figure 4.14. It is clear that simulated realization did not respect the observed trend in the data and did not reproduce the right transitioning structures. For instance, rock type one is not expected to be observed in the lower elevations as it simulated in the model using global mask. Figure 4.15 shows a comparison of local proportion reproduction using TPG methods and SIS method at elevation 700(m). Local proportions for this elevation are as follows: 0.000, 0.442, 0.075, and 0.483 for rock types one to four, respectively. The average percent errors in proportion reproduction of all four rock types using the TPG method with threshold based and MDS masks are 4.25% and 6.3%, respectively, and for SIS method, 7.13%. There is less error in reproduction of rock types' proportions using TPG methods than with SIS method, but not a very significant difference.

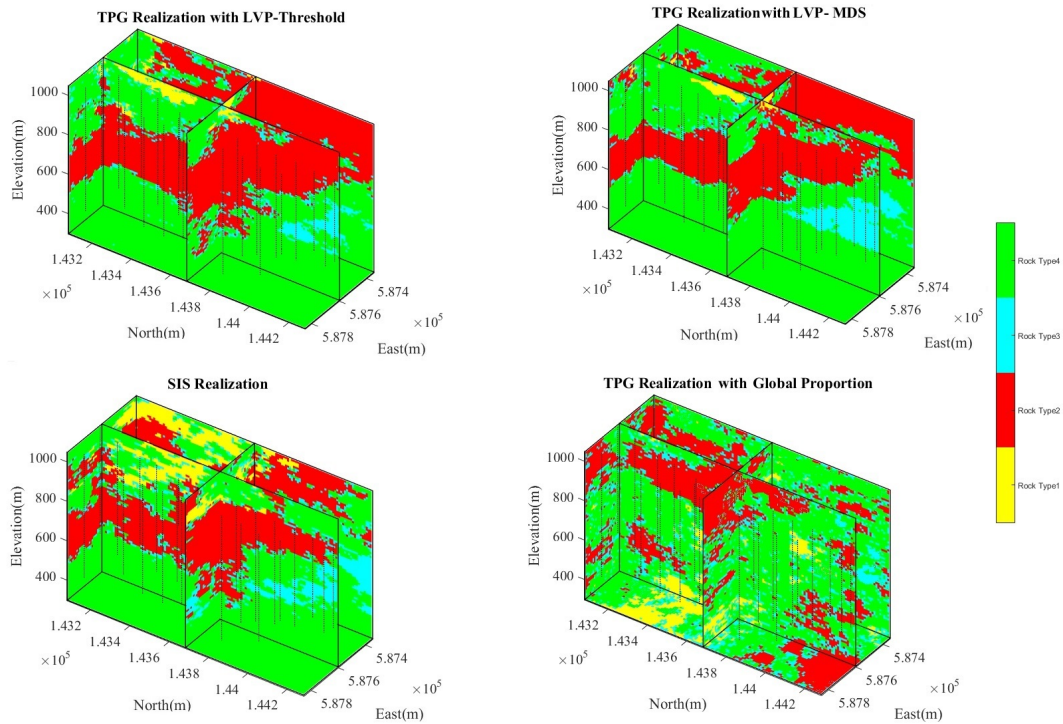


Figure 4.14: 3D view of simulated realizations. Top left: realization using TPG method with threshold based mask and top right: using MDS mask. Bottom left: generated realization with SIS method and bottom right: TPG realization using global mask.

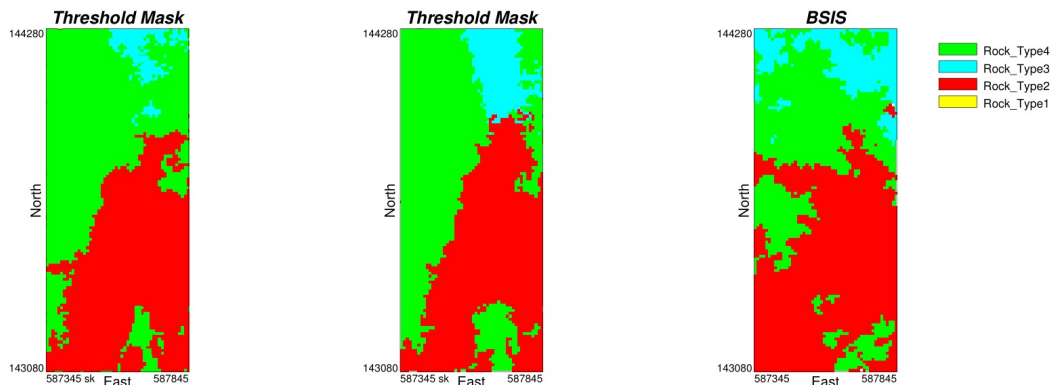


Figure 4.15: Simulated realizations at elevation 700 (m) using TPG simulation and SIS simulation methods.

4.6 Summary

In this chapter, the importance of using a locally varying mask in the presence of a trend has been demonstrated through a case study. It is usually not realistic to consider

a global truncation mask when there is a higher probability of having some rock types in some areas than in others. TPG simulation is able to impose spatial changes in the categories proportions by adopting an appropriate mask for every location. Simulation with locally varying mask generates realistic images of deposits with a complex geology. LVP with the threshold based mask is fast but required more CPU time in use of LVP with MDS mask. To address this limitation, use of an up scaled trend is possible.

Chapter 5

Correlation between Underlying Gaussian RFs in TPG Simulation

Underlying Gaussian RFs in TPG simulation should be defined in a way that describes different spatial behavior of a category or group of categories after truncation. Usually, Gaussian RFs are considered as independent variables in TPG simulation. Correlation depends on the construction of categories. Correlation between Gaussian RFs impacts the calculation of variograms and mask thresholds from the experimental proportions. Depending on the case, TPG models can be obtained by using dependent or independent Gaussian RFs, or any linear transform of RFs, or translated RFs. This chapter investigates the effects of correlated underlying Gaussian RFs on TPG simulation. Generally, a very complex truncation method or correlation between the underlying Gaussian RFs can be selected if it is required for ordering or for allowing all possible transitions between categories. Complex geological relationship between categories can be produced by choosing different Gaussian RFs.

In TPG simulation, Gaussian deviates can be correlated. [Galli et al. \(1994\)](#) showed the potential of TPG method to produce geologically realistic images by truncation of two or more Gaussian RFs, which can be either correlated or not. [Le Loch, Beucher, Galli, and Doligez \(1994\)](#) used the linear model of coregionalisation to generate correlated Gaussian RFs and showed that transition between categories approximately depends on category proportion and the correlation between Gaussian deviates. They found that even using uncorrelated Gaussian RFs, the categories in truncated simula-

tion are not independent. [Le Loch and Galli \(1997\)](#) addressed the structural analysis and conditional simulations in two steps when underlying Gaussian deviates are linked by the linear model of coregionalisation. [Armstrong and Galli \(1999\)](#) explained the mathematical theory of truncated bigaussian simulation when the second Gaussian realization is a partial derivative of the first Gaussian realization.

[Dowd, Pardo-Igúzquiza, and Xu \(2003\)](#) introduced the correlation coefficient as a tuning parameter that can be used to improve the fit of the experimental indicator semivariogram and cross semivariograms. They developed a program to calculate the goodness-of-fit between the experimental and theoretical indicator semivariograms and cross semivariograms based on semivariograms and the correlation coefficient of the Gaussian RFs. [Liu, Oliver, et al. \(2003\)](#) used correlated RFs for historic production (history-matching) to generate the conditional simulation of facies boundaries by TPG method. They pointed out that results are consistent with the geological model of observed facies as well as historic production. [Galli et al. \(2006\)](#) used an example involving algal bioconstructions in the outcrops of the Paradox basin (Utah). They considered complex horizontal and vertical transitions between the mound and inter mound facies, together with the complex geometry of the algal mounds. They used different threshold based masks for different areas; to accentuate the draping of the one facies over another, a correlation coefficient of -0.5 between the two Gaussian RFs was considered. In this case, correlation between Gaussian RFs is used to reproduce the observed geological feature in the data.

The correlation coefficient ρ can be used to introduce an additional degree of freedom and more flexibility in the modeling. The constrained propagative Gibbs sampler ([Emery et al., 2014](#)) has been generalized by [Astrakova et al. \(2015\)](#) to address the problem of conditioning of correlated Gaussian RFs to categorical data.

5.1 Correlation Matrix

Correlation varies between $-1 < \rho < 1$. The correlation matrix for two Gaussian RFs is formulated as Eq. 5.1:

$$\Sigma = \begin{pmatrix} 1 & \rho \\ \rho & 1 \end{pmatrix} \quad (5.1)$$

There are coregionalization models with two Gaussian RFs (Z_1, Z_2) in bivariate Gaussian simulation. For instance, the standard linear coregionalization model where Z_1 and Z_2 are linear combinations of independent factors can be used. Consider $Y_1(\mathbf{u})$ and $Y_2(\mathbf{u})$ as two independent Gaussian RFs ($N(0, 1)$) with the covariances $\rho_{Y_1}(\mathbf{h})$ and $\rho_{Y_2}(\mathbf{h})$. Therefore $Z_1(\mathbf{u})$ and $Z_2(\mathbf{u})$ can be defined as Eq. 5.2 (Le Loch & Galli, 1997):

$$Z_1(\mathbf{u}) = Y_1(\mathbf{u}) \quad \text{and} \quad Z_2(\mathbf{u}) = \rho Y_1(\mathbf{u}) + \sqrt{1 - \rho^2} Y_2(\mathbf{u}) \quad (5.2)$$

where:

$$\rho_{Z_1}(\mathbf{h}) = \rho_{Y_1}(\mathbf{h}) \quad \text{and} \quad \rho_{Z_2}(\mathbf{h}) = \rho^2 \rho_{Y_1}(\mathbf{h}) + (1 - \rho^2) \rho_{Y_2}(\mathbf{h}) \quad (5.3)$$

or

$$\rho_{Y_1}(\mathbf{h}) = \rho_{Z_1}(\mathbf{h}) \quad \text{and} \quad \rho_{Y_2}(\mathbf{h}) = \frac{\rho_{Z_2}(\mathbf{h}) - \rho^2 \rho_{Y_1}(\mathbf{h})}{1 - \rho^2}$$

$\rho_{Z_1 Z_2}(\mathbf{h}) = \rho \rho_{Z_1}(\mathbf{h})$ is the cross-covariance, and the covariance matrix Σ is defined as Eq. 5.4:

$$\Sigma = \begin{pmatrix} 1 & \rho & \rho_{Z_1}(\mathbf{h}) & \rho \rho_{Z_1}(\mathbf{h}) \\ \rho & 1 & \rho \rho_{Z_1}(\mathbf{h}) & \rho_{Z_2}(\mathbf{h}) \\ \rho_{Z_1}(\mathbf{h}) & \rho \rho_{Z_1}(\mathbf{h}) & 1 & \rho \\ \rho \rho_{Z_1}(\mathbf{h}) & \rho_{Z_2}(\mathbf{h}) & \rho & 1 \end{pmatrix} \quad (5.4)$$

Generally, when the correlation coefficient is zero, $Z_1(\mathbf{u}), Z_2(\mathbf{u})$ correspond to $Y_1(\mathbf{u}), Y_2(\mathbf{u})$. When the correlation coefficient is 1, $Z_1(\mathbf{u}), Z_2(\mathbf{u})$ both correspond to $Y_1(\mathbf{u})$

and is the simple truncated Gaussian method. When the correlation coefficient is -1 , $Z_1(\mathbf{u})$ correspond to $Y_1(\mathbf{u})$ and $Z_2(\mathbf{u})$ correspond to $-Y_1(\mathbf{u})$. It means that $Z_2(\mathbf{u})$ is like $Z_1(\mathbf{u})$, but with an opposite categorical ranking, for instance 1, 2, 3 becomes 3, 2, 1.

A synthetic example is considered here to illustrate the effect of correlated Gaussian RFs on the proportion of the categories, thresholds of the mask, variogram of the correlated Gaussian variable, and variogram of indicator variables.

Two independent and unconditional Gaussian realizations ($M = 2$) Y_1 and Y_2 are simulated by a sequential Gaussian simulation program (SGSIM, (C. V. Deutsch et al., 1992)) with a spherical variogram model but a different anisotropy (Figure 5.1). The modeling grid is composed of 256×256 blocks of $10 \times 10m^2$ for both realizations. Consider global proportions of categories to be 0.304, 0.175, 0.205 and 0.319, respectively for $k = 1, \dots, 4$ and Figure 5.2 as the truncation rule to truncate Gaussian deviates into categories. Here, partitions defined by rectangles are parallel to the axes and defined by four thresholds (two thresholds for each RF Z_1 and Z_2). Since there is a linear relationship between (Z_1, Z_2) and (Y_1, Y_2) based on Eq. 5.2, the rectangles in the plane (Z_1, Z_2) become parallelograms in the plane (Y_1, Y_2) . The lines parallel to Z_2 (Eq. 5.2; $Z_1 = constant$) remain parallel to Y_2 (Eq. 5.2; $Y_1 = constant$), and the lines parallel to Z_1 (Eq. 5.2; $Z_2 = constant$) become oblique (Eq. 5.2; $\rho Y_1(\mathbf{u}) + \sqrt{1 - \rho^2} Y_2(\mathbf{u}) = constant$).

Consider four thresholds to define the area of each rectangle, two threshold $[a_1, a_2]$ related to Z_1 and two threshold $[b_1, b_2]$ related to Z_2 . Consider ρ as the correlation between Gaussian RFs. Therefore, the proportion of categories at \mathbf{u} can be calculated by Eq. 5.5 (Le Loch & Galli, 1997):

$$\begin{aligned}
 p_k &= P(a_1 \leq Z_1(\mathbf{u}) < a_2 \quad \& \quad b_1 \leq Z_2(\mathbf{u}) < b_2) & (5.5) \\
 &= P(a_1 \leq Y_1(\mathbf{u}) < a_2 \quad \& \quad b_1 \leq \rho Y_1(\mathbf{u}) + \sqrt{1 - \rho^2} Y_2(\mathbf{u}) < b_2) \\
 &= P(a_1 \leq Y_1(\mathbf{u}) < a_2 \quad \& \quad \frac{b_1 - \rho Y_1(\mathbf{u})}{\sqrt{1 - \rho^2}} \leq Y_2(\mathbf{u}) < \frac{b_2 - \rho Y_1(\mathbf{u})}{\sqrt{1 - \rho^2}})
 \end{aligned}$$

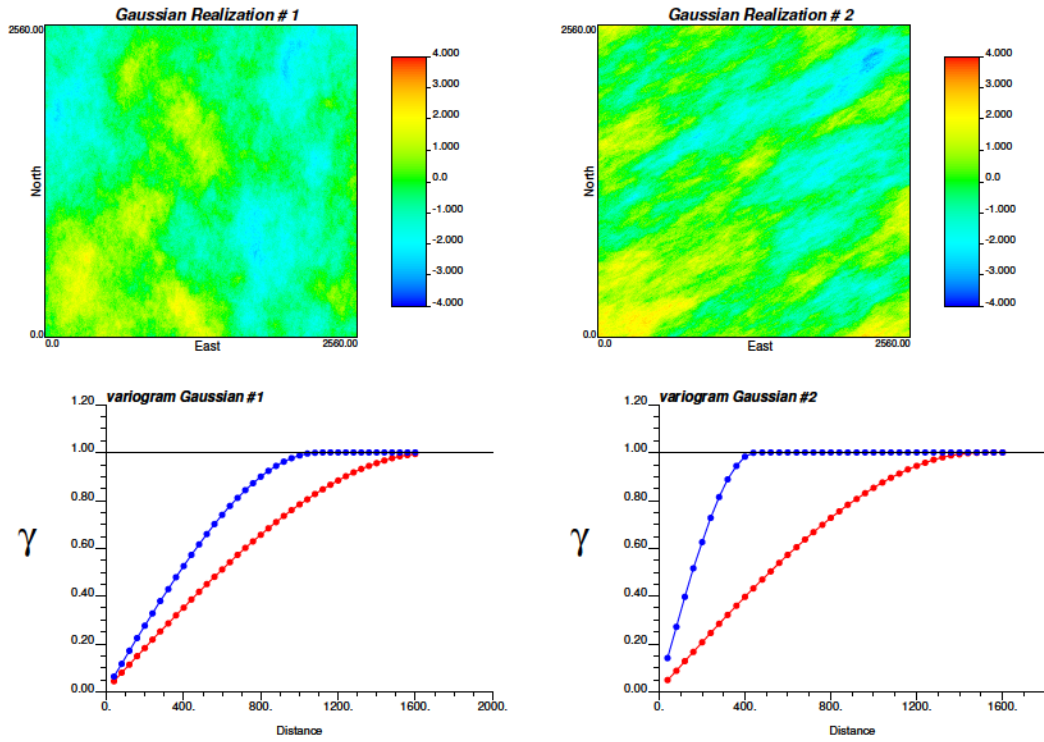


Figure 5.1: Top: two independent Gaussian variables Y_1 and Y_2 . Bottom: related variogram models of each Gaussian variables. Blue color is used for the horizontal minor direction and red is used for the horizontal major direction.

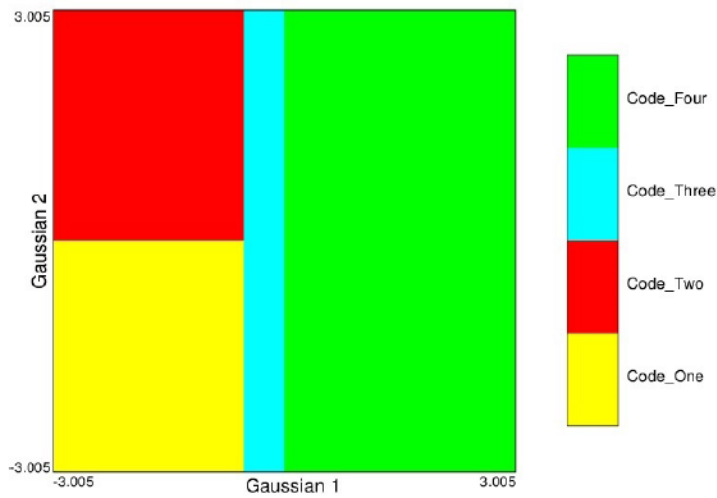


Figure 5.2: Mask for $K = 4$ categories using two Gaussian deviates.

Therefore, when one knows the thresholds and uses the independency of Gaussian variables, Y_1 and Y_2 have (Eq. 5.6):

$$\begin{aligned}
p_k &= \int_{a_1}^{a_2} \int_{\frac{b_1 - \rho w}{\sqrt{1 - \rho^2}}}^{\frac{b_2 - \rho w}{\sqrt{1 - \rho^2}}} f(\mathbf{v}) f(\mathbf{w}) dv dw & (5.6) \\
&= \int_{a_1}^{a_2} [G(\frac{b_2 - \rho w}{\sqrt{1 - \rho^2}}) - G(\frac{b_1 - \rho w}{\sqrt{1 - \rho^2}})] f(w) dw
\end{aligned}$$

where:

p_k - proportion of category k ;

$f(\cdot)$ - probability density of Gaussian distribution $f(v) = \frac{1}{\sqrt{2\pi}\sigma} e^{-\frac{1}{2}(\frac{v-\mu}{\sigma})^2}$;

$G(\cdot)$ - cumulative Gaussian distribution;

Since there is no closed form for the cumulative Gaussian distribution, numerical approximation methods (Beasley & Springer, 1985) are used to calculate the proportion of z_p for the lower tail area of Gaussian distribution related to specified value p (Eq. 5.7). This rule (Eq. 5.6) is true for all the possible configurations of threshold based of masks. For instance, in Figure 5.3 proportion of category one with known $\rho = 0$, $a_2 = -0.825$, and $b_2 = -0.521$ can be found by Eq. 5.8. The same rule is applied for all other categories.

$$\begin{aligned}
p_k &= \int_{-\infty}^{z_p} \frac{1}{\sqrt{2\pi}\sigma} e^{-\frac{1}{2}(\frac{v-\mu}{\sigma})^2} \equiv G(z_p) & (5.7) \\
& z_p = G^{-1}(p_k)
\end{aligned}$$

$$\begin{aligned}
p_1 &= \int_{-\infty}^{a_2} \int_{-\infty}^{b_2} f(\mathbf{v}) f(\mathbf{w}) dv dw = \int_{-\infty}^{-0.825} \int_{-\infty}^{-0.521} f(\mathbf{v}) f(\mathbf{w}) dv dw & (5.8) \\
&= \int_{-\infty}^{-0.825} [G(-0.521) - G(-\infty)] f(w) dw = 0.304
\end{aligned}$$

There is a one-to-one relation between the proportion of categories and the threshold values of the mask when $\rho = 0$. Therefore, by using the proportion of categories and

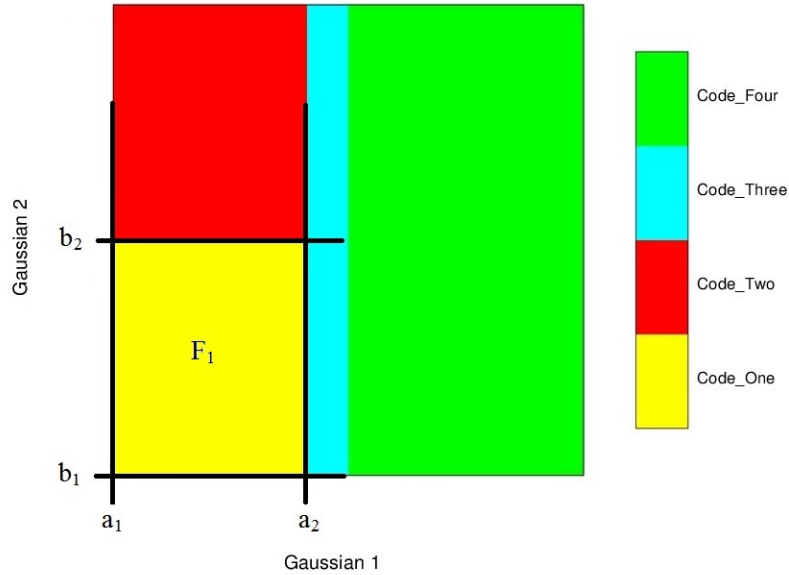


Figure 5.3: Evaluation of proportion of category one using four thresholds.

correlation between Gaussian RFs, the threshold values can be computed.

For the specified mask, distribution of the categories three and four versus the others are controlled by a threshold on Gaussian number one Z_1 . The distribution of categories one and two are controlled by a threshold on Gaussian number two Z_2 . In the next two sections, the effect of correlation on the simulated realizations and threshold mask are investigated.

5.2 Effect of Correlated Gaussian RFs on TPG Realizations

Consider using the global thresholds which are defined based on the global proportions of categories regardless of correlation between Gaussian deviates ($\rho = 0.0$). Figure 5.4 shows the behavior of the realizations when correlation ranges from -0.98 to 0.98 (Figure 5.5). In this case the Gaussian RFs are truncated based on the global thresholds regardless of correlation. In all cases the mask is constant but the proportions of categories are different for each correlation value.

As the correlation increases to positive values, category two almost disappears. Due

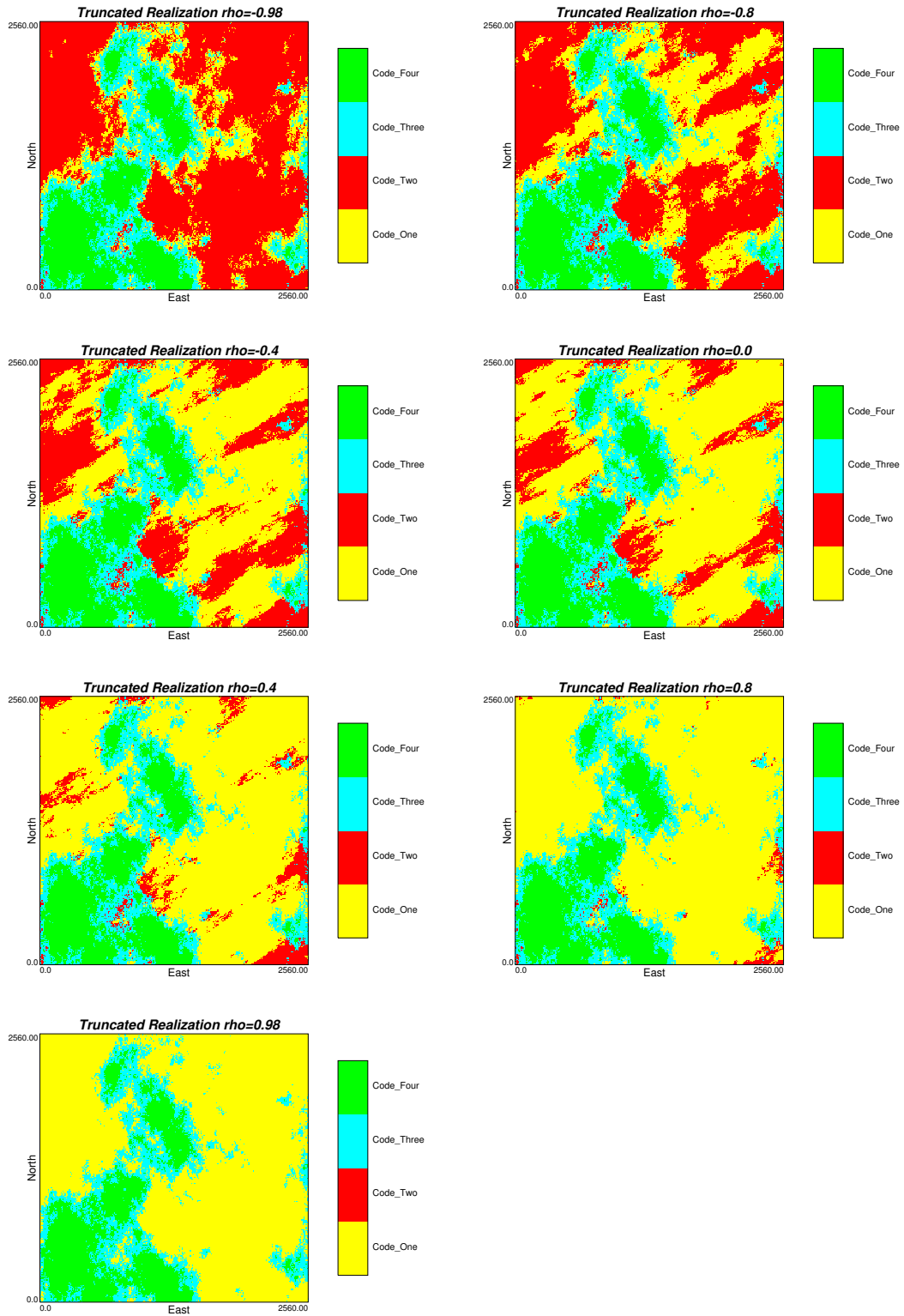


Figure 5.4: Truncated realization for different correlation between Gaussian deviates ($\rho \in (-0.98, 0.98)$) when consider global thresholds (mask).

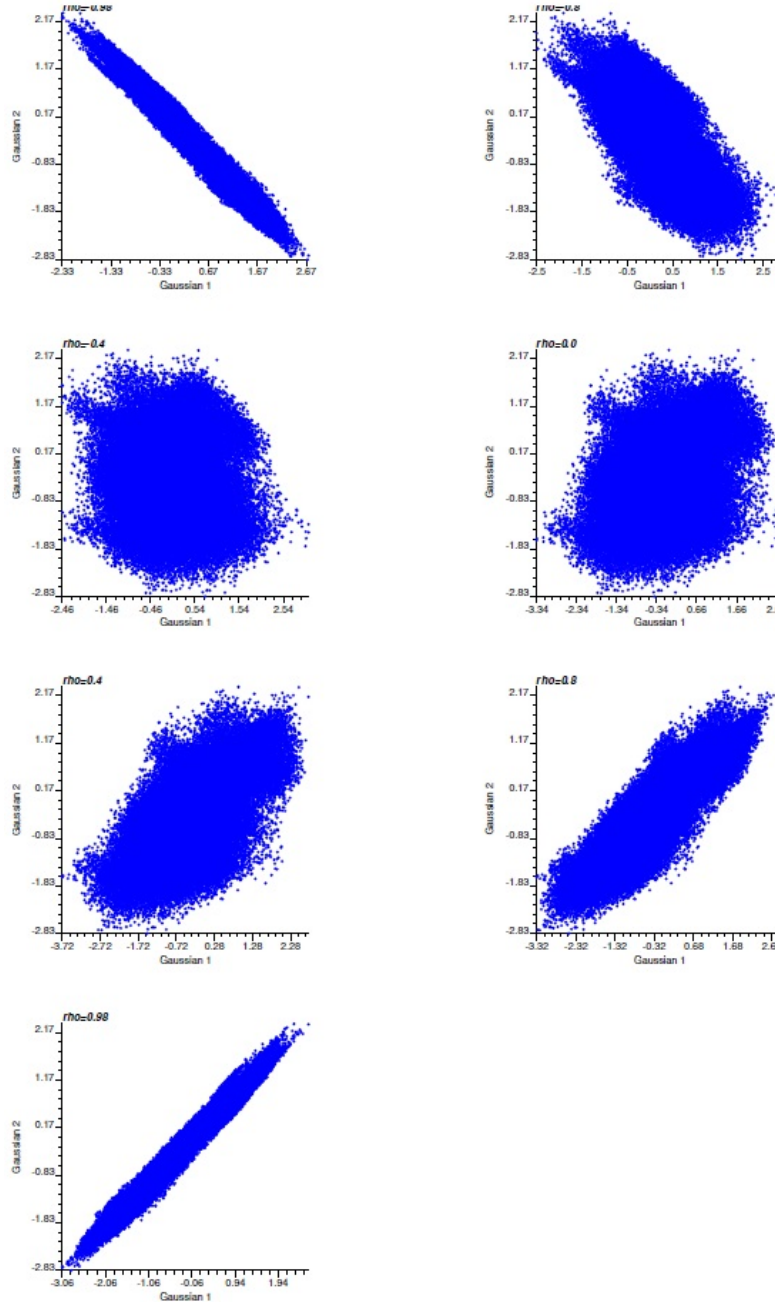


Figure 5.5: Scatter plot of variation of correlation between Gaussian deviates $(-0.98, 0.98)$.

to the completely linear relation between the Gaussian RF when $\rho = 0.98$ (Figure 5.6), there are no points in the area representing category two. Therefore, by fixing the mask and correlation coefficient between Gaussian deviates, the proportions of categories are changed. Based on the Eq. 5.2, Z_1 and Z_2 correspond to $Y_1(\mathbf{u})$ and a simple truncated Gaussian simulation (category 1, category 3, and then category 4) is the result.

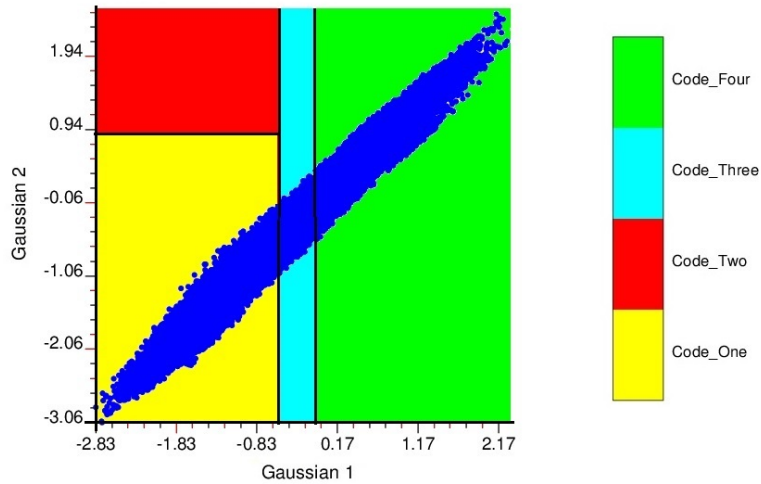


Figure 5.6: Scatter plot of Gaussian deviates with $\rho = 0.98$ and global mask.

Figure 5.7 demonstrates how the global proportion of categories vary for the mentioned mask to have fix thresholds regardless of the correlation coefficient value between Gaussian RFs. Since categories three and four are controlled by only Z_1 , correlation has no impact on the proportions of these categories as expected ($Z_1(\mathbf{u}) = Y_1(\mathbf{u})$).

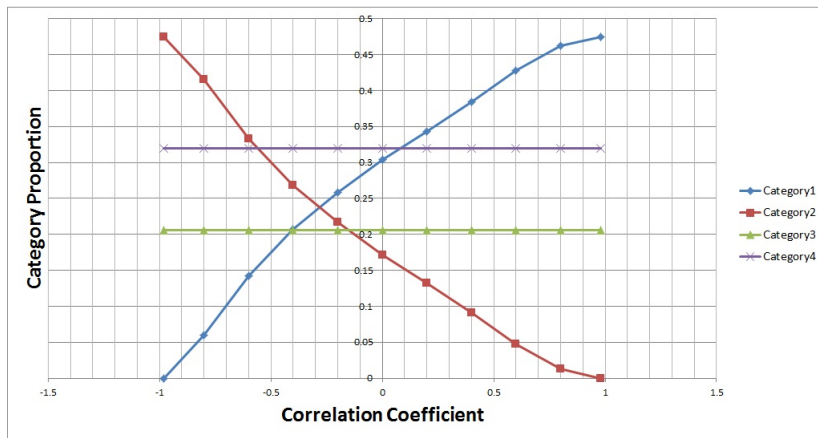


Figure 5.7: Categories proportions for each correlation coefficient with same mask.

Also, correlation has an impact on the variogram of Z_2 . As the correlation increases, the variogram of Z_2 tends to be similar to the variogram of Z_1 (Figure 5.8). When the correlation is -1 , Z_1 corresponds to $Y_1(\mathbf{u})$ and Z_2 corresponds to $-Y_1(\mathbf{u})$.

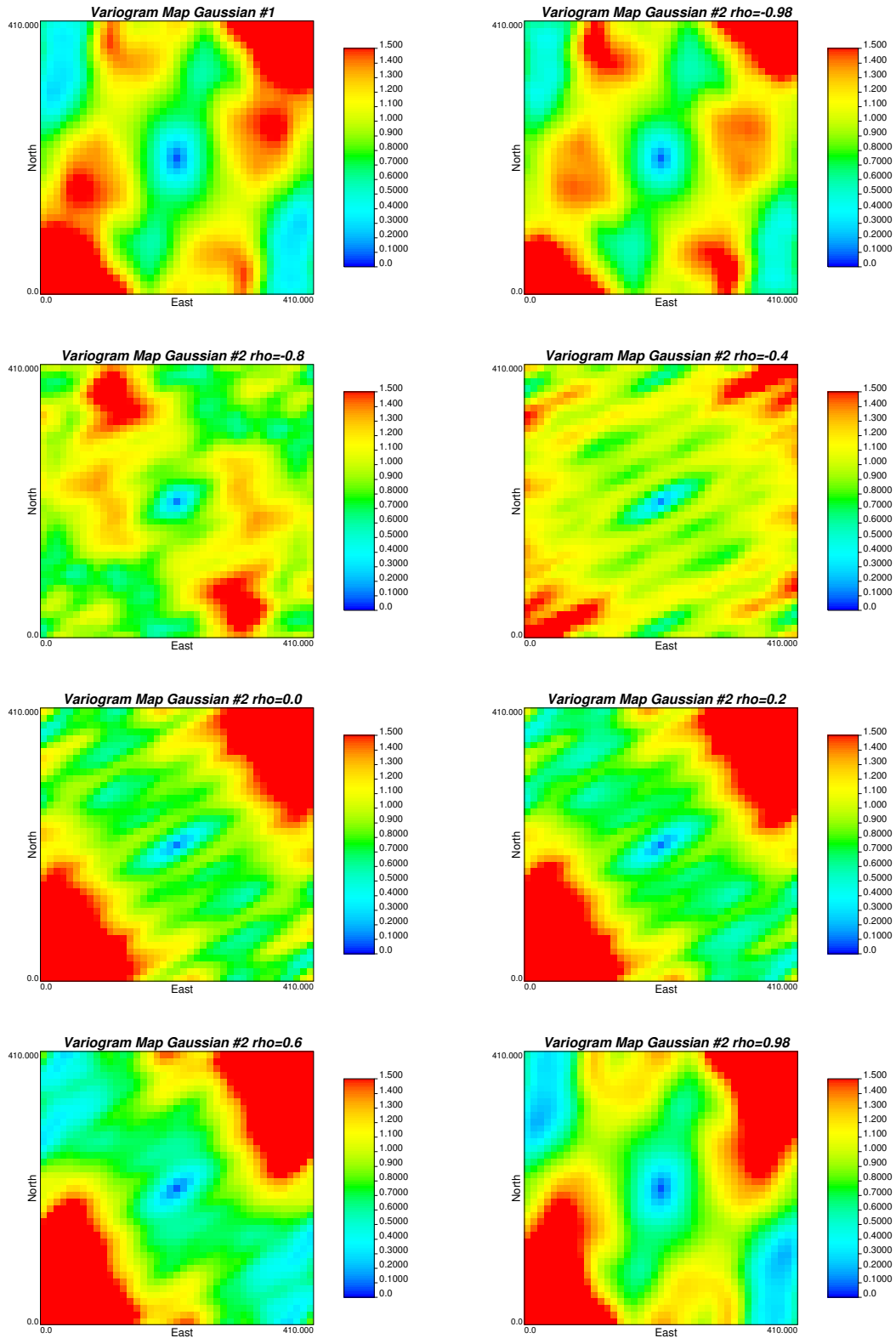


Figure 5.8: Top left: the variogram map of Gaussian RF number one. The rest are the variogram map of correlated Gaussian RF number two with different correlation coefficients.

5.3 Effect of Correlated Gaussian RFs on Mask

For a specific mask, the proportion of each category and the correlation between the underlying Gaussian RFs determine the thresholds. Consider using the global proportion of categories. To honor the global proportions of categories, if the $\rho \neq 0$, the thresholds of mask are changed. Figure 5.9 shows the behavior of truncated realization when correlation between Gaussian deviates is changing from -0.98 to 0.98 .

When the correlation is -1 , Z_1 corresponds to $Y_1(\mathbf{u})$ and Z_2 corresponds to $-Y_1(\mathbf{u})$. Therefore, Z_2 is similar Z_1 , but with an opposite categories ranking (2,1,4,3 becomes 1,2,3,4). An increasing border effect from $\rho = 0.0$ to $\rho = 0.98$ is obvious and the category two progressively wraps around the category one. The category one progressively wraps around the category two. Also, category two and three rarely transition to each other and they are almost separated by category one when the correlation is around -0.98 while the transition increases as the correlation become closer to positive value 0.98 . Figure 5.10 shows the variation of the threshold in the mask to be matched to the global proportions by changing correlation. When Gaussian one and two are independent ($\rho = 0.0$), the threshold display looks like the masks weighted by the proportions.

The correlation impacts the variogram of categories. In Figure 5.9 when the correlation is -0.98 (first image top left), it is obvious that category two is more continuous than category one, but by raising the correlation to 0.98 , opposite continuity can be seen (last image in bottom right) and category one is more continuous than category two. Variogram maps of categories by changing the correlation coefficient between the underlying Gaussian realizations are shown in Figure 5.11 to Figure 5.14.

Correlation plays an important role in the variogram of category one and two, but not three and four. The mask also is an important factor in the behavior of the variogram. Since categories three and four are controlled only by Z_1 , having constant threshold values, constant proportion and the same variogram map for these two categories, regardless of the correlation coefficient between Gaussian RFs, is predicted and expected.

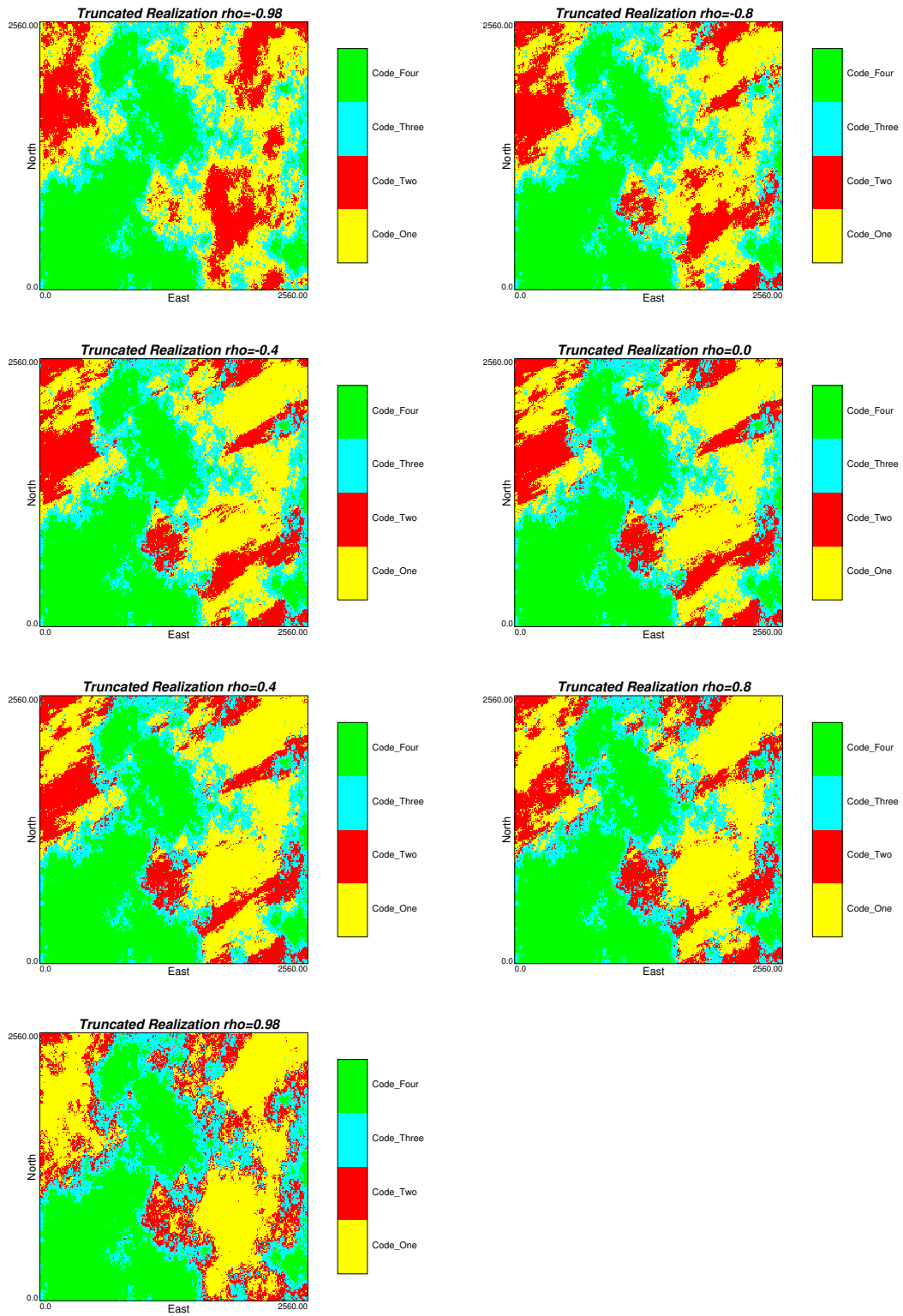


Figure 5.9: Truncated realization for different correlation between Gaussian deviates (from -0.98 to 0.98).

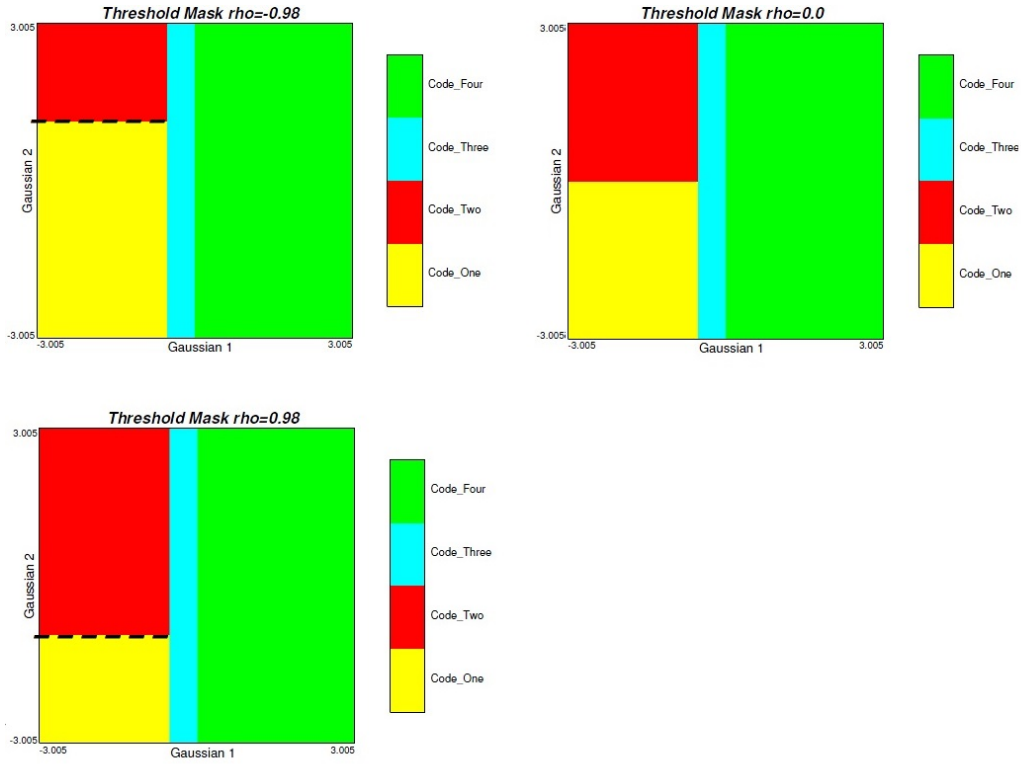


Figure 5.10: Variation of mask (thresholds) for corresponding correlation coefficient. Top left: threshold mask with $\rho = -0.98$ and top right: threshold mask with $\rho = 0.0$. Bottom: threshold mask with $\rho = 0.98$.

To honor the global proportion of categories, thresholds are adjusted based on the correlation between Gaussian functions. A program "*corr_tpgsim*" (Appendix, section A.3) is developed to simulate with correlation. The user can define any configuration of a threshold based mask and test how correlation between Gaussian RFs will change the thresholds of the mask and the resulting truncated realization. The mask thresholds and the final truncated realization are outputs of this program. In addition, for a fixed threshold mask, the user is able to check how the global proportions of categories change in TPG simulation with respect to the correlation between Gaussian RFs.

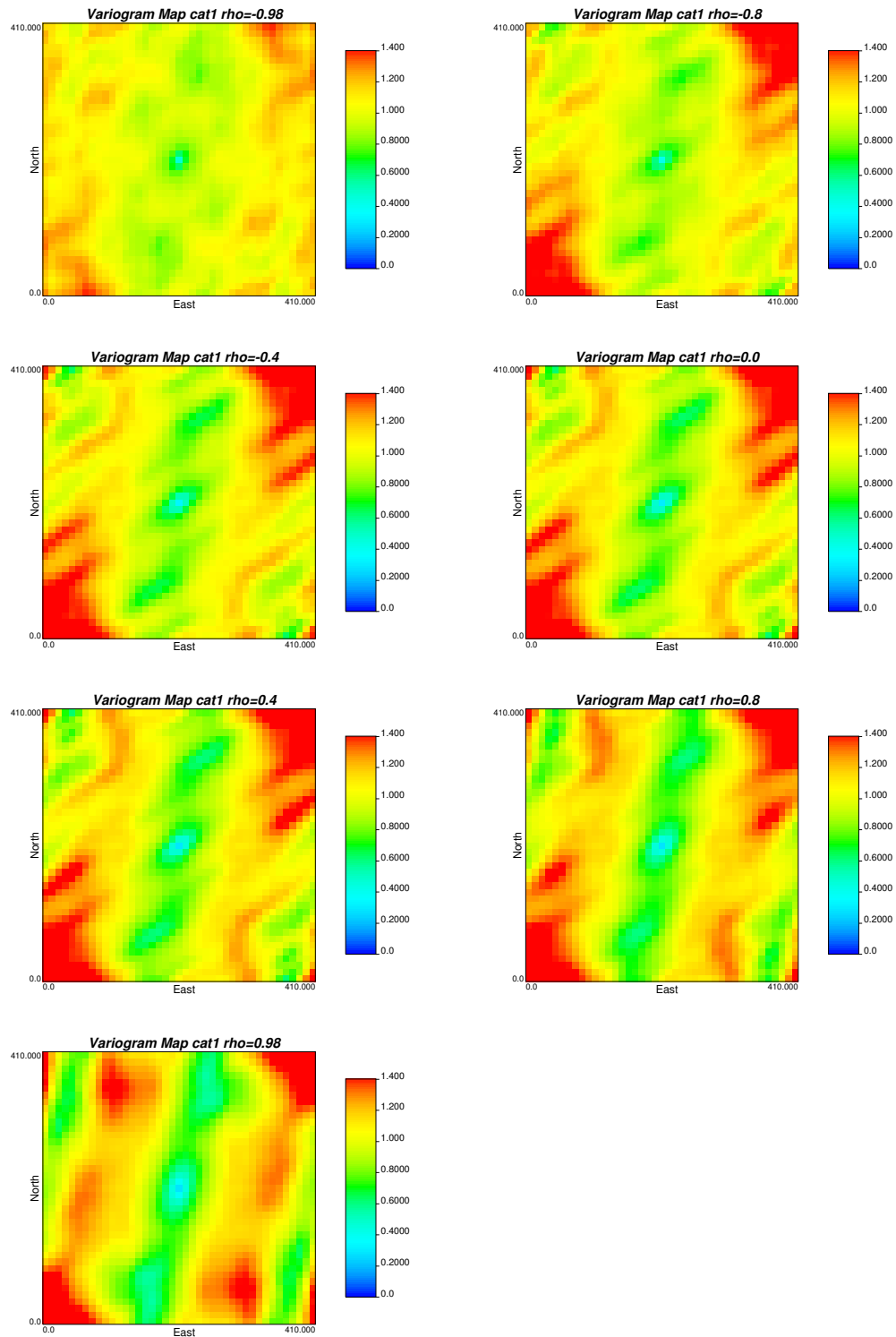


Figure 5.11: Variogram map of category number one with different correlation coefficients.

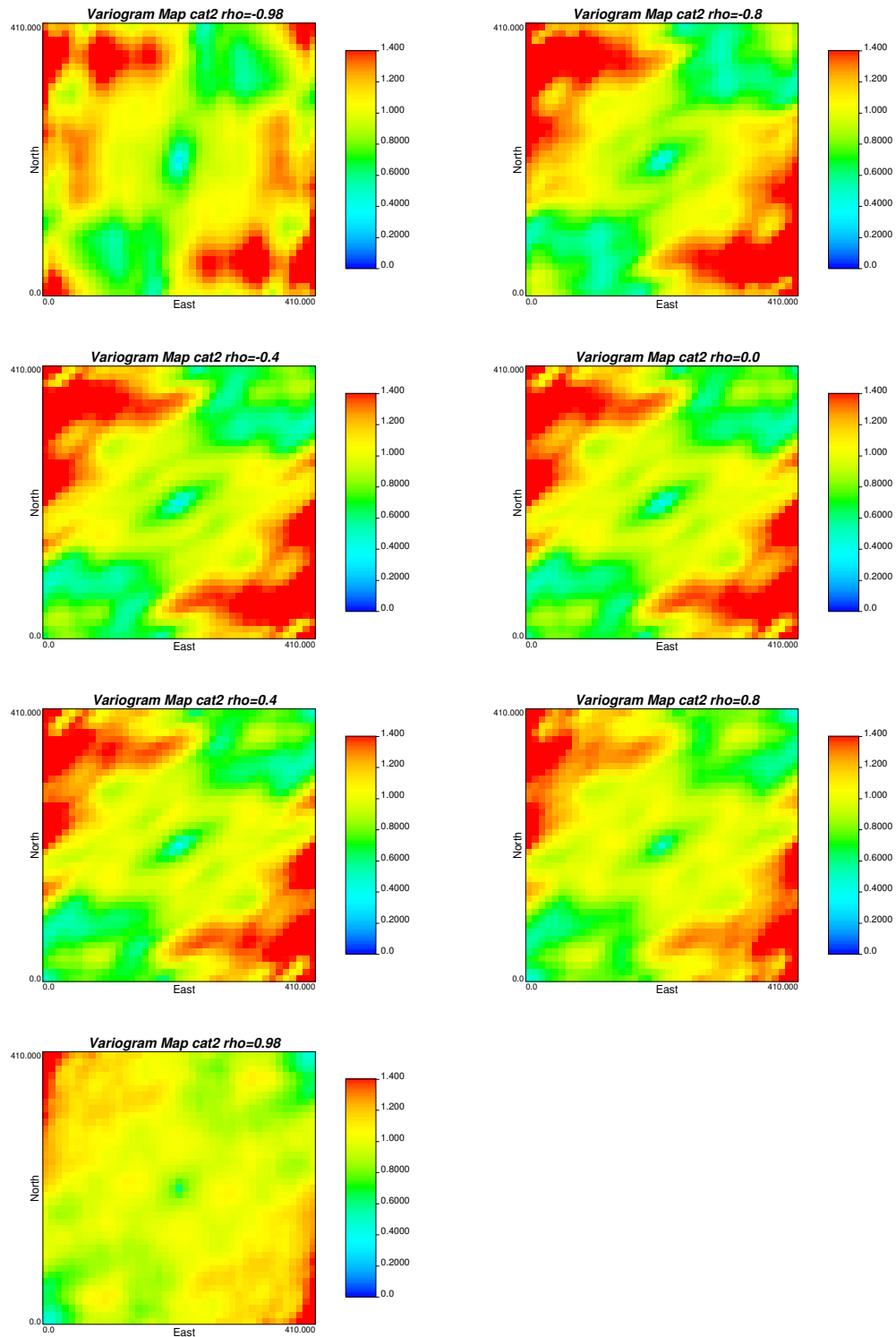


Figure 5.12: Variogram map of category number two with different correlation coefficients.

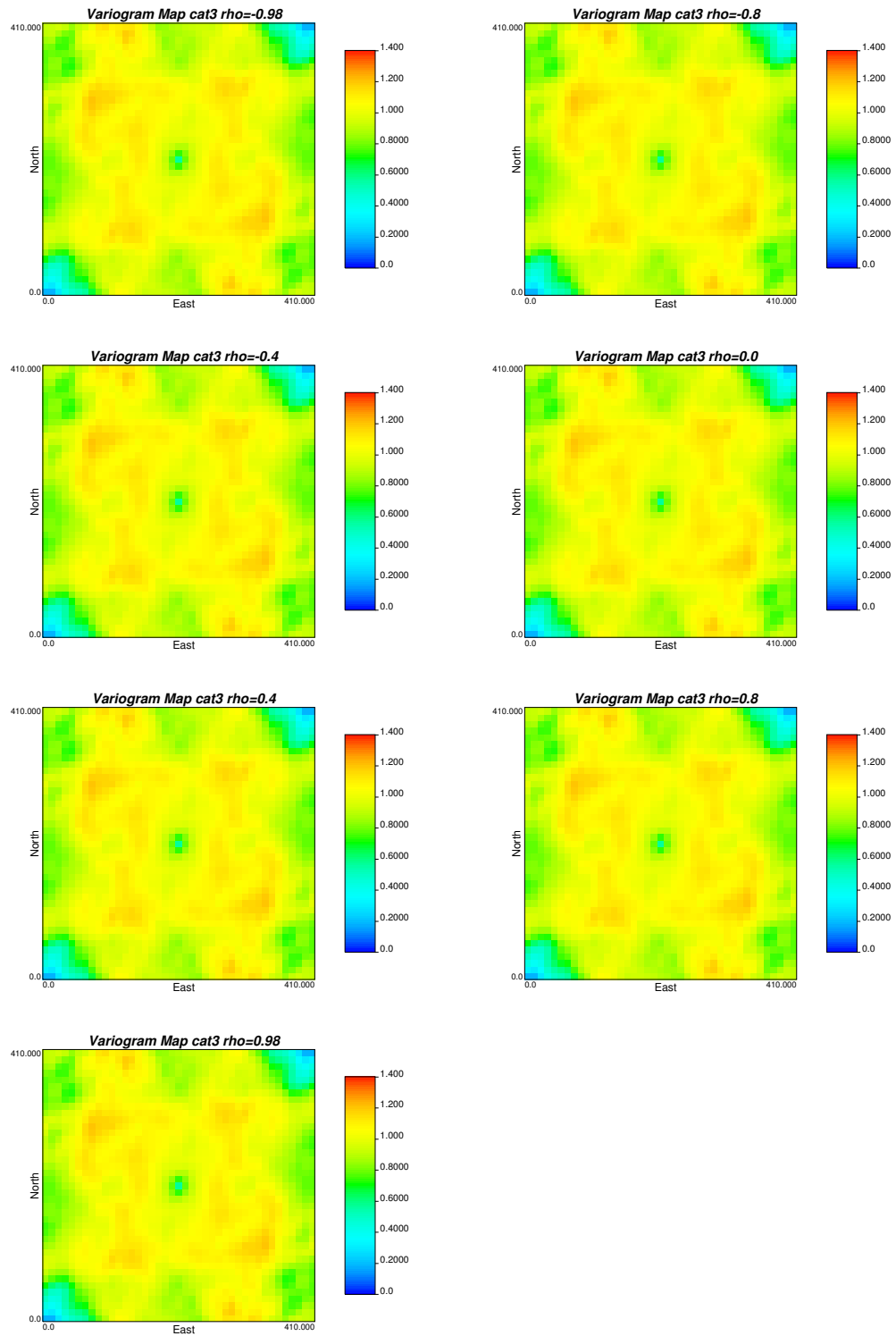


Figure 5.13: Variogram map of category number three with different correlation coefficients.

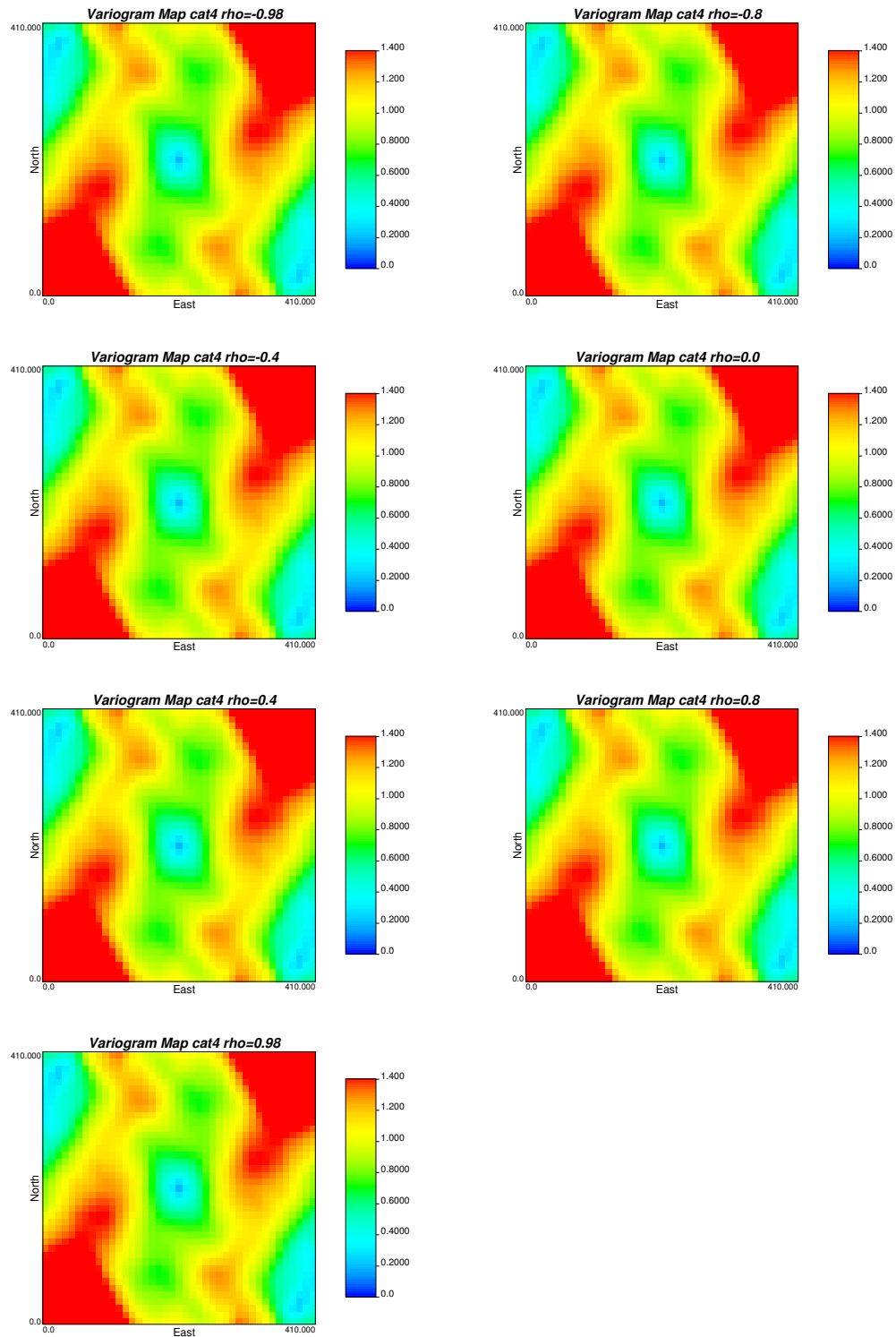


Figure 5.14: Variogram map of category number four with different correlation coefficients.

5.4 Summary

This chapter investigated the impact of correlated underlying Gaussian RFs on the threshold mask which is the most common type of mask and truncated realization. Correlation affects the mask thresholds from the experimental proportions and changes the variograms of indicator variables. Here, a specific threshold based mask is considered as an example to demonstrate the effects and a program is presented to calculate thresholds and proportions for any other configurations.

Different studies have shown that correlation between RFs can be considered due to different reasons, such as improving the fit of experimental indicator variograms, capturing observed specific geological feature, and sometimes allowing some transitions between categories. As Section 5.3 demonstrated, correlation can input the continuity of categories after truncation. Depending on the data set, correlation between RFs can make the categories more or less continuous in truncated realization. It may help to transfer the observed short range of continuity of the categorical data to the categorical model.

Correlation between Gaussian functions can change the global proportion of the categories or the thresholds of the mask and accordingly the transition between categories. Also, correlation can affect the variogram of the correlated Gaussian variable as well as the variogram of the desired indicator variables by changing the proportion of categories or mask thresholds.

In summary, considering correlated or uncorrelated Gaussian realizations is a choice that has to be made depending on whether a strong border effect is observed in the available data set. The general recommendation is to use uncorrelated Gaussian RFs to avoid any complications unless the use is helping to model some natural phenomena. The impact of the correlation between Gaussian RFs can be tested using the developed program.

Chapter 6

Variogram Optimization in TPG Simulation

The inference of the variogram models for the underlying Gaussian realizations is an important aspect of TPG simulation method. Continuity of the categories is controlled by the variogram of each Gaussian variable. The relations between all these variograms are complex functions of the truncation. These variograms should be selected in such a way that the original categorical variables have the correct spatial structure after truncation. In this chapter, three different methodologies are proposed to address this problem. In the first methodology, an optimization framework is introduced to determine the input variograms. Initially, the optimization is brute force with the best set of variograms carried forward; the second local refinement step is important in obtaining reasonable variogram reproduction models. In the second methodology, a neural network (NN) is presented to help determine the optimal input variograms. Finally, in the last methodology an optimization is proposed which targets the covariance or variance map of each categorical variable and attempts to select the optimum input variograms to best reproduce the spatial structure of each categorical variable. This method best reproduced the target categorical variable variograms.

6.1 Variogram Optimization

Variogram modeling of underlying Gaussian deviates in TPG method is very important for simulating geological domains. Direct adjustment to the experimental

variograms is not possible since the only available experimental indicator variograms are those of the indicator functions describing the categories. [Kyriakidis, Deutsch, and Grant \(1999\)](#) considered approximately transforming the calculated indicator variograms to normal scores variograms with two categories. Therefore, the variogram inversion is calculated using numerical integration of the bivariate Gaussian distribution. [Remacre and Zapparoli \(2003\)](#) used an iterative inversion approach to find the relationship between experimental indicator variograms and the covariance model of the underlying Gaussian variables. Also, [Mariethoz et al. \(2009\)](#) proposed to adjust the ranges of the variograms of the multi-Gaussian fields iteratively through an inverse procedure until the indicator variograms of the resulting truncated simulation matches the experimental indicator variograms of the field data. An ANSI computer program was developed by [Dowd et al. \(2003\)](#) to perform conditional or unconditional TPG simulations using a threshold based mask and indicator covariance and cross-covariances. But the important question here is: how the categories' variogram should be assigned to the underlying Gaussian deviates? Direct adjustment from the experimental variograms is not possible and the inference of the spatial structure of the Gaussian variables to obtain the distribution of categorical variables is very difficult.

The theoretical link between the variogram of the underlying Gaussian variables and the indicator variogram of the categorical variables for the threshold based mask is explained by [Armstrong et al. \(2011\)](#). To better match the indicator variogram of categories, an iterative approach is used to define the variogram for underlying Gaussian variables. This method is limited to the threshold based mask and is not appropriate to other types of truncation rules. Also, a numerical derivation of the variogram of the underlying Gaussian variables based on the Monte Carlo simulation is proposed by [Zagayevskiy and Deutsch \(2015\)](#). A sequence of lag distances which discretizes the correlation range of the categorical variables is independently optimized and for each lag distance thousands of pairs are simulated and the average indicator correlation after truncation is calculated. Until the convergence, the spatial correlation of the underlying Gaussian variables is adjusted. This method uses the major direction of continuity of the first important category to optimize the spatial correlation of the

underlying Gaussian variables.

In this chapter, three different techniques are adopted to address the challenge of finding the optimum spatial structure of underlying Gaussian realizations to best reproduce the spatial structure and distribution of target categorical variables.

6.2 Variogram Optimization using Local Refinement

An optimization is proposed to iteratively adjust the parameters of the variograms of the underlying Gaussian realizations. To start, the parameters of the initial variogram model, such as ranges of continuity, are defined from the experimental indicator variograms of the categorical data. Using these variogram models, a TPG simulation is constructed. Then, the indicator variogram of the categories from the simulated truncated realization is calculated. The adjustment of the initial parameters of the variograms is based on the objective function until an acceptable match between the indicator variogram model of data and the computed indicator variograms from simulated realization is achieved. Figure 6.1 represents a sketch of the refinement of the nugget effect and horizontal range of a Gaussian deviates.

The objective function (Eq. 6.1) is defined by the sum of the squared difference between the modeled indicator variogram of the input data (Figure 6.3) and the indicator variogram of categories in the simulated realization. The objective function is considered for sequence of lag distances which discretize the range of the categorical data lags weighted by lag separations to match target indicator variogram models for both horizontal and vertical directions.

$$O(\mathbf{h}) = \sum_{k=1}^K \sum_{j=1}^{nD} \frac{1}{\mathbf{h}} \times (\gamma_k(\mathbf{h}; j)^{model} - \gamma_k(\mathbf{h}; j)^{realization})^2 \quad (6.1)$$

where:

- K - the number of categories;
- nD - the number of directions for variograms (horizontal, vertical);
- h - lag distance;

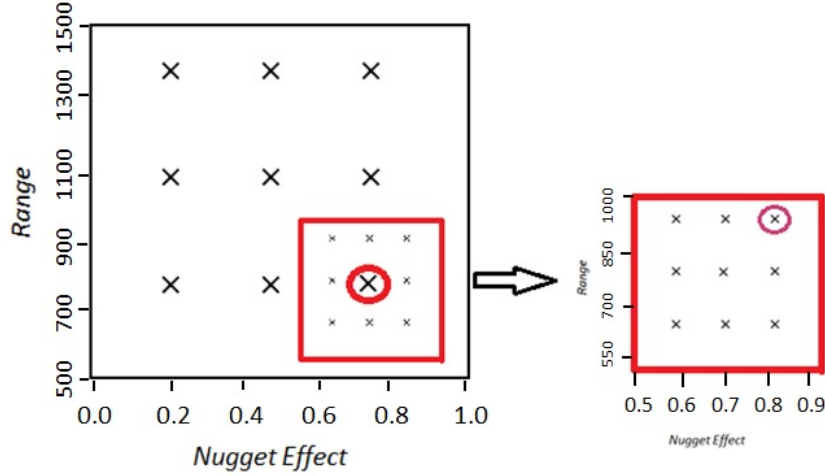


Figure 6.1: Schematic of refinement of two parameters. Large Xs represent the value of parameters for coarse optimization and the highlighted X indicates the best pair of nugget effect and range parameters. The refinement around the highlighted X provides optimal values.

Usually, the short range variogram structure is more important since it gives insight into the variability of variables of interest. So, an inverse distance weighting, $\frac{1}{h}$, is incorporated to assign higher weights to the objective function for shorter ranges. This weight is adjusted to give more or less weight to the vertical/ horizontal variograms as needed for particular applications.

As the number of categories and underlying Gaussian realizations to project increases, reproducing the variograms becomes more difficult because of the reduced flexibility using a limited number of Gaussian deviates. If certain categories are deemed more important, they could be given more weight in this scheme.

First, the optimization is constrained with the best set of variograms for the initial step. Then a second local refinement is considered to obtain a reasonable model. A case study simulating rock types at a mineral deposit is presented to illustrate the implementation of the proposed methodology.

A mineral deposit is simulated with data from drill holes with measurements for four different rock types. Figures 6.2- 6.3 demonstrates the location map of available data and the variogram models of these rock types, respectively. The transition probability between the rock types is used to define a truncation rule between the rock types in the data. The transition probability matrix (Eq. 6.2) for this data is as follows:

$$\mathbf{tp}(h) = \begin{bmatrix} 0.9089 & 0.0067 & 0.0000 & 0.0844 \\ 0.0002 & 0.9778 & 0.0002 & 0.0219 \\ 0.0000 & 0.0010 & 0.9369 & 0.0621 \\ 0.0036 & 0.0390 & 0.0168 & 0.9406 \end{bmatrix} \tag{6.2}$$

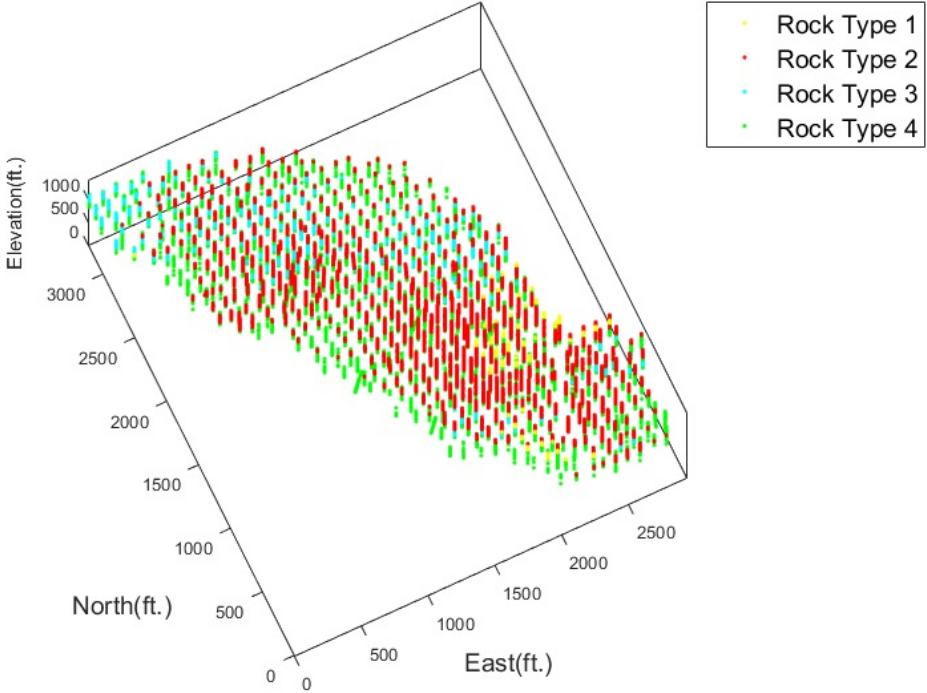


Figure 6.2: Location map of available data.

From the transition probability matrix, it is expected that rock types two and four are connected to all other rock types and rock type one is connected occasionally to rock type three. Figure 6.4 shows the truncation mask for this data set (see Section 4.2);

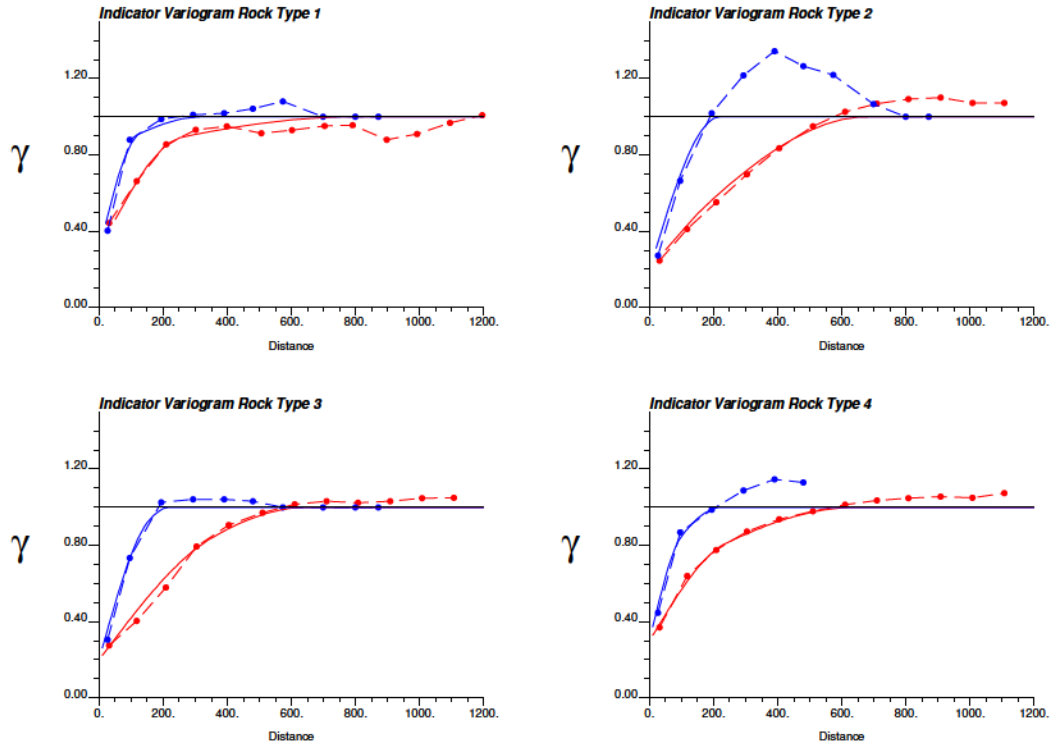


Figure 6.3: Experimental and fitted variograms in horizontal (red) and vertical (blue) directions for available rock types.

the two axes correspond to the values of the underlying Gaussian realizations (Y_1 and Y_2) with mean zero and variance of one, $N(0,1)$, and the color codes correspond to the domain of the different rock types.

The surface area of the different rock types in the threshold based mask corresponds to their respective global proportions that are estimated by analyzing the available drill hole data. The global proportions of rock type one, two, three, and four are 0.014, 0.57, 0.086, and 0.33, respectively. The corresponding thresholds of the threshold based mask are shown in Figure 6.4 ($t_1 = 0.176$, $t_2 = -1.84$, and $t_3 = 0.84$).

Two Gaussian random realizations, Y_1 and Y_2 , are considered, with Gaussian variogram models with two structures for both underlying Gaussian realizations. Generally, Gaussian covariance provides smoother boundaries between the rock types than other types of variograms (Pyrz & Deutsch, 2014). The Gaussian model has the parabolic shape at the short distances and provides more continuity. As Figure 6.4 illustrated, transition between rock types one, three, and four are controlled more by Y_2 and tran-

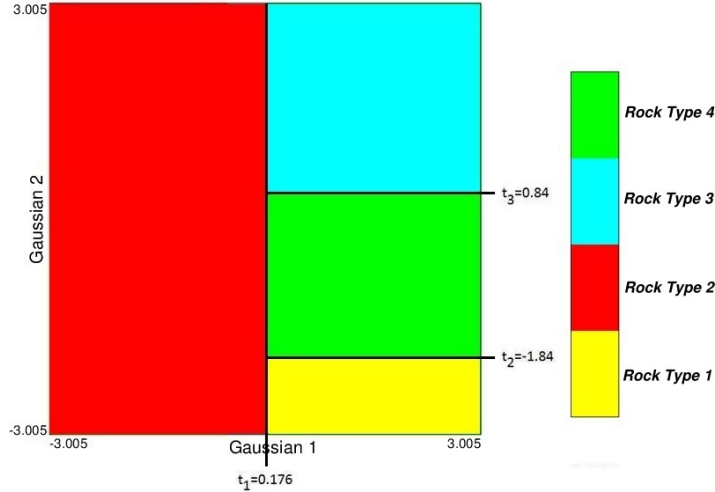


Figure 6.4: Global threshold based mask with four rock types.

sition of rock type two to other rock types is controlled more by Y_1 .

To reproduce the variogram model of all the rock types, the determination of the initial input variograms to generate the Gaussian realizations is important. To achieve this goal, a N -dimensional space for variogram parameters of the underlying Gaussian deviates is created for each underlying Gaussian variable and a simultaneous optimization is considered. Here, N is the number of parameters that is required to build an isotropic variogram model with two nested structures. Consider $N = 6$, which represents the horizontal and vertical directions' ranges for each structures, nugget effect, and contribution of the first structure. Boundaries of this space for horizontal and vertical directions are selected based on the maximum and minimum ranges between all four rock types. In the first step, to achieve the best initial solution, optimization is carried forward with possible combinations of parameters for the underlying variogram model. Improvement of variogram reproduction of rock types is checked through the objective function in each combination. The set of parameters with the lowest objective value is considered as the best initial solution. In the next step, a local refinement is implemented and optimization is brute forced with the best set of variograms carried forward. In this step, an optimization search to obtain the optimum solution is limited to the neighborhood of the best set of variograms from the previous step.

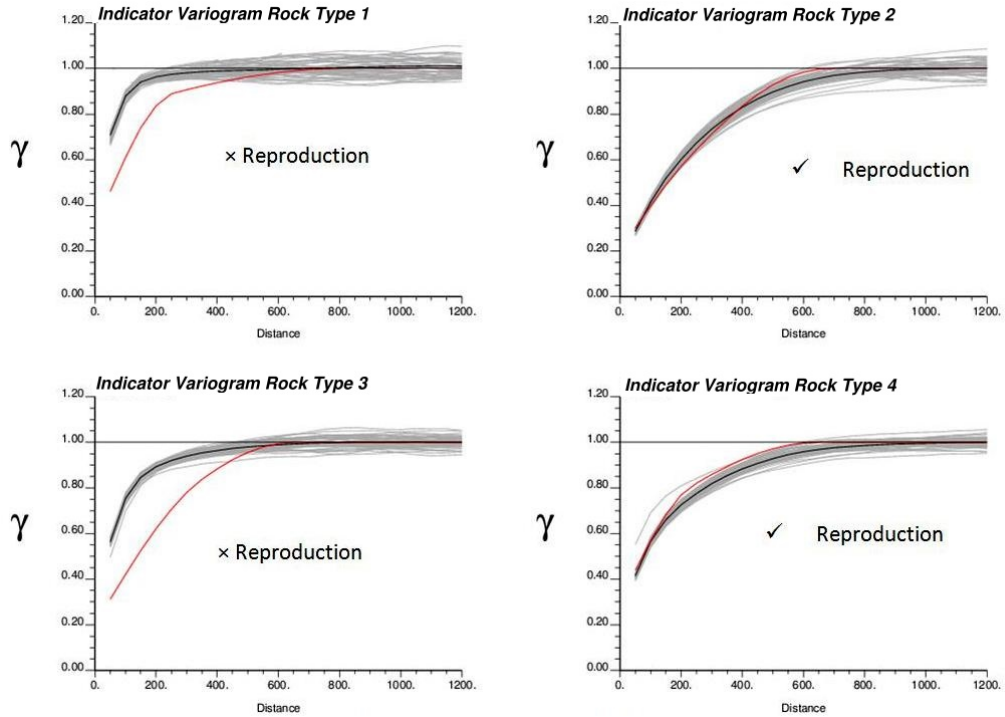
Finding a balance between the variogram reproductions of all rock types is necessary

and local refinement is applied for this purpose. Depending on the importance of the rock types, the final variograms can be selected.

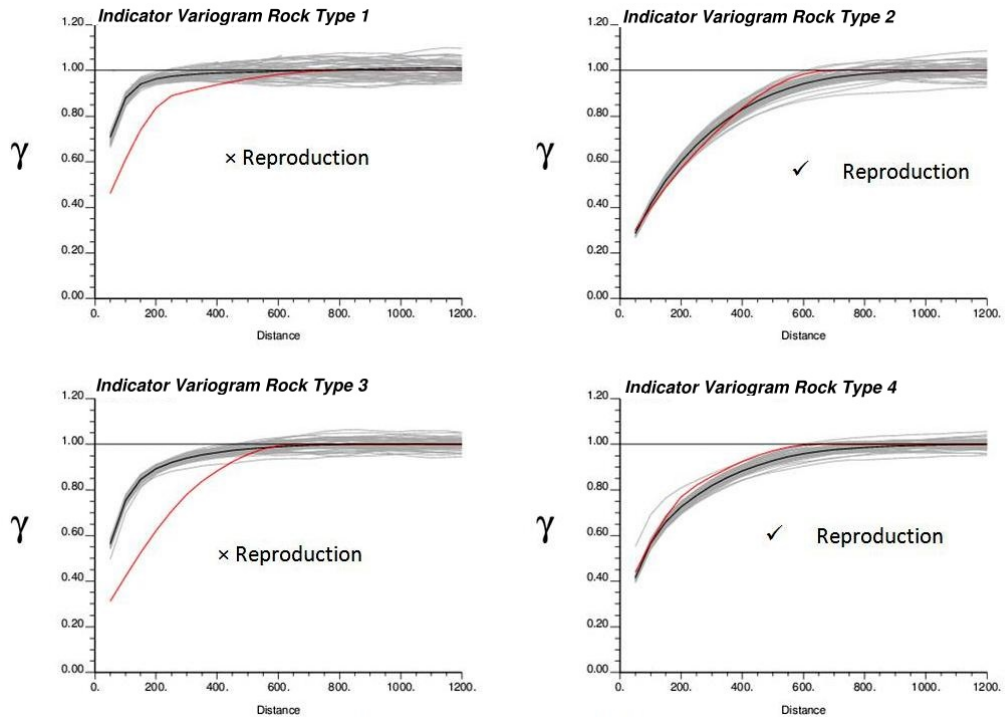
Figure 6.5(a) puts higher weight on the variogram reproduction of rock type four, Figure 6.5(b) puts higher weight on the variogram reproduction of rock types one and three, and Figure 6.6 shows a balanced approach that attempts to reproduce all four rock types for both horizontal and vertical directions. Based on the results, rock type two always shows good reproduction.

With optimized parameters, Gaussian function Y_1 is modeled with a Gaussian covariance model with two nested structures with ranges of 600 (ft.) in the horizontal direction and 180 (ft.) vertically with a nugget effect of 0.05. The ranges of Gaussian function Y_2 are longer than Y_1 in all directions. The ranges are 700 (ft.) and 280 (ft.) in horizontal and vertical directions, respectively. Y_2 also has a Gaussian variogram. Reproduction of input proportions of the rock types is shown in Figure 6.7. The input proportions are reproduced well. In addition, transition probabilities are calculated from the final TPG realization to compare to the transition probability matrix calculated from the data. TPG simulation reproduced the data transition probabilities from rock types two and four to other rock types well. There is a slight error in transition reproduction of data for rock types one and three to other rock types that is the result of the low global proportion of these rock types (Eq. 6.3 and Figure 6.8).

$$\mathbf{tp}(h) = \begin{bmatrix} 0.5704 & 0.1627 & 0.0000 & 0.2669 \\ 0.0024 & 0.8757 & 0.0285 & 0.0934 \\ 0.0000 & 0.1384 & 0.7108 & 0.1507 \\ 0.0061 & 0.1445 & 0.0480 & 0.8014 \end{bmatrix} \quad (6.3)$$

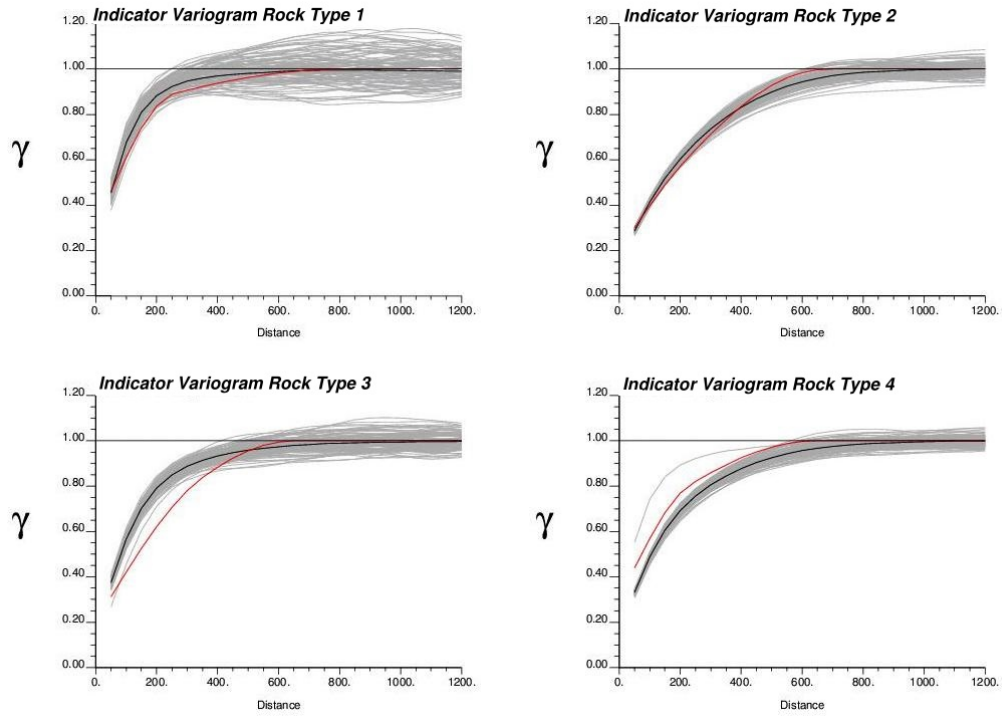


(a) Good variogram reproduction of rock types two and four

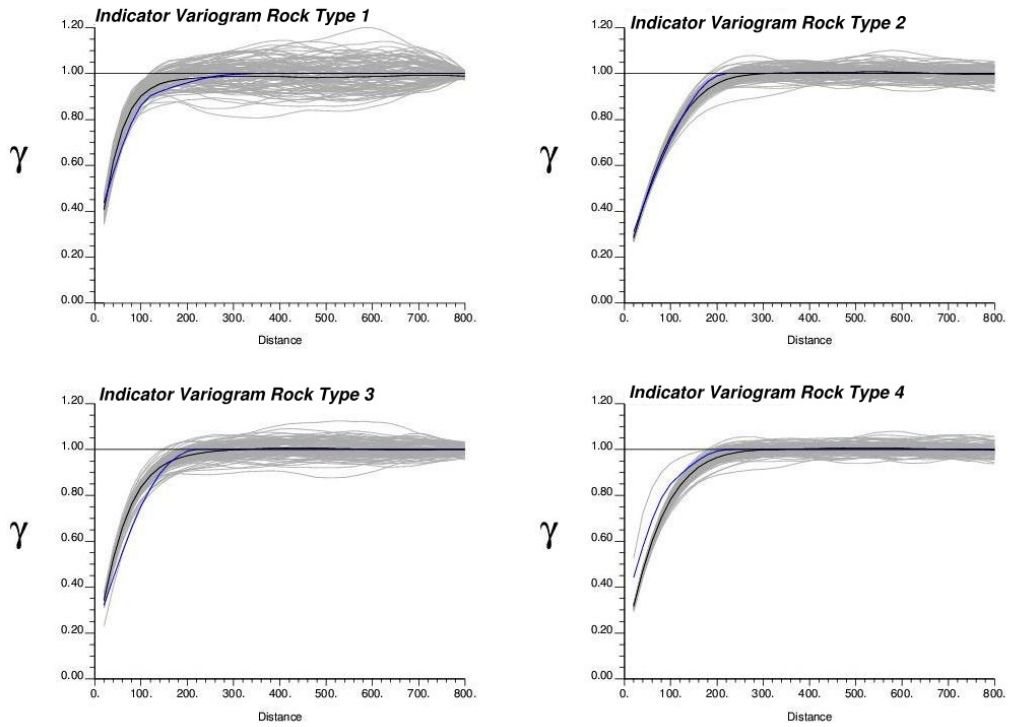


(b) Good variogram reproduction of rock types one and three

Figure 6.5: Variogram reproductions of horizontal direction(gray lines). Red and black lines represent variogram model of rock types and and the average reproduction of 50 realizations.



(a) Variogram reproductions of horizontal direction



(b) Variogram reproductions of vertical direction

Figure 6.6: Balanced reproduction of model variograms of all four rock types with TPG method (gray lines), and the average of 50 realizations (black line).

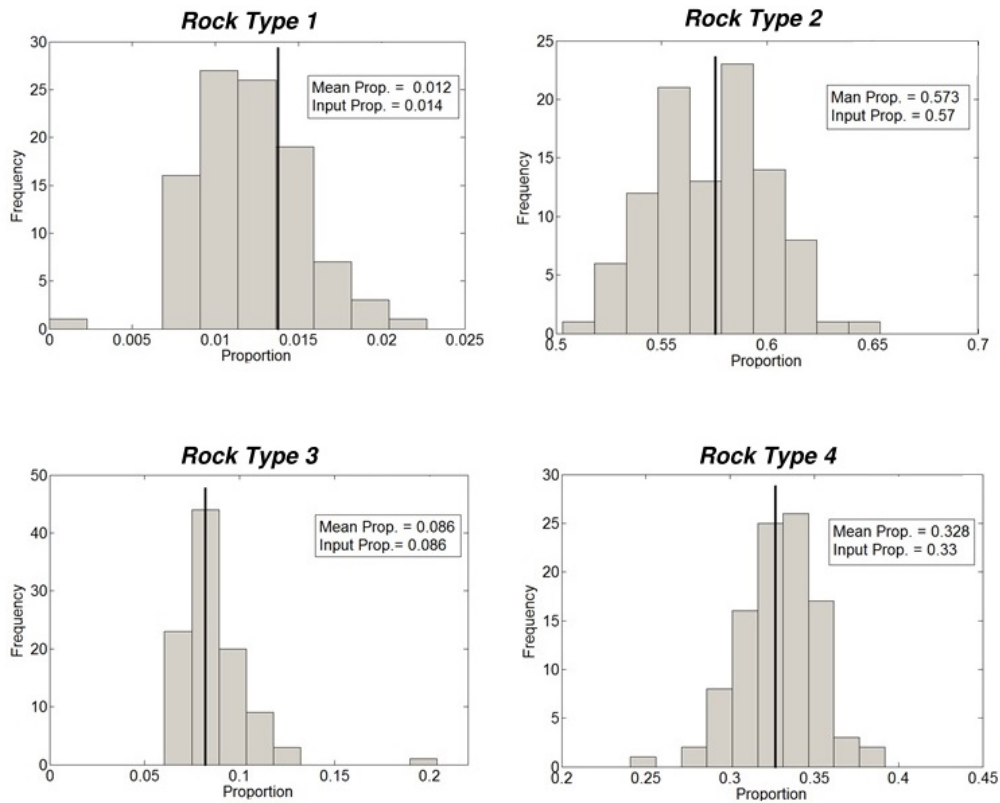


Figure 6.7: Input proportion reproduction for all four categories with TPG simulation for 50 realizations. The input proportions are shown with the black line.

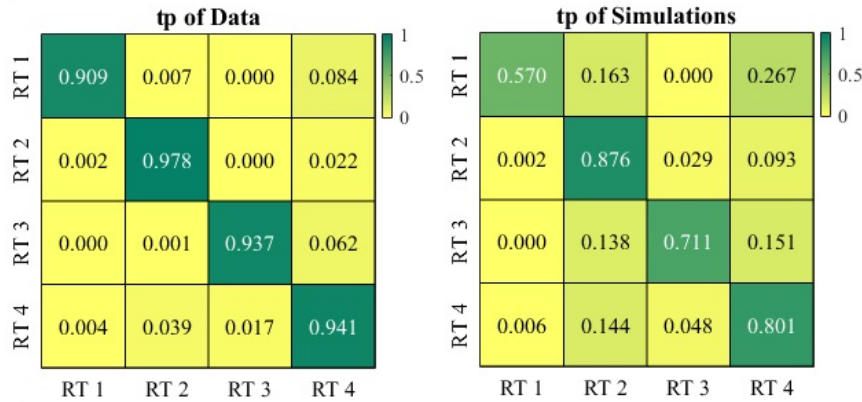


Figure 6.8: Transition probability matrix of data and averaged transition probability matrix of rock types for 50 simulated realizations colored by transition probability values from zero to one.

Remarks

The proposed optimization finds reasonable local optimums for a given set of indicator variograms but depends on the initial parameters; random restarts are important.

The proposed method is iterative and provides reasonable variograms for the Gaussian variables in TPG simulation in an effort to reproduce the desired variograms and often can be used directly; in some cases, the practitioner may want to manually adjust the final variogram fit depending on site specific concerns. The limitation of this work flow is the required computational time for optimization as the number of rock types increase. Also, defining the best set of variograms to start the optimization is a challenge. The entire solution space is not fully explored as this is found to be very computationally expensive.

6.3 Variogram Optimization using a Neural Network

NN offers a non-algorithmic approach to geostatistical simulation with the possibility of automatic recognition of correlation structure. A NN is presented in this section to help determine the optimal input variograms used to generate the underlying Gaussian realizations.

The field of NNs has been applied widely in the past fifteen years and is still developing quickly. NNs have been trained to perform complex functions in several fields of application such as pattern recognition, identification, classification, speech, vision and control systems. Currently, problems that are difficult for human or conventional computers can be addressed by NNs.

6.3.1 Artificial Neural Network (ANN)

Figure 6.9 shows a typical network diagram. Each processing element (or unit) in the network can be schematically represented as a node. Also, connections between units are indicated by the arcs. The arrowheads on the connections represent the direction of information flow in the network. An input on the left layer of processors can activate many units of the hidden-layer (second-layer). The activity on the hidden layer activates the units that are recognized on the output layer. The comparison of the output and the target is used as a measurement to adjust the network until the network output matches the target. Simple elements are working in a parallel way in the form of a directed graph in NNs. The connections between elements define the

network function. When one adjusts the values of the connections between elements, a NN can be trained to perform a certain function. The NN can offer a feasible solution and better understanding of the problem. To train a network in the supervised learning, many input/output pairs are usually used.

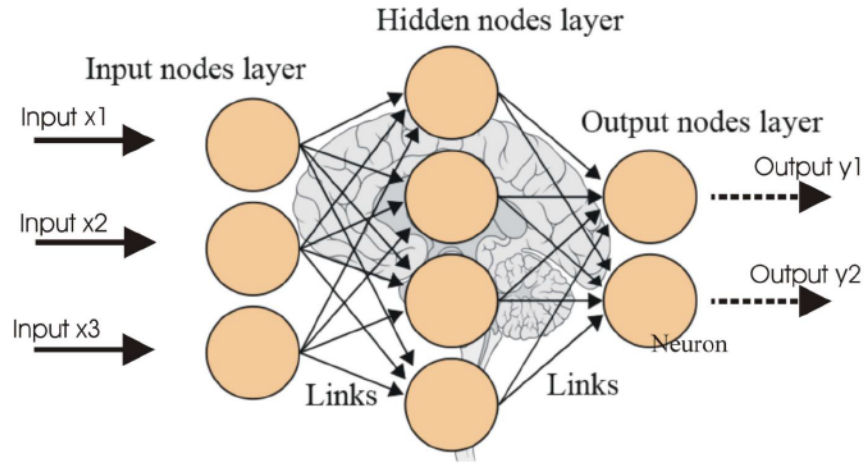


Figure 6.9: Schematic representation of ANN. (Tadiou, n.d.)

There are different training methods, but the supervised training methods are frequently used. Other networks can be obtained from unsupervised training techniques or from direct design methods (Hastie, Tibshirani, & Friedman, 2009). For instance, to identify groups of data an unsupervised network can be used. A binary threshold unit as a computational model for an artificial neuron is proposed by McCulloch and Pitts (1943) (Figure 6.10). This mathematical neuron computes a weighted sum of its n input signals, $x_{ij} = 1, 2, \dots, n$ and generates an output of 1 if this sum is above a certain threshold \mathbf{u} . Otherwise, an output of 0 results. Mathematically, Eq. 6.4:

$$y = \theta \left[\sum_{j=1}^n w_j x_j - \mathbf{u} \right] \quad (6.4)$$

where:

- θ - a unit step function at 0;
- w_j - the synapse weight associated with the j^{th} input;

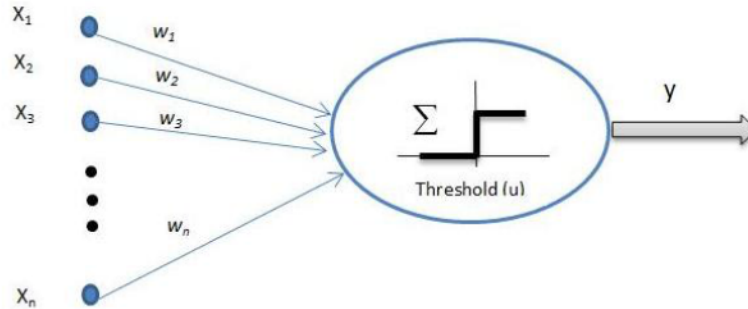


Figure 6.10: McCulloch-Pitts model of a neuron (McCulloch & Pitts, 1943).

A positive weights model relates to excitatory synapses and a negative weights model relates to inhibitory synapses. The McCulloch-Pitts method has been developed in several different models, for instance, in the use of other activation functions instead of the threshold function (Gaussian, Piecewise linear, Sigmoid, Softplus and Rectified linear), as shown in Figure 6.11. ANNs can be grouped into two groups based on the connection design:

- Feed-forward networks: have no loops in graphs
- Recurrent (or feedback) networks: have loops due to feedback connections

Different network behaviors are found based on different connectivities. In general, feed-forward networks are static and one set of output values is produced instead of a sequence of values from a certain input. The important property of feed-forward networks is that they are memory-less which means their response to an input is independent of the previous network state. Alternatively, feedback (recurrent) networks are dynamic organizations. The neuron outputs are calculated, once a new input is presented. Because of the feedback paths, the inputs to each neuron are then modified, which leads the network to enter a new state. Different learning algorithms are required for different network designs.

The ability to learn is an important attribute of intelligence. In the ANN for learn-

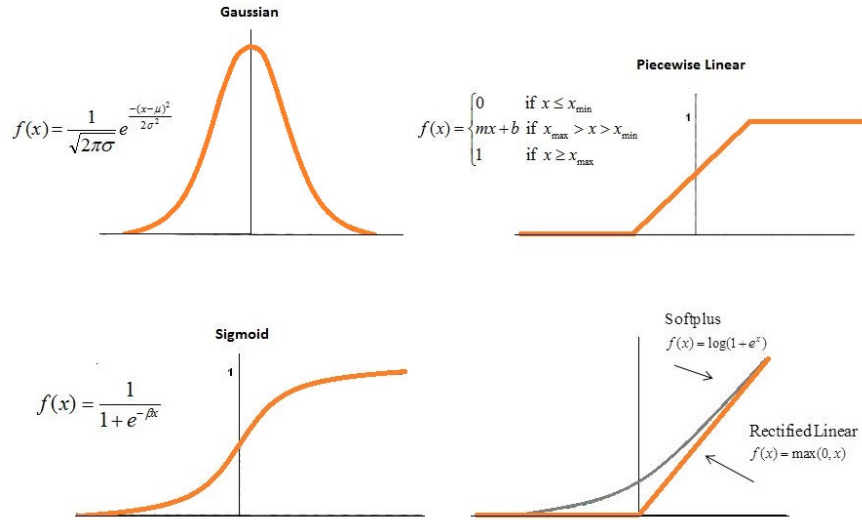


Figure 6.11: Different types of activation functions. Top from left to right: Gaussian, Piecewise linear. Bottom from left to right: Sigmoid, Softplus and Rectified linear.

ing, network design and connection weights should be updated properly. From the available training data, the network must learn the connection weights. By iteratively updating the weights in the network, performance is improved. One of the most important advantages of ANN is that it learns the underlying rules between the variables of an interested population from the relation of a given input/ output instead of following the rules that assigned by humans.

6.3.2 Application

Section 6.3.1 introduced the basic concepts of an ANN model and its learning algorithms. Now an application of ANN is discussed to illustrate how a one layer feed-forward network is used in variogram parameters optimization. Categorical data are available and the proportions of categories and the transition probability between the data set are known from the available data. The relations between the categories can be different depending on the type of geology, and the selected mask imposes the relations and contacts between the categories. Here, the transition probability between the categories is used to characterize the spatial distributions between the categories in the data.

In this study a synthetic 2D example with three categories and two underlying Gaussian random realizations is considered to test the potential of ANN in variogram optimization. Figure 6.12 shows two reference realizations that are generated with spherical variogram models.

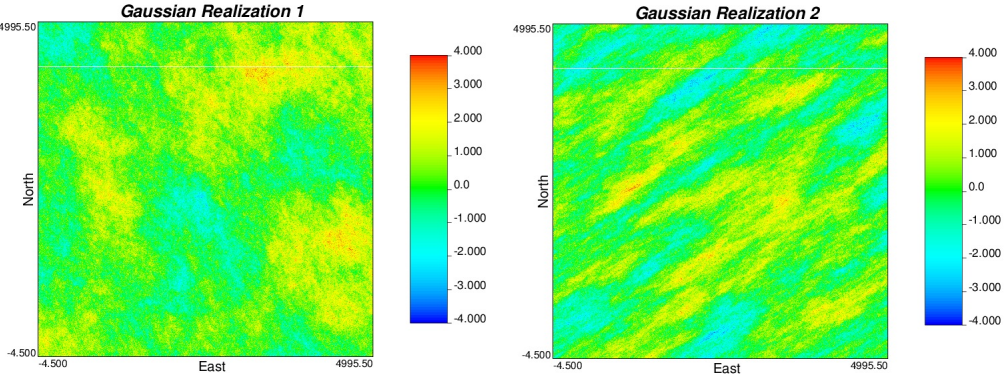


Figure 6.12: Underlying Gaussian realizations (500×500 cells).

Gaussian function Y_1 is modeled with a spherical covariance model with one nested structures with the ranges of 1318 ft. in the minor horizontal direction and 2010 ft. in the major horizontal direction. The nugget effect equal to 0.30 has been selected for this realization. The ranges of Gaussian function Y_2 are shorter than Y_1 on all directions. The ranges are 416 ft. and 1527 ft. in minor and major horizontal directions with azimuth of 153° degree from north for both realizations. Y_2 also has a spherical variogram with nugget effect equal to 0.27. These two realizations are truncated using an MDS mask to create interested categories (Figure 6.13).

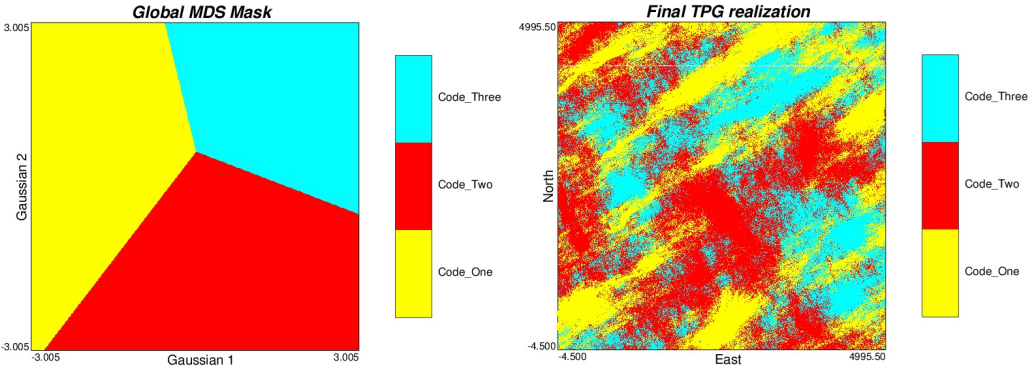


Figure 6.13: MDS mask with 3 categories and a corresponding truncated bigaussian simulation.

A feed-forward ANN is used for ANN modeling. The nodes are considered as computational units and ANN considers the nodes as artificial neurons. In the first step a data base that defines the relation between input and output is built. The inputs of this network are the indicator variogram parameters of categories in the categorical data set. The network is trained for different ranges of inputs. For a 2D categorical data set, there are four relevant parameters for each category with one spherical structure: Nugget effect, strike, maximum range of continuity, and minimum range of continuity. Three hundred pairs of Gaussian realizations with random variogram parameters are generated. A specific transition probability matrix and mask for sequence set of proportions of categories are considered for truncation of simulated Gaussian realizations. The indicator variograms of categories are calculated and fed as inputs to the ANN, while the output of ANN is the variogram parameters that have been used to generate the underlying Gaussian realizations.

Connection strengths and transfer functions control how much of the activation value is passed on to the next node. The accumulated activation value that each node receives from its own activation function is modified based on its transfer function and passed through the network to the next node. To develop a good ANN, the transfer function must be selected properly. For instance, a neuron may have a bell-curve style firing pattern, threshold, sum its inputs, or average them, or something completely complicated. The activation flows through the network in one direction, from input nodes, through the hidden layers, until eventually the output nodes are activated. If a network is suitably trained, this output should match the known values in some meaningful way. In this study, a full connection is considered. The network has 12 inputs and 8 outputs (Figures 6.14). Based on these relations, connection strengths, inhibition/excitation conditions, and transfer functions can be determined. Table 6.1 summarizes the results of the ANN based on five different activation functions.

The most popular method of learning is Back-Propagation. To begin, the network is initialized; all the connections are set randomly. A network that has twelve inputs, one hidden layer with ten nodes and eight output neurons created in PyBrain ([Schaul](#)

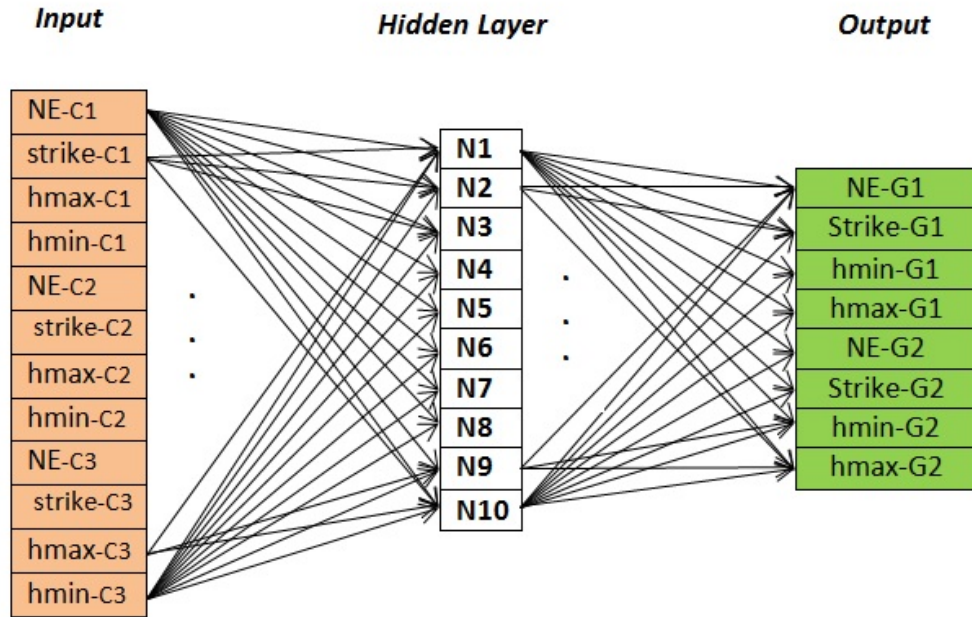


Figure 6.14: Designed neural network with full connections and one hidden layer.

Table 6.1: Summary of results for created ANN based on different activation functions.

	SigmoidL	GaussianL	LinearL	TanhL	SoftmaxL	True
NE1	0.35	0.22	0.34	0.23	0.23	0.3
Strike1	186.9	273.3	182.2	210.3	187.9	153.0
hmin1	998.3	1238.3	991.3	1164.8	944.8	1318.0
hmax1	2040.4	2031.7	1907.5	2029.2	2072.0	2010.0
NE2	0.26	0.21	0.25	0.26	0.22	0.27
Strike2	186.3	311.8	189.0	200.5	187.5	239.0
hmin2	474.5	473.1	442.3	453.7	480.5	416.0
hmax2	1319.4	1286.0	1251.3	1260.1	1268.1	1527.0

et al., 2010). The number of nodes in a hidden layer is usually between the size of the node in the input and the output layers. Hidden layers are connected with full connection objects. The network is trained for 1000 epochs. An epoch is a forward and one backward pass through the entire training set. A back propagation trainer (Rumelhart, McClelland, Group, et al., 1988) is used for set up a trainer that basically takes the network and training data set as input. Five different PyBrain supervised trainers are used. Table 6.2 summarizes the percent error in each parameter for each activation function. ANN with sigmoid and hyperbolic tangent activation functions predicts the outputs with fewer errors.

Table 6.2: Summary of the percent error in each parameter for each activation function

	SigmoidL	GaussianL	LinearL	TanhL	SoftmaxL
NE1	17.52	23.86	15.96	10.00	22.18
Strike1	22.17	78.63	19.09	37.45	22.81
hmin1	24.25	6.04	24.78	11.61	28.31
hmax1	1.51	1.08	5.09	0.95	3.09
NE2	1.74	22.69	6.51	1.40	20.16
Strike2	21.82	103.79	23.54	1.40	20.16
hmin2	14.08	13.73	6.33	9.07	15.51
hmax2	13.59	15.78	18.04	17.48	16.95
Average % Error	14.58	33.20	14.92	14.88	18.94

Remarks

ANN algorithms can be used to detect complex nonlinear relationships between input variables and all possible interactions between output variables. The proposed optimization addresses the problem of variogram reproduction for two Gaussian variables in a 2D case for a specific mask. The major disadvantages of this algorithm are its black box nature and limited flexibility in handling a verity of inputs. It can be hard to adjust and verify that the network is well trained.

6.4 Variogram Optimization by Iteratively Adding Complexity

The key to the modeling approach presented in this section is adopting an optimization to find the optimum variograms of underlying Gaussian deviates to obtain the appropriate indicator variogram reproduction of each category after truncation. The proposed optimization targets the covariance or variance map of each categorical variable and attempts to select the optimum input variograms to best reproduce the spatial structure of each categorical variable. A novel optimization method is proposed which iteratively increases the complexity of the covariance functions to obtain the best fit for the original categories.

Optimization begins with a simple initial random covariance function; optimization is used to obtain a local minimum. The initial parameterization of the variogram is as simple as possible (one structure and no horizontal anisotropy for each Gaussian deviate). Gradient optimization or simulated annealing optimization can be selected to find the optimal covariance map for the underlying Gaussian realizations. As with any optimization methods, the important part is the formulation of an objective function. The emphasis of the proposed optimization is on finding the appropriate covariance map for underlying Gaussian realizations that honor the pattern statistics in the original model and minimize the objective function. In successive iterations, complexity is added to the variogram in the form of additional variogram structures and anisotropy, improving the fit to the desired categorical variable variograms. This procedure is repeated for the desired number of variogram structures. Each step increases the difficulty of optimization and always results in a closer match to the desired categorical variograms. The balance between simplicity and better variogram reproduction is discussed. A synthetic example is presented to illustrate the implementation of the proposed method.

6.4.1 Application

This section explains the use of the proposed method to optimize variograms of underlying Gaussian deviates. In the first step, a simple random variogram model with one structure and no horizontal anisotropy for each Gaussian deviate is considered as the initial parameterization. The next step is the integration of the multivariate Gaussian probability distribution to simulate Gaussian values. LU simulation (LU) is applied here to simulate the Gaussian deviates using the spatial covariance matrix with a large number of points. In this method, the covariance matrix C is decomposed by Cholesky decomposition to the lower matrix (L) and upper matrix (U). A random number generator generates a vector of uncorrelated standard normal values (W), and then the correlated values are calculated by Eq. 6.5:

$$Y(\mathbf{u}) = LW(\mathbf{u}), \quad \mathbf{u} \in D \quad (6.5)$$

A TPG simulation is constructed by truncation of the generated Gaussian realizations using an appropriate mask. Here, an MDS mask is used to obtain the truncation mask automatically from the transition probabilities determined from the input data; thus, in the proposed work flow, the truncation rules are automatically calculated as well as the input variograms for each Gaussian deviate.

The adjustment of the initial parameters of the variogram is based on the objective function until an acceptable match between the covariance map of data and the computed covariance map from the simulation results for each category is achieved. The objective function (Eq. 6.6) is the difference between the modeled covariance maps of the indicator variables ($Cov_k^{model}(\mathbf{h}_i)$) and the covariance maps of unconditional truncated simulation ($Cov_k^{realization}(h_i)$) weighted by the inverse lag distance of covariance points in the covariance map to center of covariance map and also weighted by categories proportions. The N lag separation vectors (\mathbf{h}) which are the most compact arrangement (see Figure 6.15) are used to calculate objective function. Based on Eq. 6.7, for each category, any lag vector between two points is considered by decomposing the

separation vector into three principal components (x_i , y_i , and z_i) which are within 3 dimensional range of spatial continuity. Optimization and random restarts are used to obtain the optimal parameters of the initial simplified covariance structure.

$$O = \sum_{k=1}^K p_k \sum_{i=1}^N \frac{1}{(\mathbf{h}_i(k))^w} (Cov_k^{model}(\mathbf{h}_i(k)) - Cov_k^{realization}(\mathbf{h}_i(k)))^2 \quad (6.6)$$

$$\mathbf{h}_i(k) = \sqrt{\left(\frac{x_i}{a_{hmax}(k)}\right)^2 + \left(\frac{y_i}{a_{hmin}(k)}\right)^2 + \left(\frac{z_i}{a_{vert}(k)}\right)^2} \quad (6.7)$$

where:

- a - the spatial extent (i.e., ranges) of variability for each principal direction;
- K - the number of categories;
- w - the weight term;

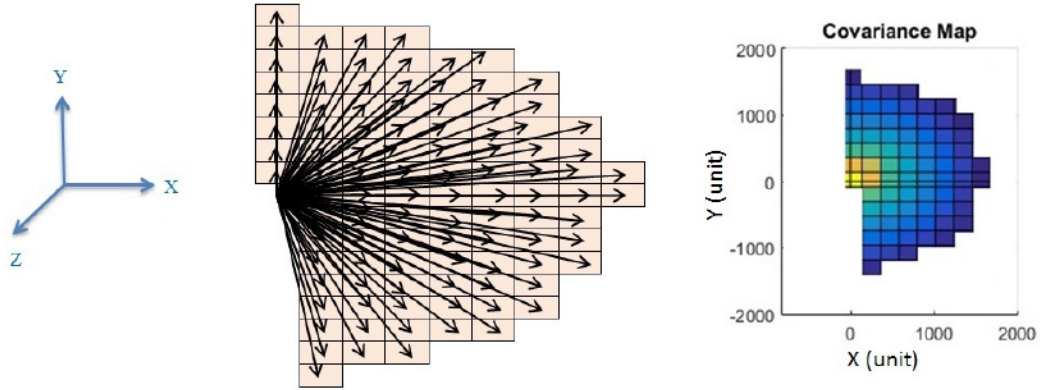


Figure 6.15: Polar plot of the lag vectors to calculate the objective function (C. V. Deutsch & Cockerham, 1994).

The spatial extent of the variability for each principal direction is different for each nested structure and each category. These ranges are often referred to as the major horizontal direction, minor horizontal direction and vertical direction, according to

the GSLIB convention (C. V. Deutsch & Cockerham, 1994). By convention, w varies between 0 and 2 and a series of studies indicate that $w = 1$ works the best. Higher the w value, assigns less weight to the covariance values that are far from the origin, and those points make very little contribution to the outcome.

Two types of optimization are considered here: the Fletcher-Reeves method, which is a gradient base optimization, and the SA algorithm. Optimization begins with a random set of variogram parameters to build the initial covariance map and then iteratively adjusts the parameters to minimize the objective function. After obtaining the initial solution for variables using the mentioned optimization, more complexity can be added to the algorithm in the next step by adding more structures. The optimum solution and objective value of the previous step is used as an initial input and objective value to the process. The new set of parameters is adjusted iteratively for a certain number of iterations or until the best match is achieved. Figure 6.16 shows the work flow for the optimization using a covariance map of categorical variables in TPG simulation method.

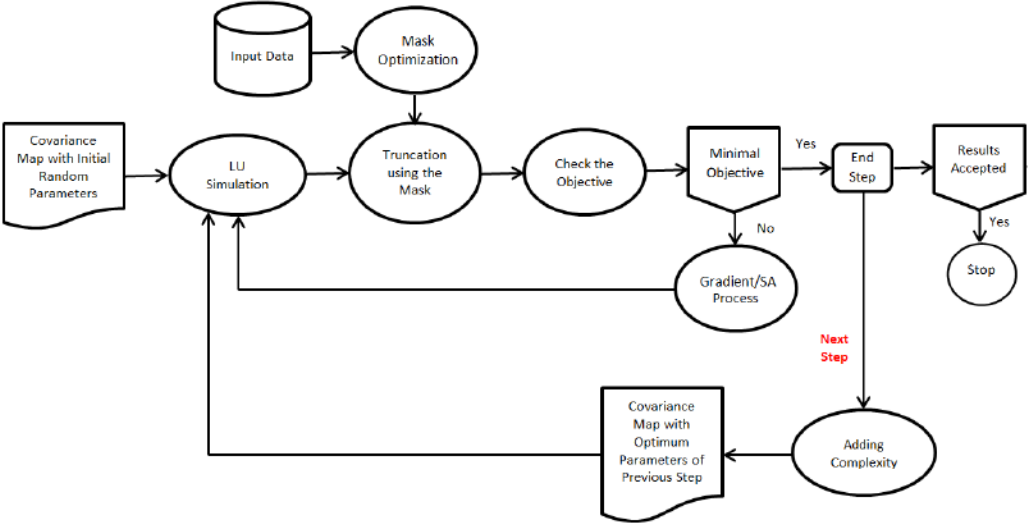


Figure 6.16: Work flow for covariance map optimization of categorical variable in TPG simulation method.

The proposed optimization is developed in a program "*vargopt_tpg*" (Appendix, section A.4) to obtain the best fit for the variogram models of underlying Gaussian

deviates in TPG simulation. This program is able to deal with the complex spatial continuity of categorical variables. Two types of semivariogram models are specified in this program to model Gaussian variables: the Gaussian type and stable variogram type. The Gaussian model is defined by an effective range a and positive variance contribution value c (Eq. 6.8). Note that instability problems are often encountered with the Gaussian model with no nugget effect (Posa (1989); Stein and Handcock (1989)). Therefore, using a very small nugget effect is suggested in this case. The stable variogram model is defined by Eq. 6.9, with power term wt which varies between 1 and 2 (Chiles & Delfiner, 2009). For anisotropic variogram models, the inner ratio $\frac{h}{a}$ is modified as shown in Eq. 6.10, where a_{max} , a_{min} , and a_{med} are the ranges of spatial continuity in principal directions of major, minor, and medium continuities. In this case, wt is added as a parameter to optimization algorithm.

$$\gamma(h) = c. \left[1 - \exp\left(-\frac{(3h)^2}{a^2}\right) \right] \quad (6.8)$$

$$\gamma(h) = c. \left[1 - \exp\left(-3\left(\frac{h}{a}\right)^{wt}\right) \right] \quad (6.9)$$

$$\frac{h}{a} = \sqrt{\left(\frac{h_{max}}{a_{hmax}(k)}\right)^2 + \left(\frac{h_{min}}{a_{hmin}(k)}\right)^2 + \left(\frac{h_{med}}{a_{med}(k)}\right)^2} \quad (6.10)$$

Case Study

Two Gaussian variables are simulated and truncated to generate a categorical model that is used as reference (Figure 6.17). The Gaussian variable Y_1 is simulated using a Gaussian variogram with ranges of 16 units in the major direction (West-East) and eight units in the minor direction (South-North). The Gaussian variable Y_2 is simulated with a isotropic Gaussian variogram with a range of 16 units. The truncation rule is defined

by the MDS mask with proportions of 0.5, 0.25 and 0.25 for categories one, two and three, respectively. The transition probability matrix is calculated from the available data (Eq. 6.11). Figure 6.18 shows the MDS based mask and reference categorical data.

$$\mathbf{tp}(h) = \begin{bmatrix} 0.9268 & 0.0461 & 0.0271 \\ 0.0720 & 0.8733 & 0.048 \\ 0.0784 & 0.1014 & 0.8201 \end{bmatrix} \quad (6.11)$$

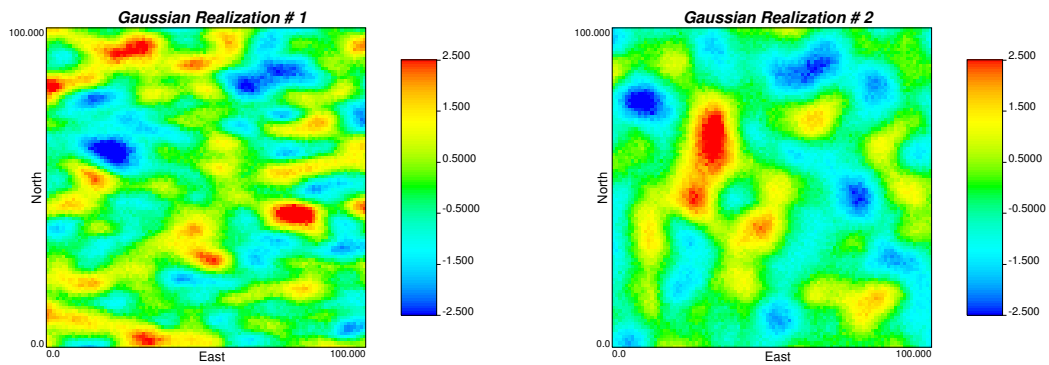


Figure 6.17: Underlying Gaussian realizations.

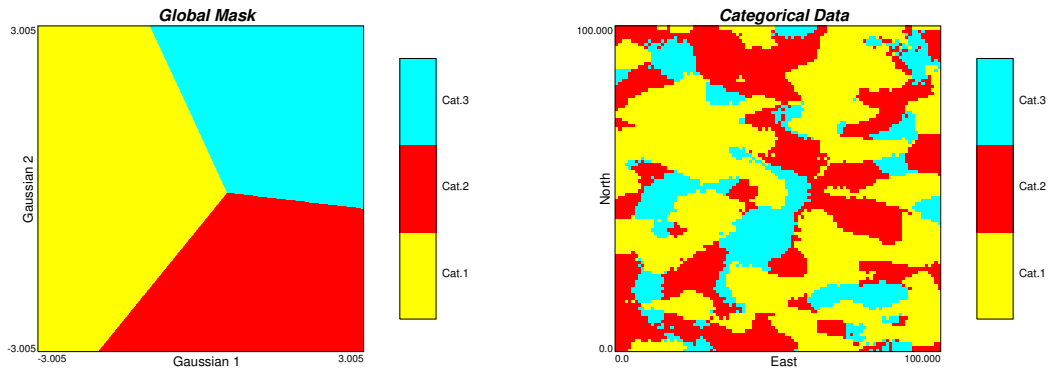


Figure 6.18: Left: truncation rule using MDS mask and right: categorical data.

Figure 6.19 and Figure 6.20 show a slice of 3D representation of covariance of the off sets for three available categories and the experimental indicator variograms of the resultant categorical model.

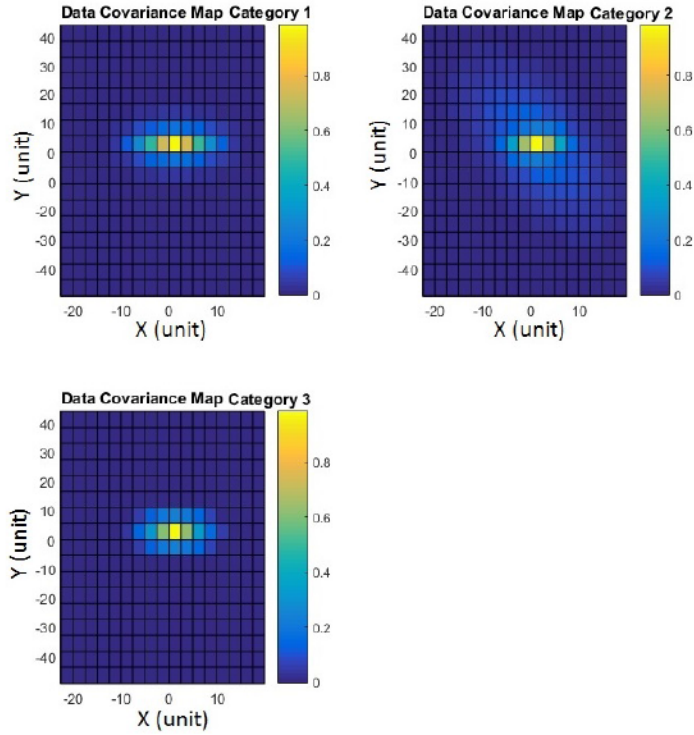


Figure 6.19: Slice of representation of covariance of off sets for each available category colored by covariance values.

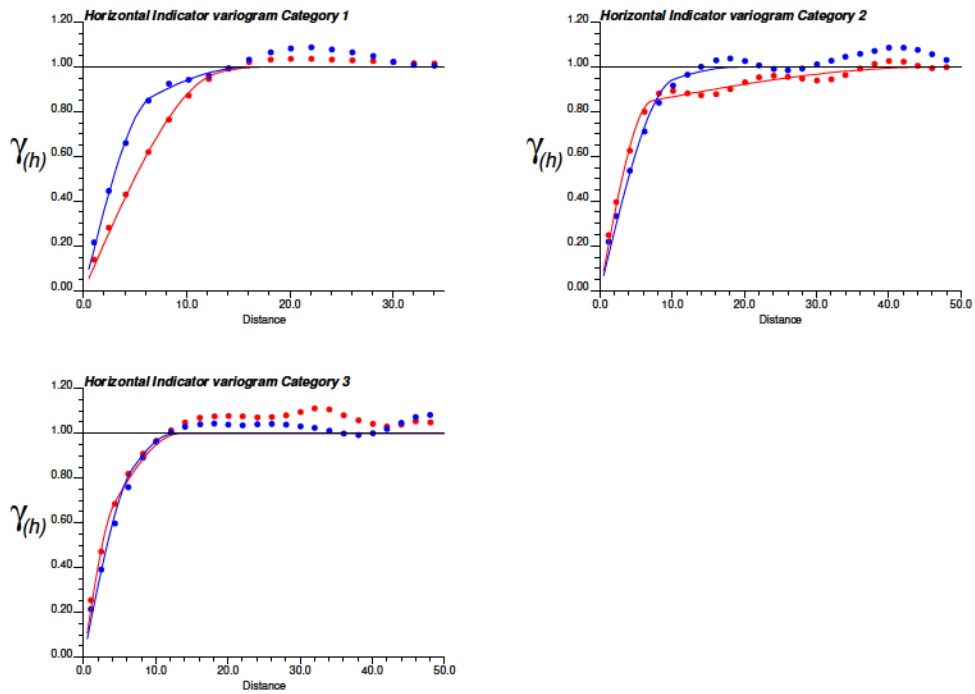


Figure 6.20: Experimental and fitted variograms model in major (red) and minor (blue) horizontal directions.

In the first step, one anisotropic Gaussian structure with random variogram parameters of underlying Gaussian deviates is considered. The optimization method continuously modified the initial parameters until the objective function optimized. This procedure is optimized for 100 different random restarts and the one with the smallest objective value is considered as the best match. The algorithm started with an objective value of 7.18 and stopped with a final objective value of 2.45. Here, the Gaussian function Y_1 is modeled with a Gaussian covariance model with one nested structure with a horizontally anisotropic variogram. A nugget effect of 0.01 has been selected for these realizations. In the next step, another structure is added to the previous covariance/variogram model. The optimization algorithm begins with the optimum parameters from the previous step. A contribution for each nested structure is added as an optimization parameter. Input proportions of categories among 100 unconditional simulations is reproduced very well and presented in Figure 6.21. The final variograms reproduction among 100 simulations with optimized parameters for both structures is shown in Figure 6.22. By adding one more structure, the final objective value reduced to 0.226 and the variogram reproduction of categories improved by 5%.

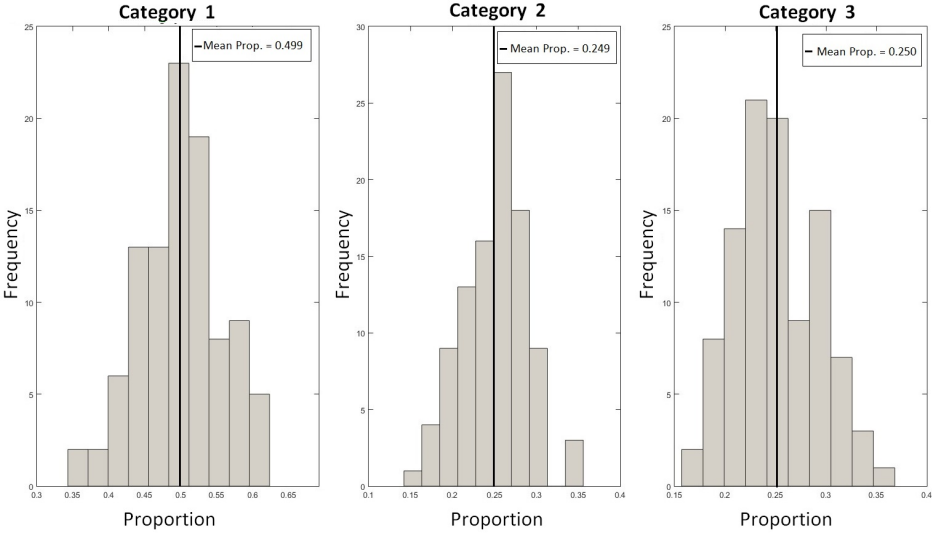


Figure 6.21: Input proportion reproduction for all three categories with TPG simulation for 100 realizations. The input proportions are showed with the black line.

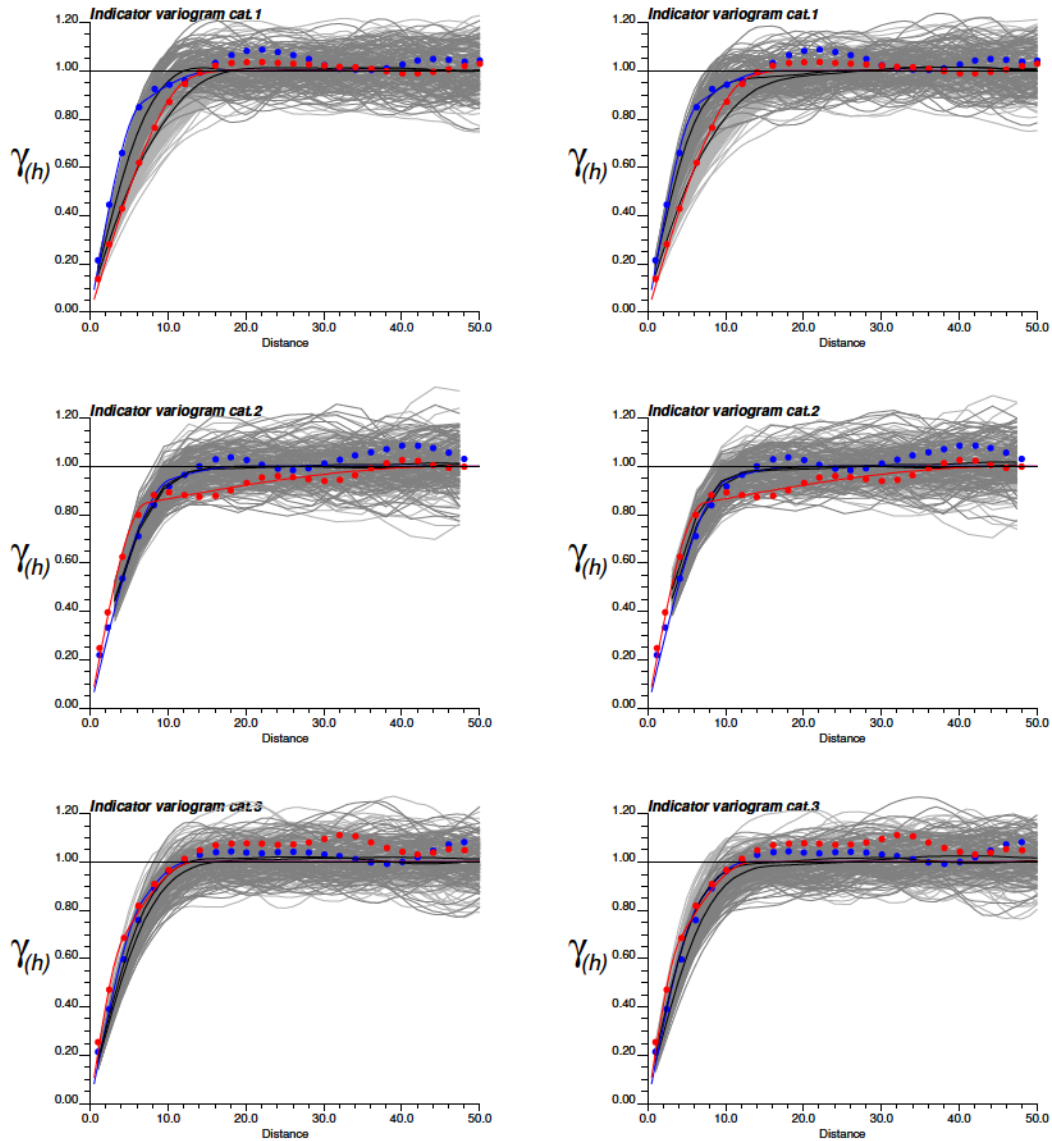


Figure 6.22: Reproduction of model variograms with TPG in major (red) and minor (blue) directions using two Gaussian deviates and one nested structures (left) and two nested structures (right) for all three categories.

Figure 6.23 shows the reference, initial and optimized underlying Gaussian realizations and categorical data. The optimized ranges for Y_1 are 16 units in the major direction (90° degree) and 11 units in the minor direction. Y_2 also has a Gaussian covariance with optimized ranges of 12 units in the major direction (173° degree) and 10 units in the minor direction. Figure 6.23(c) shows that spatial distribution of reference categories (Figure 6.23(a)) are preserved in TPG simulation using optimized underlying variograms models.

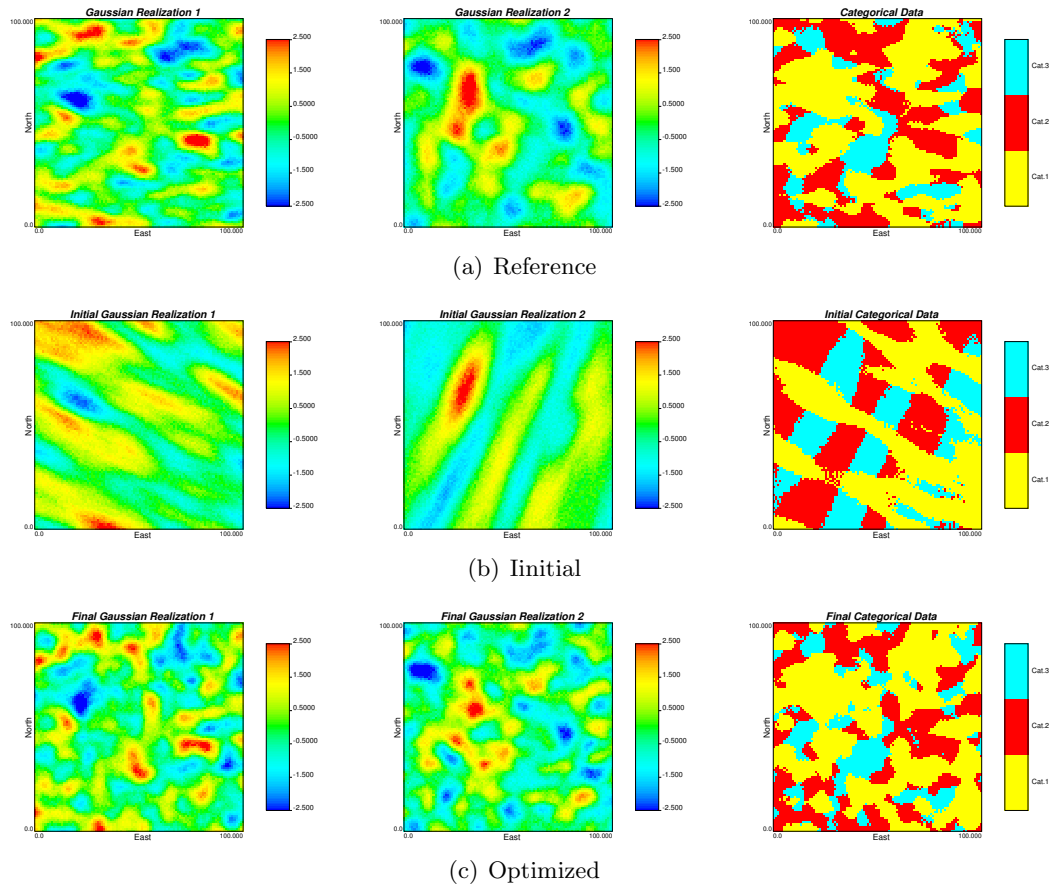


Figure 6.23: Underlying Gaussian realizations and categorical data.

A slice through the representation of covariance of the off sets using initial and optimized variogram parameters for three available categories is shown in Figure 6.24. Figure demonstrates how the optimization started with a very different covariance map as categorical data and converged to the target covariance map of categories in finite steps.

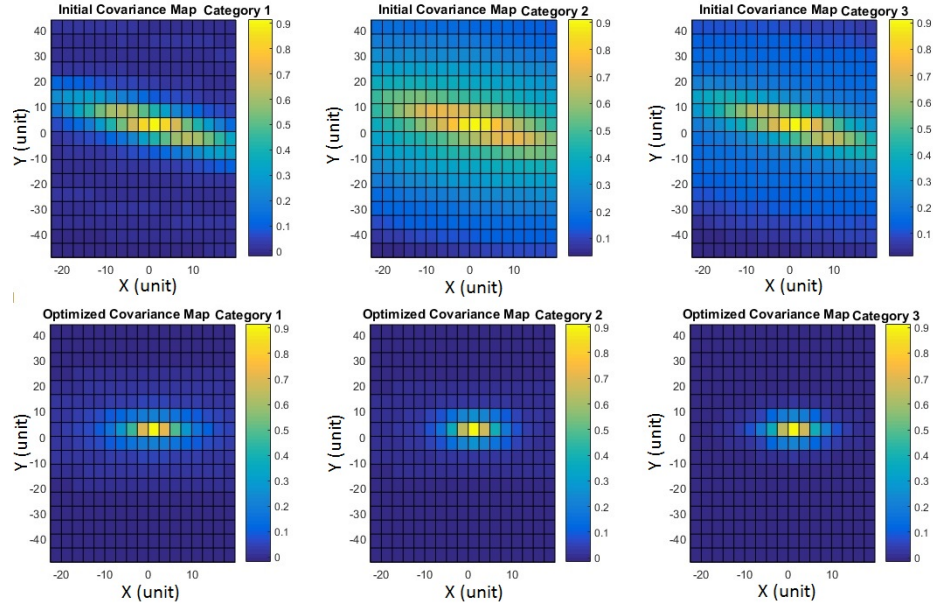


Figure 6.24: Slice through the representation of covariance of off sets. Top: using the initial variogram parameters and bottom: using the optimum variogram parameters for three available categories.

6.5 Summary

Three different methodologies for inferring the variogram of the underlying Gaussian deviates are explained in this chapter. The first relies on iteratively adjusting the set of variograms parameters of the underlying Gaussian realizations to obtain the initial optimum solution and then a local refinement is applied to balance variogram reproduction of all the categories. In this method, initial sets of parameters are required that can be difficult to assign.

In the second optimization methodology, an ANN algorithm is adopted to find the optimum parameters of the variograms of the underlying Gaussian deviates. This a learning algorithm which learns the underlying rules between given input/ output variables. ANN is a powerful method which can be trained to perform complex functions in different fields. However, it is a black box and can be hard to adjust and ensure that the network is well trained. Also, this is a training process and requires a huge data base which is not always available. In variogram optimization, there are many different scenarios that an ANN should be trained for, such as different masks, transition

probabilities and categories proportions. It is very difficult to build this data base for all possible scenarios.

Lastly, a variogram optimization is introduced which targets the covariance map of each categorical variable. The procedure begins with a simple variogram model which is easier to optimize and find a reasonable local minimum. Variogram reproduction is mapped in successive iterations as complexity is added to the variogram model. In the proposed work flow, the truncation rules are automatically calculated as well as the input variograms for each Gaussian deviate. The relationships between the parameters are complex and the objective function is non-convex; therefore the use of random restarts is required. The limitation of this method comes with the required CPU time. Time does increase linearly with the increasing number of random restarts.

Chapter 7

Case Study

The following chapter uses data from the Red Dog mine, Alaska to study the performance of the developed methodologies in a complex geological setting. The chapter begins with an overview of the geology and background of data and continues with showing the application of TPG simulation on the data set.

Section 7.1 explains the settings, description of the data, the geology and the geologic domains of the case study. Sections 7.2 and 7.3 document details of the implementation of the proposed method. Also, geostatistical models are evaluated in terms of accuracy, precision and prediction of the geologic domains in Section 7.3. The results are compared to the production data.

7.1 Available Data

The data set in this case study is from the Red Dog mineral deposit. Red Dog mine is the largest zinc (Zn) producer in the world and it is located 90 miles north of Kotzebue, Alaska, USA. The deposit consists of sulphide ore zones in sedimentary exhalative (sedex) deposits, and is characterized by the presence of multiple metals and multiple ore types (Ayuso et al. (2004); De Vera, McClay, and King (2004); Moore, Young, Modene, and Plahuta (1986)). This mine consists of five geological mineralized plates based on structural and sedimentary characteristics: Upper, median, lower, sub lower, and host rock. In total, there are 31 geology codes based on the block model geology codes. For this case study, the selected area contains four geological mineralized

plates (median, lower, sub lower, and host rock) and each is the combination of different rock types. The median plate is the combination of median plate lower grade exhalite ($< 15\%Zn$) including silica rock and silicified Ikalukrok shale, median plate Ikalukrok vein unit, median plate higher grade exhalite ($> 15\%Zn$), and median plate Ikalukrok barite. The lower plate is the combination of lower plate lower grade exhalite ($< 15\%Zn$) and includes silica rock and silicified Ikalukrok shale, lower plate lower grade exhalite ($< 15\%Zn$), lower plate Ikalukrok barite, and lower plate higher grade exhalite ($> 15\%Zn$). The sub lower plate consists sub lower Plate barite, sub lower plate vein unit, and sub lower plate lower grade exhalite ($< 15\%Zn$) and includes silica rock and silicified Ikalukrok shale. The host plate is the combination of the remaining rock types in the selected area. Figure 7.1 shows the experimental indicator variogram and variogram model of these rock types in the horizontal and vertical directions. There is no clear horizontal anisotropy to consider directional variograms; therefore horizontal omnidirectional and vertical indicator variograms are calculated for the four rock types. Figure 7.2 shows the projection of the available drill hole data (DH) onto different cross sections.

The selected area for this case study is based on the production data. The coordinate limits of the model for this study are summarized in Table 7.1 and the geostatistical models will be simulated at $12.5(ft.) \times 12.5(ft.) \times 12.5(ft.)$ resolution. This model consisted of a total of 3,590,400 blocks.

Table 7.1: Dimension parameters of the block model utilized for the construction of the implementation of TPG simulation.

Direction	Origin	Block Model	Number of Block	Block Size(ft.)
Easting	585400		264	12.5
Northing	145000		200	12.5
Elevation	450		68	12.5

The predictive ability of the resulting models is tested by dense blasthole (BH) data since often there are a plenty of exhaustive data available. There are a total 82355 available BH data for comparison. Figure 7.3 shows the projection of DH data versus BH data onto an East-North cross sectional view.

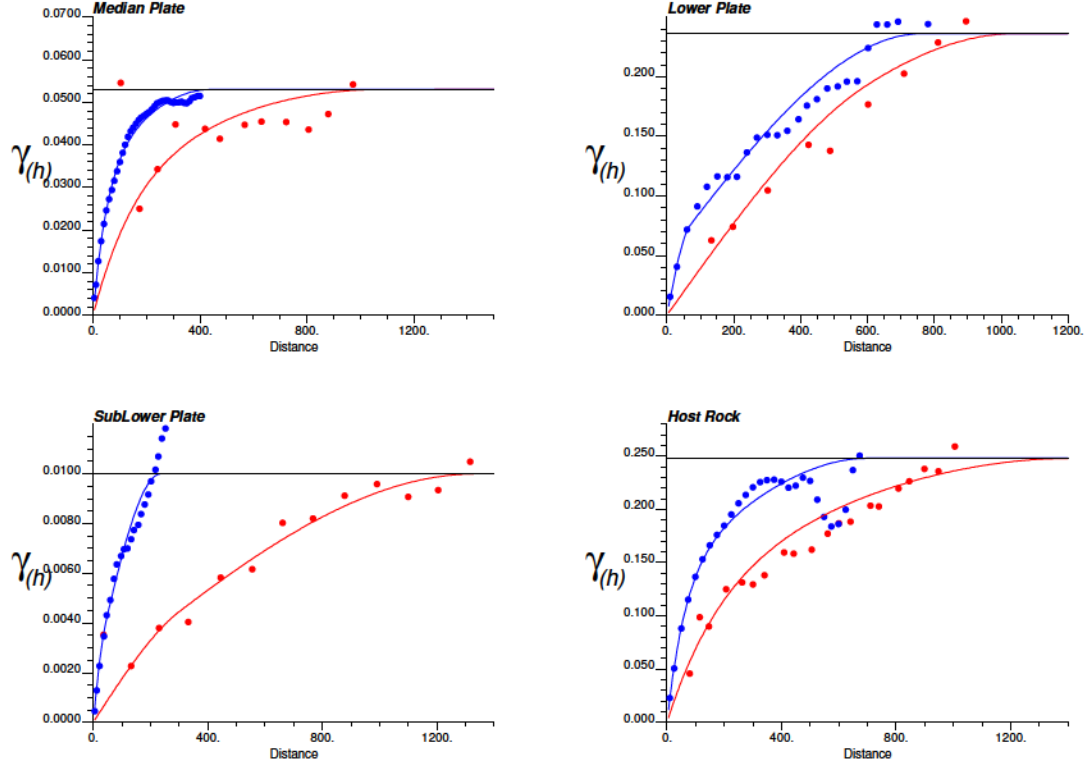


Figure 7.1: Experimental indicator and fitted variograms in horizontal direction (red) and vertical direction (blue).

7.1.1 Data Analysis

The global proportions of rock types in the data are summarized in Table 7.2. Transition probability (Eq. 7.1) is used as the measure of spatial variability for the truncation rule. From the transition probability matrix, it is not expect to see the lower plate and host rock be connected to all other rock types, and the median plate and sub lower plate to be connected occasionally.

$$\text{tp}(h) = \begin{matrix} \textit{Median} \\ \textit{Lower} \\ \textit{Sublower} \\ \textit{Host} \end{matrix} \begin{bmatrix} 0.9455 & 0.0034 & 0.0000 & 0.0511 \\ 0.0005 & 0.9798 & 0.0001 & 0.0196 \\ 0.0000 & 0.0024 & 0.9446 & 0.0530 \\ 0.0054 & 0.0138 & 0.0010 & 0.9798 \end{bmatrix} \quad (7.1)$$

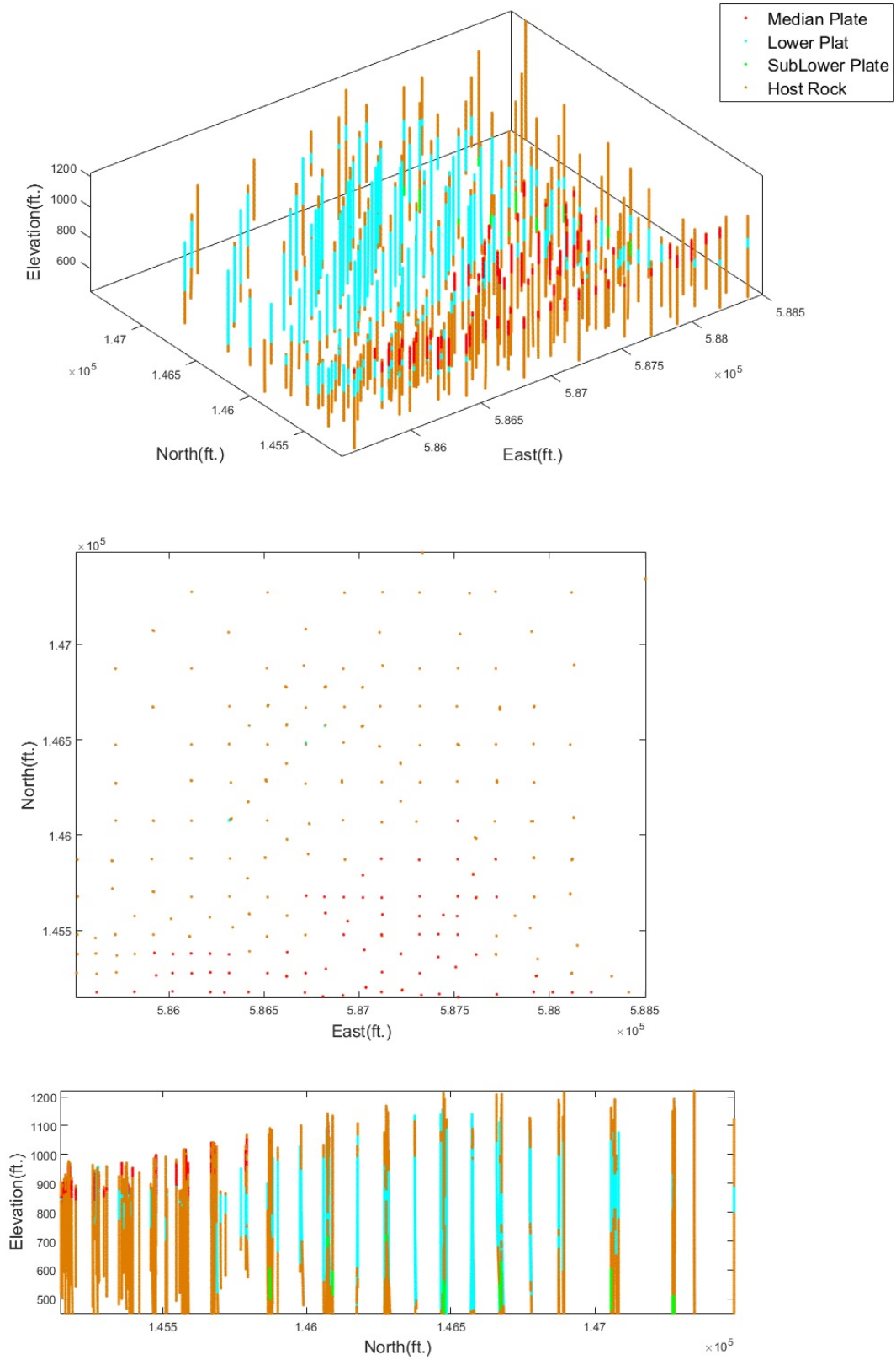


Figure 7.2: Top: location map of available DH data, middle: projected onto a North-East cross section, and bottom: North-Elevation cross sectional view.

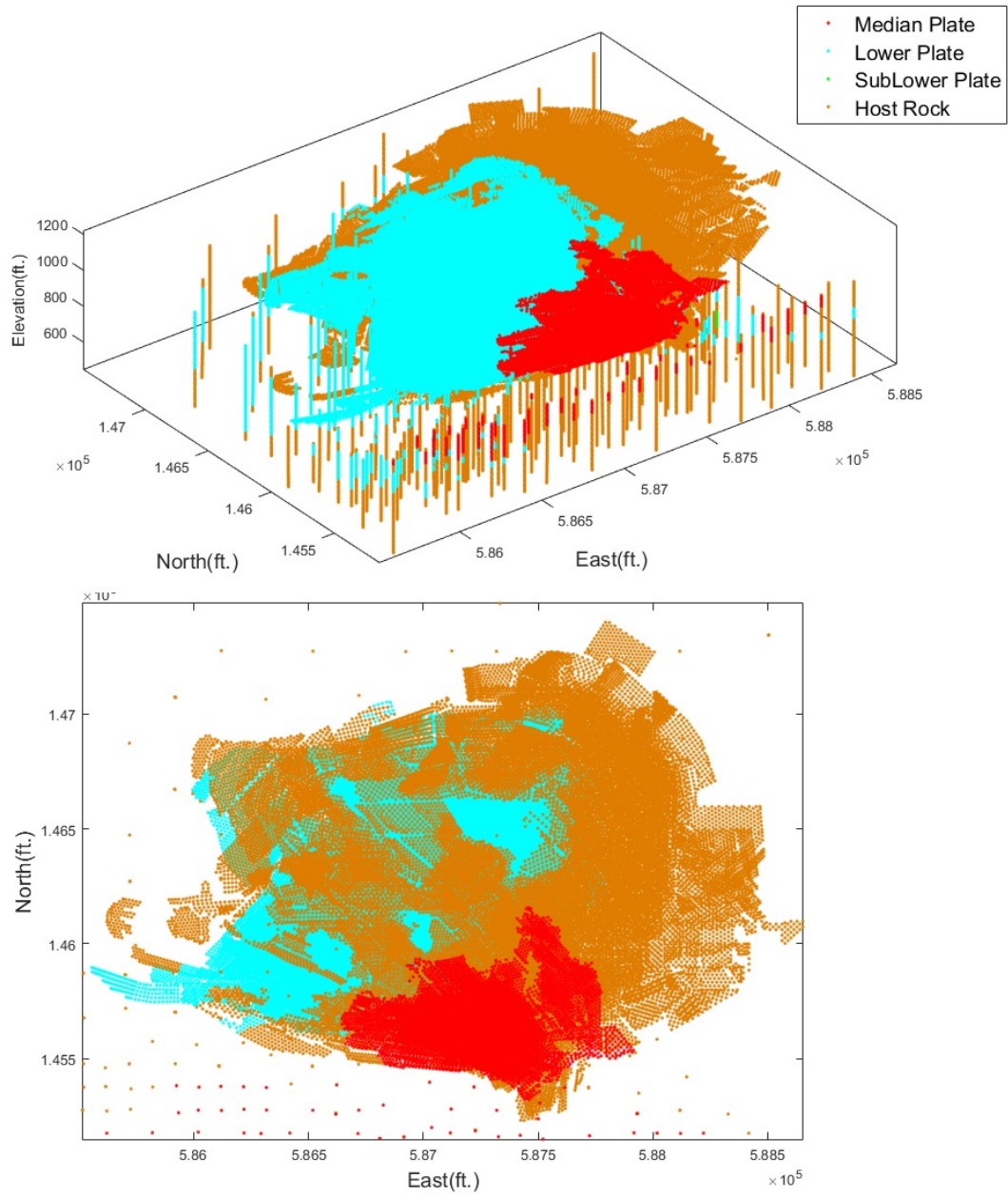


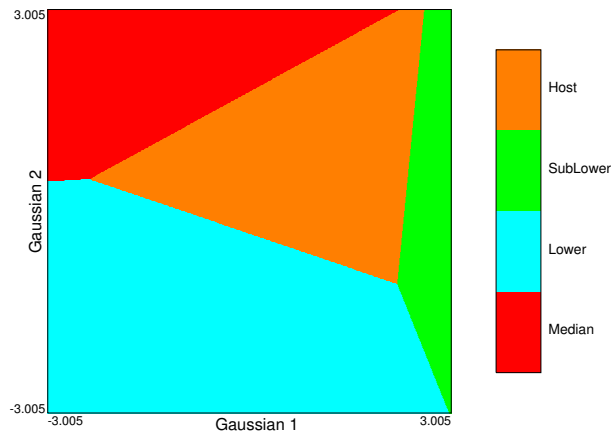
Figure 7.3: Top: location map of available BH and DH data and bottom: DH data versus BH data an East-North cross sectional view.

Table 7.2: Summary of rock types' declustered proportions in DH data and BH data.

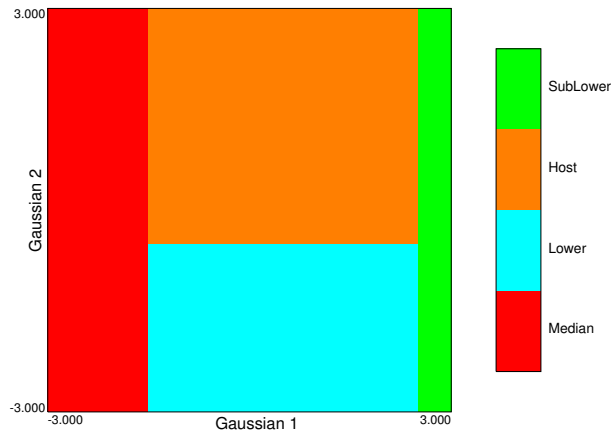
Rock Type	Median Plate	Lower Plate	SubLower Plate	Host Rock
DH Prop.	0.043	0.327	0.018	0.612
BH Prop.	0.089	0.399	0.000	0.511

7.1.2 Global Mask

The threshold mask and MDS mask are two mask frameworks that are considered in this study. Figure 7.4 demonstrates the truncation rule with MDS and threshold based method.



(a) MDS Mask



(b) Threshold based Mask

Figure 7.4: Global truncation rules for Red Dog data set with four rock types. The two axes correspond to the values of the underlying Gaussian realizations (Y_1 and Y_2), and the color codes correspond to the domain of the different rock types.

7.2 Variogram Optimization of Underlying Gaussian Realizations

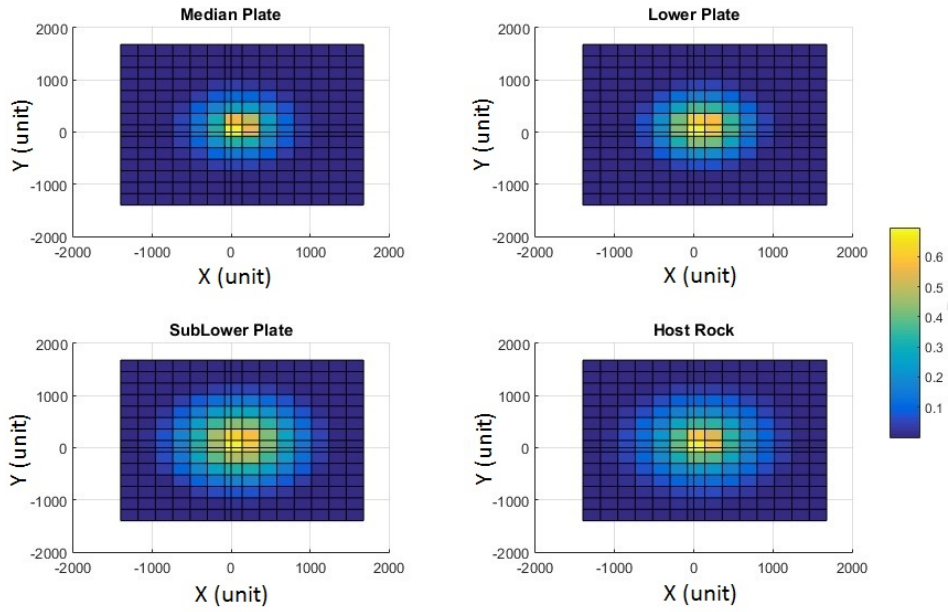
Variogram modeling of underlying Gaussian deviates in TPG method is very important for simulating geological domains. After the definition of the truncation rule, the next step is to define the spatial structure of the Gaussian variables in a way that they match the indicator variograms of the categories after truncation. For this study, variogram optimization using the covariance map as explained in section 6.4 is considered and variogram reproduction of rock types with two and three Gaussian deviates is checked. The addition of more Gaussian deviates is discussed and compared.

Optimization begins with an initial random covariance function; optimization is used to obtain a local minimum. The initial parameterization of the variogram is as simple as possible (one structure and no horizontal anisotropy for each Gaussian deviate). The adjustment of the initial variogram parameters is based on the objective function using SA optimization until an acceptable match between the variogram model of rock types in the data set and the computed variogram model of rock types from the simulation results is achieved. As mentioned in Section 6.4, the objective function is the difference between the modeled covariance maps of the rock types and the covariance maps of truncated simulations. Figure 7.5 shows the a slices of 3D representation of covariance of off sets for data onto X-Y and Y-Z cross sections for the four available rock types.

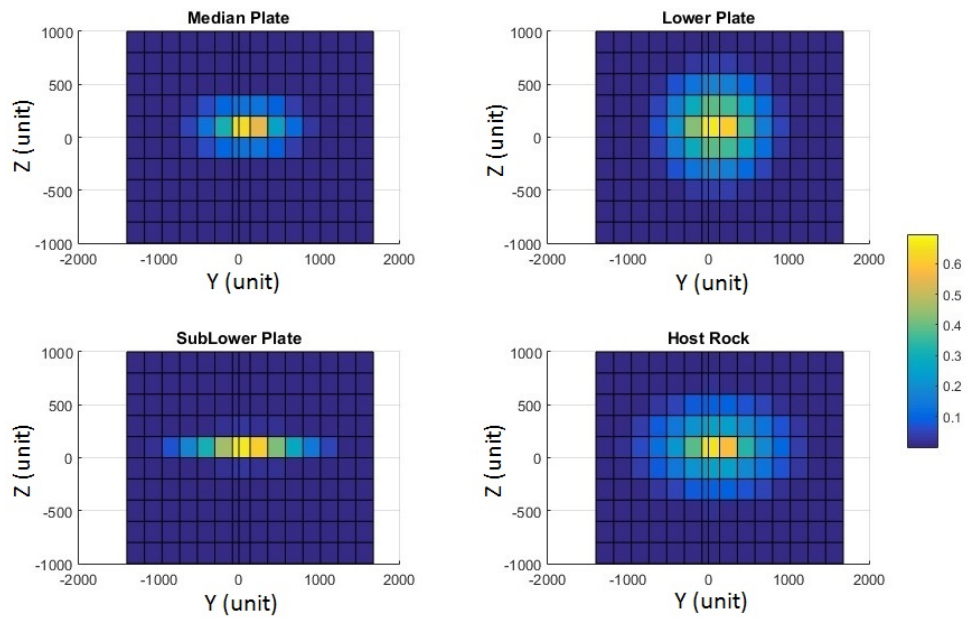
Results have been compared by using two and three Gaussian realizations. All the Gaussian realizations have Gaussian covariance/variogram models and a Gaussian distribution with mean zero and variance of one ($N(0, 1)$).

Variogram Optimization using Two Gaussian Deviates

In the first step of variogram optimization, one isotropic Gaussian structure is considered and SA is used to optimise the variogram of the underlying Gaussian deviates until the objective function is minimized and the target covariance map of rock types is reproduced. A Gaussian covariance model characterizes phenomena with very high



(a) X-Y cross sectional view



(b) Y-Z cross sectional view

Figure 7.5: slices of 3D representation of covariance of off sets for data for four available rock types colored by covariance values.

spatial continuity and has the smaller nugget variance due to its parabolic behavior at the origin. The nugget effect of 0.01 has been selected for these realizations since a matrix instability problem may occur by the Gaussian covariance model (Posa (1989); Stein and Handcock (1989)).

Optimization is performed with 500 different random restarts and the one with the smallest objective value is considered as the best match. Table 7.3 summarizes the optimized parameters with the proposed method. The algorithm started with an objective value of 2.15 and stopped with a final objective value of 0.99.

Here, the Gaussian function Y_1 is modeled with a Gaussian covariance model with one nested structure with a horizontally isotropic variogram. The optimized ranges for Y_1 are 890 ft. and 526 ft. in the horizontal and vertical directions, respectively. Y_2 also has a Gaussian covariance with optimized ranges of 1038 ft. and 703 ft. in the horizontal and vertical directions, respectively. The final reproduction of variograms with optimized parameters for both horizontal and vertical directions is shown in Figure 7.6. There is a noticeable fluctuation in variogram reproduction of the median plate and sub lower plate which is expected due to the low proportions of these two rock types. Reproduction of input proportions of the categories among 100 unconditional simulations is presented in Table 7.4. The input proportions are reproduced well.

Table 7.3: Summary of optimized variogram parameters using proposed optimization for both Gaussian deviates and one nested structure.

γ Parameters	h_a of G_1	h_v of G_1	h_a of G_2	h_v of G_2
Optimized	890 (ft.)	526 (ft.)	1038 (ft.)	703 (ft.)

Table 7.4: Reproduction of input proportions of the categories using 100 unconditional simulations with one nested structure.

Plate	Median	Lower	SubLower	Host Rock
DH Prop.	0.058	0.382	0.010	0.550
Reproduced Prop.	0.057	0.377	0.010	0.556

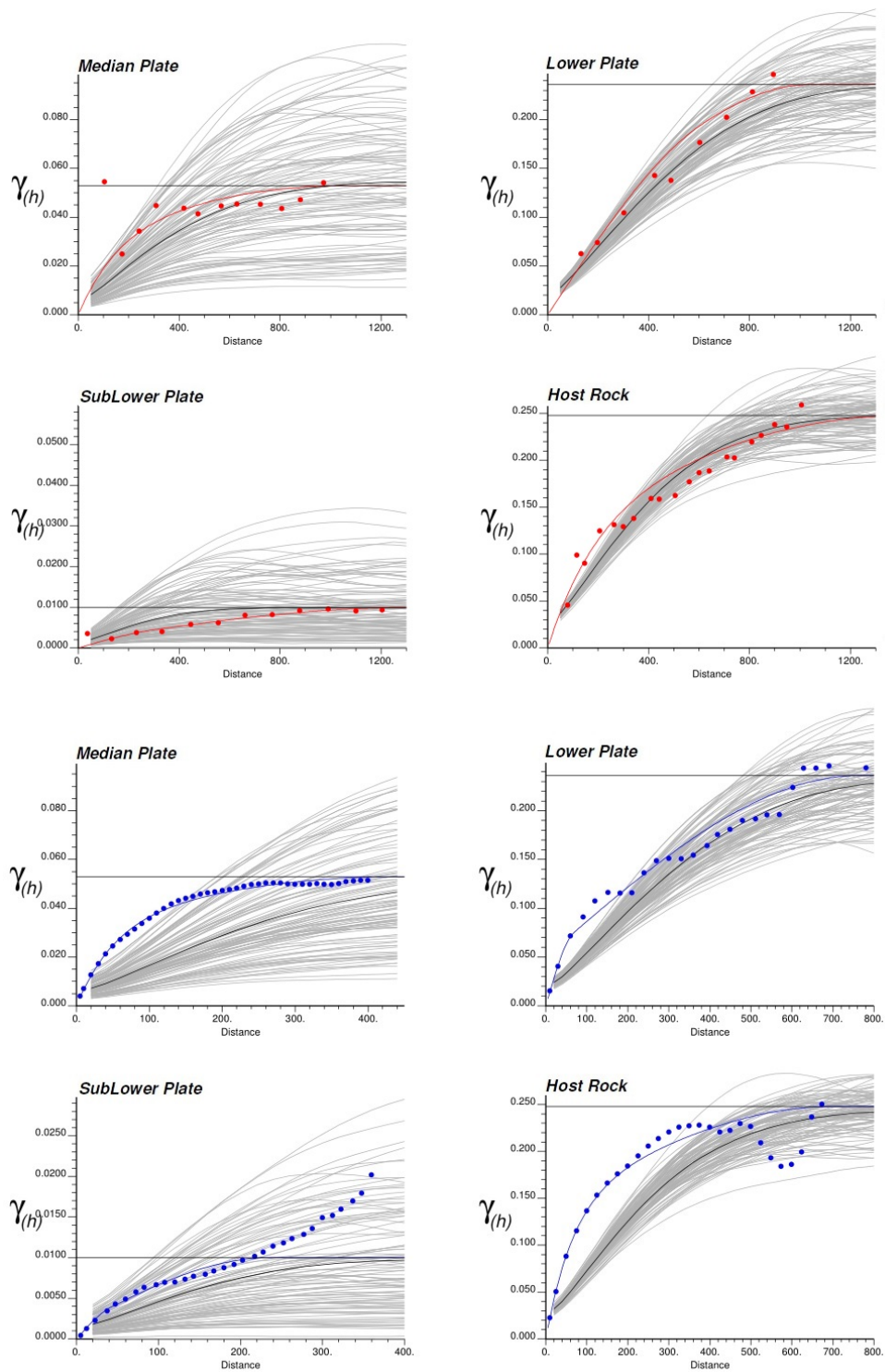


Figure 7.6: Reproduction of model variograms with TPG in horizontal (red) and vertical (blue) directions using two Gaussian deviates and one nested structure. Gray lines are the variograms of 100 unconditional simulated realizations.

Here, optimization began with a simple variogram model and one structure to find the local minimum but indicator variograms of all rock types are not well reproduced. Therefore, another step is required to improve variogram reproduction.

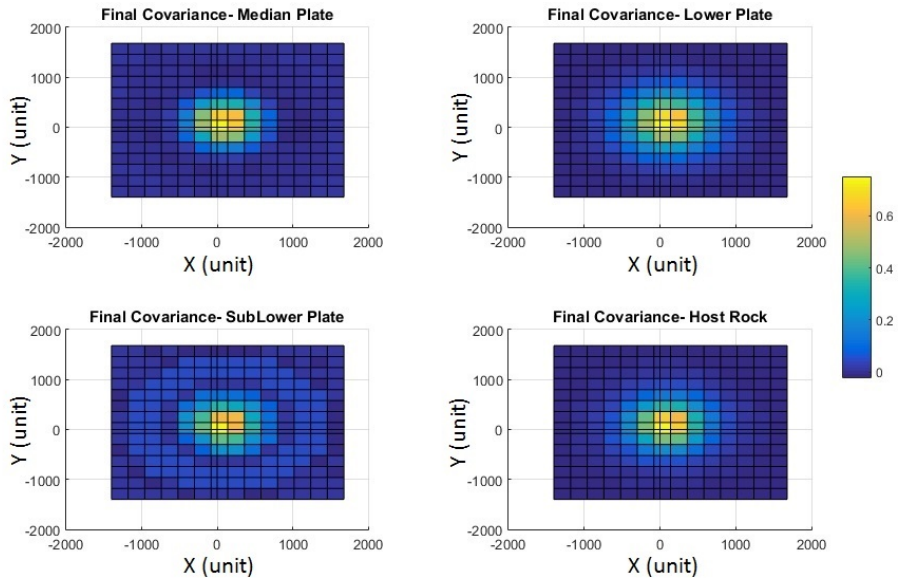
So, in the second step, another Gaussian structure is added to the variogram model of optimum solution and the optimization algorithm is started with the optimum solution from the previous step. Contribution for each nested structure is another optimization parameter. The new set of parameters is iteratively adjusted to minimize the objective function and find the global minimum. Slices of a 3D representation of covariance of off sets for data using optimized variogram parameters of categories onto X-Y and Y-Z cross sections for four available rock types are shown in Figure 7.7. For instance, it is noticeable how the covariance map of the indicator variable which represents the sub lower plate in the simulation came close to covariance map of sub lower plate in data. Also, the final variogram reproduction with optimized parameters for both horizontal and vertical directions is shown in Figure 7.8. By adding one more structure, the objective value reduced to 0.84 and the results represent an improvement by 7%. Input proportions of the rock types among 100 simulations are reproduced well and presented in Table 7.5. Table 7.6 summarizes the optimized covariance/variogram parameters from the proposed methods.

Table 7.5: Reproduction of input proportions of the categories using 100 unconditional simulations with two nested structures.

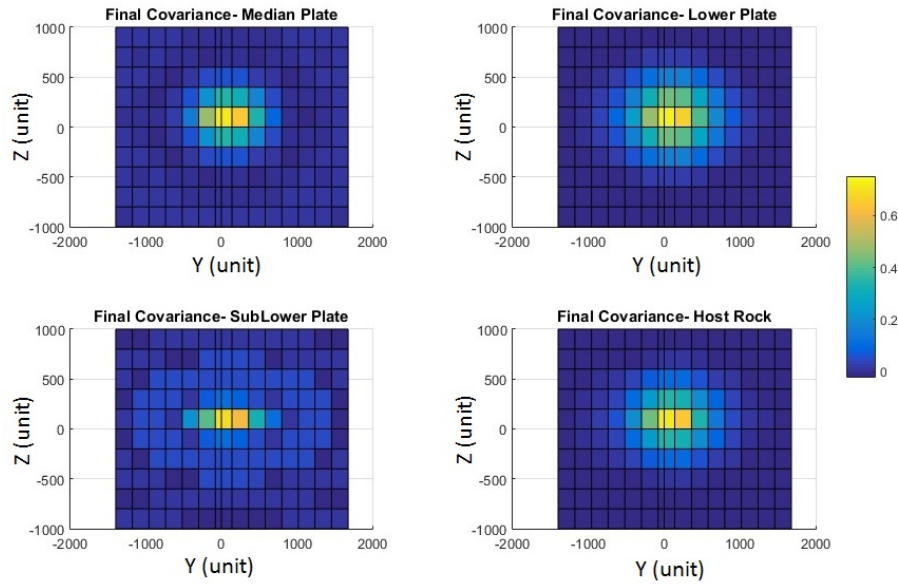
Plate	Median	Lower	SubLower	Host Rock
DH Prop.	0.058	0.382	0.010	0.550
Reproduced Prop.	0.056	0.381	0.009	0.554

Table 7.6: Summary of optimized variogram parameters for both Gaussian deviates and two nested structures.

γ Parameters	h_a of G_1	h_v of G_1	$C-G_1$	h_a of G_2	h_v of G_2	$C-G_2$
Optimized-St_1	826 (ft.)	103 (ft.)	0.54	859 (ft.)	617 (ft.)	0.39
Optimized-St_2	1844 (ft.)	809 (ft.)	0.45	1028 (ft.)	668 (ft.)	0.60



(a) X-Y cross section



(b) Y-Z cross section

Figure 7.7: Slices of a 3D representation of covariance of off sets using optimized variogram parameters for four available rock types with two nested structures.

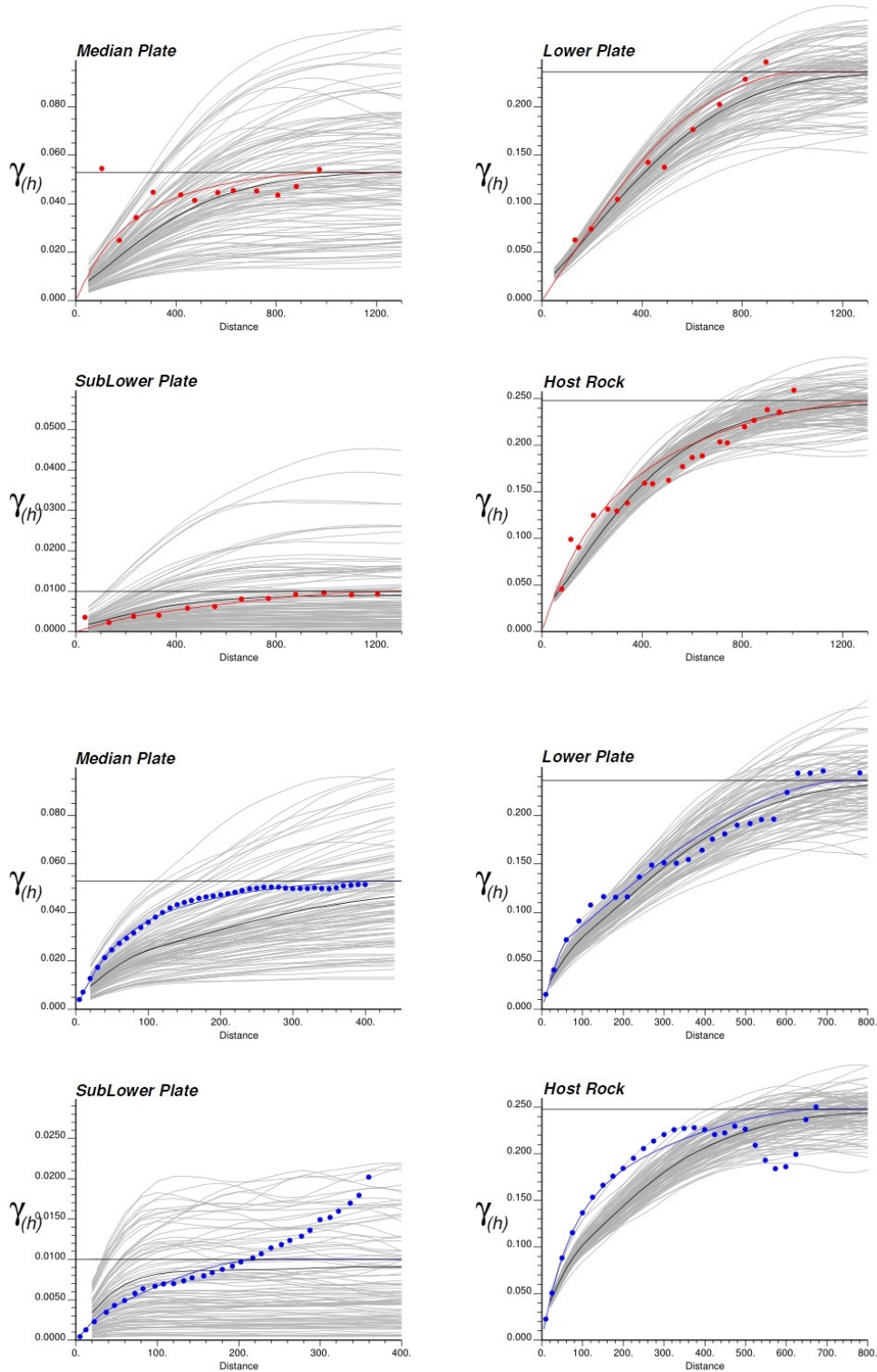


Figure 7.8: Reproduction of model variograms with TPG in horizontal (red) and vertical (blue) directions using two Gaussian deviates and two nested structures. Gray lines are the variograms of 100 unconditional simulated realizations.

Variogram Optimization using Three Gaussian Deviates

Variogram reproduction of rock types is also checked with use of three underlying Gaussian deviates. Figure 7.9 demonstrates the global MDS mask for three Gaussian deviates. Here, Gaussian functions Y_1 , Y_{21} , and Y_3 are first modeled with a Gaussian covariance model with one nested structure with a horizontally isotropic variogram and then a second nested structure is added. A nugget effect of 0.01 is selected for these realizations. Final reproduction of model variograms with optimized parameters for both horizontal and vertical directions with three Gaussian deviates is shown in Figure 7.10 and Figure 7.11. The input proportions are reproduced well. By comparing the mismatch between the target indicator variogram model and the averaged variogram of the resulting 100 simulated indicator values for the successive lag distances, the variogram reproduction is found to be improved by 16% with three Gaussian deviates. Figure 7.12 shows the improvement in variogram reproduction (Eq. 7.2) for all four rock types in vertical and horizontal directions.

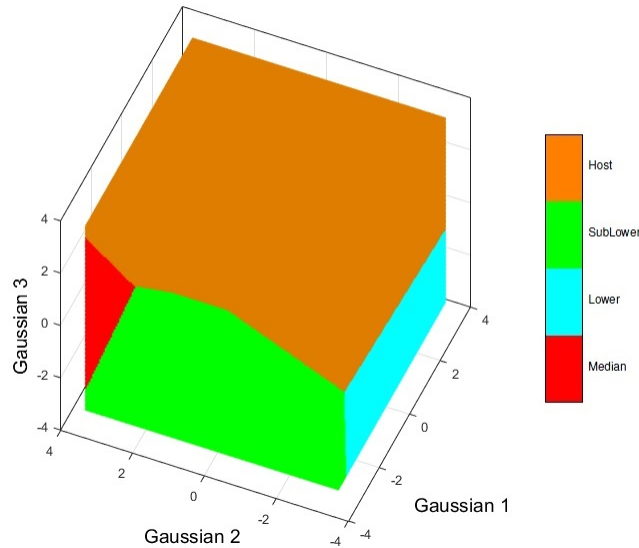


Figure 7.9: Truncation rule based on the MDS with three Gaussian deviates.

$$Error\%(\mathbf{h}; \mathbf{k}) = \frac{|\gamma_k(\mathbf{h})^{model} - \gamma_k(\mathbf{h})^{Average}|}{\gamma_k(\mathbf{h})^{model}} \times 100, \quad k = 1, \dots, K \quad (7.2)$$

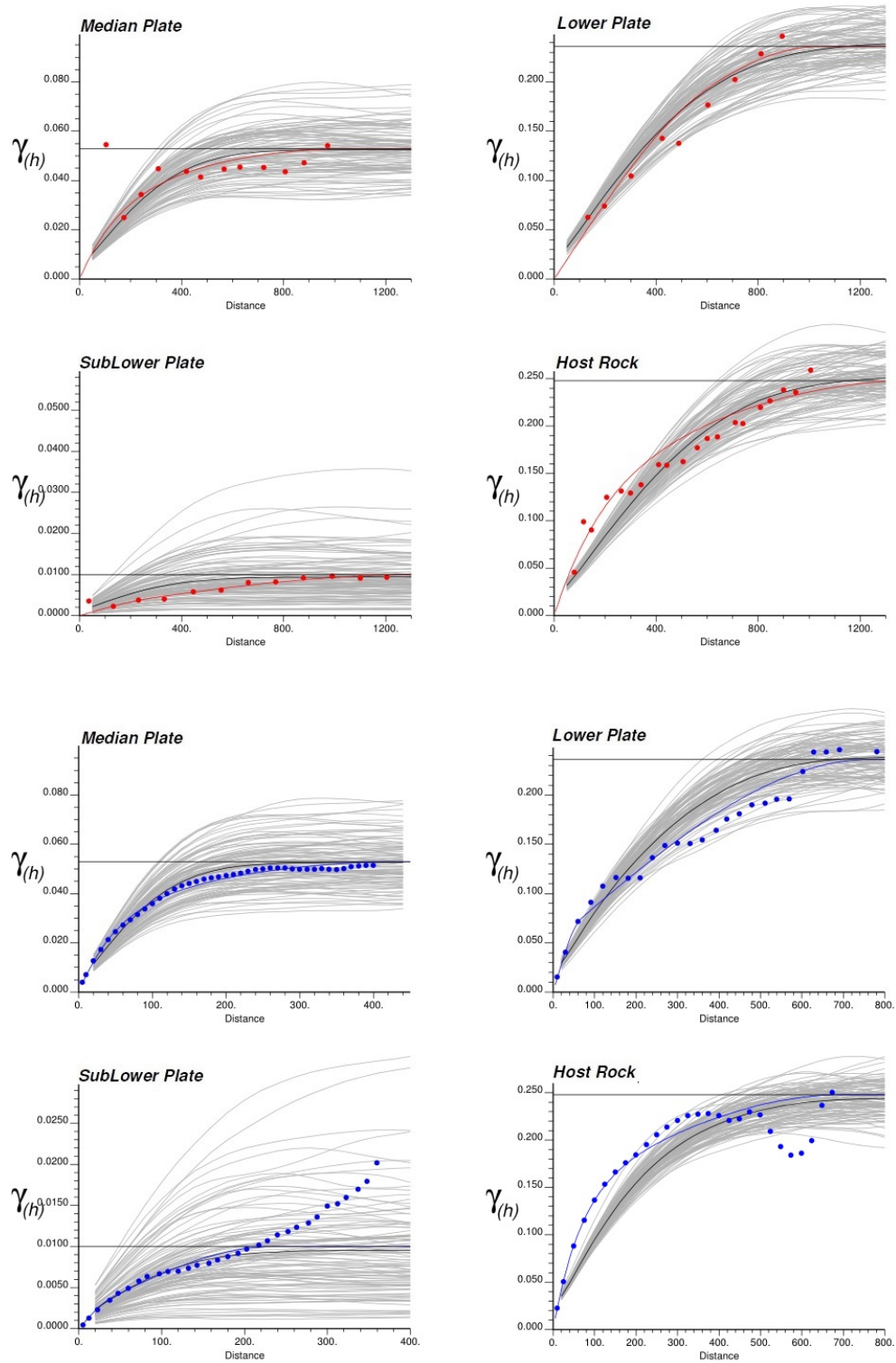
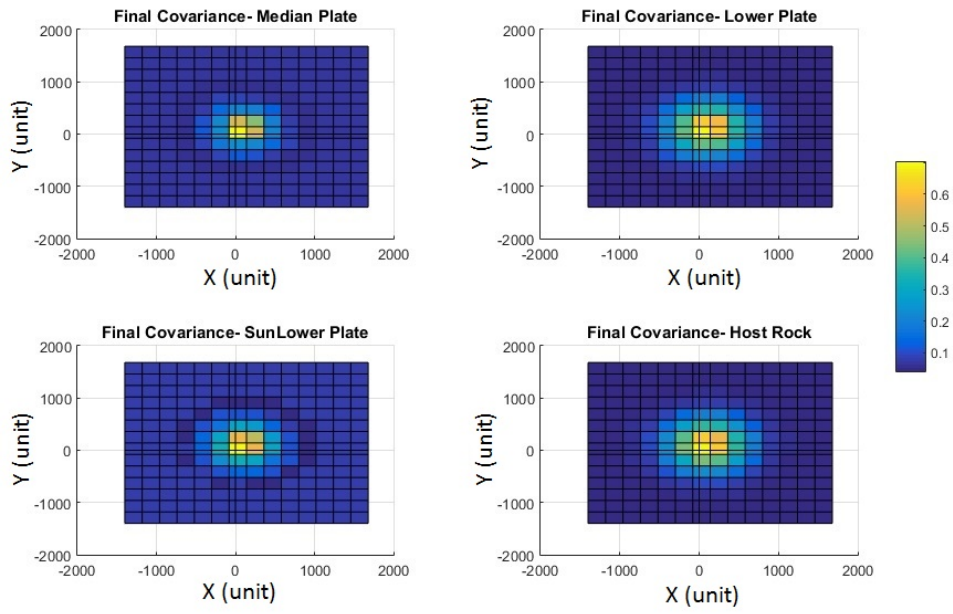
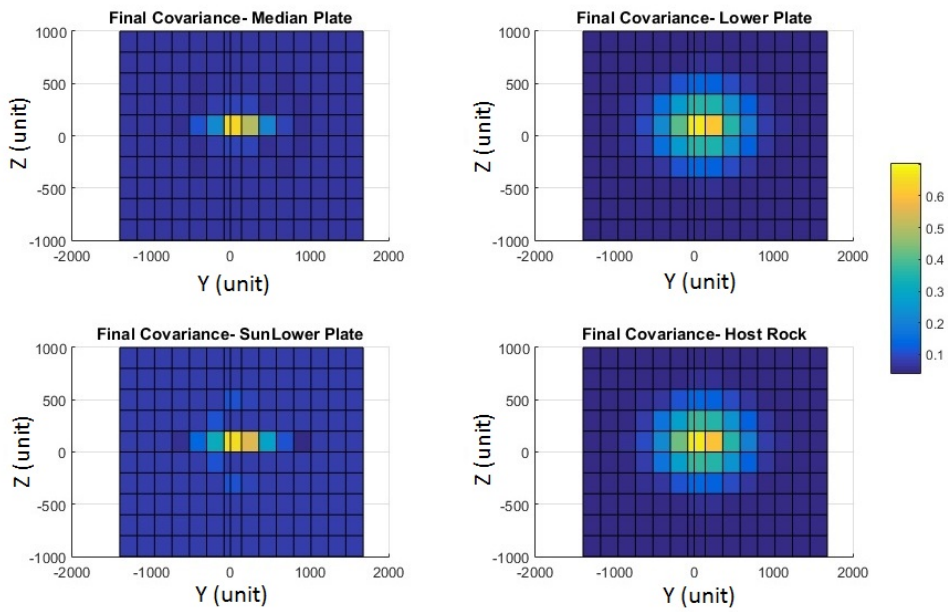


Figure 7.10: Reproduction of model variograms with TPG in horizontal (red) and vertical (blue) directions using three Gaussian deviates. Gray lines are the variograms of 100 unconditional simulated realizations.



(a) X-Y cross section



(b) Y-Z cross section

Figure 7.11: Slices of a 3D representation of covariance of off sets using optimized variogram parameters for four available rock types with three Gaussian deviates colored by covariance values.

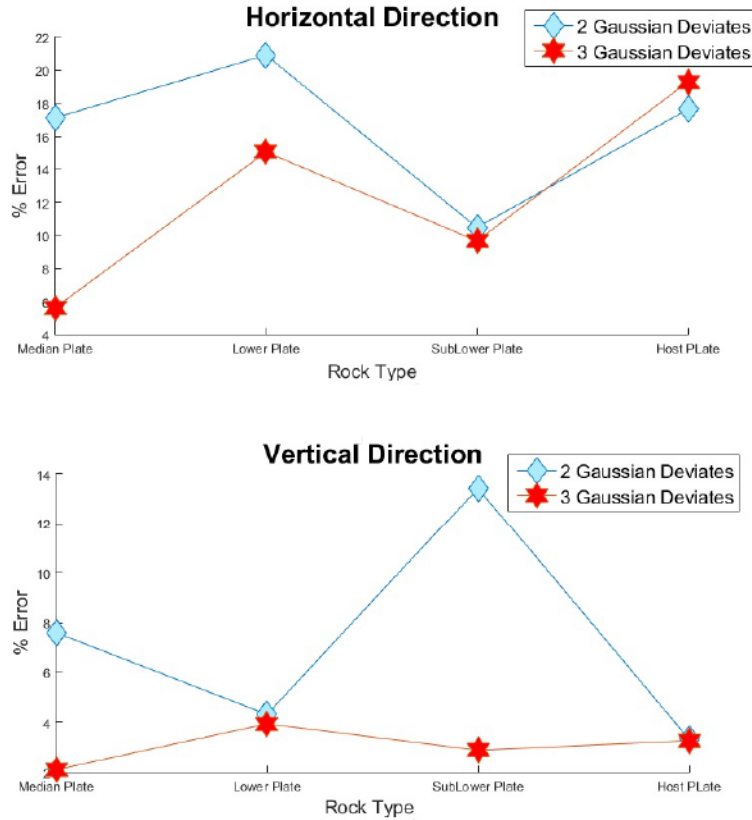


Figure 7.12: Percent error in variogram reproduction of rock types. Top: in horizontal direction and bottom: vertical direction. Red color using three underlying Gaussian Deviates and blue color using two underlying Gaussian Deviates.

Variogram Reproduction Comparison

Here, variogram reproduction of TPG simulation is compared with the results of the proposed MCS based methodology by [Zagayevskiy and Deutsch \(2015\)](#) which is developed by [D. S. Silva and Deutsch \(2016b\)](#). This approach obtains the Gaussian variograms numerically using Monte Carlo simulation. Variograms reproduction of the MCS based method for both horizontal and vertical directions using three underlying Gaussian realizations is shown in Figure 7.13.

Using the proposed covariance optimization, an excellent variogram reproduction for the median plate, lower plate in the horizontal direction and the median plate and sub lower plate in the vertical direction is achieved. Variogram reproductions for other two rock types in both directions are reasonable. Also, the MCS based approach

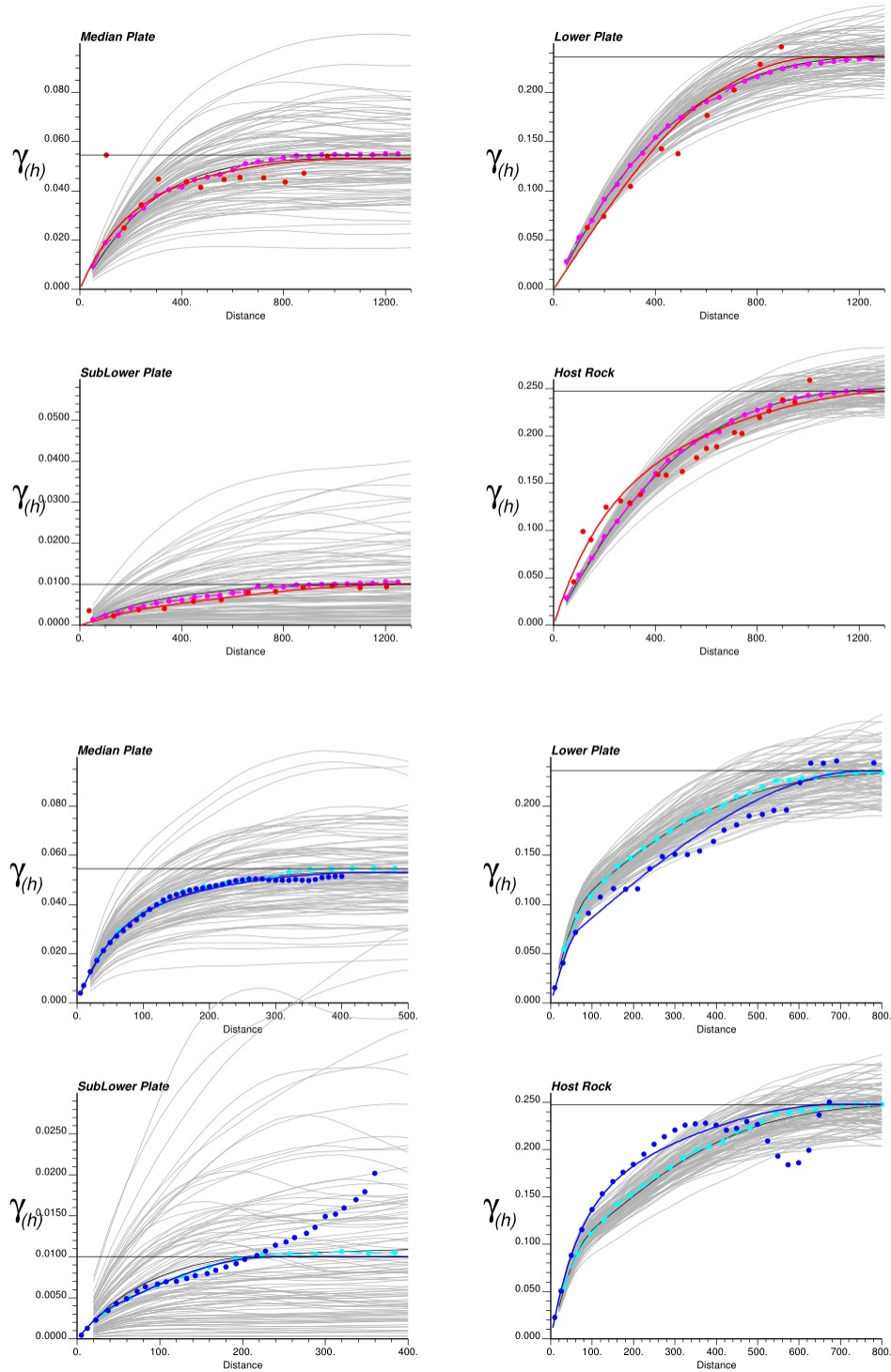


Figure 7.13: Reproduction of model variograms in horizontal (red) and vertical (blue) directions using MCS based methodology using three underlying Gaussian realizations. The solid black lines are the average variograms calculated from all realizations. Markers in violet and light blue color are the optimized points from MCS based method for the indicator variograms. Gray lines are the variograms of 100 unconditional simulated realizations.

obtained a good reproduction for the mentioned rock types.

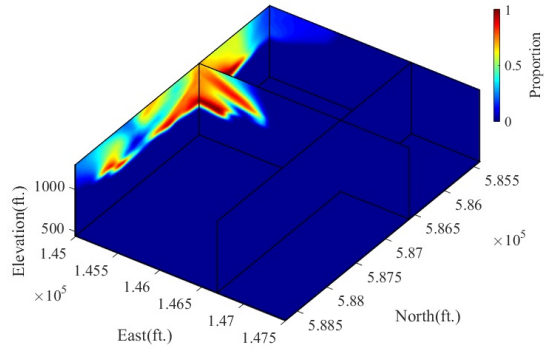
Finding the covariance/variogram of the underlying Gaussian deviates in TPG simulation to reproduce the indicator variogram of all indicator variables is challenging. In this study, a novel idea with optimization methods addressed this barrier.

7.3 Locally Varying Proportions

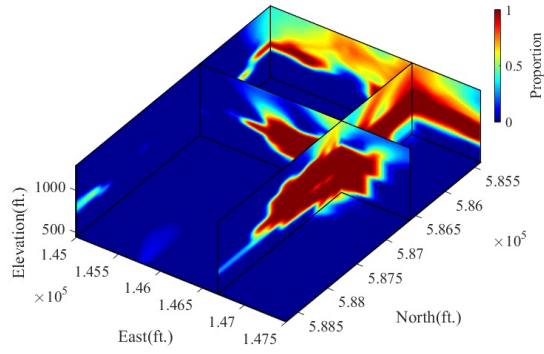
The use of locally varying masks for the incorporation of trend is discussed in this section. Comparisons are made between the simulated categorical model using a threshold based mask and a MDS mask framework as well as block sequential indicator simulation (BSIS) model. Results demonstrate that the relationships between rock types are better reproduced in TPG models. BH data is used to validate the models generated from the available DH data.

Figure 7.14 shows the trend model that has been generated using a GSLIB program "maketrend" (Manchuk & Deutsch, 2011) for four rock types. The trend model demonstrates the locally varying proportion of each plate in different locations of the area of interest. The spatial distribution of the proportions of rock types is shown in Figure 7.15. The variation of the rock types' proportion in the vertical direction is clear. The locally varying mask is used to handle LVP and truncate underlying Gaussian realizations. To generate the Gaussian realizations, the optimized variogram of the previous section for two underlying Gaussian realizations with two nested structures are used. A cross section through two generated Gaussian realizations is shown in Figure 7.16.

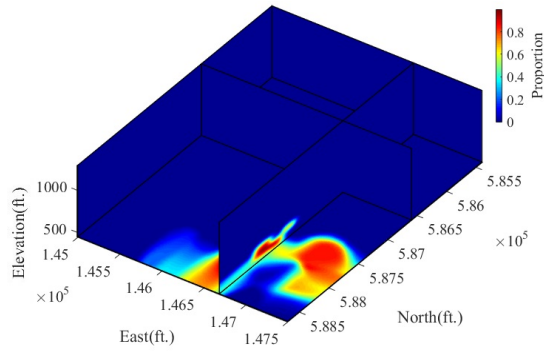
BSIS method is also used to simulate the plates in the presence of the trend. Figure 7.17 shows a 3D view of one individual simulated realization for all four methods. Visually, it is clear that the TPG realizations for both types of mask appear much smoother than BSIS realization.



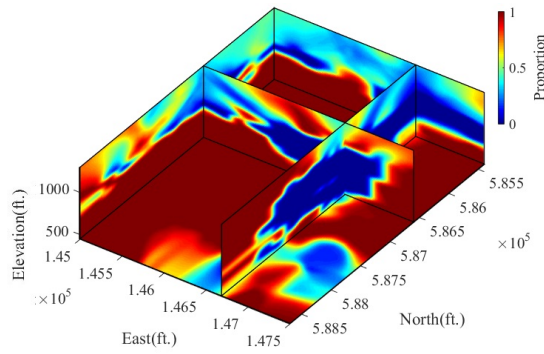
(a) Trend model for median plate



(b) Trend model for lower plate



(c) Trend model for sublower plate



(d) Trend model for host rock

Figure 7.14: 3D view of generated trend model for each plate based on the data sets.
141

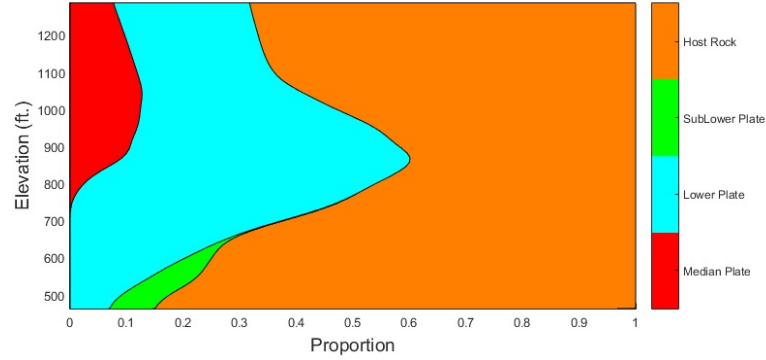


Figure 7.15: Global VPC for the Red Dog deposit.

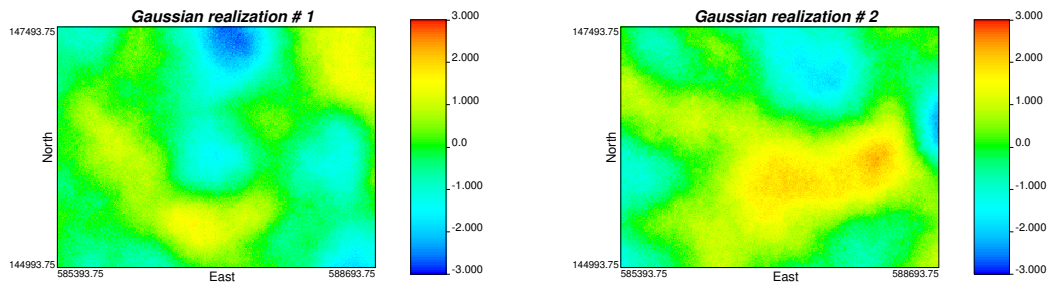
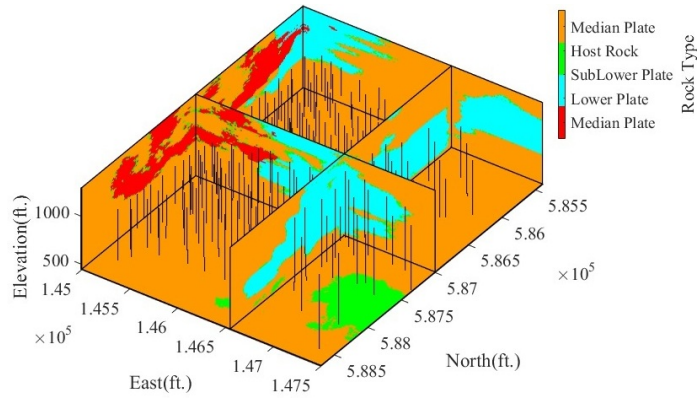


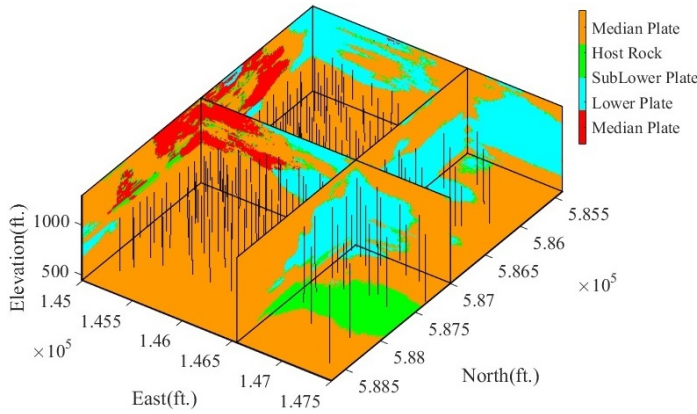
Figure 7.16: Cross section through generated Gaussian realizations with the optimized variograms.

An important check is the histogram of the simulated values. Statistical fluctuations are natural in stochastic simulation; however, these fluctuations should be reasonable and unbiased. In total, 50 realizations are generated and the summary statistics checked for reproduction. Histograms of all four plates were reproduced within reasonable statistical fluctuations for both threshold based mask and MDS based mask (Figure 7.18 and Figure 7.19).

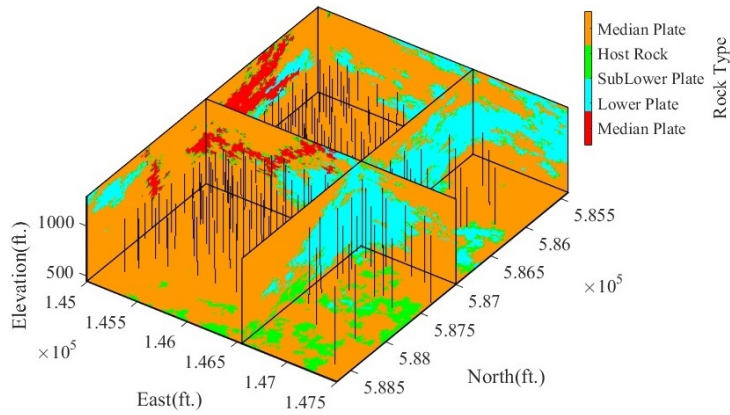
In addition to visual inspection of the realization and histogram, the error in the reproduction of observed transition probabilities in data is calculated using 50 realizations. Both TPG simulations reproduced the data transition probabilities well. When BSIS is used, transitions that are not expected to exist are present; transitions from median to sub lower and median to host are observed. Direct transitions of plates are reproduced better in TPG methods. The summary of the absolute error in transition probability reproduction ($Error = |\mathbf{tp}_{kk'}^{data} - \mathbf{tp}_{kk'}^{realization}|$) between rock types is shown in Figure 7.20.



(a) TPG simulation with threshold based mask



(b) TPG simulation with MDS mask



(c) BSIS method

Figure 7.17: 3D view of simulated realizations using TPG simulation with threshold based mask, TPG simulation with MDS mask, BSIS method.

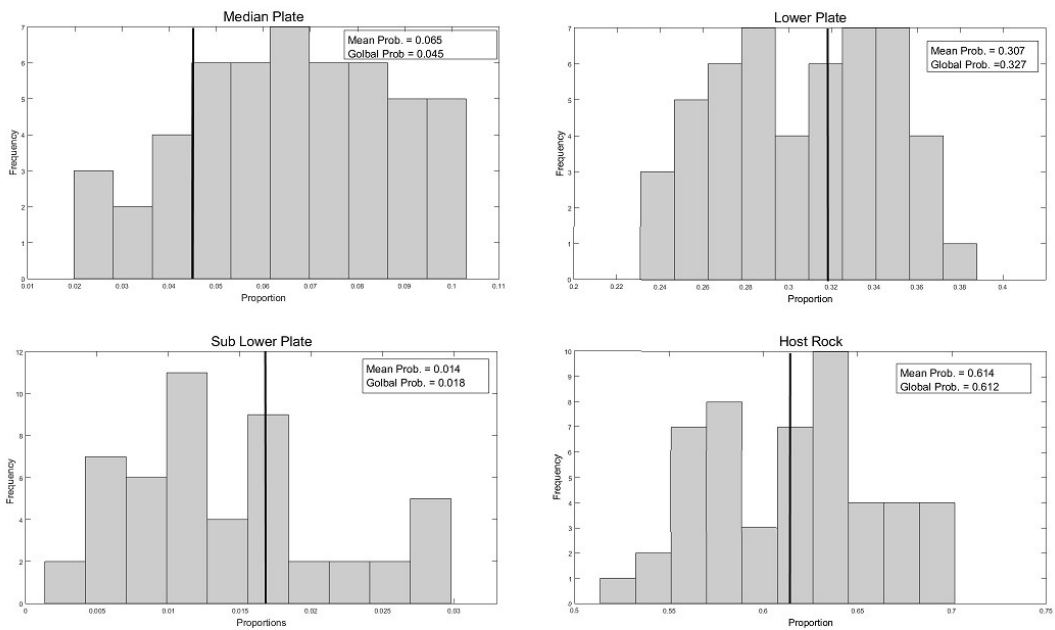


Figure 7.18: Global proportion reproduction for all four rocks with TPG simulation with threshold based mask for 50 unconditional realizations. The declustered global proportions are indicated with the black solid line.

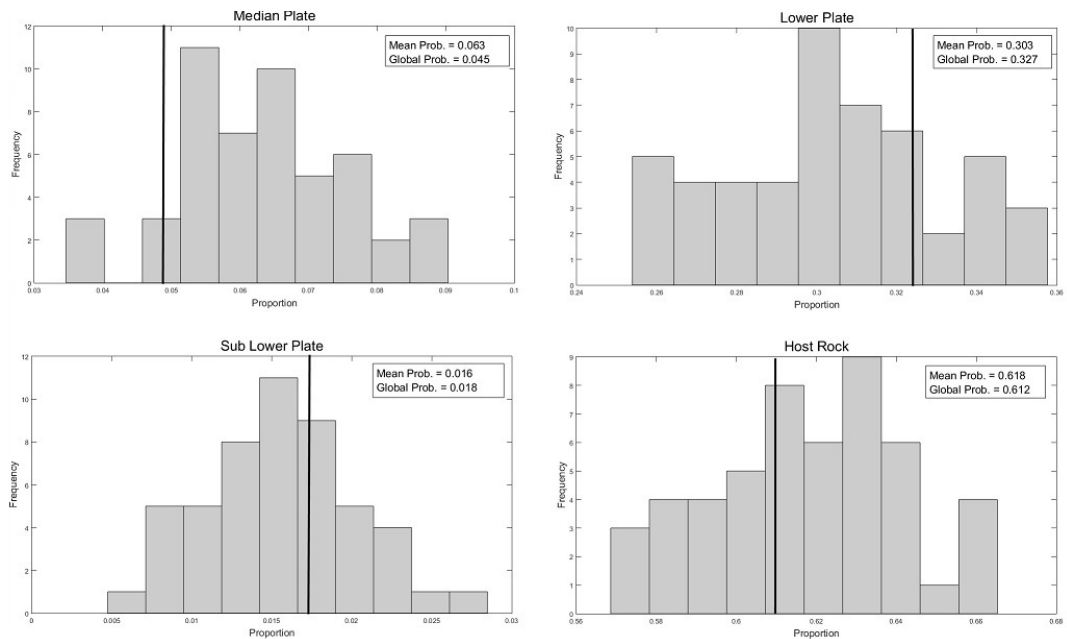


Figure 7.19: Global proportion reproduction for all four rocks with TPG simulation with MDS mask for 50 unconditional realizations. The declustered global proportions are indicated with the black solid line.

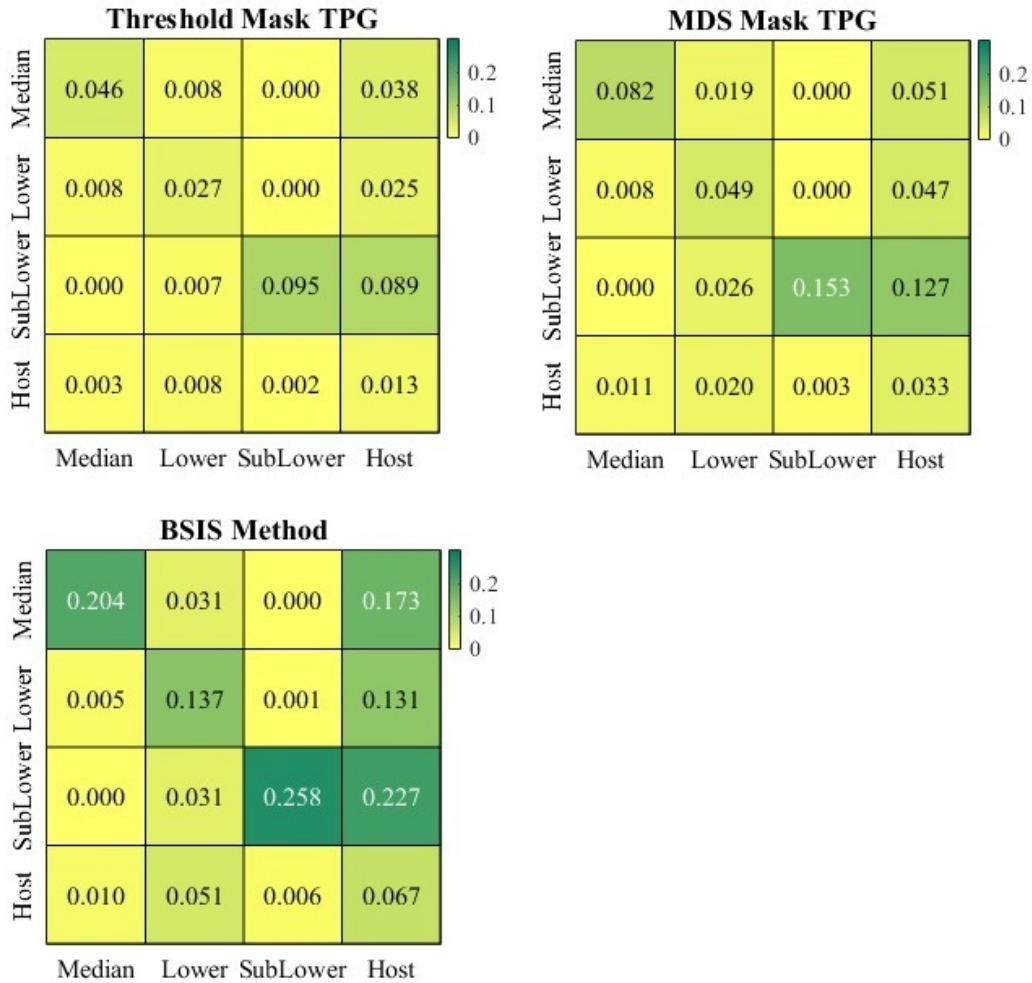


Figure 7.20: Error in transition probability reproduction using TPG methods and BSIS method colored by absolute error between transition probabilities.

The color scale characterizes the amount of error in transition probability reproduction. Darker green represents more error in **tp** reproductions. In total, TPG models have lower error than BSIS models. Also, Table 7.7 shows the total error in the reproduction of transition probabilities observed in data for the direct and cross transitions.

Table 7.7: Summary of performance in transition probabilities reproduction using TPG simulation and BSIS method.

Method	Total Error
Threshold Mask	0.369
MDS Mask	0.629
BSIS	1.301

Validation using BH Data

Cross validation is one of the most important steps in a geostatistical modeling. BH data was excluded from the input data so that it can be used to check the models and compare techniques. The error estimate refers to the expected value at each location, calculated based on the local distribution constructed using the 50 realizations. For all 50 realizations, the percentage of errors of the model to predict the expected value at BH locations is measured and then an average is calculated. Figure 7.21 shows the error estimate in a threshold based mask, MDS mask, BSIS methods. Diagonal values indicate the percentage of correctly simulated rock types at BH locations, while off diagonal terms are the percentage of incorrectly simulated rock types at BH locations. The sub lower plate does not exist in the BH area and it is not simulated in the models. The summary of the performance of each method in matching categorical observations from BH data is shown in Table 7.8.

Table 7.8: Summary of performance in reproduction of BH data using TPG simulation and BSIS method. Results are relative to TPG technique with threshold mask.

Method	% Correct	% Error
Threshold Mask	100.0	0.0
MDS Mask	99.9	0.1
BSIS	87.8	12.2

The total error in BSIS method is 1.332, while both TPG methods have smaller error in reproduction of BH rock types. The total error in classification of rock types using TPG method with threshold based mask and MDS mask is 0.369 and 0.726, respectively. Therefore, ordering relationships is reproduced better in TPG simulations.

TPG models are constructed using the threshold and MDS masks to account for the trend and outperformed BSIS. Each model is validated by checking the reproduction of representative histogram and with additional data (BH). The comparison shows the improvement of the geologic representation of the models simulated by developed TPG simulation. The relationships between rock types are better reproduced in the TPG models.

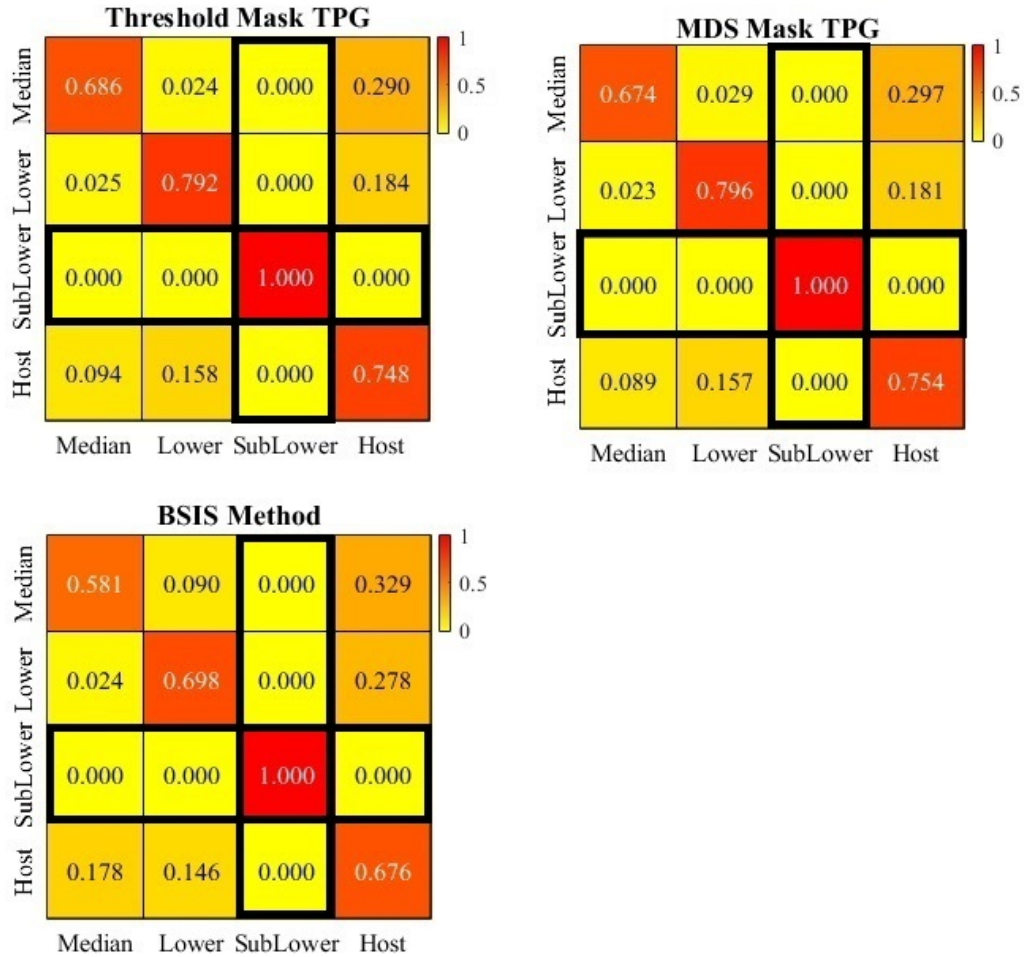


Figure 7.21: Error in matching categorical observations from BH data. Diagonal values indicate the percentage of correctly simulated rock types at BH locations, while off diagonal terms are the percentage of incorrectly simulated rock types at BH locations. The sub lower plate is not exist in the BH area.

7.4 Summary

An illustrative case study has been presented and applied to a real data set with four rock types. A new development is proposed here for categorical variable modeling using TPG simulation. Some barriers in TPG simulation such as determining the variogram of the underlying Gaussian realizations and locally varying proportions in categorical data have been addressed and the improvement using proposed methodology is shown through this case study.

The developed TPG improvements are used to create reasonable realizations that are more accurate and precise than SIS model, for instance. Also, simulated models provide better matches to the transitions observed in data and the categorical data observations from production data.

Chapter 8

Summary and Future work

There are a number of techniques available for the stochastic simulation of a categorical variable. A choice between the different techniques for stochastic categorical modeling is based on several factors: the scale of the problem, the objective of the model, the type and density of available data, and the conceptual depositional model to be reproduced (C. V. Deutsch, 2002). SIS is a well-known categorical variable modeling technique in the petroleum and mining industry. SIS does not account for ordering relationship between categories and is useful for diagenetically controlled facies or rock types due to the inherent high variability. This is a two point statistical method which is parameterized by range, direction and two points in each lag vector. MPS is another categorical variable modeling method which is widely used to characterize curvilinear features common in naturally occurring deposits. Using multiple rather than two point statistics makes this method capable of capturing complex features such as sinuous fluvial and deep water channels, dispersive patterns in lobes, and mounds associated with patch reefs. Still, finding a representative training image is often difficult and is the main drawback of this method.

TPG simulation is another method in variogram based modeling. Sometimes categories are genetically ordered due to depositional processes, climate changes and geological settings results in consistent ordering. For instance, a retrograding coast leads in a natural upward transition from fluvial to shore face to marine. TPG simulation is a powerful method for simulating categories with known ordering relationship. If the

available methods are applied properly, accurate models of categories can be obtained.

The aim is to improve TPG simulation to facilitate the use of this technique for categorical variable modeling. TPG method is reasonable to be applied to heterogeneous facies or rock types that have been genetically ordered because of depositional process (Pyrzcz & Deutsch, 2014) and have no clear geometric shapes. When there is a visible ordering between geometries, TPG simulation can be implemented to reproduce these natural orderings as well as the spatial continuity of each category. This chapter summarizes the main contributions and ends with future work.

8.1 Mask Optimization

A difficult problem in TPG simulation is the inference of a mask that reproduces the desired spatial arrangement of the categories. The determination of a truncation procedure for complicated geological environments is not an obvious task. The truncation rules control the proportions and ordering of categories in the simulation. The layout of the mask must be suitably chosen to reflect contacts between different categories. Four different methodologies have been discussed in Chapter 3 and Chapter 4.

1. **Discretized mask:** A random discretized mask is iteratively corrected using SA to impart the desired spatial features in the final TPG realization. This is an automatic mask optimization for two underlying Gaussian RFs which relies on the use of the transition probabilities of categories to find the best configuration automatically. SA is used as an optimization technique in the discretized mask optimization. SA is a powerful probabilistic technique which avoids being trapped in the local minimal and attempts to find the global minimal. However, limitation comes from the required CPU time for the convergence to the optimal mask using SA.
2. **Object based mask:** An object based mask places a number of shapes as objects randomly in the bigaussian mask. Gradient optimization is adopted to iteratively adjust the objects using sequential search directions to obtain the optimum mask. This is a fast automatic mask optimization. However, as the

number of objects and categories increases, complexity of optimization increases and since the objective function is not convex function, it would be hard to handle. Many different examples with different complexities are considered and it is found that obtaining the optimal solution for more than five categories is difficult due to the fact that the gradient technique uses the gradient value of all the parameters simultaneously for finding the optimum directions, and more categories and shapes result in more parameters in a non-convex optimization space.

3. **Threshold based mask:** The threshold based mask is the most common type of mask ([Armstrong et al., 2011](#)). A program ("*tpgsim*", Appendix, A.1) is developed which is flexible and covers most common combinations between categories. The layout of the threshold based mask is determined from the practitioners' geological knowledge. The main contribution of this work is in the handling of the spatial changes in the categories proportion. Usually, there is non-stationarity in proportions due to geological trends, and the threshold based mask is able to deal with LVP and is very fast. It is necessary to use a proper truncation mask which represents the correct relationship between the categories in each location of a domain in the presence of a trend. A developed mask is able to address the trend efficiently.
4. **MDS mask:** The MDS mask is initially developed by [J. L. Deutsch and Deutsch \(2014\)](#) and then generalized to handle LVP in categories. This method attempts to optimize the truncation mask parametrized with Voronoi polygon at every location in the presence of LVP. The methodology can be scaled to any number of underlying Gaussian variables for TPG simulation. A program "*mds_tpg_LVP*" is developed (Appendix, A.2) to deal with LVP. Due to the optimization process, CPU time can be an issue. To handle this limitation, use of a scaled trend is proposed.

Recommendations for Mask Selection

When the geological architecture of a deposit or reservoir is well understood the use of the threshold based mask is recommended to impose the known geological knowledge. This type of mask also has the advantage of considering geological trend in categories proportion.

MDS mask, discretized mask and object based mask are three proposed masks optimization that do not require input from the practitioner; they rely solely on the transition probability between the categories calculated from data. This is an important advantage which makes TPG simulation easier to implement when the transitions are complex. However, the involvement of geological knowledge in the mask is reduced in these methodologies.

The discretized mask and object based mask account for two underlying Gaussian deviates and are useful to define the contact between up to five categories. When the relationship between categories are very complicated or the use of more than two underlying Gaussian realizations is required, the MDS mask is ideal because it can be automatically scaled to any number of underlying Gaussian variables for TPG simulation.

8.2 Correlated Gaussian functions

TPG simulation is based on the truncation of Gaussian variables. Gaussian RFs should be defined in a way that describes the different spatial behavior of a category or group of categories after truncation. These Gaussian variables can be considered correlated or independent variables in TPG simulation. The effects of correlated underlying Gaussian RFs on TPG simulation are investigated in Chapter 5.

A complex geological relationship between categories can be produced by choosing different Gaussian RFs. Studies showed that correlation between them can introduce more flexibility and freedom in the modeling to capture observed specific geological features, and also can be used as a tuning parameter to improve the fit of experimental indicator variograms. However, a number of considerations has to be taken into

account. Correlation between RFs (1) can change the global proportion of the categories in the final truncated simulation; (2) can change the thresholds of the mask and accordingly the transition between categories.

Considering correlated or uncorrelated Gaussian realization is a choice that has to be made based on the observed feature in the available data set and there is no general extension to all deposits. An example is demonstrated in Chapter 5 to show different scenarios. A program "*corr_tpgsim*" (Appendix, section A.3) is developed to deal with correlation and the user is able to test these relationships for any configuration of the threshold mask.

8.3 Variogram Optimization

Another important aspect of TPG simulation is the inference of the variogram models for the underlying Gaussian RFs. Since only the indicator functions describing the categories are available, direct adjustment of the experimental variograms is difficult. In Chapter 6, three different methodologies are proposed to address this problem.

The proposed covariance map optimization ("*vargopt_tpg*", Appendix, A.4) targets the covariance or variance map of each categorical variable to optimize the variogram of the underlying Gaussian RFs. This method attempts to find the optimum input variogram parameters to best reproduce the spatial structure of each categorical variable by iteratively adding complexity to the variogram model of underlying Gaussian RFs. The optimization relies on a global mask. A case study demonstrated the potential of this method and results showed a reasonable match between the indicator variogram models of the categories in the data and simulated realization. However, it can be computational expensive to find the optimum solution since the methodology relies on finding the global minimum using random restarts. The convergence time for finding the optimum results in the case study was about 16 hours with 500 random restarts

8.4 Remarks

The main practical challenge in the application of TPG simulation is the inference of the variogram models for the underlying Gaussian deviates. This is achieved through the proposed technique in Chapter 6. The procedure may fall into local optimums depending on the initial set of parameters. Therefore, the use of many random restarts to avoid trapping is proposed, this requires a significant amount of CPU time. The other limitation of the method is that the variogram of underlying Gaussian deviates are not defined with respect to locally varying proportion of categories. TPG simulation relies on a stationary application of the Gaussian model.

8.5 Future Work

In the he following section, some ideas are suggested for future research to improve categorical variable modeling using TPG simulation as follow:

- Conditional simulation is always important in geostatistical modeling. Usually, the only available variables are those of the indicator functions describing rock types or facies which are observed in drill holes or wells. Transferring categorical data to continuous values for conditional simulation of underlying Gaussian deviates is an essential step in TPG simulation. There are some techniques available (Chapter 4), but still there are limitations in the application of TPG simulation. Accordingly, improvement is necessary to obtain the correct categories on the back transformation with the same spatial structure.
- In this work new methodologies have been developed for obtaining an optimum mask that implies global optimization. However, still there are limited numbers of truncation rules in their flexibility. Developing an automatic fully arbitrary truncation mask to back transform continuous variables to categorical simulation would be interesting.
- The flexibility of TPG technique comes from the use of multiple underlying Gaussian RFs to transfer categorical variables to a continuous space. In reality, any

number of Gaussian realizations can be used to simulate and define the relationship between categories. However, visualization of more than three Gaussian variables is very difficult. One area for future work is to facilitate the use of multiple underlying Gaussian RFs to model many categories with respect to the geological knowledge and also remain practical.

- Incorporating any sort of secondary data in TPG simulation, whether the data are coming from another source of sampled data, such as production data, or whether they are coming from exhaustive geophysical surveys, such as magnetic, seismic, or gravitational data, would improve modeling to generate a geological model that looks more realistic and represents geological complexity better.

References

- Alabert, F. (1987). Stochastic imaging of spatial distributions using hard and soft infonilation. *Msc. thesis, stanford university*.
- Alabert, F., et al. (1989). Non-gaussian data expansion in the earth sciences. *Terra Nova*, 1(2), 123–134.
- Allard, D., Dor, D., Biver, P., & Froidevaux, R. (2012). Non-parametric diagrams for pluri-gaussian simulations of lithologies. In *9th international geostatistical congress, oslo, norway* (Vol. 1115).
- Antoniou, A., & Lu, W.-S. (2007). *Practical optimization: algorithms and engineering applications*. Springer Science & Business Media.
- Armstrong, M., & Galli, A. (1999). Derivative based plurigaussian simulations. In *Proceedings of iamg* (Vol. 99, pp. 591–596).
- Armstrong, M., Galli, A., Beucher, H., Loc'h, G., Renard, D., Doligez, B., ... Geffroy, F. (2011). *Plurigaussian simulations in geosciences*. Springer Science & Business Media.
- Arpat, G. B. (2003). A multiple-scale, pattern-based approach to reservoir characterization. *International Student Paper Contest*.
- Arroyo, D., Emery, X., & Peláez, M. (2012). An enhanced gibbs sampler algorithm for non-conditional simulation of gaussian random vectors. *Computers & Geosciences*, 46, 138–148.
- Astrakova, A., & Oliver, D. S. (2015). Conditioning truncated pluri-gaussian models to facies observations in ensemble-kalman-based data assimilation. *Mathematical Geosciences*, 47(3), 345–367.

- Astrakova, A., Oliver, D. S., & Lantuéjoul, C. (2015). Truncation map estimation based on bivariate probabilities and validation for the truncated plurigaussian model. *arXiv preprint arXiv:1508.01090*.
- Ayuso, R., Kelley, K., Leach, D., Young, L., Slack, J., Wandless, J., . . . Dillingham, J. (2004). Origin of the red dog zn-pb-ag deposits, brooks range, alaska: evidence from regional pb and sr isotope sources. *Economic Geology*, *99*(7), 1533–1553.
- Beasley, J., & Springer, S. (1985). The percentage points of the normal distribution. In *Applied statistics algorithms* (pp. 188–191). JSTOR.
- Beucher, H., Galli, A., Le Loch, G., Ravenne, C., Group, H., et al. (1993). Including a regional trend in reservoir modelling using the truncated gaussian method. In *Geostatistics tróia92* (pp. 555–566). Springer.
- Boisvert, J. B. (2007). Mineral deposit modeling with pseudo-genetically constructed training images. *Msc. thesis, Alberta university*.
- Boisvert, J. B., Pyrcz, M. J., & Deutsch, C. V. (2007). Multiple-point statistics for training image selection. *Natural Resources Research*, *16*(4), 313–321.
- Boucher, A. (2009). Sub-pixel mapping of coarse satellite remote sensing images with stochastic simulations from training images. *Mathematical Geosciences*, *41*(3), 265–290.
- Busetti, F. (2003). Simulated annealing overview. *JP Morgan, Italy*.
- Carle, S. F., & Fogg, G. E. (1996). Transition probability-based indicator geostatistics. *Mathematical geology*, *28*(4), 453–476.
- Carnevali, P., Coletti, L., & Patarnello, S. (1985). Image processing by simulated annealing. *IBM Journal of Research and Development*, *29*(6), 569–579.
- Carrasco, P., Ibarra, F., Rojas, R., Le Loch, G., & Séguret, S. (2007). Application of the truncated gaussian simulation method to a porphyry copper deposit. In *Proceedings of the 33rd international symposium on application of computers and operation research in the mineral industry apcom* (pp. 31–39).
- Carrillat, A., Sharma, S. K., Grossmann, T., Iskenova, G., Friedel, T., et al. (2010). Geomodeling of giant carbonate oilfields with a new multipoint statistics workflow. In *Abu Dhabi international petroleum exhibition and conference*.

- Chiles, J.-P., & Delfiner, P. (2009). *Geostatistics: modeling spatial uncertainty* (Vol. 497). John Wiley & Sons.
- Chiu, S. N., Stoyan, D., Kendall, W. S., & Mecke, J. (2013). *Stochastic geometry and its applications*. John Wiley & Sons.
- Chong, E. K., & Zak, S. H. (2013). *An introduction to optimization* (Vol. 76). John Wiley & Sons.
- Christakos, G. (1990). A bayesian/maximum-entropy view to the spatial estimation problem. *Mathematical Geology*, *22*(7), 763–777.
- Christakos, G. (2012). *Modern spatiotemporal geostatistics*. Courier Corporation.
- Chugunova, T. L., & Hu, L. Y. (2008). Multiple-point simulations constrained by continuous auxiliary data. *Mathematical geosciences*, *40*(2), 133–146.
- David, M. (1977). Geostatistical ore reserve estimation: Elsevier sci. Publ. Co., New York.
- Delbari, M., Loiskandl, W., & Afrasiab, P. (2010). Uncertainty assessment of soil organic carbon content spatial distribution using geostatistical stochastic simulation. *Soil Research*, *48*(1), 27–35.
- De Marsily, G., Delay, F., Gonçalves, J., Renard, P., Teles, V., & Violette, S. (2005). Dealing with spatial heterogeneity. *Hydrogeology Journal*, *13*(1), 161–183.
- Deutsch, C., & Tran, T. (2002). Fluvsim: a program for object-based stochastic modeling of fluvial depositional systems. *Computers & Geosciences*, *28*(4), 525–535.
- Deutsch, C. V. (1992). *Annealing techniques applied to reservoir modeling and the integration of geological and engineering (well test) data* (Unpublished doctoral dissertation). stanford university.
- Deutsch, C. V. (2002). *Geostatistical reservoir modeling*. Oxford university press.
- Deutsch, C. V., & Cockerham, P. W. (1994). Practical considerations in the application of simulated annealing to stochastic simulation. *Mathematical Geology*, *26*(1), 67–82.
- Deutsch, C. V., Journel, A. G., et al. (1992). Geostatistical software library and users guide. *New York*, *119*, 147.

- Deutsch, J. L., & Deutsch, C. V. (2014). A multidimensional scaling approach to enforce reproduction of transition probabilities in truncated plurigaussian simulation. *Stochastic environmental research and risk assessment*, 28(3), 707–716.
- De Vera, J., McClay, K., & King, A. (2004). Structure of the red dog district, western brooks range, alaska. *Economic Geology*, 99(7), 1415–1434.
- Dimitrakopoulos, R., Mustapha, H., & Gloaguen, E. (2010). High-order statistics of spatial random fields: exploring spatial cumulants for modeling complex non-gaussian and non-linear phenomena. *Mathematical Geosciences*, 42(1), 65–99.
- Dowd, P., Pardo-Igúzquiza, E., & Xu, C. (2003). Plurigau: a computer program for simulating spatial facies using the truncated plurigaussian method. *Computers & geosciences*, 29(2), 123–141.
- Dubrule, O. (1989). A review of stochastic models for petroleum reservoirs. In *Geostatistics* (pp. 493–506). Springer.
- Dubrule, O. (1993). Introducing more geology in stochastic reservoir modelling. In *Geostatistics tróia92* (pp. 351–369). Springer.
- Dupanloup, I., Schneider, S., & Excoffier, L. (2002). A simulated annealing approach to define the genetic structure of populations. *Molecular Ecology*, 11(12), 2571–2581.
- Emery, X. (2004). Properties and limitations of sequential indicator simulation. *Stochastic Environmental Research and Risk Assessment*, 18(6), 414–424.
- Emery, X. (2007). Simulation of geological domains using the plurigaussian model: new developments and computer programs. *Computers & Geosciences*, 33(9), 1189–1201.
- Emery, X. (2010). On the existence of mosaic and indicator random fields with spherical, circular, and triangular variograms. *Mathematical Geosciences*, 42(8), 969–984.
- Emery, X., Arroyo, D., & Peláez, M. (2014). Simulating large gaussian random vectors subject to inequality constraints by gibbs sampling. *Mathematical Geosciences*, 46(3), 265–283.
- Emery, X., Ortiz, J., & Cáceres, A. (2008). Geostatistical modelling of rock type

- domains with spatially varying proportions: application to a porphyry copper deposit. *Journal of the Southern African Institute of Mining and Metallurgy*, 108(5), 284–292.
- Fachri, M., Tveranger, J., Braathen, A., & Schueller, S. (2013). Sensitivity of fluid flow to deformation-band damage zone heterogeneities: A study using fault facies and truncated gaussian simulation. *Journal of Structural Geology*, 52, 60–79.
- Fletcher, R., & Reeves, C. M. (1964). Function minimization by conjugate gradients. *The computer journal*, 7(2), 149–154.
- Fontaine, L., & Beucher, H. (2006). Simulation of the muyumkum uranium roll front deposit by using truncated plurigaussian method. In *6th international mining geology conference, "rising the challenge"* (p. 5p).
- Galli, A., Beucher, H., Le Loch, G., Doligez, B., et al. (1994). The pros and cons of the truncated gaussian method. In *Geostatistical simulations* (pp. 217–233). Springer.
- Galli, A., Le Loch, G., Geffroy, F., & Eschard, R. (2006). An application of the truncated pluri-gaussian method for modeling geology.
- Gandin, L. S., & Hardin, R. (1965). *Objective analysis of meteorological fields* (Vol. 242). Israel program for scientific translations Jerusalem.
- Goovaerts, P. (1997). *Geostatistics for natural resources evaluation*. Oxford University Press on Demand.
- Grammer, G. M., Eberli, G. P., Van Buchem, F. S., Stevenson, G. M., & Homewood, P. (1996). Application of high-resolution sequence stratigraphy to evaluate lateral variability in outcrop and subsurface desert creek and ismay intervals, paradox basin..
- Guardiano, F. B., & Srivastava, R. M. (1993). Multivariate geostatistics: beyond bivariate moments. In *Geostatistics troia92* (pp. 133–144). Springer.
- Haldorsen, H., & Chang, D. (1986). Notes on stochastic shales: From outcrop to simulation model, reservoir characterization. *LW Lake, HB Carroll*, 445–485.
- Haldorsen, H., MacDonald, C., et al. (1987). Stochastic modeling of underground reservoir facies (smurf). In *Spe annual technical conference and exhibition*.

- Haldorsen, H. H., Lake, L. W., et al. (1984). A new approach to shale management in field-scale models. *Society of Petroleum Engineers Journal*, 24(04), 447–457.
- Hastie, T., Tibshirani, R., & Friedman, J. (2009). Unsupervised learning. In *The elements of statistical learning* (pp. 485–585). Springer.
- Hestenes, M. R., & Stiefel, E. (1952). *Methods of conjugate gradients for solving linear systems* (Vol. 49). NBS.
- Holden, L., Hauge, R., Skare, Ø., & Skorstad, A. (1998). Modeling of fluvial reservoirs with object models. *Mathematical Geology*, 30(5), 473–496.
- Hu, L. Y., Joseph, P., Dubrule, O., et al. (1994). Random genetic simulation of the internal geometry of deltaic sandstone bodies. *SPE Formation Evaluation*, 9(04), 245–250.
- Jeng, F.-C., & Woods, J. W. (1990). Simulated annealing in compound gaussian random fields [image processing]. *IEEE Transactions on Information Theory*, 36(1), 94–107.
- Journal, A., & Huijbregts, C. (1978). *Mining geostatistics*. Academic Press, London.
- Journal, A., & Isaaks, E. (1984). Conditional indicator simulation: application to a saskatchewan uranium deposit. *Journal of the International Association for Mathematical Geology*, 16(7), 685–718.
- Journal, A. G. (1974). Geostatistics for conditional simulation of ore bodies. *Economic Geology*, 69(5), 673–687.
- Journal, A. G. (1983). Nonparametric estimation of spatial distributions. *Journal of the International Association for Mathematical Geology*, 15(3), 445–468.
- Journal, A. G. (2004). Beyond covariance: the advent of multiple-point geostatistics. *In Geostatistics 2004*,. (Banff, Canada)
- Journal, A. G., & Alabert, F. (1989). Focusing on spatial connectivity of extreme-valued attributes: Stochastic indicator models of reservoir heterogeneities. *AAPG Bull.:(United States)*, 73(CONF-890404-).
- Journal, A. G., & Zhang, T. (2006). The necessity of a multiple-point prior model. *Mathematical Geology*, 38(5), 591–610.
- Koltermann, C. E., & Gorelick, S. M. (1996). Heterogeneity in sedimentary deposits:

- A review of structure-imitating, process-imitating, and descriptive approaches. *Water Resources Research*, 32(9), 2617–2658.
- Krige, D. G. (1951). A statistical approach to some mine valuation and allied problems on the witwatersrand. *Msc. thesis, university of Witwatersrand*.
- Kyriakidis, P. C., Deutsch, C. V., & Grant, M. L. (1999). Calculation of the normal scores variogram used for truncated gaussian lithofacies simulation: theory and fortran code. *Computers & Geosciences*, 25(2), 161–169.
- Langlais, V., & Doyle, J. (1993). Comparison of several methods of lithofacies simulation on the fluvial gypsy sandstone of oklahoma. In *Geostatistics tróia92* (pp. 299–310). Springer.
- Lantuéjoul, C. (2013). *Geostatistical simulation: models and algorithms*. Springer Science & Business Media.
- Lantuéjoul, C., Desassis, N., & Fouedjio, F. (2012). Simulation of a gaussian random vector: a propagative approach to the gibbs sampler. *9th Int. Geostat. Congr., Oslo, Norway*.
- Le Loch, G., Beucher, H., Galli, A., & Doligez, B. (1994). Improvement in the truncated gaussian method: combining several gaussian functions. In *Ecmor iv-4th european conference on the mathematics of oil recovery*.
- Le Loch, G., & Galli, A. (1997). Truncated plurigaussian method: theoretical and practical points of view. *Geostatistics wollongong*, 96(1), 211–222.
- Liu, N., Oliver, D. S., et al. (2003). Automatic history matching of geologic facies. In *Spe annual technical conference and exhibition*.
- Lyster, S. J. (2009). *Simulation of geologic phenomena using multiple-point statistics in a gibbs sampler algorithm* (Unpublished doctoral dissertation). Alberta university.
- Maharaja, A. (2008). Tgenerator: object-based training image generator. *Computers & Geosciences*, 34(12), 1753–1761.
- Manchuk, J., & Deutsch, C. (2011). *A short note on trend modeling using moving windows* [CCG Annual Report 17]. CCG Paper 2011-403, Centre for Computational Geostatistics, Edmonton, AB: University of Alberta.

- Mariethoz, G., Renard, P., Cornaton, F., & Jaquet, O. (2009). Truncated plurigaussian simulations to characterize aquifer heterogeneity. *Ground Water*, 47(1), 13–24.
- Matheron, G. (1962). Traite de geostatistique appliquee. *Technip, Paris, France*.
- Matheron, G. (1963). Principles of geostatistics. *Economic geology*, 58(8), 1246–1266.
- Matheron, G. (1965). Les variables regionalisees et leur estimation. *Une appli.*
- Matheron, G. (1971). *The theory of regionalized variables and its applications* (Vol. 5). École nationale supérieure des mines.
- Matheron, G. (1973). The intrinsic random functions and their applications. *Advances in applied probability*, 439–468.
- Matheron, G., Beucher, H., De Fouquet, C., Galli, A., Guerillot, D., Ravenne, C., et al. (1987). Conditional simulation of the geometry of fluvio-deltaic reservoirs. In *Spe annual technical conference and exhibition*.
- Mattfeldt, T. (1996). Stochastic geometry and its applications. *Journal of Microscopy*, 183(3), 257–257.
- McCulloch, W. S., & Pitts, W. (1943). A logical calculus of the ideas immanent in nervous activity. *The bulletin of mathematical biophysics*, 5(4), 115–133.
- Mead, C., & Ismail, M. (2012). *Analog vlsi implementation of neural systems* (Vol. 80). Springer Science & Business Media.
- Metropolis, N., Rosenbluth, A. W., Rosenbluth, M. N., Teller, A. H., & Teller, E. (1953). Equation of state calculations by fast computing machines. *The journal of chemical physics*, 21(6), 1087–1092.
- Miall, A. (2013). *The geology of fluvial deposits: sedimentary facies, basin analysis, and petroleum geology*. Springer.
- Miall, A. D. (1985). Architectural-element analysis: a new method of facies analysis applied to fluvial deposits.
- Michiels, W., Aarts, E., & Korst, J. (2007). *Theoretical aspects of local search*. Springer Science & Business Media.
- Moore, D., Young, L., Modene, J., & Plahuta, J. (1986). Geologic setting and genesis of the red dog zinc-lead-silver deposit, western brooks range, alaska. *Economic Geology*, 81(7), 1696–1727.

- Moysey, S., & Knight, R. (2003). Full-inverse statistical calibration: A monte carlo approach to determining field-scale relationships between hydrologic and geophysical variables. In *Agu fall meeting abstracts* (Vol. 1, p. 03).
- Murray, C. J. (1994). Identification and 3-d modeling of petrophysical rock types.
- Oliver, D. S. (2002). Conditioning channel meanders to well observations. *Mathematical geology*, *34*(2), 185–201.
- Pennsylvanian. (n.d.). Retrieved from www.isgs.illinois.edu/outreach/geology-resources/pennsylvanian-rocks-illinois/
- Posa, D. (1989). Conditioning of the stationary kriging matrices for some well-known covariance models. *Mathematical Geology*, *21*(7), 755–765.
- Pyrzcz, M. J. (2004). *The integration of geologic information into geostatistical models* (Unpublished doctoral dissertation). Alberta university.
- Pyrzcz, M. J., & Deutsch, C. V. (2005). Conditioning event-based fluvial models. In *Geostatistics banff 2004* (pp. 135–144). Springer.
- Pyrzcz, M. J., & Deutsch, C. V. (2014). *Geostatistical reservoir modeling*. Oxford university press.
- Pyrzcz, M. J., McHargue, T., Clark, J., Sullivan, M., & Strebelle, S. (2012). Event-based geostatistical modeling: description and applications. In *Geostatistics oslo 2012* (pp. 27–38). Springer.
- Pyrzcz, M. J., & Strebelle, S. (2006). Event-based geostatistical modeling: application to deep-water systems. In *Reservoir characterization: Integrating technology and business practices, gulf coast section, sepm twenty-sixth annual research conference* (pp. 893–922).
- Ravenne, C., Galli, A., Doligez, B., Beucher, H., & Eschard, R. (2002). Quantification of facies relationships via proportion curves. In *Geostatistics rio 2000* (pp. 19–39). Springer.
- Remacre, A. Z., & Zapparolli, L. H. (2003). Application of the plurigaussian simulation technique in reproducing lithofacies with double anisotropy. *Brazilian Journal of Geology*, *33*(2), 37–42.
- Reza, Z. A., Pranter, M. J., & Weimer, P. (2006). Moddre: A program to model

- deepwater-reservoir elements using geomorphic and stratigraphic constraints. *Computers & geosciences*, *32*(8), 1205–1220.
- Rondon, O. (2009). A look at plurigaussian simulation for a nickel laterite deposit. In *7th international mining & geology conference, held in perth, wa* (pp. 17–19).
- Rozenberg, G., Bck, T., & Kok, J. N. (2011). *Handbook of natural computing*. Springer Publishing Company, Incorporated.
- Rumelhart, D. E., McClelland, J. L., Group, P. R., et al. (1988). *Parallel distributed processing* (Vol. 1). IEEE.
- Schaul, T., Bayer, J., Wierstra, D., Sun, Y., Felder, M., Sehnke, F., . . . Schmidhuber, J. (2010). PyBrain. *Journal of Machine Learning Research*, *11*, 743–746.
- Seifert, D., & Jensen, J. (1999). Using sequential indicator simulation as a tool in reservoir description: issues and uncertainties. *Mathematical Geology*, *31*(5), 527–550.
- Serrano, R. P., Guadagnini, L., Giudici, M., Guadagnini, A., & Riva, M. (2012). Application of the truncated plurigaussian method to delineate hydrofacies distribution in heterogeneous aquifers.
- Serrano, R. P., Guadagnini, L., Riva, M., Giudici, M., & Guadagnini, A. (2014). Impact of two geostatistical hydro-facies simulation strategies on head statistics under non-uniform groundwater flow. *Journal of Hydrology*, *508*, 343–355.
- Shmaryan, L., & Deutsch, C. (1999). Object-based modeling of fluvial/deepwater reservoirs with fast data conditioning: methodology and case studies. In *Spe annual technical conference* (pp. 877–886).
- Sichel, H. S. (1952). *New methods in the statistical evaluation of mine sampling data*.
- Silva, D. A., & Deutsch, C. V. (2014). A multiple training image approach for spatial modeling of geologic domains. *Mathematical Geosciences*, *46*(7), 815–840.
- Silva, D. S., & Deutsch, C. (2016b). *Variogram inference in truncated plurigaussian simulation* [CCG Annual Report 18]. CCG Paper 2016-409, Centre for Computational Geostatistics, Edmonton, AB: University of Alberta.
- Silva, D. S., & Deutsch, C. V. (2016a). Multiple imputation framework for data assignment in truncated pluri-gaussian simulation. *Stochastic Environmental Research*

and Risk Assessment, 1–13.

- Stein, M. L., & Handcock, M. S. (1989). Some asymptotic properties of kriging when the covariance function is misspecified. *Mathematical Geology*, *21*(2), 171–190.
- Straubhaar, J., Renard, P., Mariethoz, G., Froidevaux, R., & Besson, O. (2011). An improved parallel multiple-point algorithm using a list approach. *Mathematical Geosciences*, *43*(3), 305–328.
- Strebelle, S. (2002). Conditional simulation of complex geological structures using multiple-point statistics. *Mathematical Geology*, *34*(1), 1–21.
- Strebelle, S., & Journel, A. G. (2000). Sequential simulation drawing structures from training images. *In 12th International Geostatistics Congress*,. (Cape Town, South Africa)
- Sun, T., Meakin, P., Jøssang, T., & Schwarz, K. (1996). A simulation model for meandering rivers. *Water Resources Research*, *32*(9), 2937–2954.
- Tadiou, K. M. (n.d.). Retrieved from www.futurehumanevolution.com/artificial-intelligence-future-human-evolution/artificial-neural-networks/
- Teles, V., Delay, F., & De Marsily, G. (2004). Comparison of genesis and geostatistical methods for characterizing the heterogeneity of alluvial media: Groundwater flow and transport simulations. *Journal of hydrology*, *294*(1), 103–121.
- Tetzlaff, D. M., & Harbaugh, J. W. (1989). *Simulating clastic sedimentation*. Springer.
- Triki, E., Collette, Y., & Siarry, P. (2005). A theoretical study on the behavior of simulated annealing leading to a new cooling schedule. *European Journal of Operational Research*, *166*(1), 77–92.
- Van Buchem, F. S., Doligez, B., Eschard, R., Lerat, O., Grammer, G. M., & Ravenne, C. (1998). Stratigraphic architecture and stochastic reservoir simulation of a mixed carbonate/siliciclastic platform (upper carboniferous, paradox basin, usa). *In Overpressures in Petroleum Exploration: Workshop Proceedings*,. (Pau, France, (22), 109. Editions TECHNIP)
- Van Laarhoven, P. J., & Aarts, E. H. (1987). *Simulated annealing*. Springer.
- Vargas-Guzmán, J., & Al-Qassab, H. (2006). Spatial conditional simulation of facies objects for modeling complex clastic reservoirs. *Journal of Petroleum Science*

and Engineering, 54(1), 1–9.

- Viseur, S. (1999). Stochastic boolean simulation of fluvial deposits: a new approach combining accuracy with efficiency. In *Spe annual technical conference*.
- Wickelmaier, F. (2003). An introduction to mds. *Sound Quality Research Unit, Aalborg University, Denmark*, 46.
- Xia, W., & Wu, Z. (2005). An effective hybrid optimization approach for multi-objective flexible job-shop scheduling problems. *Computers & Industrial Engineering*, 48(2), 409–425.
- Xie, Y., Cullick, A. S., Deutsch, C. V., et al. (2001). Surface-geometry and trend modeling for integration of stratigraphic data in reservoir models. In *Spe western regional meeting*.
- Xu, C., Dowd, P. A., Mardia, K. V., & Fowell, R. J. (2006). A flexible true plurigaussian code for spatial facies simulations. *Computers & geosciences*, 32(10), 1629–1645.
- Xu, W. (1995). *Stochastic modeling of reservoir lithofacies and petrophysical properties* (Unpublished doctoral dissertation). stanford university.
- Zagayevskiy, Y., & Deutsch, C. (2015). *Numerical derivation of gaussian variogram models for truncated pluri-gaussian simulation* [CCG Annual Report 17]. CCG Paper 2015-213, Centre for Computational Geostatistics, Edmonton, AB: University of Alberta.
- Zhang, C., & Li, W. (2007). Comparing a fixed-path markov chain geostatistical algorithm with sequential indicator simulation in categorical variable simulation from regular samples. *GIScience & Remote Sensing*, 44(3), 251–266.
- Zhang, F., Reynolds, A., Oliver, D., et al. (2003). The impact of upscaling errors on conditioning a stochastic channel to pressure data. *SPE Journal*, 8(01), 13–21.
- Zhang, Y., Yan, H., Zou, X., Tao, F., & Zhang, L. (2016). Image threshold processing based on simulated annealing and otsu method. In *Proceedings of the 2015 chinese intelligent systems conference* (pp. 223–231).

Appendix A

TPG Simulation Software

In this chapter parameter files of all the developed programs for TPG simulation are explained in details. Origin for gridded data files is the same as all of the GSLIB data files.

A.1 Locally Varying Mask with Linear Thresholds

The ”*tpgsim*” program operates in the GSLIB fashion. With this program, threshold based masks are generated based on the LVP of categories. The parameter file used by the program is shown below and a detailed line by line description is given.

```
1   START OF PARAMETERS:
2 Southern.dat   - file with data
3 4             - number of categories to include
4 2 1 5 3       - category identifiers (integers)
5 2 3 4         - columns for X, Y, Z coordinates
6 1 5           - columns for drill hole, category
7 1             - type of mask:0=Global; 1=LVP
8 .5 .04 .08 .38 - category Global prop.(if option=0)
9 trend.out     - input trend file (if option=1)
10 50 587350 10 - nx,xmn,xsiz
11 120 143085 10 - ny,ymn,ysiz
```



```

12 75      300  10  - nz,zmn,zsiz
13 1  2  3  4      - column number of prop.(if option=1)
14 2  2  0          - numbers of rectangles (nL,nC,nR)
15 0  1  1          - position of rectangles:1=V.;0=H.
16 mask.out        - mask output for trend/global prop.
17 mask-data.out   - mask output for input data
18 gauss-data.out  - output(transfer cat. to Gaussian)
19
20 NOTES:
21
22 Order of categories in this program is
23 In vertical position:from left side to right side
24 In horizontal position:from bottom to up
25 Mask:
26 If nL=2, nC=2, nR=2 & position:left=0,center=0,right=1
27 Number of categories=6
28
29  |--- |-----|---|---|
30  | 2  |   4  | 5  | 6  |
31 t3|    |-----|    |    |
32 t1|----|   3  |    |    |
33  | 1  |        |    |    |
34  |--- |-----|---|---|
35      t2      t4  t5

```

1. Indicates start of parameter and must be present.
2. Specifies data file, which can be from drill hole data set or well data set.
- 3-4. Specifies the number of categories on line 4 and category identifiers on line 5.
- 5-6. Specifies the column numbers for coordinates of data on line 5 and columns for drill hole id and categories on line 6.

7. Specifies the type of mask. If the mask is based on the global proportions (option= 0), the output file contains only the threshold values for the global mask.
8. Specifies the category global proportions. It is necessary input if the global mask (option= 0) has been selected.
9. Specifies the input trend model file. It is necessary input file if the LVP mask (option= 1) has been selected.
- 10-12. Next three lines are reserved for the grid specification: number of cells in X direction with minimum value of X and cell size is entered on line 10, number of cells in Y direction with minimum value of Y and cell size is entered on line 11, and number of cells in Z direction with minimum value of Z and cell size is specified on line 12.
13. Specifies column number for proportion of categories in the input trend file.
14. Specifies the number of rectangles in each three zones (Left, center, and right).
15. Specifies the position of rectangles in the each zones (1= vertical, 0= horizontal).
16. Specifies the output file for the mask based on the global proportions or trend model. In case of trend model, this output file contains the local mask (threshold values) for all locations and in the case of global proportions contains only one mask that is representing the threshold values for global proportions.
17. Specifies the corresponding mask output file for data values and is shown the local mask at each location with data values.
18. Specifies the corresponding Gaussian values for data. The categorical data must be transferred into continuous Gaussian conditioning data for conditional simulation of the Gaussian variables. This output file contains the data value (which is the category) and the corresponded Gaussian values with respect to the truncation rule.

A.1.1 Truncating Conditional Gaussian for Threshold Mask

The "*truncation - tp*" program operates in the GSLIB fashion. This program takes the truncation mask output by "*tpgsim*" and truncates bivariate Gaussian values to

categorical values. The parameter file used by the program is shown below and a detailed line by line description is given.

```
1  START OF PARAMETERS:
2  realz1.out      - input data file (Gaussian#1)
3  realz2.out      - input data file (Gaussian#2)
4  50  587350  10  - nx,xmn,xsiz
5  120 143085  10  - ny,ymn,ysiz
6  75   300  10  - nz,zmn,zsiz
7  1              - column for value
8  1              - input mask size;1:realz 2:data
9  mask.out       - input file with thresholds (mask)
10 1  2  3        - columns for X, Y, Z coordinates
11 4              - number of categories to include
12 4 5 6          - column numbers for thresholds
13 2 2 0          - numbers of rectangles (nL,nC,nR)
14 0 1 1          - position of rectangles:1=V.;0=H.
15 Newmask.out    - output file(if option=2)
16 cat-thre.dat   - output file truncated realization
17
18 NOTES:
19
20 Order of categories in this program is
21 In vertical position:from left side to right side
22 In horizontal position:from bottom to up
23 Mask:
24 If nL=2, nC=2, nR=2 & position:left=0,center=0,right=1
25 Number of categories=6
26
```

```

27  |--- |-----|---|---|
28  | 2  |   4  | 5  | 6  |
29 t3|    |-----|    |    |
30 t1|----|   3  |    |    |
31  | 1  |    |    |    |
32  |--- |-----|---|---|
33      t2      t4  t5

```

1. Indicates start of parameter and must be present.
- 2-3. Specifies input realization files to be truncated using the mask that comes from the "tpgsim" program. Generally, conditional/ unconditional simulation results using GSLIB "sgsim" program can be considered as input files.
- 4-7. Next three lines are reserved for the grid specification: number of cells in X direction with minimum value of X and cell size is entered on line 4, number of cells in Y direction with minimum value of Y and cell size is entered on line 5, and number of cells in Z direction with minimum value of Z and cell size is specified on line 7.
7. Specifies the column number of input realizations. It assumed that the column number in both realizations is the same.
8. the status of input mask. If there is a threshold based mask for any location of input realizations, then option one should be selected. In this case, the LVP mask is available for the whole simulation grids and there are $K - 1$ threshold values for each location in the mask file. If the input threshold masks are calculated only for those locations with data value, then option two should be selected. In this case, the nearest mask to the location of input realizations is selected to be used as the truncation rule.
9. Defines the input file for the mask for LVP.
10. Contains the column numbers for X, Y, Z coordinated if thresholds of mask are defined for available data and coordinates of data are specified; otherwise put 0 as column numbers.

11. Specifies number of categories to include.
12. Specifies column number for threshold values in the input mask file.
13. Specifies the number of rectangles in each three zones (Left, center, and right).
14. Specifies the position of rectangles in the each zones (1= vertical, 0= horizontal).
- 15-16. The output files are specified. The output file for the mask at each location with data values on line 15 and the truncated realization output file on line 16.

A.2 Locally Varying Mask with MDS

The "*mds_tpg_LVP*" program operates in the GSLIB fashion. This program is MDS of the transition probability matrix and optimization for TPG simulation using LVP of categories. The first version of program is written by Jared L. Deutsch for global mask and it is modified for considering trend. The parameter file used by the program is shown below and a detailed line by line description is given.

```

1  START OF PARAMETERS:
2  Southern.dat      - input data file
3  2  3  4           - columns for X, Y, Z
4  1  5             - columns for drill hole, category
5  tpmat-South.dat  - input transition prop. matrix
6  4                - number of categories (K)
7  1  2  3  5       - category identifiers (integers)
8  .04  .5  .08  .38 - category proportions (Global)
9  trend.dat        - input trend model (prop.)
10 50  587350  10   - nx, xmn, xsiz
11 120 143085  10   - ny, ymn, ysiz
12 75   300  10   - nz, zmn, zsiz
13 1  2  3  4       - column numbers for LVP prop.
14 0                - upscale trend model: 0=No; 1=Yes
15 5 5 3           - number of grid to upscale trend

```

```

16 2          - number of Gaussian to project(M)
17 tpg_points.out - file for control point output
18 2          - debugging level (0, 1 or 2)
19 mds_tpg.dbg  - file for debugging output
20 10000       - number of points for MC integration
21 3           - optimization level (0, 1)
22 200  0.03   - max. iterations;early exit level
23 0.4         - move magnitude
24 trendcoord.out - output trend model with coordinates
25 data-trend.dbg - output with data and their trend
26 upscaled-t.dbg - output with up scaled trend data
27
28
29 NOTES:
30 The number of points for MC integration directly
31 affects the speed of the program
32 1: very low number of points <10000 -->not recommended
33 2: low number of points 20000-40000 -->do recommended
34 3: medium number of points 50000-10000 -->recommended
35 4: high number of points >11000 --> is not recommended
    (very time consuming)

```

1. Indicates start of parameter and must be present.
2. Specifies a data file, which can be from the drill hole data set or well data set.
- 3-4. Specifies the column number for coordinates (X, Y, Z) of data on line 3 and drill hole id and categories on line 4.
5. Specifies a data file with the transition probability matrix, which can be calculated from drill hole data using a GSLIB program " *tpmat_tpg*".
- 6-8. Specifies the number of categories on line 6, category identifiers on line 7 and global proportions of categories on line 8.

9. Specifies the trend model (local proportions) as an input file.
- 10-12. Next three lines are reserved for the grid specification: Number of cells in X direction with minimum value of X and cell size are entered on line 10, number of cells in Y direction with minimum value of Y and cell size are entered on line 11, and number of cells in Z direction with minimum value of Z and cell size are specified on line 12.
13. Contains the column numbers for the local proportions for each category.
14. Specifies option for re-sizing the trend model. If upscale trend is requested, put 1; otherwise put 0.
15. Specifies number of cells to be merged in X, Y, and Z directions.
16. Specifies the number of Gaussian variables to project on, which must be less than the number of categories.
17. Specifies the output file which contains the control points.
- 18-19. The debugging level and output file, which can used to output intermediate matrices and optimization steps, are specified on lines 21 and 22, respectively.
20. Specifies the number of points to use for Monte Carlo integration.

Integration of the multivariate Gaussian probability distribution is necessary to optimize the control points. Monte Carlo integration is used in this program. After each movement of the control points, Monte Carlo integration is performed again and the objective function is checked. The number of Monte Carlo integration directly affects the speed of the program and may cause some error in proportion optimization. The wise decision should be made about this number.

There are two main factors that should be considered. First, the number of categories with low proportions (1% – 5%). Second, the percentage of error in proportion that is acceptable for your work. Based on the experience, in terms of time and possible error level in proportion reproduction, the Monte Carlo points between (10000, 40000) will be optimum. For instance, the average percent error (Eq. A.1) for these numbers is around 1% to 4% when there is one category with low proportion and the possible error on that category would be around 2% to 6%. When there are two categories with low proportions, the average percent

error would be around 3% to 6% and the possible error on those low proportion categories would be around 8%.

$$\overline{Error}\% = \sum_{k=1}^K \frac{|p_k^* - p_k|}{p_k} \quad (\text{A.1})$$

where:

- p_k^* - estimated proportion;
- p_k - desired proportion [global or local];

As the number of categories with low proportion increases, the percentage of error increases. In this case using more points for Monte Carlo integration is recommended. Using more than 100000 points, however, will be very time consuming and would result in little gain in accuracy.

- 21. Specifies the optimization level (0= no optimization, 1= optimization for integration).
- 22-23. Specifies the optimization parameters. Maximum iterations and early exit level for objective function on line 22. Move magnitude (modify if optimization difficult) on line 23.
- 24-26. Specifies output file with the trend model with coordinates on line 24, the debugging files for data with their corresponding local proportions on line 25 and the up scaled trend on line 26.

A.2.1 Truncating Conditional Gaussian for MDS Mask

The "*trans_tpg_LVP*" program operates in the GSLIB fashion. This program takes the truncation mask output by "*mgs_tpg_LVP*" and truncates a set of Gaussian values to categorical values. The parameter file used by the program is shown below and a detailed line by line description is given.


```

1   START OF PARAMETERS :
2   5           - number of category
3   2           - number of Gaussian variables (M)
4   gaussdata.dat - input data (Simulated realizations)
5   0 1  2  3   0 - columns for dh,x,y,z,secvar
6   4  5           - column for Gaussians m=1,...,M
7   tpg_points.out - input with tpg points
8   catvalue.dat  - output for transformed data
9
10  NOTES :
11
12  Corresponding Gaussian variables must be ordered
13  All the Gaussian variables should be in one file.

```

1. Indicates start of parameter and must be present.
2. Specifies number of categories.
3. Specifies the number of Gaussian variables to truncate, which must be less than the number of categories.
4. Specifies an input file corresponding to Gaussian variables and must be ordered as $m = 1, \dots, M$. If "sgsim" program is used for individual Gaussian simulations, then a CCG merging utility such as "merge_multi" should be used to collect Gaussian variables in one file.
5. Specifies the data file name. This file must contain Gaussian realization number two.
6. Contains the column number for drill hole id and coordinates (X, Y, Z) of Gaussian realizations and secondary variable if it is available.
7. Specifies column number for Gaussian variables
8. Specifies the input file which contains the control points comes from "mds_tpg_LVP" program.

9. Specifies the truncated realization output file.

A.3 Correlation Coefficient in Truncated Plurigaussian Simulation

The "*corr_tpgsim*" program operates in the GSLIB fashion. This program is developed to deal with correlation between underlying Gaussian RFs. Practitioners can define any of the explained cases in the parameter file for any configuration of threshold based mask and receive the global proportions and the mask thresholds as well as the final truncated realization. The parameter file used by the program is shown below and a detailed line by line description is given.

```
1  START OF PARAMETERS :
2  1                - 1:Gaussians input 2:generate MC
3  R1.out           - if 1;file for Gaussian real. #1
4  R2.out           - if 1;file for Gaussian real. #2
5  256 10.0 10.0    - nx,xmn,xsiz
6  256 10.0 10.0    - ny,ymn,ysiz
7  1  0.0  1.0      - nz,zmn,zsiz
8  1                - column for value
9  100000           - if 2;number of points for MC
10 4                - number of categories in tpmat (K)
11 1 2 3 4          - category identifiers(integers)
12 .30 .18 .21 .32  - category global proportions
13 2  2  0          - numbers of rectangle in L,C,R
14 0  1  1          - position of rectangle in L,C,R
15 69058            - random number to generate MC points
16 0.8              - correlation between two Gaussians
17 2                - 1:matching global thr. 2: global P.
18 mask.out         - mask output; 1:local; 2:global P.
```

```

19 prop.out          - output of cat. proportions in sim.
20 Gauss-Trun.out   - output of Gaussians & truncated
21
22 NOTES:
23
24 Order of categories in this program is
25 In horizontal position:from left side to right side
26 In vertical position:from bottom to top
27 Mask example:
28 If nL=2, nC=2, nR=2 & position:left=0,center=0,right=1
29 Number of categories=6
30
31  |--- |-----|---|---|
32  | 2  |   4  | 5 | 6 |
33 t3|    |-----|   |   |
34 t1|----|   3  |   |   |
35  | 1  |       |   |   |
36  |--- |-----|---|---|
37      t2      t4  t5

```

1. Indicates start of parameter and must be present.
2. Option for 1: giving Gaussian realizations as input files or 2: generating them internally.
3. Specifies the data file name. This file must contain Gaussian realization number one.
4. Specifies the data file name. This file must contain Gaussian realization number two.
- 5-7. Next three lines are reserved for the grid specification: number of cells in X direction with minimum value of X and cell size is entered on line 5, number of cells in Y direction with minimum value of Y and cell size is entered on line

- 6, and number of cells in Z direction with minimum value of Z and cell size is specified on line 7.
8. Specifies the column number of Gaussian variables (should be the same in both files)
 9. Specifies the number of points to use for Monte Carlo integration
 10. Specifies number of available categories.
 11. Specifies category identifiers (ID)
 12. Global proportion of categories should be defined in this line.
 13. Specifies the number of rectangles in each three zones (Left, center, and right) in the mask.
 14. Specifies the position of rectangles in the mask for each zones (1= vertical, 0= horizontal).
 15. Seed number for the generation of random numbers. This is used to generate points for Monte Carlo integration.
 16. Specifies correlation coefficient between underlying Gaussian realizations.
 17. Specifies the option for matching global thresholds and finding a new proportion of categories with respect to correlation between Gaussian realizations (option = 1) or matching the global proportions and finding the new threshold values with respect to correlation between Gaussian realizations (option = 2).
 18. Specifies the output file for the mask which contains the threshold values which is based on the new proportions (option = 1) or based on the global proportions (option = 2).
 19. Specifies the output file for proportion of categories for selected option.
 20. Specifies the output file for Gaussian realizations and truncated simulation with respect to correlation coefficient and selected option for matching global thresholds values or global proportion of categories.

A.4 Covariance Map Optimization

The "vargopt_tpg" program operates in the GSLIB fashion. This program is developed to obtain the best fit for the variogram models of underlying Gaussian deviates in TPG simulation with a flexible methodology. The parameter file used by the program is shown below and a detailed line by line description is given.

```
1   START OF PARAMETERS:
2   tpg_points.dat   - File for control point input
3   vargsmodel.var   - File for categories' varg models
4   4                - Number of categories
5   2                - number of Gaussian variables (M)
6   2                - Number of structures
7   1                - 0:start with nst; 1:use sequential
8   1                - 0:Anisotropic;1:Isotropic
9   0                - 0:3D case; 1:2D case
10  50               - Number of random restart
11  1                - Optimization; 0:GA 1:SA
12  1500            - If SA:number of iterations
13  40              - If GA:number of iterations
14  0               - Gaussian type; 0:regular;1:stable
15  0               - Power of inverse distance weight
16  600            - Number of point for LU simulation
17  10 10 10       - The lowest possible range(a1,a2,v)
18  2700 2700 1400 - The highest possible range(a1,a2,v)
19  69069          - Random number seed
20  parameter.dat   - Output of initial/final parameters
21  objective.dat    - Output of initial/final objective
22  optimum.dat     - Output parameters for optimum run
```

1. Indicates start of parameter and must be present.
2. Specifies an input file which contains the control points of the mask which is the output file of " *mds_tpg*" program.
3. Specifies an input file which contains the variogram model of categories in one file.
- 4-5. Specifies the number of categories and underlying Gaussian deviates to truncate, which must be less than the number of categories.
6. Specifies number of structures of variogram/covariance model.
7. Specifies the way that optimization should deal with structures. To use proposed sequential methodology for structures (first *st=1*, then adding *st=2*, then ...), select option 1; otherwise option 0. With option 0, optimization starts directly with mentioned number of structures.
8. Specifies option for considering anisotropy in covariance model for underlying Gaussian realizations. Option 0 uses anisotropic variogram model and option 1 uses isotropic variogram model.
9. Specifies the dimension of data set (3 dimensional or 2 dimensional) for optimization. In case of 3D (option 0), there is a vertical range to be optimized for each underlying Gaussian.
10. Specifies number of random restart for optimization. Since there is no unique solution, program uses different random restart in each step and the one with the smallest objective value is considered as the best match.
11. Specifies type of optimization. By selecting 0, Gradient optimization is used and by selecting 1, SA is applied.
12. Specifies the number of iterations in each random restart for SA optimization. The number of iterations for this type of optimization should be more than 1000. SA requires a large number of iterations to converge.
13. Specifies the number of iterations in each random restart for Gradient optimization. This type of optimization does not need too many iterations (≤ 100).
14. Specifies the variogram/ covariance type to use. Two models are considered in this program to build the covariance of Gaussian variables; Gaussian type and

stable type. Option 0: regular Gaussian type; 1: stable Gaussian type.

15. Specifies power of inverse distance in objective function (weight to the covariance values from the origin).
16. Specifies the number of points to use for LU simulation.
- 17-18. Specifies the lowest and highest possible values for variogram ranges (a_{hmax} , a_{hmin} , a_{vert}) for optimization. These values can be defined based on the lowest and highest indicator variogram ranges of categories (from data set) \pm sufficient variation.
19. Specifies seed number for the generation of random numbers. This is used to generate points for simulation of underlying Gaussian deviates using LU method.
20. Specifies output file of initial and final parameters for each structure in each random restart.
21. Specifies output file of initial and final objective values for each structures in each random restart.
22. Specifies output file of initial and final parameters for optimum run.